The mineralogy of some synthetic sulphosalts

Alan James Hall

THE MINERALOGY OF SOME SYNTHETIC SULPHOSALTS

A THESIS SUBMITTED FOR THE DEGREE OF DOCTOR OF PHILOSOPHY IN THE UNIVERSITY OF DURHAM

by

ALLAN JAMES HALL, B.Sc. (Edinburgh)

GRADUATE SOCIETY

OCTOBER, 1971.

ABSTRACT

'The Mineralogy of some Synthetic Sulphosalts'

Allan J. Hall

The mineralogy of the sulphosalts is not well understood, principally because of the very wide variations in chemical composition of the natural examples and their common admixture with other sulphide mineral species.

The synthesis of pure sulphosalt compositions is considered to be a valuable means of solving the problems involved. Changes in characteristic physical properties can then be measured as elements are substituted systematically into the structure.

A typical sulphosalt, tetrahedrite, general formula $(CuAg)_{10}(ZnFeCu)_2(SbAs)_4S_{13}$ was selected for study by synthesis in sealed evacuated silica glass capsules.

The phase relations of the Cu-Sb-S system were studied. Phases obtained were: tetrahedrite, $Cu_{12}Sb_4S_{13}$; non-stoichiometric tetrahedrite, $Cu_{12.12}Sb_{3.34}S_{13}$ to $Cu_{13.04}Sb_{3.86}S_{13}$, which has high and low temperature cubic polymorphs; stibioluzonite, Cu_3SbS_4; chalcostibite, $CuSbS_2$; and Cu_3SbS_3.

Substitution of As for Sb in tetrahedrite (the tetrahedrite-tennantite series) was found to result in a decrease in cubic cell edge, increase in microhardness, decrease in reflectivity and slight changes in quantitative colour measurements. Non-stoichiometry of the series also affected these properties.

Substitution of Zn and Fe for Cu in tetrahedrite

resulted in an increase in cubic cell edge, increase in microhardness and increase in reflectivity. Substitution of Ag for Cu resulted in an increase in unit cell edge, decrease in microhardness and decrease in reflectivity. Only Ag substitution proved to be temperature dependant, the low temperature breakdown products of Ag-tetrahedrite being $(CuAg)_3SbS_4$ and $(AgCu)_3SbS_3$.

Chemical bonding in the phases synthesised is discussed in detail. Substitution and the resultant effect on physical properties are discussed in relation to the atomic properties of the substituting element.

ACKNOWLEDGEMENTS

The author wishes to thank Professor G. M. Brown, Head of the Geology Department, for the facilities provided for this study.

The author also wishes to thank Mr. R. Phillips, for suggesting this topic, supervising the study and for critically reading the manuscript.

Special thanks are due to: Dr. Saunders, of the Applied Physics Department, for his advice on the construction of the experimental apparatus; Mrs. Dennison, for translating the paper by Cambi and Elli (1965); Dr. A. Peckett and D. Robinson, for advice on the use of the electron microprobe correction programs; U. Win Htein, for use of his colour measurement programs and advice on the measurement of reflectivity; and K. Ashworth, for his contribution to the x-ray diffraction work.

The technical staff of the Science Site Workshop and the Department of Geology are thanked for their assistance in the construction of the apparatus and the preparation of material for this thesis. The glassblowers of the Chemistry Department are acknowledged for their skill in making and sealing the silica glass capsules.

Finally the author wishes to thank the Natural Environment Research Council for financing this study.

TABLE OF CONTENTS

page

TABLES

FIGURES

PLATES

INTRODUCTION

Introduction to present study

The sulphosalts are a group of sulphide minerals. An indication of the chemistry of the group is given by the general formula - $A_m B_n X_p$

where A is a metal, e.g. Cu, Ag, Pb or Hg

B is a semi-metal, e.g. Sb, As or Bi

X is a non-metal, e.g. S or Se

Sulphosalts commonly exhibit extensive substitution. They are usually intergrown with other minerals in ore deposits. The consequent difficulties in chemical analysis have resulted in uncertainties in the basic formula of many individual sulphosalts and in the possible extent of substitution by different elements. The mineralogical properties of individual sulphosalts change with variations in chemistry, the result being that natural sulphosalts are difficult to identify without complete analysis.

The variation in composition and properties of sulphosalts has not yet been adequately explained by mineralogical theory. The collection of systematic data is required before theories which have been formulated to explain mineralogical observations on simple sulphides can be extended to the sulphosalts. This should be made possible by the synthesis of pure sulphosalt compositions and the study of changes, due to substitution, in certain characteristic physical properties.

A typical sulphosalt, tetrahedrite, was selected for study. Several other sulphosalts which also occur in the

Cu-Sb-S system were also synthesised.

The present study required an examination of previous work on natural tetrahedrites in order to define their features and problems (Chapter 1). The technique of synthesis which was used is described in Chapter 2. Previous work on the Cu-Sb-S system was found to be incomplete and experiments on the phase relations of tetrahedrite in the central area of this system were undertaken (Chapter 3). Substitution of Sb by As, the tetrahedrite-tennantite series, is the subject of Chapter 4. Substitution of Cu by Zn, Fe and Ag in tetrahedrite is the subject of Chapter 5. In order to understand substitution in tetrahedrite an understanding of the chemical bonding in tetrahedrite is necessary and this is the subject of Chapter 6.

CHAPTER 1

Substitution in Natural Tetrahedrites

Summary of Previous Work on Natural Tetrahedrites

Extensive substitution in tetrahedrite has long been recognised. The general formula of substituted tetrahedrite (or fahlerz), $(CuAg)_{10}(ZnFeCu)_2(SbAsBi)_4S_{13}$, was suggested by Tschermak (1894).

Machatschki (1928a) gave $a_o = 10.41\text{Å}$ for antimonian fahlerz from Colquechaca, Bolivia and $a_o = 10.29\text{Å}$ for a specimen from Felsobanya. Machatschki (1928b) gave $a_o = 10.189\text{Å}$ for tennantite from Redruth, Cornwall and $a_o = 10.205\text{Å}$ for binnite, a variety of tennantite. Machatschki (1928a, b) determined the structures of tetrahedrite and tennantite and derived the general formula $Cu_{12}(SbAs)_4S_{12}$. Thereafter the existence of the '13th' sulphur atom has been the subject of much controversy.

Pauling and Neuman (1934) determined the structure of binnite, from Binnenthal, Wallis, Switzerland. From the recalculated chemical analysis of tetrahedrite by Kretschmer (1911) they derived the ideal formula suggested by Tschermak (1894). They noted that recent analysis by Prior of binnite supported the formula $Cu_{12}As_4S_{12}$ of Machatschki (1928b), but for a slight excess of sulphur, which induced them to accept the formula $Cu_{12}As_4S_{13}$ for binnite. They found that $a_o = 10.19\text{Å}$, the unit cell formula being $2(CuFe)_{12}As_4S_{13}$.

In a classification of sulphosalts, Berry (1943) recognised a TETRAHEDRITE group with -

tetrahedrite $2(Cu_{12}Sb_4S_{13})$ T_d^3-$I\bar{4}3m$ $a_o = 10.32\text{Å}$

tennantite $2(Cu_{12}As_4S_{13})$ " $a_o = 10.19\text{Å}$

Edwards (1947) included the tetrahedrite-tennantite series, $Cu_{12}(SbAs)_4S_{13}$, in a list of sulphosalts capable of producing solid solutions at normal temperatures.

Harada and Kitahama (1952) quoted cell edges of tetrahedrite, $(CuFe)_3(SbAs)S_3$, from Japan -

Mata Mine $a_o = 10.35\text{Å}$

Teine Mine $a_o = 10.38\text{Å}$

Bernard (1957, 8) noted substitution of Cu, in tetrahedrite from the Slovak Mountains, by Hg (0.5-19%), Fe (1-10%), Zn (0.5-10%) and Ag ($1X10^{-2}$-1%). Substitution by Hg and As produced the strongest effects on the cell size.

Kostov (1957) noted that there is a constancy of Sb:As ratio among most members of isomorphous series quoted by Edwards (1947). Tetrahedrite and tennantite, however, are an exception to this statement. A plot of Sb v As content of natural compositions indicated a large variability in composition for tetrahedrite whereas tennantite had a more restricted composition and only special varieties contained a significant proportion of Sb. It was concluded that a large content of As in tetrahedrite and a limited Sb content in tennantite is due to easier substitution of small As atoms for large Sb atoms than vice versa. A member of the series, zandbergerite, has the Sb:As ratio of 1:1 corresponding to the ratio in other sulphosalts. The form of the Sb-As binary (Kostov Fig.1) was considered significant in this respect since three phases occur, antimony, stibarsene and arsenic, due to 13.8% difference in the atomic radii.

Hellner (1958) in a structural classification of sulphides, grouped together tetrahedrite, Cu_3SbS_3, tennantite, Cu_3AsS_3, and wittichenite, Cu_3BiS_3.

The structure of tetrahedrite was refined by Wuensch (1964) using a natural specimen from Horhausen, Westerwald, Germany. Analysis (Kretschmer 1911) gave the formula.

$$Cu_{10.19}Zn_{1.71}Fe_{0.34}Pb_{0.06}Ag_{0.02}Sb_{4.04}S_{13.17}$$

$$(Cu_{10.06}Zn_{1.69}Fe_{0.34}Ag_{0.02}Sb_{3.99}Bi_{0.04}S_{13})$$

The cell edge was found to be $10.390 \pm .0006$Å. The ideal formula, $Cu_{12}Sb_4S_{13}$, was accepted for tetrahedrite.

Bohmer (1964) analysed natural tetrahedrite-tennantites and showed a compositional gap between 6 and 11 at%.As which was interpreted as being a miscibility gap for varieties having 2.5 at% Ag. A continuum of unit cell dimensions from 10.30Å to 10.55Å was noted. Neither natural, nor several synthetic specimens, showed evidence of an order-disorder relationship therefore Bohmer suggested that it was misleading for Wuensch (1964) to conceive of tetrahedrite in terms of ordered Sb or As substitution in tetrahedral Cu sites.

Graeser (1965), in a description of minerals from Binnenthal, Switzerland, described specimens of the fahlerz group (tetrahedrite-tennantites). An Ag_2S content of 1.4 wt% was noted to increase the unit cell edge of members of the tetrahedrite-tennantite series (with 0.5 wt% Ag_2S or less) by about 0.02Å. The following cell edges were quoted -

tetrahedrite - rich in Ag, a_o = 10.39Å

low in Ag, a_o = 10.37Å

tennantite - rich in Ag, a_o = 10.23Å

low in Ag, a_o = 10.21Å

Novotný and Novak (1966) in a mineralogical and geochemical study of Špani Dolina, central Slovakia, noted a ferro-zincian tetrahedrite with 30 mol% tennantite and a_o = 10.299-10.320Å.

The structure of binnite, a variety of tennantite, from Lengenbach, Canton Wallis, Switzerland, was refined by Wuensch, Takéuchi and Nowacki (1966a). Analyses of the specimen gave the formulae -

by microprobe - $Cu_{9.54}Zn_{1.18}Fe_{0.69}As_{3.97}S_{15.09}$

$(Cu_{8.22}Zn_{1.02}Fe_{0.59}As_{3.42}S_{13})$

by spectroscope - $Cu_{11.30}Zn_{1.29}Ag_{0.26}As_{2.90}Sb_{0.44}S_{12.08}$

$(Cu_{12.16}Zn_{1.39}Ag_{0.28}As_{3.12}Sb_{0.47}S_{13})$

by Prior and Spencer (1899) - $Cu_{11.69}Fe_{0.30}Ag_{0.26}Pb_{0.01}As_{3.79}S_{12.83}$

$(Cu_{11.85}Fe_{0.30}Ag_{0.26}Pb_{0.01}As_{3.84}S_{13})$

by Prior (1916) - $Cu_{9.84}Zn_{1.77}Fe_{0.17}Ag_{0.17}As_{3.93}S_{13.02}$

$(Cu_{9.82}Zn_{1.77}Fe_{0.17}Ag_{0.17}As_{3.92}S_{13})$

The analyses of Prior and Spencer and Prior were considered to be the most accurate. The semi-metal site occupancy was given as $As_{0.87}Sb_{0.13}$. The cell edge was calculated as 10.232±.005Å.

Wuensch et al. (1966b) noted that tetrahedrite and binnite are isostructural and have a curious superstructure based on a distorted sphalerite-like arrangement of atoms but the nature of the distortions differ in the two struc-

tures. This may be explained in terms of a slightly different mode of sulphur packing.

Sakharova (1966) examined tetrahedrite-tennantite ores and derived the general formula $R^{+}_{n}R^{++}_{m}((SbAs)_{b}S_{3b})S_{2}$. X-ray diffraction analysis indicated that the size of the unit cell edge depends on the atomic ratio Sb:As and may serve as a criterion in determining the ratios of these elements in the formula.

Trdlička (1967) in a mineralogical study of four tetrahedrites from Fichtenhübel, Slovakia, noted Zn = 1.15 - 4.69% and Fe = 3.62 - 7.14%. Cell edges ranged from 10.370 to 10.402Å.

Boyle (1968) noted that the following substitutions may take place in tetrahedrite -

for Cu : Fe, Mn,Zn,Cd,Ag,Au,Hg,Pb,Ni,Co,Ge,Ba,Sn,V,In

for Sb : As,Bi

for S : Se,Te

With the exception of Hg no apparent relationship between the content of silver and the various substituting elements in tetrahedrite-tennantite was noted. Argentian tetrahedrites are low in Hg and mercurian tetrahedrites are low in Ag. The differences in covalent radii, Ag(1.53Å), Cu(1.35Å) and atomic radii, Ag(1.40Å), Cu(1.24Å), of copper and silver were regarded as being significant yet it was noted that substitution by Ag of Cu in tetrahedrite-tennantite up to 25% had been reported by Staples and Warren (1946).

Microprobe analysis of tetrahedrites from various localities are given by Springer (1969). The general formula $(CuAg)_{2.50}(FeZn)_{0.50}(AsSbBiTe)S_{3.25}$ was established. A practically complete interchange of Sb and As was noted.

In some specimens the ratio Sb:As varied but the sum of the at% Sb and at% As remained the same. Springer also noted that pure $Cu_3AsS_{3.25}$ is rare, the divalent cation normally being represented by Zn and Fe rather than Cu.

Nowacki (1969) in a structural classification of sulphosalts grouped tetrahedrite ($(SbS_3)_4$ S $Cu_6^{III}Cu_6^{IV}$) and binnite ($(AsS_3)_4$ S $Cu_6^{III}Cu_6^{IV}$). The superscript is co-ordination number.

Yui (1970), using the electron microprobe, analysed tetrahedrite-tennantites from various localities in Japan. The general formula $(CuAg)_{10}(ZnFe)_2(AsSb)_4S_{13}$ was accepted. Single grains of tetrahedrite-tennantite were observed to be inhomogenous with three or more distinct 'phases' with different Sb, As and Ag contents. Tetrahedrites, with the Zn:Fe ratio varying zonally, were observed.

Discussion of Substitution in Natural Tetrahedrites

In this section relationships between elements in natural tetrahedrites are described. The main features found are listed at the end of this section.

In this section and throughout the text the basic formula of tetrahedrite - $Cu_{12}Sb_4S_{13}$ has been used. There are four reasons for using this formula -

(a) The 12:4:13 ratio has been established by recent microprobe analyses of natural tetrahedrites (Springer 1969) and microprobe analyses of synthetic tetrahedrites (this study).

(b) The atomic proportions are represented as small whole numbers.

(c) This formula has become established in the literature.

(d) Wuensch (1964) determined a possible structure of tetrahedrite with the unit cell formula - $^{2}(Cu_{12}Sb_{4}S_{13})$.

The term 'stoichiometric' is used in the text when discussing tetrahedrite and is taken to mean a constancy in the ratio metal:semi-metal:non-metal = 12:4:13. The ratios of metals (e.g. Cu:Zn:Ag) or semi-metals (e.g. Sb:As) in the structure may vary due to substitution but tetrahedrite remains stoichiometric if the metal:semi-metal:non-metal ratio is maintained.

In substituted tetrahedrites each structural site may contain more than one element and one particular element may enter more than one site. The substitution of a particular element into the structure may depend on an external phenomenon - such as temperature, or an internal phenomenon - such as the presence of a certain element. Thus, the variation in element content of substituted tetrahedrites may be the result of a number of different factors. 'Factor Analysis' can resolve the intercorrelations within a set of variables. Analysis of variance, however, depends on the independent variation of groups of variables (elements in this case). In the case of substitution in tetrahedrite, the variations of all the elements are interrelated and Factor Analysis proved to contribute little to understanding the relationships between substituting elements. Only correlations between elements and groups of certain elements will therefore be discussed.

Analyses of a number of tetrahedrites (69) were obtained from Dana (1944) and Springer (1969) (Tables 1-1 and 1-3). The older analyses are less reliable because of the probability

of impurity inclusions - some analyses in Dana involving corrections due to the presence of gangue. All analyses were converted to atomic % (Tables 3-2 and 3-4) since the weight % of a non-varying element in the structure will change as the ratio of a substituting pair of elements change.

The correlation matrix for major elements found in tetrahedrite is given in Table 1-5. The summary statistics permit the recognition of elements of high variance (greater than 5), which represent the major substituting elements, and elements of low variance (less than 5), which represent elements not involved in substitutions or elements which only occur in a few tetrahedrites.

Sulphur has a low variance indicating a lack of substitution and suggesting a constancy in the general formula of natural tetrahedrites. A C_o-Bi-S association can, however, be recognised. The two possible interpretations are that Co,Bi-tetrahedrites are non-stoichiometric with high S contents or that the particular tetrahedrites analysed contained a Co-Bi-S phase as an impurity.

Correlations between low variance elements and high variance elements are suspect since the correlations need not represent associated variances. In the case of Pb, for example, there are only a few tetrahedrites with Pb. The content of Cu in these tetrahedrites is quite variable and dependent mainly on the extent of major substitutions. The correlation coefficient between Cu and Pb, therefore, has little significance as an indicator of Cu-Pb substitution.

Correlations between high variance elements are compiled in Table 1-6. Sb v As gives the strongest -ve correlation and indicates extensive Sb-As substitution. This strong correlation results in opposed secondary correlations, X v Sb

and X v As, where X is varying due to substitution by another element. Secondary correlations are ringed in Table 1-6. Secondary correlations indicate more extensive Ag, Fe and Zn substitution for Cu in Sb rich natural tetrahedrites. This could well be a sampling phenomenon, i.e. more analyses of Sb rich tetrahedrites are available.

The low correlation coefficients in Table 1-6 are because of variations in an element due to substitution by elements other than the major substituting element. The significant (significance level greater than 99% (Davies 1957))'- ve' correlations (corr. coeff. 0.40 or greater) are Sb v As, Zn v Fe and Cu v Fe.

From the sum of the means of the analyses of each element (Table 1-5) the general formula of natural tetrahedrite, $(CuAgFeZn)_{12}(SbAs)_4S_{13}$, can be derived (only the major substituting elements are included). From the correlation coefficient matrix (Table 1-6) zinc and iron compete for Cu sites (Zn v Fe, corr. coeff. = -0.55). The maximum zinc and maximum iron contents do not exceed 6.90 at% in the case of analyses from Springer (1969) and only five analyses from Dana (1944) exceed this total. In Table 1-5 the lack of -ve correlation of Ag with other substituting cations indicates that Ag is not competing for Fe,Zn type sites. This is also apparent from the increase in correlation from Cu v Zn+Fe+Hg to Cu+Ag v Zn+Fe+Hg (Table 1-5).

These points are emphasised by stating the general formula of tetrahedrite as - $(CuAg)_{10}(ZnFeCu)_2(SbAs)_4S_{13}$. This formula is valid for the majority of the analyses.

In Fig.1-1 the ratio of Sb:As observed in natural tetrahedrites is shown. Miscibility gaps, suggested by Kostov (1957), are not obvious but the greater range of

Sb:As ratio in Sb rich members than in As rich members is apparent. This may be due to the limited number of analyses available.

In Fig.1-2 the Cu:Fe+Zn+Hg:Ag ratios of the natural substituted tetrahedrites have been plotted. Only five of the eight cations (metals) analysed for are represented in this diagram. A spread in the distribution of points (i.e. low Cu values) is therefore to be expected. The distribution of points in this diagram is interpreted as being due to substitution of Cu by divalent cations corresponding to the general formula $Cu_{10}(ZnFeHg)_2(SbAs)_4S_{13}$. Note that silver in tetrahedrite is associated with the Cu:Zn+Fe+Hg ratio of 5:1 there being a spread of values about the dashed line representing this ratio in Fig.1-2.

Summary of Main Features of Natural Tetrahedrites

(1) Extensive substitution is evident in tetrahedrite. The main substituting elements are: As for Sb; and Zn, Fe and Ag for Cu. Special varieties of tetrahedrite are rich in Hg or Bi.

(2) Substitution of Sb by As between the two end-members, tetrahedrite and tennantite, is incomplete and the possibility of one (or two) miscibility gaps remains.

(3) Substitution of Cu by Zn and Fe corresponds to the formula $Cu_{10}(ZnFe)_2Sb_4S_{13}$ and this may represent the limit of substitution of Zn and Fe in tetrahedrite.

(4) Substitution of Cu by Ag takes place mainly in divalent cation rich tetrahedrites there being an association of Ag content with the Cu:Zn+Fe+Hg ratio of 5:1. A definite saturation value is not evident for Ag.

It is difficult coming to definite conclusions on the extent and limits of substitution possible in tetrahedrite from a study of natural tetrahedrites. This is because of the wide range in substituting elements present, the uncertainty of the validity of chemical analysis of macroscopic specimens and the possibly limited range in compositions available in natural occurrences. The value in studying synthetic minerals is that these problems do not arise.

Experimental work was therefore undertaken to contribute to the understanding of substitution in natural tetrahedrites and to establish relationships between composition and mineralogical properties of substituted tetrahedrites. The features listed above were used as a guide.

TABLE 1-1 Analyses of tetrahedrites from Dana (1944) (wt%)

Spec. No.	Cu	Fe	Zn	Ag	Hg	Pb	Ni	Co	Bi	Sb	As	S	Date
2	45.39	1.32	-	-	-	0.11	-	-	-	28.85	-	24.48	1899
3	41.55	1.02	2.63	-	-	0.62	-	-	0.83	28.32	-	24.33	1899
4	37.75	1.10	6.51	0.11	-	0.71	-	-	0.53	28.66	-	24.61	1911
5	37.70	5.13	3.87	-	-	-	-	-	-	26.81	-	26.49	1926
6	37.42	6.60	1.72	-	-	-	0.23	-	-	29.28	-	25.70	1906
7	37.22	0.86	6.59	1.51	-	0.33	-	-	-	26.61	0.38	25.16	1900
8	38.95	4.77	2.21	0.02	-	-	-	-	-	27.00	1.40	25.66	1911
9	39.16	2.00	4.87	-	-	-	-	0.23	-	25.71	1.68	24.48	1909
10	37.93	0.60	7.57	0.45	-	-	-	-	-	26.12	1.84	25.21	1911
11	38.59	1.05	6.16	0.68	-	-	-	-	-	24.98	2.25	25.35	1911
12	38.52	0.94	7.05	0.08	-	-	-	-	-	25.26	2.69	25.22	1911
13	36.10	0.78	6.44	1.51	-	2.72	-	-	-	24.00	2.75	24.99	1911
14	40.57	4.53	1.61	0.03	1.52	-	-	-	-	20.60	5.07	25.21	1911
15	37.87	0.95	7.58	1.49	-	-	-	-	-	21.30	5.54	25.66	1910
16	38.15	3.77	5.05	-	-	0.53	-	-	1.63	17.47	6.75	25.58	1906
17	40.91	2.57	4.85	0.23	0.80	-	-	-	-	15.77	9.03	26.34	1911
18	42.35	4.31	1.48	0.09	-	-	-	-	-	14.51	10.24	26.38	1911
19	33.39	4.64	3.53	4.86	-	-	-	-	0.34	25.22	1.46	25.74	1926
20	34.15	3.79	4.86	5.94	-	-	-	-	-	25.24	1.21	25.22	1906
21	22.14	0.93	6.22	11.20	-	9.38	-	-	-	28.22	0.23	21.68	1895
22	29.99	3.29	2.49	12.74	-	0.25	-	-	-	26.42	0.58	23.71	1911
23	30.56	3.51	-	15.26	-	0.05	-	-	-	27.73	-	23.15	1899

TABLE 1-1 (Contd.)

Spec. No.	Cu	Fe	Zn	Ag	Hg	Pb	Ni	Co	Bi	Sb	As	S	Date
24	25.23	3.72	3.10	17.71	-	0.05	-	-	-	26.63	-	23.52	1829
25	32.76	1.46	0.38	1.51	13.71	-	-	-	-	27.90	0.84	20.60	1902
26	32.19	1.41	0.10	-	17.32	-	-	0.23	1.57	23.45	0.31	21.90	1865
27	33.30	2.66	5.32	1.70	0.75	0.83	2.49	-	-	23.44	4.48	23.83	1911
28	30.04	9.83	0.59	-	-	0.26	3.46	-	-	28.82	1.50	24.48	1906
29	33.83	6.40	-	1.37	-	-	-	4.21	4.55	4.72	6.98	26.40	1865
30	30.10	13.08	-	-	-	-	-	-	-	29.61	-	27.01	1873
31	35.64	0.80	8.19	0.18	2.67	-	-	-	-	28.07	-	24.74	1854
32	35.72	6.51	-	0.04	-	-	-	1.20	13.07	2.19	11.44	29.10	1870
33	35.72	0.42	6.90	13.65	-	0.86	-	-	-	0.13	17.18	25.04	1892
34	42.22	10.90	0.63	-	-	-	-	-	-	-	13.34	29.09	1936
35	42.05	1.48	6.09	0.04	-	-	-	-	-	10.87	12.57	27.12	1911
36	43.40	0.10	9.26	0.06	-	0.15	-	-	-	4.35	18.80	23.00	1920
37	44.50	0.62	7.28	0.02	-	0.35	-	-	-	-	18.76	27.58	1924
38	42.03	0.62	7.76	1.24	-	-	-	-	-	-	19.80	28.08	1916
39	42.15	5.44	2.62	1.31	-	-	-	-	-	4.66	16.68	27.61	1911
40	48.50	2.77	-	0.23	-	-	-	-	-	2.44	18.82	27.04	1911
41	44.12	3.68	-	4.77	-	-	-	-	-	-	20.49	26.94	1899
42	49.83	1.11	-	1.87	-	0.17	-	-	-	-	19.04	27.60	1899
43	53.24	1.58	0.23	-	-	-	-	-	-	-	18.29	26.54	1911

TABLE 1-2 Analyses of tetrahedrites from Dana (1944) (at%)

Spec. No.	Cu	Fe	Zn	Ag	Hg	Pb	Ni	Co	Bi	Sb	As	S
2	41.08	1.36	-	-	-	0.03	-	-	-	13.63	-	43.90
3	38.23	1.07	2.35	-	-	0.18	-	-	0.23	13.60	-	44.35
4	34.48	1.14	5.78	0.06	-	0.20	-	-	0.15	13.66	-	44.54
5	33.13	5.13	3.31	-	-	-	-	-	-	12.30	-	46.13
6	33.10	6.64	1.48	-	-	-	0.22	-	-	13.52	-	45.05
7	33.96	0.83	5.84	0.81	-	0.09	-	-	-	12.67	0.29	45.49
8	34.57	4.82	1.91	0.01	-	-	-	-	-	12.51	1.05	45.13
9	35.68	2.07	4.31	-	-	-	-	0.23	-	12.22	1.30	44.19
10	34.05	0.61	6.61	0.24	-	-	-	-	-	12.24	1.40	44.85
11	34.66	1.07	5.38	0.36	-	-	-	-	-	11.71	1.71	45.11
12	34.42	0.96	6.12	0.04	-	-	-	-	-	11.78	2.04	44.65
13	33.02	0.81	5.72	0.81	-	0.76	-	-	-	11.45	2.13	45.29
14	35.97	4.57	1.38	0.02	0.43	-	-	-	-	9.53	3.81	44.29
15	33.26	0.95	6.47	0.77	-	-	-	-	-	9.76	4.13	44.66
16	33.60	3.78	4.32	-	-	0.14	-	-	-	8.03	5.04	44.65
17	34.96	2.50	4.03	0.12	0.22	-	-	-	-	7.03	6.55	44.60
18	36.11	4.18	1.23	0.05	-	-	-	-	-	6.46	7.41	44.57
19	30.23	4.78	3.11	2.59	-	-	-	-	0.09	11.91	1.12	46.17
20	30.81	3.89	4.26	3.16	-	-	-	-	-	11.88	0.93	45.08
21	22.92	1.10	6.26	6.83	-	2.98	-	-	-	15.25	0.20	44.47
22	28.56	3.57	2.31	7.15	-	0.07	-	-	-	13.13	0.47	44.75

TABLE 1-2 (Contd.)

Spec. No.	Cu	Fe	Zn	Ag	Hg	Pb	Ni	Co	Bi	Sb	As	S
23	29.41	3.84	-	8.65	-	0.02	-	-	-	13.93	-	44.15
24	24.40	4.09	2.91	10.09	-	-	-	-	-	13.44	-	45.07
25	34.08	1.73	0.38	0.93	4.52	-	-	-	-	15.15	0.74	42.47
26	33.53	1.67	0.10	-	5.72	-	-	0.26	0.50	12.75	0.27	45.20
27	30.57	2.78	4.75	0.92	0.22	0.23	2.47	-	-	11.23	3.49	43.35
28	27.20	10.13	0.52	-	-	0.07	3.39	-	-	13.62	1.15	43.92
29	31.17	6.71	-	0.74	-	-	-	4.18	1.27	2.27	5.46	48.20
30	26.41	13.06	-	-	-	-	-	-	-	13.56	-	46.97
31	32.66	0.83	7.29	0.10	0.78	-	-	-	-	13.42	-	44.92
32	30.55	6.33	-	0.02	-	-	-	1.10	3.40	0.98	8.30	49.33
33	30.94	0.41	5.81	6.96	-	0.23	-	-	-	0.06	12.62	42.97
34	34.00	9.99	0.49	-	-	-	-	-	-	-	9.11	46.42
35	35.12	1.41	4.94	0.02	-	-	-	-	-	4.74	8.90	44.88
36	37.28	0.09	7.74	0.03	-	0.04	-	-	-	1.94	13.70	39.19
37	36.19	0.57	5.75	0.01	-	0.09	-	-	-	-	12.94	44.45
38	34.05	0.57	6.11	0.59	-	-	-	-	-	-	13.61	45.07
39	34.28	5.03	2.07	0.63	-	-	-	-	-	1.98	11.51	44.50
40	39.56	2.57	-	0.11	-	-	-	-	-	1.04	13.02	43.70
41	36.20	3.44	-	2.31	-	-	-	-	-	-	14.26	43.80
42	40.48	1.03	-	0.90	-	0.04	-	-	-	-	13.12	44.43
43	43.16	1.46	0.18	-	-	-	-	-	-	-	12.58	42.63

TABLE 1-3 Analyses of tetrahedrites from Springer (1969) (wt%)

Spec. No.	Cu	Fe	Zn	Ag	Hg	Bi	Sb	As	S
1	38.10	-	7.40	-	-	-	28.80	-	25.20
2	37.90	0.70	6.80	-	-	-	28.90	-	24.90
3	38.80	2.50	5.20	-	-	-	21.30	5.60	26.00
4	37.10	3.30	4.00	1.00	-	-	28.90	0.30	25.50
5	37.80	3.00	4.40	-	-	-	25.00	2.40	25.60
6	42.30	5.60	1.90	-	-	-	2.20	18.90	28.50
7	42.70	0.10	8.50	-	-	-	0.50	19.80	28.50
8	37.90	1.90	5.50	1.20	-	-	27.30	1.50	25.20
9	29.80	0.60	6.50	11.00	-	-	28.00	-	24.30
10	30.50	5.10	1.70	10.90	-	-	28.40	-	24.60
11	33.70	5.80	0.80	5.40	-	-	26.90	1.20	24.90
12	36.30	5.00	2.10	2.70	-	-	27.70	1.00	24.90
13	43.20	7.00	-	-	-	-	2.60	18.40	28.40
14	41.70	-	8.30	-	-	-	3.30	18.10	27.70
15	39.00	0.70	7,30	1.10	-	-	19.60	6.80	26.70
16	50.70	-	-	-	-	-	1.20	19.30	28.20
17	51.20	-	-	-	-	-	1.20	19.30	28.20
18	44.80	3.70	-	-	-	-	10.00	13.50	27.50
19	50.30	0.40	-	-	-	-	1.30	19.40	28.40
20	44.30	6.20	-	-	-	-	-	20.20	27.70
21	42.90	0.20	8.10	-	-	-	0.80	19.70	28.20
31	37.40	2.70	1.40	-	9.60	-	18.50	6.50	24.70
32	39.30	3.40	2.80	-	3.00	-	17.80	7.70	26.20
33	39.30	4.40	-	-	4.20	-	21.90	4.40	25.20
34	39.40	2.80	1.30	-	4.80	-	21.70	4.60	25.30
41	39.20	6.10	0.80	-	-	12.50	1.80	12.90	25.10
42	38.90	2.50	4.80	-	-	15.90	2.10	12.00	26.30

TABLE 1-4 Analyses of tetrahedrites from Springer (1969) (At%)

Spec. No.	Cu	Fe	Zn	Ag	Hg	Bi	Sb	As	S
1	34.56	-	6.52	-	-	-	13.63	-	45.29
2	34.54	0.73	6.02	-	-	-	13.74	-	44.97
3	34.01	2.49	4.43	-	-	-	9.74	4.16	45.16
4	33.37	3.38	3.50	0.53	-	-	13.56	0.23	45.44
5	33.96	3.07	3.84	-	-	-	11.72	1.83	45.58
6	34.07	5.13	1.49	-	-	-	0.93	12.91	45.48
7	34.27	0.09	6.63	-	-	-	0.21	13.48	45.32
8	33.97	1.94	4.79	0.63	-	-	12.77	1.14	44.76
9	28.10	0.64	5.96	6.11	-	-	13.78	-	45.41
10	28.26	5.38	1.53	5.95	-	-	13.73	-	45.16
11	31.02	6.07	0.72	2.93	-	-	12.92	0.94	45.41
12	32.92	5.16	1.85	1.44	-	-	13.11	0.77	44.75
13	34.73	6.40	-	-	-	-	1.09	12.55	45.24
14	34.26	-	6.63	-	-	-	1.42	12.61	45.09
15	33.49	0.68	6.09	0.56	-	-	8.78	4.95	45.44
16	41.03	-	-	-	-	-	0.51	13.25	45.22
17	41.27	-	-	-	-	-	0.51	13.19	45.04
18	37.28	3.50	-	-	-	-	4.34	9.53	45.35
19	40.51	0.37	-	-	-	-	0.55	13.25	45.32
20	35.91	5.72	-	-	-	-	-	13.89	44.49
21	34.60	0.18	6.35	-	-	-	0.34	13.48	45.06
31	34.32	2.82	1.25	-	2.79	-	8.86	5.06	44.91
32	34.30	3.38	2.38	-	0.83	-	8.11	5.70	45.31
33	35.49	4.52	-	-	1.20	-	10.32	3.37	45.10
34	35.58	2.88	1.14	-	1.37	-	10.23	3.52	45.28
41	34.90	6.18	0.69	-	-	3.38	0.84	9.74	44.28
42	33.94	2.48	4.07	-	-	4.22	0.96	8.88	45.46

TABLE 1-5

Natural Substituted Tetrahedrites - Correlation Coefficient Matrix

Analyses from Dana (1944) and Springer (1969). Raw Data in Atomic %.

	Cu	Fe	Zn	Ag	Hg	Pb	Ni	Co	Bi	Sb	As	S	Fe+Zn+Hg
Cu	-1.00												-0.74
Fe	-0.40	1.00											
Zn	-0.22	-0.57	1.00										
Ag	-0.63	0.01	0.04	1.00									
Hg	0.01	-0.08	-0.22	-0.10	1.00								
Pb	-0.37	-0.13	0.21	0.31	-0.05	1.00							
Ni	-0.25	0.27	-0.05	-0.05	-0.03	0.03	1.00						
Co	-0.12	0.20	-0.18	-0.04	-0.00	0.03	-0.03	1.00					
Bi	-0.06	0.17	-0.13	-0.11	-0.02	-0,05	-0.05	-0.30	1.00				
Sb	-0.48	0.07	0.18	0.27	0.20	0.18	0.15	-0.15	-0.27	1.00			0.34
As	0.52	-0.16	-0.14	-0.26	-0.18	-0.14	-0.11	0.01	0.12	-0.97	1.00		
S	-0.28	0.37	-0.18	-0.08	-0.11	-0.06	-0.17	0.43	0.31	0.02	-0.17	1.00	
Cu+Ag													-0.90

TABLE 1-5 (Contd.)

Summary Statistics At%

	Cu	Fe	Zn	Ag	Hg	Pb	Ni	Co	Bi	Sb	As	S
Var.	13.70	6.97	6.42	5.16	0.89	0.14	0.25	0.27	0.58	31.19	27.96	1.49
Max.	43.16	13.06	7.74	10.09	5.72	2.98	3.39	4.18	4.22	15.25	14.26	49.33
Min.	22.92	0.00	0.00	0.00	0.00	0.00	0.00	0.00	0.00	0.00	0.00	39.19
Mean	33.95	3.00	3.00	1.07	0.26	0.07	0.09	0.09	0.20	7.99	5.40	44.88
Sum					41.54					13.59		44.88
(Tetrahedrite $Cu_{12}Sb_4S_{13}$)					(41.37)					(13.79)		(44.82)

TABLE 1-6

Natural Substituted Tetrahedrites

Summary Matrix - High Variance (>5) Elements

	Cu	Fe	Zn	Ag	Sb	As
Cu	1.00					
Fe	-0.40	1.00				
Zn	-0.20	-0.55	1.00			
Ag	-0.65	0.00	0.05	1.00		
Sb	-0.50	0.05	0.20	0.25	1.00	
As	0.50	-0.15	-0.15	-0.25	-0.95	1.00

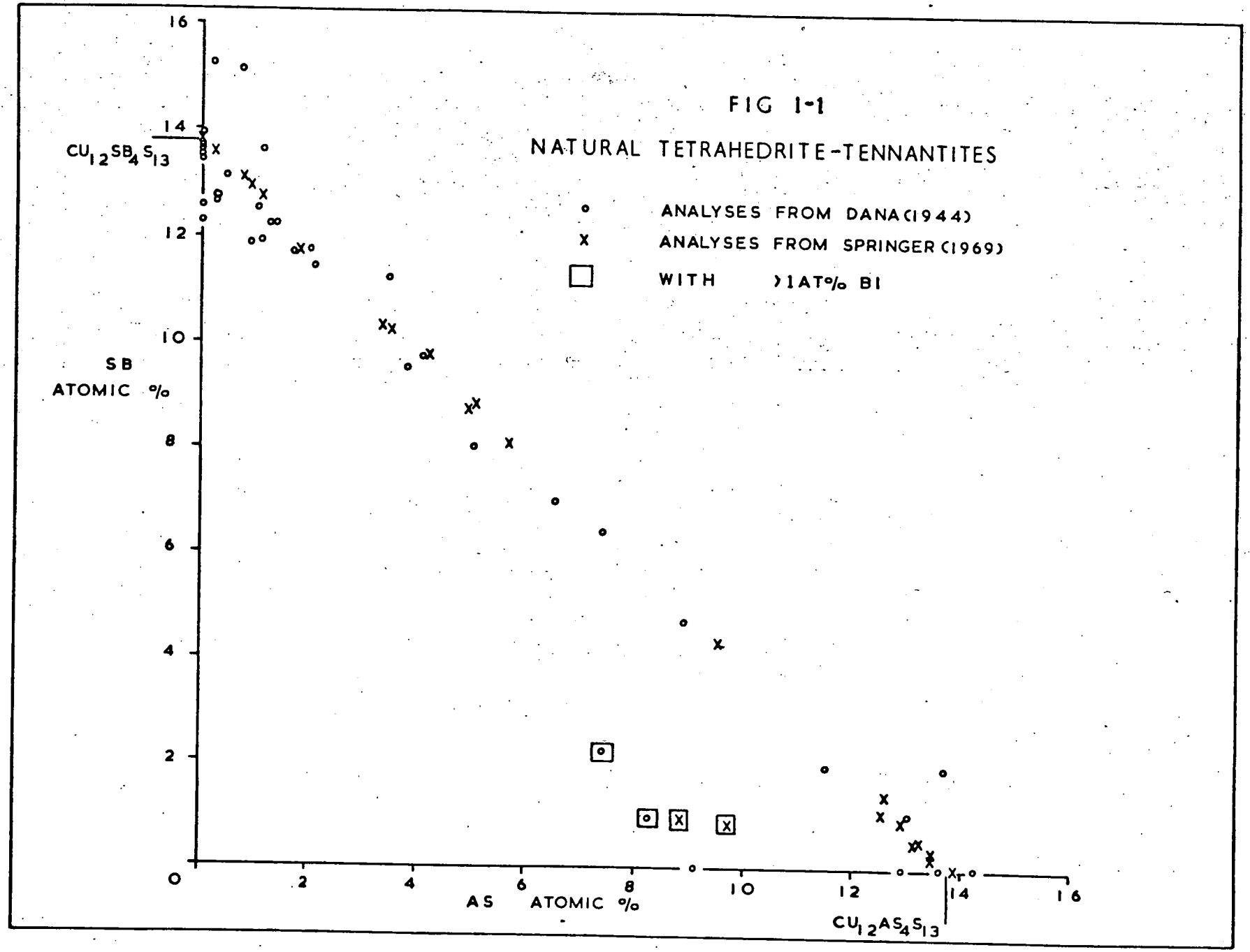
FIG 1-1
NATURAL TETRAHEDRITE-TENNANTITES
ANALYSES FROM DANA (1944)
ANALYSES FROM SPRINGER (1969)
WITH >1AT% BI
$Cu_{12}Sb_4S_{13}$
$Cu_{12}As_4S_{13}$
SB ATOMIC %
AS ATOMIC %
0
2
4
6
8
10
12
14
16

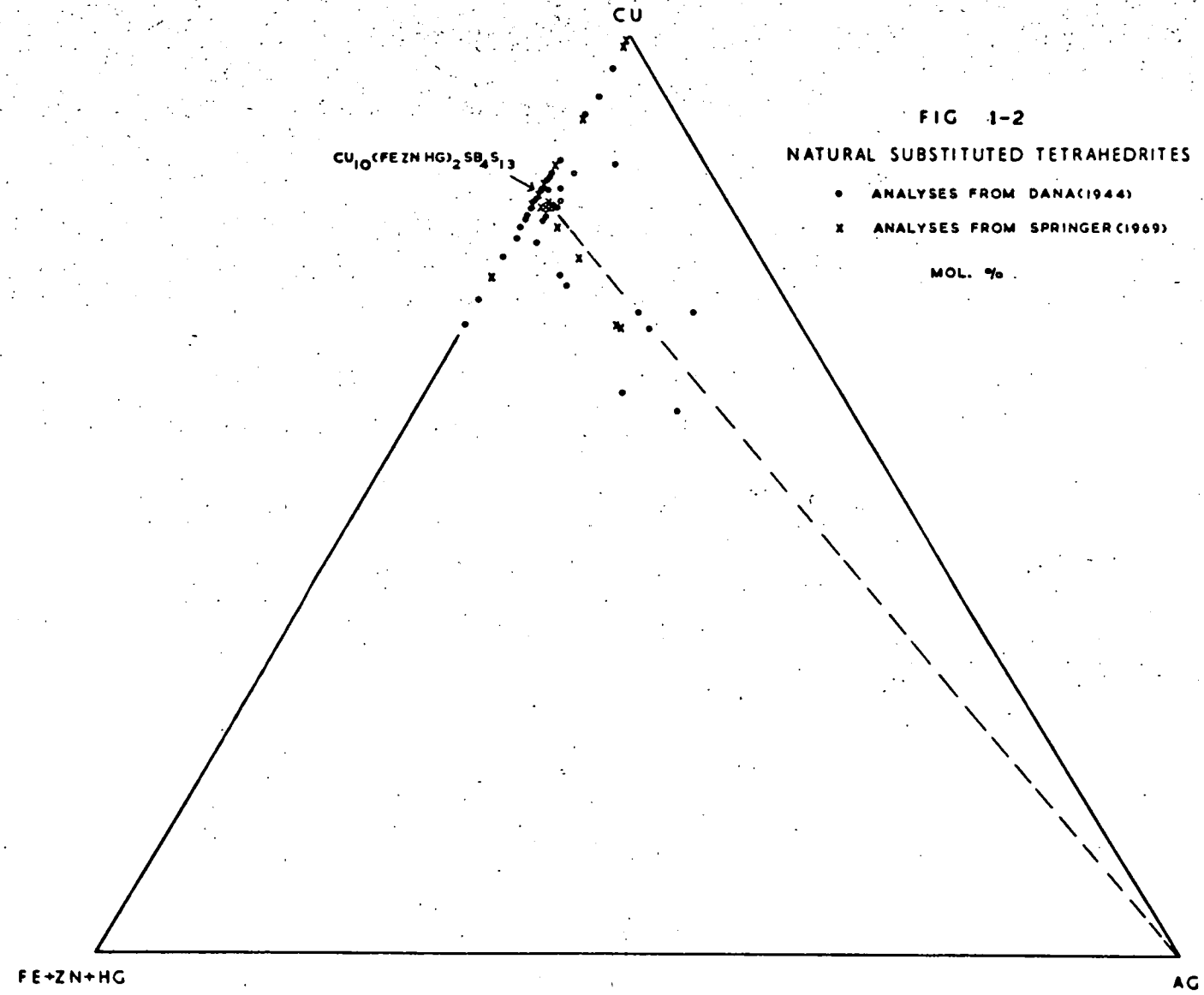

FIG 1-2

NATURAL SUBSTITUTED TETRAHEDRITES

• ANALYSES FROM DANA(1944)

x ANALYSES FROM SPRINGER(1969)

MOL. %

CHAPTER 2

Synthesis and Analysis of Sulphosalts - Description of Apparatus and Procedure

Introduction

When this project was started there was no comprehensive account of the experimental details of the techniques of sulphide synthesis. Dry sulphide synthesis in sealed evacuated silica glass capsules was chosen as the most appropriate technique for a general study of synthetic sulphide mineralogy. The technique described here has developed from a combination of published information and practical experience. An attempt was made to keep the apparatus of general applicability and this has resulted in its limited usefulness in certain aspects of synthetic sulphide research. The determination of sulphide phase equilibrium diagrams, for example, requires a carefully calibrated quench furnace with a minimal temperature range over the length of the specimen. Single crystal growth, on the other hand, requires a furnace with a carefully controlled temperature gradient over the length of the specimen. In quench furnaces the specimen drops rapidly out of the furnace whereas in crystal growth furnaces it is lowered slowly.

The furnace described here is best suited to growing polycrystalline aggregates of sulphide phases, in the temperature range 0-850°C, suitable for general mineralogical studies. Only qualitative, or at best, semi-quantitative conclusions regarding phase relations can be made.

Chemicals Used and Weighing Procedure

The failure rate of early experiments was high. For reasons of economy, therefore, limited purity chemicals were used, high purity chemicals being used once the success of a run could be guaranteed. The chemicals which have been used are listed in Table 2-1. All chemicals were stored in a dessicator. The 99.95% copper powder was reduced in a stream of coal gas immediately before use. The metal rods were filed to a powder immediately before use.

The powders, totalling 1.0g of specimen, were weighed directly into a perspex tube to an accuracy of 0.00005g on a Mettler Single Pan Balance. Three perspex balls were added and the components carefully mixed by hand shaking. Violent automatic shaking was avoided after one specimen exploded. The specimens were stored in a dessicator for short periods of 1 to 24 hours before loading into silica glass capsules. Processing losses were less than 1% and were not significant in this study. Specimen numbers were written on the capsules using a diamond tipped pen.

Silica Glass Capsules

Thin walled, high purity, transparent vitreosil tubing (grade A) of a range in diameters has been used. This was obtained from Thermal Syndicate, Wallsend.

A prepared capsule is shown in Plate 2-1. The silica glass cone, which fitted onto the evacuating equipment, could be reused about twelve times. The join between the capsule and the cone was drawn into a capillary. The long neck of the capsule separated the highly reactive chemicals from the sealing flame. The neck was made narrow in order to minimise the vapour space in the capsule. The capsule

design was preferred to that commonly used where a close fitting silica rod occupies the space above the specimen. Experience showed that the elements could react spontaneously at room temperature if left for more than a few minutes under high vacuum and that the heat of the sealing flame could readily cause reaction. A narrow capillary, as described above, was therefore necessary to facilitate rapid sealing - and this precludes the insertion of a solid rod.

The vapour space above the specimen in the capsule is about 1cc. The sulphur lost to the vapour can be calculated approximately. The vapour pressure of sulphur over pyrrhotite in equilibrium with pyrite at 600°C is approximately 10^{-2}mm Hg (Toulmin and Barton 1964). The vapour pressure over sulphides in the Cu-Sb-S system will be in this order of value. Assuming sulphur behaves as an ideal gas and consists of S_2 molecules, the sulphur loss (m) can be calculated from the formula -

$$m = \frac{P.V.MW}{R.T}$$

where P = pressure in mm Hg

V = volume in cc

MW = molecular weight (64.132)

R = gas constant (62361)

T = temperature °K

At 600°C the sulphur loss will be in the order of 0.01 x 10^{-6}g/cc. This loss is insignificant in this study.

The vapour pressure over pure sulphur at 500°C is 1605mm Hg (West and Menzies 1929). If excess sulphur is present in the specimen a loss of about 0.002g/cc will take place at 500°C. Compositions with excess sulphur have not been used in this study. Unreacted sulphur, however, may on

occasion be present and it is important that the silica glass capsules can withstand the large internal pressure. Silica tubes with a wall thickness of 0.5 to 1 mm. are usually quite capable of withstanding pressures of up to 50 atmospheres. Pressures of this magnitude are only experienced in the most sulphur-rich portions of sulphide systems at temperatures approaching 1000°C. (Naldrett, personal communication).

Vacuum Equipment

The vacuum equipment is shown in Plate 2-2 and Fig.2-1. The rotary vacuum pump was an Edwards, Two Stage Gas Ballast, Rotary High Vacuum Pump (Model ED35), capable of 0.0005 torr (1 torr = 1 mm. Hg). The vacuum was monitored by an Edwards, Pirani Gauge Head (Model G6A) and an Edwards, Pirani Vacuum Gauge (Model B5), over the pressure range 0.5 to 0.001 torr. The vacuum system included a cold trap, situated between the specimen and the Pirani Head and vacuum pump, in order to trap vapours emitted when the specimen reacted during sealing. Silicone grease was applied to all joints and valves.

Sealing Procedure

The pump valve was closed and the specimen valve opened (Fig.2-1). The pump was switched on and left about thirty minutes to warm up. The capsule was attached (Fig.2-1), the pump valve opened very slowly and, as the system was slowly evacuated, the specimen was tapped gently in order to ease the escape of air. Rapid evacuation caused the powder to be drawn out of the capsule. When a suitable vacuum was attained (0.01 - 0.001 torr), the capsule was quickly sealed with an oxygen-gas flame, the capsule being held wrapped in wet asbestos tape. A second person was required in order to close

the specimen valve immediately should anything have gone wrong. The sealing process took about fifteen minutes per capsule.

Furnace

The furnace assembly with furnace tube, temperature controller and temperature recorder is shown in Plate 2-3.

Kanthal wire was wound round and cemented to a fused mullite tube (5 cm. internal diameter and 50 cm. long) giving a resistance of about 40 ohms. This tube was held in a syndanyo box packed with vermiculite (Fig.2-2).

A stainless steel specimen container, attached to a metal rod, was suspended by a wire on a pulley and could be raised or lowered out of the furnace (Plate 2-3 and Fig. 2-2). Stainless steel containers were used because in early experiments the capsules often exploded. Several container designs were tried but that illustrated (Fig.2-3a) has proved the most satisfactory. The specimen holder used in quench runs (Fig.2-3b) was lowered rapidly out of the furnace, the capsules picked out with tweezers, and plunged into cold water.

The central steel support rod enclosed a chromel-alumel thermocouple which was close to the capsules, but protected from them, should they have burst. The specimen temperature was not known accurately but since the specimen - thermocouple distance was constant the temperature difference between different runs could be measured and temperature histories were repeatable. Temperature measurement was not critical for this study. The specimen temperature was continuously monitored by a Kent, Multelec Mark II, single point microvolt recorder. A safety device was built into the

chart recorder so that if the temperature controller had lost control the furnace would have been automatically switched off when a set temperature was reached.

The temperature controller used was a Eurotherm, stepless, indicating controller with thyristor output and thermocouple input (PID/SCR/10A/240v/PA/0-1200°C NiCr/NiAl).

Temperature control was excellent, the specimen temperature not measurably exceeding ± 3°C. variation over several days. The controller was used in two ways; automatically, to maintain the furnace at a set temperature; and manually, to raise or lower the furnace temperature. The manual control permitted temperature change in very small steps. A mechanical device attached to the controller allowing continuous, steady temperature change would have been advantageous. Several positions were tried for the thermocouples. The position shown (Fig.2-2) should give the best control as the delay time from temperature change to controller reaction is minimal. This positioning was a late feature of the furnace and has the disadvantage that the controller temperature reading is much less than that of the recorder. Several thermocouples in circuit, positioned in cavities drilled into the inner alumel furnace tube, would be the ideal arrangement. Other improvements in design which would improve the stability of temperature would be to minimise the internal volume of the furnace and increase the insulation.

Run Histories

The details of each run are given where appropriate in the text. A general requirement was that the furnace temperature was changed slowly in order to avoid damaging the

furnace windings. Specimens were always allowed to react at a low temperature (2-400°C.) for at least twelve hours before being raised to the maximum temperature. This step was necessary to avoid possible detonation of the specimen by rapid reaction.

Opening Capsules

The capsules often burst violently when being opened and, on occasion, would shatter spontaneously when being handled. On removal from the furnace, the capsules were therefore stored immediately in plastic tubes and before opening they were wrapped in cellotape. Using the usual glass-tube cutting technique the sealing end of the capsule was cut off then the specimen section of the capsule split (Plate 2-1). Opening of the capsules took place in a fume cupboard since small amounts of sulphurous vapour were emitted. The usual product was a solid button, vesicular or consisting of welded grains.

TABLE 2-1

Chemicals used in Synthesis

(a)

Low Purity

Element	Material	Purity	Manufacturer
Cu	Copper powder	99.95%	Koch-Light
Sb	antimony powder	98.5%	B.D.H.
As	arsenic trisulphide (lump)	optical grade	Koch-Light
S	sulphur crystals	-	B.D.H.
Zn	zinc sulphide (luminous)	-	B.D.H.

(b)

High Purity

Element	Material	Purity	Manufacturer
Cu	powder	imp = 10 ppm	J. Matthey
	rod	"	"
Sb	powder	99.9999%	Koch-Light
As	powder	99.999%	Koch-Light
S	powder	99.9999%	Koch-Light
Fe	rod	imp = 15 ppm	J. Matthey
Ag	rod	imp = 10 ppm	J. Matthey
Zn	rod	imp = 10 ppm	J. Matthey

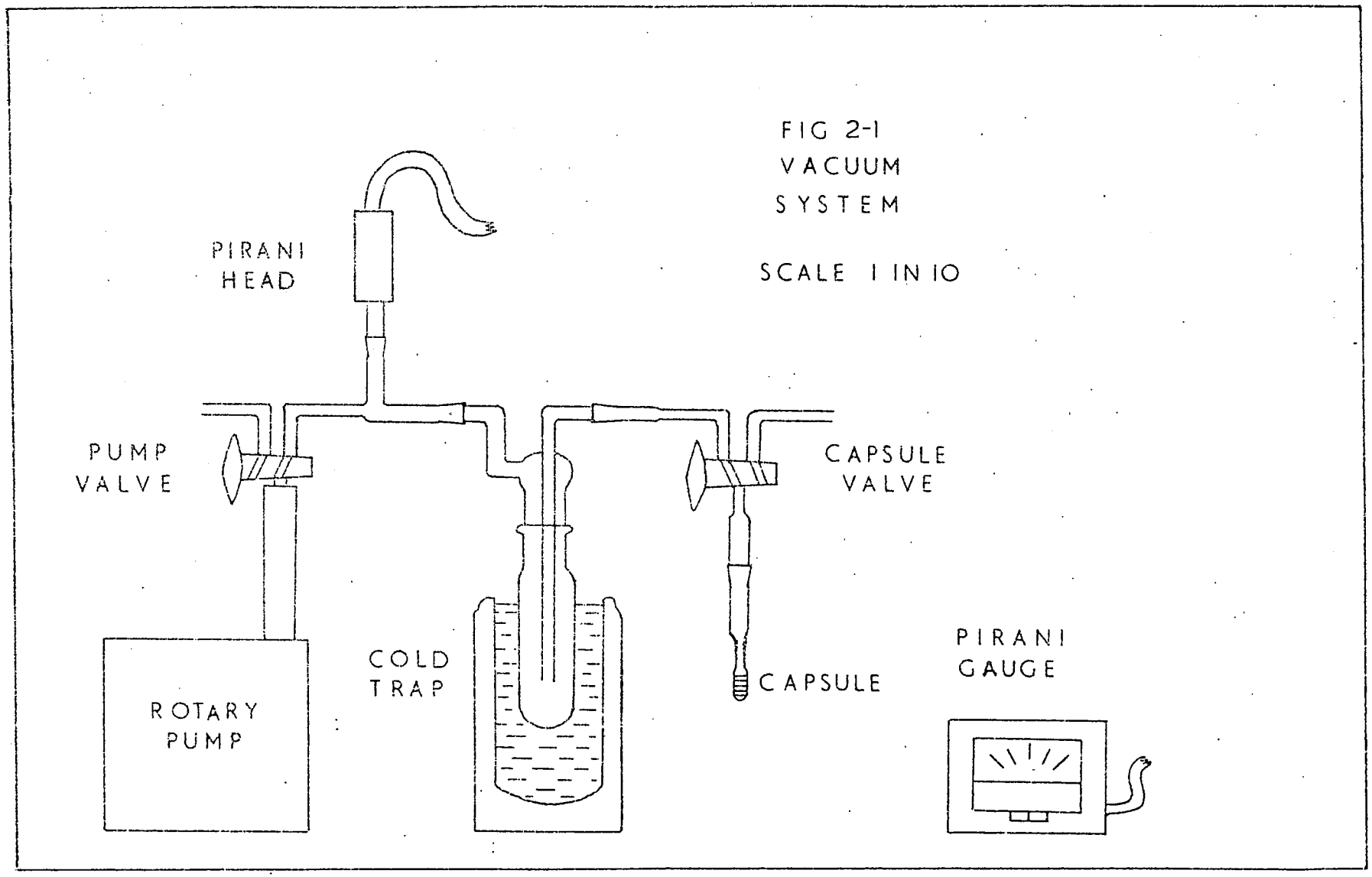
FIG 2-1
VACUUM
SYSTEM
SCALE 1 IN 10
PIRANI
HEAD
PUMP
VALVE
CAPSULE
VALVE
ROTARY
PUMP
COLD
TRAP
CAPSULE
PIRANI
GAUGE

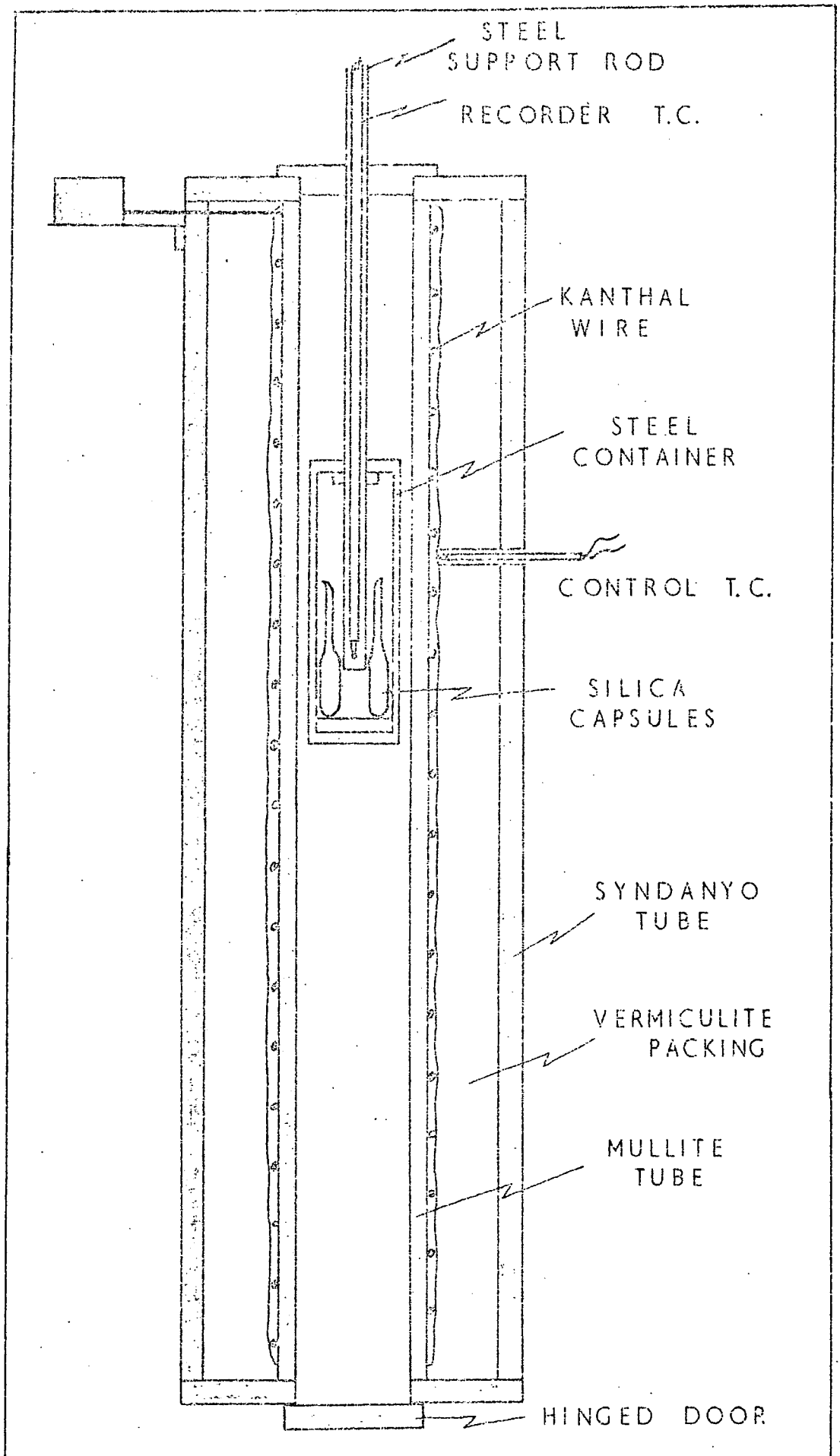

FIG 2-2
VERTICAL RESISTANCE FURNACE
SCALE 1 IN 2.5

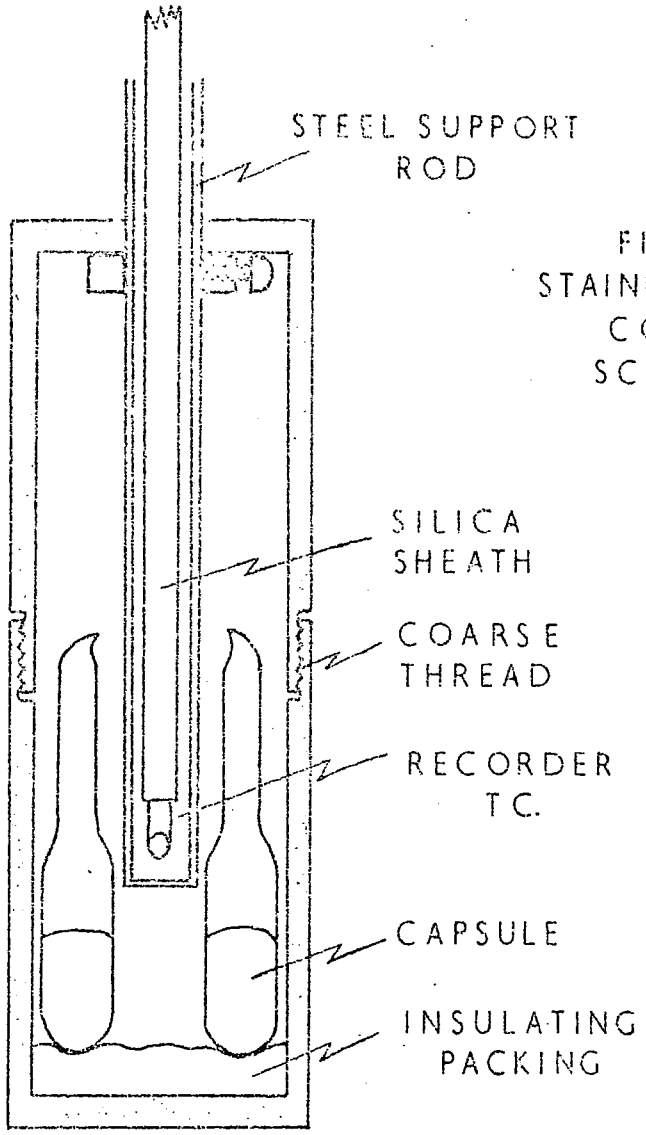

FIG 2-3A
STAINLESS STEEL CONTAINER
SCALE 1 IN 1

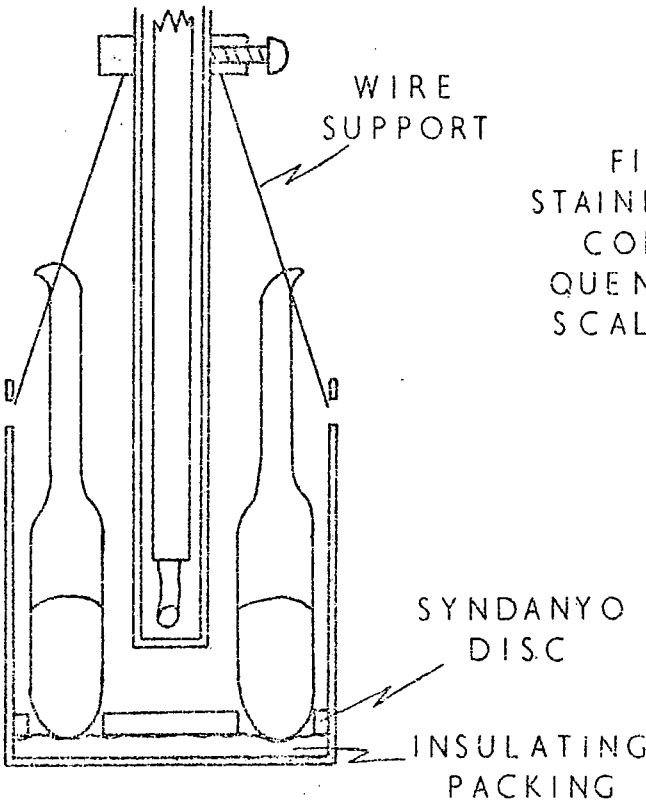

FIG 2-3B
STAINLESS STEEL CONTAINER
QUENCH RUNS
SCALE 1 IN 1

PLATE 2-1

Silica Glass Capsules

Note the capillary joining the capsule to the cone. The long narrow-neck capsules proved successful whereas, when using a simple capsule (centre), the specimen often reacted on sealing.

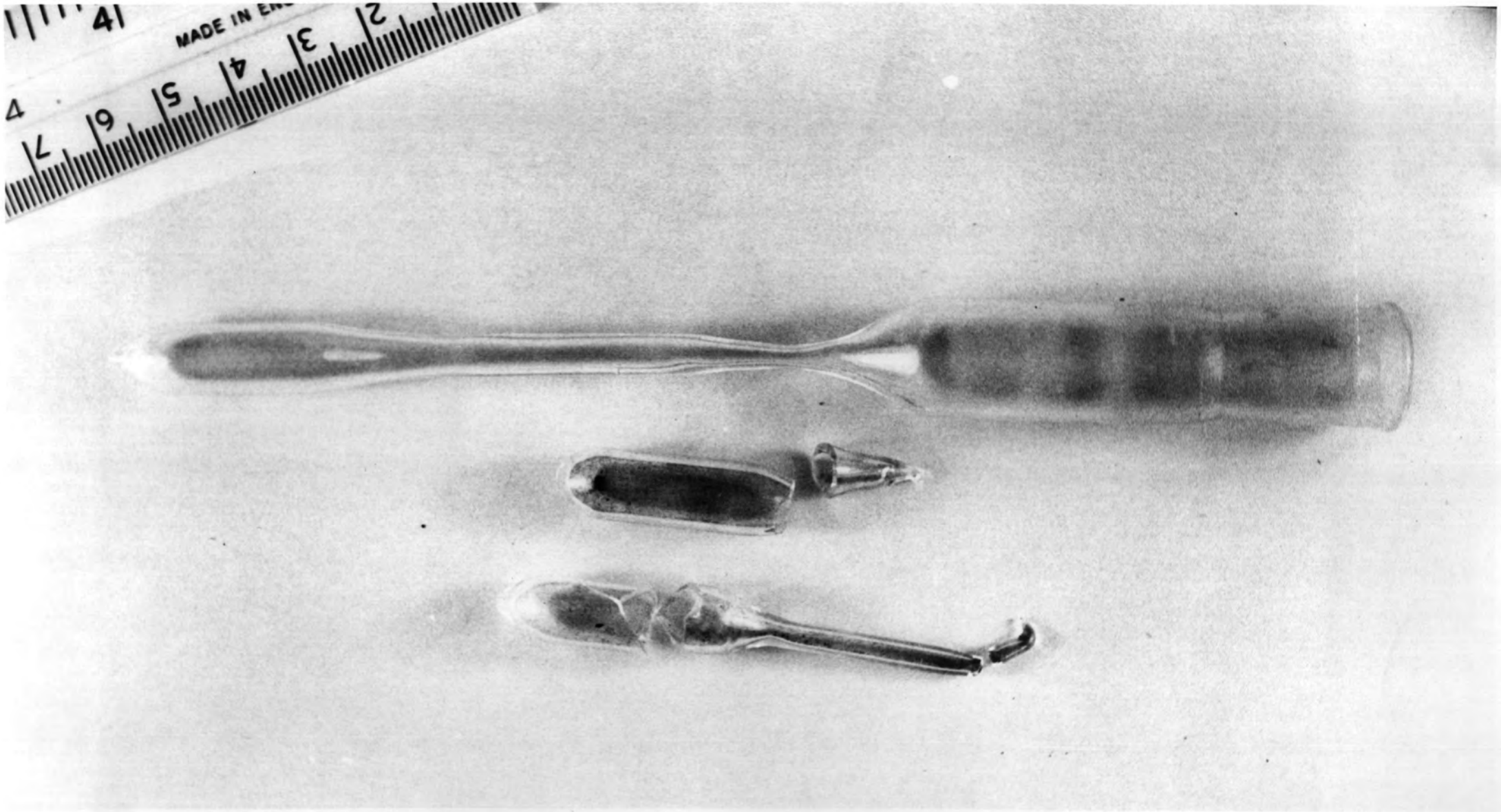
MADE IN

PLATE 2-2

Vacuum Equipment (see Fig.2-1). Note that the Pirani Gauge Head is situated between the Rotary Vacuum Pump and the cold trap.

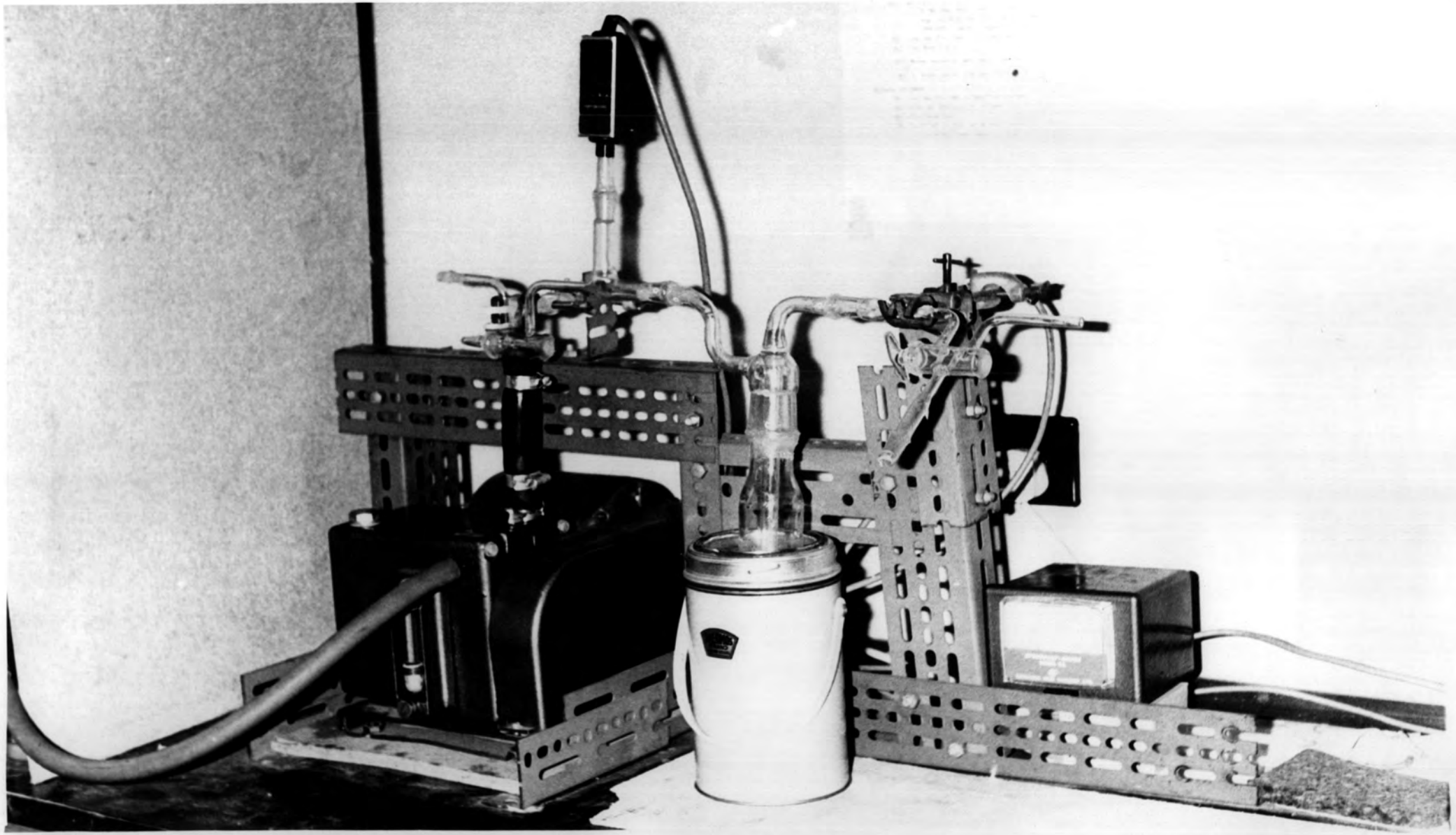

PLATE 2-3

The Furnace Assembly

Specimens are raised into and lowered out of the furnace tube by means of the pulley. The specimen temperature is monitored on the Kent Temperature Recorder, below which is situated the Eurotherm Temperature Controller. The Ammeter, to the left of the Controller, monitors the current supplied to the furnace.

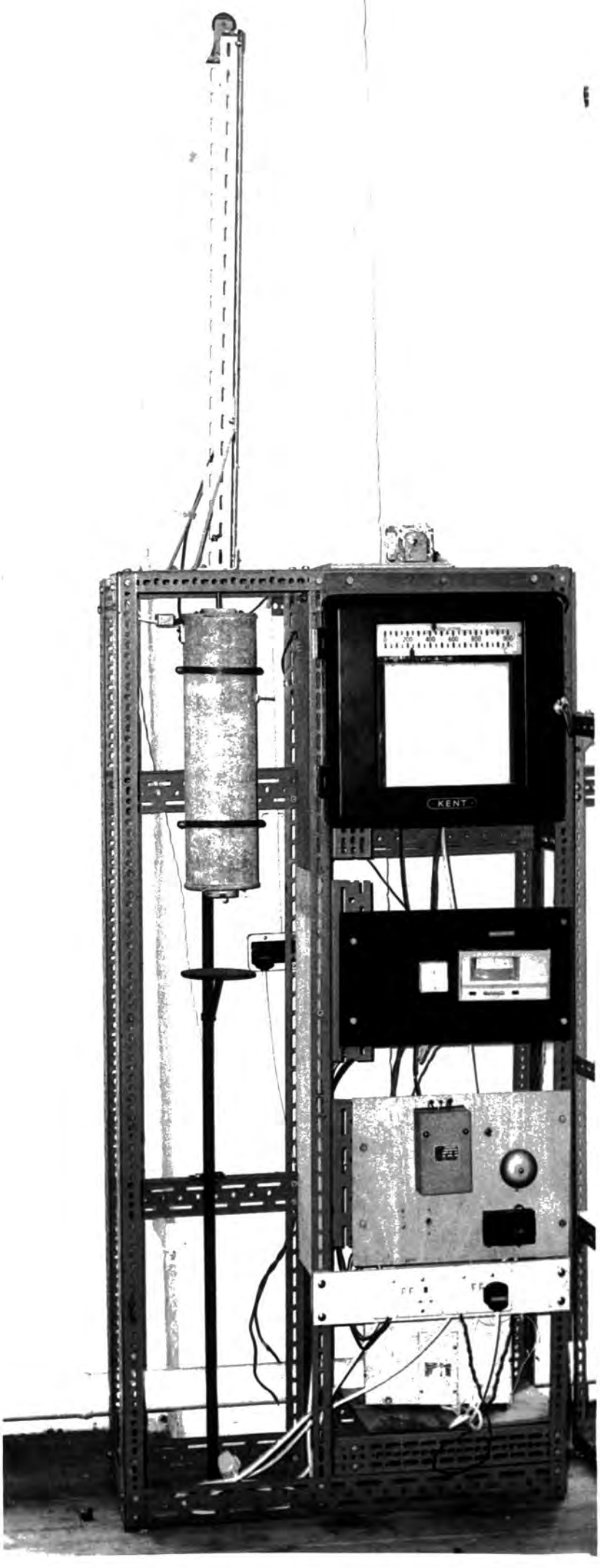
KENT

PLATE 2-4

Specimen Container (see Fig.2-2)

The stainless steel specimen container is attached to a metal rod which is suspended by a wire on a pulley. The thermocouple which monitors the specimen temperature is situated within the metal rod.

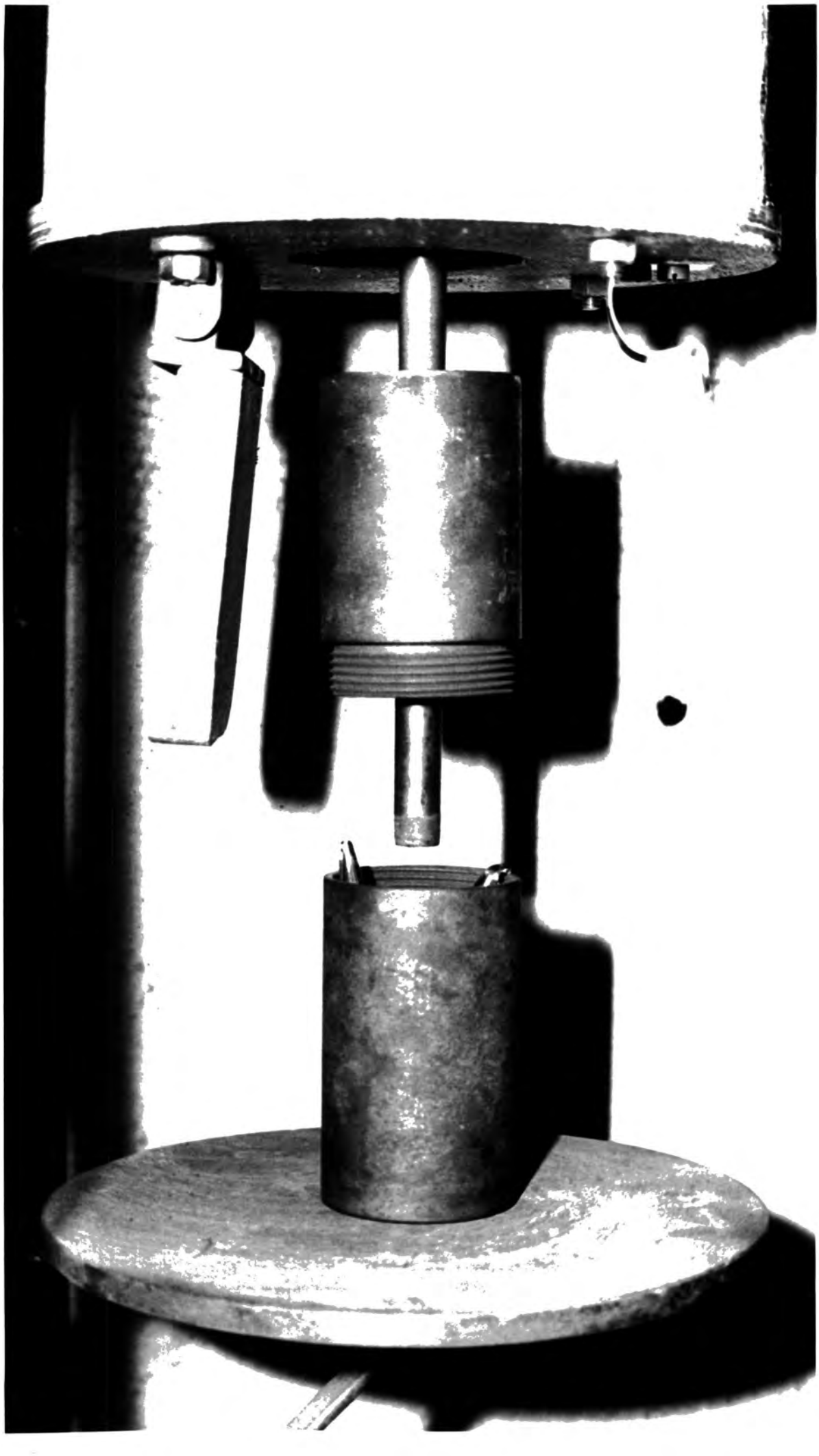

Techniques Employed in the Examination of the Sulphides Synthesised

Reflected Light Microscopy

Several fragments of each specimen were distributed in resin, polished, and examined by reflected light using a Zeiss Ultraphot. The phases obtained were identified and their textural relationships interpreted. Interesting features were photographed.

Optical examination has proved to be an essential step in the mineralogical study of synthetic sulphides. Interpretation of textures leads to an understanding of phase relations and has contributed to the planning of temperature histories of the synthesis of certain phases. Phenomena exhibited by the synthetic sulphides include -

skeletal crystal growth, dendritic crystal growth, eutectic intergrowths, two liquid texture, mutual boundary texture, reaction relationships, reaction rims, exsolution, eutectoid breakdown, inversion twinning, growth twinning, metastability, scratch induced inversion and colour change.

Electron Microprobe Analysis

Fragments chosen for microprobe analysis were drilled out from the polished specimen and mounted in a 0.5 mm. resin core suitable for mounting in the microprobe standard holder. Specimens and standards were carbon coated simultaneously. A Cambridge Geoscan, a two spectrometer microprobe with a 75° take off angle was used for analysis. A counting rate of 10 secs. was used exclusively in obtaining the count rate on standard, standard background, specimen and specimen background. The counter dead time was 4 microseconds.

Two programmes have been used in obtaining, from the raw data, the final corrected wt% of the elements present.

(1) TIM (Duncumb and Jones)

Uncorrected wt% values were calculated by hand. Corrected wt% values were computed using TIM. A correction for fluorescence was not made on the standard by TIM. The fluorescence correction required on the compound standards employed is small and has therefore been neglected. It is possible using TIM to determine one element by difference.

(2) EMPADR VII (Rucklidge and Gasparrini 1969)

Uncorrected and corrected wt% values are computed by EMPADR from the raw counts obtained from the microprobe. All necessary corrections are applied to both standard and specimen. The range in ratio of a substituting pair of elements can be determined conveniently using the 'Fixed Stoichiometry' option of EMPADR. For example, with $(CuAg)_{12}Sb_4S_{13}$, simultaneous determination of Cu and Ag can be carried out on many points in one or more specimens. EMPADR calculates the uncorrected wt% Cu and Ag, from the stoichiometry calculates the wt% Sb and S, and then computes the corrected wt% values.

Under ideal conditions an accuracy of 1% of the wt% present is possible using the electron microprobe (Long 1967). Springer (1969) analysed natural tetrahedrites and quoted an experimental error of approximately $\pm 2\%$ of the wt% present.

Analyses of the sulphides synthesised have usually given high totals. Tetrahedrite, stibioluzonite and Cu_3SbS_3 were analysed by Dr. A. Peckett of this department. His totals were about 0.5 wt% less than those given in Table 3-5.

No single element was responsible for the higher totals given in Table 3-5 but Cu and Sb contributed slightly more than S. The high totals, therefore, do not affect the conclusions drawn from the normalised results.

When one element (Cu) was computed by difference using TIM, this element was consistently low. This technique was used occasionally, however, because it was found that greater precision in the comparison of Cu-Sb-S phases was possible when Cu (using elemental Cu as a standard) was not determined.

Powder Diffraction

A Phillips high angle PW 1012/10 goniometer was used to obtain diffraction profiles of suitable specimens across a selected range in 2θ. Smear and rotating cavity mounts have been used. Because of the inevitable admixture of impurity in the large samples required and the lack of published diffraction data on Cu-Sb-S synthetic phases, this technique was of little value in this study.

Material for powder diffraction photographs was normally obtained from the polished specimen by drilling out or picking out with a needle - 'picked' sample. This could be carried out while the specimen was in view under the microscope. This technique was adopted because it minimised the risk of, and contributed to the identification of, any impurities in the sample. The powder so obtained was mounted on a silica glass fibre using a collodion solution. In some cases fragments of specimen were ground under acetone and powder obtained - 'ground' sample.

Debye-Scherrer powder photographs mounted in the Straumanis position were obtained using a 114.95 mm. diameter

Phillips camera. Narrow collimator and beam trap were used exclusively. Exposure times of the order of 2-10 hours were required when using the spot focus of Co K_α radiation from a 2 Kw generator.

Measurement of Powder Photographs

The photographs were mounted on a standard Hilger and Watts film measuring scale with a vernier capable of measuring to 0.005 cm. Theta values of diffracted lines could therefore be measured to 0.0125°. Since 'd' is a function of $\sin\theta$ ($d = \lambda/2\sin\theta$) the d-values of the lines can be determined at higher values of θ.

$$d\ (\text{precision}) = \frac{0.0125.d}{\tan\theta}$$

The values of 2θ, $\sin^2\theta$, d and $\sin^2\theta_n/\sin^2\theta_1$ (where 1 = line 1, n = nth line), were computed for the $\bar{\alpha}$, α_1 and α_2 lines using a program, DPOW, specially written by the author. Since the film was mounted in the Straumanis position the calculation could allow for film shrinkage (Klug and Alexander 1962). A necessary correction was applied to bring all $\sin^2\theta$ values to equivalent $\sin^2\theta_{\alpha_1}$ values before the $\sin^2\theta_n/\sin^2\theta_1$ values were computed (Klug and Alexander 1962).

For 'Co' radition $\sin^2\theta_{\alpha_1} = \sin^2\theta_{\alpha_2} \times 0.99570$

$\sin^2\theta_{\alpha_1} = \sin^2\theta_{\bar{\alpha}} \times 0.99856$

Indexing and Calculation of Cell Parameters

Cubic Minerals

The $\sin^2\theta_n/\sin^2\theta_1$ values computed in DPOW were used to obtain a factor, N_1, the $h^2 + k^2 + l^2$ value of the first line which, when divided into the $\sin^2\theta_n/\sin^2\theta_1$ values, brought them to approximate integers. This was done by trial and error using the list of $\sin^2\theta_n/\sin^2\theta_1$ values.

If the hkl value of the first line was known then $N_1 = h^2 + k^2 + l^2$.

N_1 was then used in DPOW to compute the approx. N values $(h^2 + k^2 + l^2)$ of each line -

$$N_n \text{ (approx.)} = \frac{\sin^2\theta_n}{\sin^2\theta_1/N_1}$$

In DPOW, N was rounded to the nearest integer and used to calculate the apparent cubic unit cell edge of each line -

$$a_n = \sqrt{\frac{N.\lambda^2}{4\sin^2\theta}}$$

During this process the $\sin^2\theta_1/N_1$ value was recalculated, after indexing each line of relative intensity greater than 20, using the N value (integer) just established for the line -

$$\sin^2\theta_1/N_1 = \frac{\sin^2\theta_n}{N_n}$$

This is necessary because of the low accuracy in measurement of $\sin^2\theta_n$ at low 2 θ values as a result of line displacements due to absorption of the X-ray beam by the sample (Klug and Alexander 1962). Also, the precision in measurement of $\sin^2\theta$ is poorer at low 2θ values.

According to Nelson and Riley (1945) the absorption error, eccentricity error and error in camera constants give an error in the apparent unit cell dimension which is proportional to $1/2(\cos^2\theta/\sin\theta + \cos^2\theta/\theta)$, the Nelson-Riley Extrapolation Function, and reduces to zero at $\theta = 90^\circ$. The 2θ values and apparent cell edge of selected high angle lines (usually only α_1 and α_2 back reflections) were used to compute the true cubic cell edge. A program called NELRIL was written. This program calculated the Nelson-Riley extrapolation function value for each 2θ value and by means

of a linear regression through the plots of 'Nelson-Riley extrap. func.' v 'cell edge (a_n)' calculated the cell edge at $\theta = 90^{o}$. The procedure was repeated twice rejecting points which plotted outside 1.5 standard deviations from the best fit straight line. The 'standard error of the intercept' was calculated and given as the error of the extrapolated cell edge -

$$\text{stnd. err. of intcpt.} = \sqrt{\frac{\sum_{1}^{n}(y-y_c)^2 \cdot \sum_{1}^{n}x^2}{(n-2).(n.\sum_{1}^{n}x^2 - (\sum_{1}^{n}x)^2)}}$$

where x = Nelson-Riley extrap. func. value

y = Observed cell edge for a line

y_c = Calculated cell edge for a line

n = Number of lines

Non-Cubic Minerals

The d-spacings of the diffracted lines were obtained from the powder photographs using DPOW. Two programs, GENSTRUK and COHEN, used for indexing and calculating the unit cell parameters respectively, are described in a report published by the UKAEA (Marples and Shaw 1966).

GENSTRUK produces a listing of line positions on being given non-cubic unit cell parameters. Observed d-values may be given as input and these lines are indexed by comparison with the generated lines. Indices allocated to the observed lines which do not fit the space group of the mineral must be rejected manually.

COHEN calculates, using Cohen's method (Klug and Alexander 1962), the 'least squares' best lattice parameters and their standard deviations on being given an indexed set of d-values. The program will reject lines not in agreement with the majority.

Vickers Microhardness Measurements

The diamond indentation method of microhardness determination was used. The instrument employed was a 'G.K.N. Microhardness Tester.'

The size of the impression obtained is related to the microhardness of the specimen. Since only isometric phases were examined, the mean of the two axial dimensions of the diamond impression was calculated. The microhardness given by the equation -

$$HD = \frac{2P.\sin\theta}{D^2}$$

where HD = hardness

P = the load in grams

θ = half the included angle of the pyramid (68^{o})

D = the diagonal of the indentation in mm,

was read from tables (G.K.N. 1958).

A number of indentations was made on each specimen allowing the standard deviation of the Vickers Microhardness to be calculated. Indentations with excessive fracturing were discarded.

Reflectivity Measurements

The general instrumental conditions are given in Table 2-2. The apparatus and technique has been described by Tansel (1970) and Akinci (1970). The reflectivities of the minerals were determined by comparison with a NPL standard (Table 2-3). The reflectivity of the specimen at a given wavelength was calculated from the equation -

$$R_{sp} = ((G_{sp} - G_{bb}).R_{std})/(G_{std} - G_{bb})$$

where R = reflectivity, G = galvonometer reading,

sp = specimen, std = standard and

bb = black box (primary glare correction).

Maximum and minimum readings of the galvo. were taken in triplicate for the standard, the specimen, the standard and finally the black box. The mean readings were then calculated and used in the above equation.

During the determination of the spectral reflectivities of synthesised members of the tetrahedrite-tennantite series the measurements at different wavelenths were all made on the same area of the specimen. During the measurement of the reflectivities of substituted tetrahedrites (Cu substituted) the reflectivities of several grains in the same specimen were determined enabling the standard deviation of the measurements to be calculated.

Colour Measurements

The unreliability of the human eye in colour perception makes the quantitative evaluation of mineral colours invaluable. The 'spectrophotometric method' described in the Science of Colour (1953) has been used in this study.

Tristimulus Values

Any colour can be produced by mixing the three primary colours blue, green and red. The three tristimulus values (X, Y and Z) are related to the proportions of these three colours required to produce a given colour. The tristimulus values can be computed from -

(a) The spectral reflectivity curve.

(b) The spectral distribution of energy in the illuminant, and certain psychological-physiological coefficients adopted by the Commission Internationale de L'Eclairage (C.I.E.) as 'Tristimulus Values of

the Spectrum Colours' (Piller 1966).

Reflectivities are required at thirty standard wavelengths for the calculation of each tristimulus value. In the present study the standard reflectivity values were calculated by extrapolation from the measured spectral reflectivity curve by means of a computer program written by U. Win Htein of this department. There are three standard light sources, A (tungsten light), B (direct sunlight) and C (average daylight), and the X, Y and Z tristimulus values were computed for each using the factors given in Table 16 of the Science of Colour. The Y value indicates the relative brightness of the specimen on a scale that represents an absolute black by zero and perfect white by 100% (Piller 1966). The X and Z values do not have simple representations.

Chromaticity

A given colour can be represented by its dominant wavelength and % purity (i.e. the proportion of dominant wavelength and white light). These two values specify the chromaticity and can be obtained from the standard 'Chromaticity Diagram' given in Fig.2-4 (C.I.E. 1931). All the spectrum colours are represented on the curve (spectrum locus) in Fig.2-4 and have 100% purity. The three standard illuminants are also plotted in this diagram. To represent colours in the diagram the chromaticity co-ordinates, x, y and z, are computed from the tristimulus values, X, Y and Z. The chromaticity co-ordinates are related thus -

$$x = \frac{X}{X+Y+Z} \qquad y = \frac{Y}{X+Y+Z} \qquad z = \frac{Z}{X+Y+Z}$$

Only x and y are required for plotting points in the chromaticity diagram.

The dominant wavelength and excitation purity of a colour are obtained as shown in Fig.2-4 for a specimen (sp) using illuminant A.

This can be done graphically but is inaccurate. In the present study, therefore, the dominant wavelength and the excitation purity were computed using a program written by U. Win Htein of this department.

Colour Discrimination

There are threshold values of colour measurements which must be exceeded in order that the human eye can perceive colour differences. These threshold values were determined by MacAdam (1942) and used to construct the threshold ellipse in Fig.4-8. The colour differences between the selected point at the centre of the ellipse and all points lying within the ellipse are indistinguishable by the human eye.

TABLE 2-2

Instrumental Conditions for Reflectivity Measurements

Photoelectric Apparatus	EMI - II stage 6094B Photomultiplier Stabilized voltage supplied by Farnell Inst. Ltd. E2 type stabilized EHT power supply. Output of the photomultiplier fed to DM 2005 type Dynanco Ltd. Digital Voltmeter.
Light Source	8 volt - 48 watt Tungsten Filament Lamp Stabilized voltage supplied by Farnell Inst. Ltd. TSV 70 Stabilized Voltage Supply.
Microscope	Vickers Inst. Ltd. Ore Microscope.
Objective	X40, 0.85 na.
Filter	Veril B-200, Jena Glassworks, Mainz No.B-34716 Continuous Filter Monochromator
Aperture	5

TABLE 2-3

Reflectivity of Carborundum Standard, NPL No.2538.27

Wavelength (nm)	Reflectivity (%)
440	21.0
460	20.8
480	20.6
500	20.5
520	20.4
540	20.3
560	20.2
580	20.1
600	20.0
620	20.0
640	19.9
660	19.9

FIG 2-4 CHROMATICITY DIAGRAM

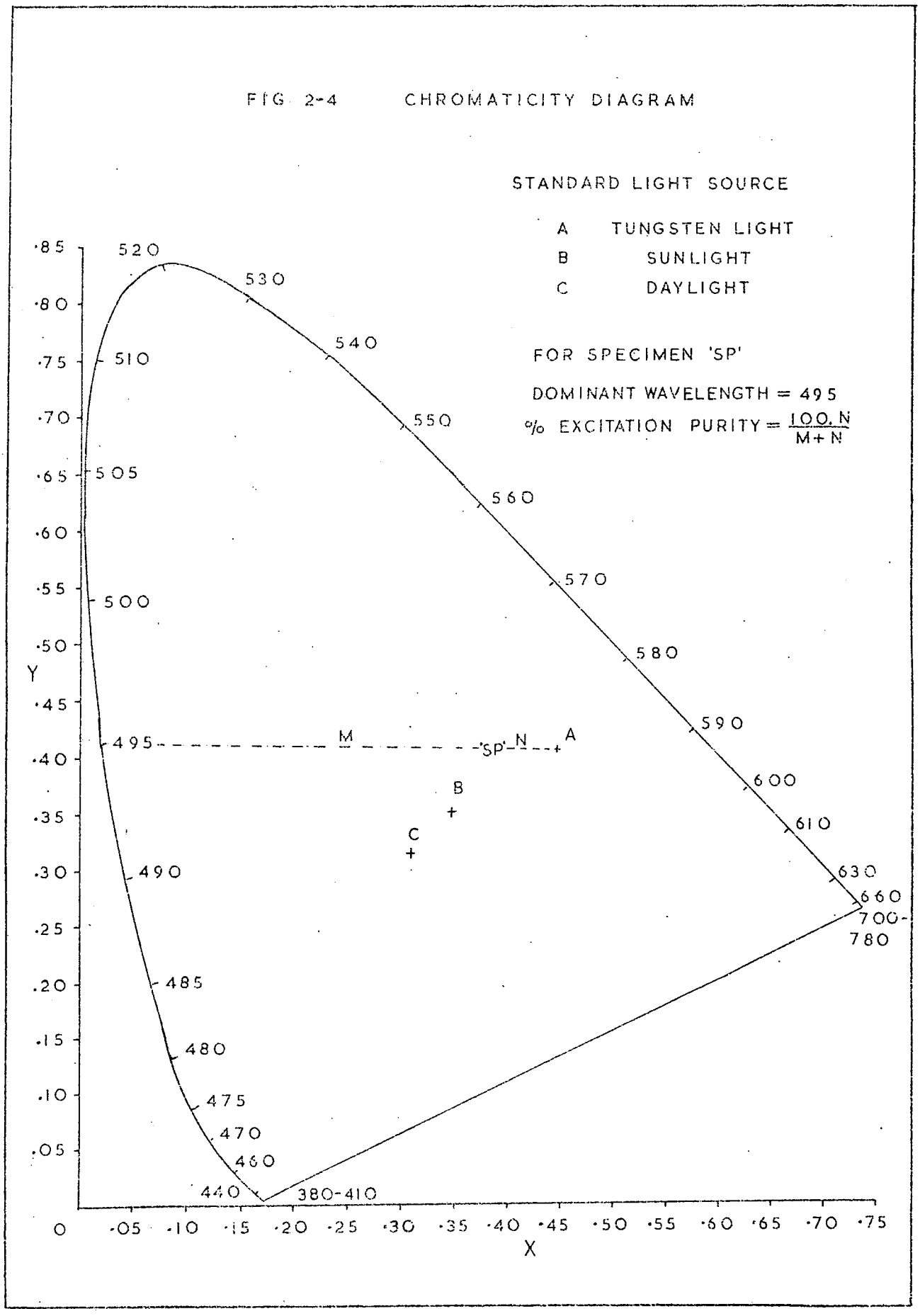

CHAPTER 3

THE CU-SB-S SYSTEM

Introduction

A knowledge of the phase relations of a compound can contribute to its successful synthesis. Valuable facts include - (a) the composition range; (b) the composition at the melting point; (c) whether the melting is congruent or incongruent and (d) whether there are temperature dependant crystal structure inversions (polymorphism). Using the technique of sulphide synthesis by crystal growth from the melt the ideal compound is stoichiometric, melts congruently and has no polymorphism.

A literature survey was undertaken in an attempt to obtain the above facts for tetrahedrite and other phases in the Cu-Sb-S system.

Although the general form of the Cu-Sb-S system was established from a variety of sources, no recent work using modern techniques of phase diagram determination has been published on the ternary and the phase relations of tetrahedrite remained uncertain. Selected runs were therefore undertaken in order to confirm the form of the ternary system and an attempt was made to establish the subsolidus phase relations of tetrahedrite below 500°C.

Previous Work on the Cu-Sb-S System

The binary phase relations of Cu-S and Sb-S are well established but the Cu-Sb system has not been recently revised.

The Cu-S Binary (Fig.3-1)

The details required for Fig.3-1 were taken mainly from Kullerud (1958, 60) and Roseboom (1966) who has revised the system.

The high temperature portion is well established but the low temperature (<100°C) portion between CuS and Cu_2S is the subject of continuing publications. The low temperature details are, however, insignificant in this study as in most work on dry sulphide phase relations.

Low temperature orthorhombic chalcocite (Cu_2S) inverts at 103°C to a non-quenchable hexagonal polymorph which remains stable to 435°C where it inverts to a cubic polymorph. Digenite ($Cu_{1.76-79}S$) inverts to non-quenchable cubic high-digenite at 76-83°C. With increasing temperature the composition range of high digenite increases and includes Cu_2S at 435°C. On cooling, a variety of low temperature breakdown products of high digenite are possible depending on the Cu:S ratio. In the present study, in runs in the Cu-Sb-S system, breakdown products have been quite variable in appearance but have, in total, been labelled $Cu_{2-x}S$.

The Sb-S Binary (Fig.3-2)

This system is described by Hansen and Anderko (1958). The high temperature cubic polymorphism of stibnite was reported by Prouvost (1963). Stibnite was synthesised in this study by slow cooling from the melt. Well developed acicular crystal were obtained (Plates 3-5,6). Rapid cooling of the composition Sb_7S_3 from 620°C resulted in the production of a two liquid texture (Plates 3-7,8).

The Cu-Sb Binary (Fig.3-3)

This system is described by Hansen and Anderko (1958).

The data were obtained mainly by thermal and resistometric analyses. The portion from 20 to 30 atomic % Sb was described by Elliott (1965) and was obtained using x-ray techniques. The complexities of this diagram are of little consequence in the present study of the central part of the Cu-Sb-S system.

The Cu-Sb-S Ternary

A summary of early attempts at synthesis of phases in this system can be obtained from Gmelin (1961).

The Cu_2S-Sb_2S_3-Sb-Cu area was studied using thermal analyses and texture studies by Guertler and Meissner (1921). Because of the technique used their results only give an indication of the form of the system but the main tie lines were established. From their tabulated data the Cu_2S-Sb join has been constructed and is presented with the diagram given by Guertler and Meissner in Fig.3-4. Two two-liquid fields were established by Guertler and Meissner though from their own tabulated data (i.e. specimen 2), it is possible that the two liquid field extends continuously across the diagram. The ternary phases tetrahedrite, given as Cu_3SbS_3, and chalcostibite, $CuSbS_2$, were recognised.

The existence of the compounds Cu_3SbS_3 and $CuSbS_2$ were confirmed by thermoanalyses and microscopic examination in a study of the Cu_2S-Sb_2S_3 join (Parravano and De Cesaris, 1912). Cu_3SbS_3 was named stilotipo (Italian). Dana (1944) noted that natural stylotypite $(CuAgFe)_3SbS_3$ has been shown to be a mixture of tetrahedrite and other phases. Parravano and De Cesaris do not say if Cu_3SbS_3 was recognised as being a non-cubic phase and not tetrahedrite. The eutectic temperatures for Cu_2S-Cu_3SbS_3 = 610°C, Cu_3SbS_3-$CuSbS_2$ = 542°C and $CuSbS_2$-Sb_2S_3 = 490° were established.

As a result of isothermal reduction of Cu_2S-Sb_2S_3 mixtures by H_2 at 400°C the following solid-solutions were obtained by Schenck et al. (1939) -

(a) $3Cu_2S.Sb_2S_3$ - $5Cu_2S.3Sb_2S_3$

(b) $Cu_2S.Sb_2S_3$ - $4Cu_2S.5Sb_2S_3$

(c) $3Cu_2S.4Sb_2S_3$ - $2Cu_2S.3Sb_2S_3$

The central area of the Cu-Sb-S system was studied by Gaudin and Dicke (1939). Several Cu:Sb ratios, with excess and deficient sulphur, were heated in iron containers to 525°C and quenched at 300-500°C. The ternary phases tetrahedrite, famatinite (stibioluzonite) and chalcostibite were obtained and shown by selective irridescent filming to have a range in composition. Tetrahedrite and chalcostibite were reported to melt incongruently.

Wernick and Benson (1957) synthesised Cu-Sb-S ternary compounds in sealed quartz tubes containing N_2 at $^2/_3$ atmos. pressure. The following data were reported - tetrahedrite, Cu_3SbS_3, cubic, M.P. = 555°C; famatinite (= stibioluzonite), Cu_3SbS_4, cubic, M.P. = 555°C; wolfsbergite (= chalcostibite), $CuSbS_2$, orthorhombic, M.P. = 535°C.

The Cu_2S-Sb_2S_3 join was studied by Cambi and Elli (1965). The diagram they presented is given in Fig.3-5 and was established by dry thermal synthesis, hydrothermal synthesis, thermal analysis, x-ray diffraction, wet chemical analysis and polished specimen study. It was concluded that tetrahedrite has a range in composition from $3Cu_2S.Sb_2S_3$ to $4Cu_2S.Sb_2S_3$, that the low temperature polymorph, 'α' (a_o = 10.31 ± 0.02Å), inverts at 500-530°C to a high temperature cubic polymorph, 'β' (a_o = 10.44 ±0.03Å), which melts congruently at 610°C. In thermal synthesis 'α' and

'β' tetrahedrites were obtained resulting in a splitting of all the peaks on the diffraction profile but after reheating to 400°C only the 'α' tetrahedrite peaks were retained. Only 'α' tetrahedrite was obtained by hydrothermal synthesis. The x-ray diffraction profile obtained for chalcostibite showed doubling of the most intense peaks. The resolution of these peaks had not previously been reported.

The Cu_2S-Sb_2S_3 join was also investigated by Godovikov et al. (1970). The new sulphosalt, Cu_3SbS_3, which has a structure similar to orthorhombic wittichenite, Cu_3BiS_3, and melts incongruently from 593° to 618°C to tetrahedrite, was reported.

Conclusions

The information obtained from these publications has enabled the construction of the Cu-Sb-S ternary and the 600°C isothermal section is given in Fig.3-6. The publication by Godovikov et al.(1970) arrived too late to contribute to the series of experiments which were planned from this Cu-Sb-S working diagram.

The conclusion drawn from the study of previous work on the Cu-Sb-S system was that the general form of the Cu-Sb-S ternary diagram and the ternary phases present had been established. The work of Cambi and Elli (1965) was the most thorough and it was decided to confirm their results as well as synthesise tetrahedrite. Preliminary runs in the Cu-Sb-S system were therefore selected with the following objectives -

(a) To synthesise the major phases and establish optical identification criteria.

(b) To confirm the form of the Cu_2S-Sb_2S_3 binary published by Cambi and Elli (1965).

These preliminary experiments were accomplished during the

development of the technique of synthesis and therefore involved a variety of experimental conditions. The conclusions reached were that, while most of the established Cu-Sb-S ternary diagram appeared to be correct, the phase relations of tetrahedrite were more complex than suggested by Cambi and Elli (1965). A more detailed study of the central part of the Cu-Sb-S ternary was therefore undertaken.

The study of the central part of the Cu-Sb-S system will first be outlined before describing certain selected runs in the system. The appearance of the ternary phases (sulphosalts) in polished specimen will then be described and diffraction data given. Finally the results will be summarised and discussed.

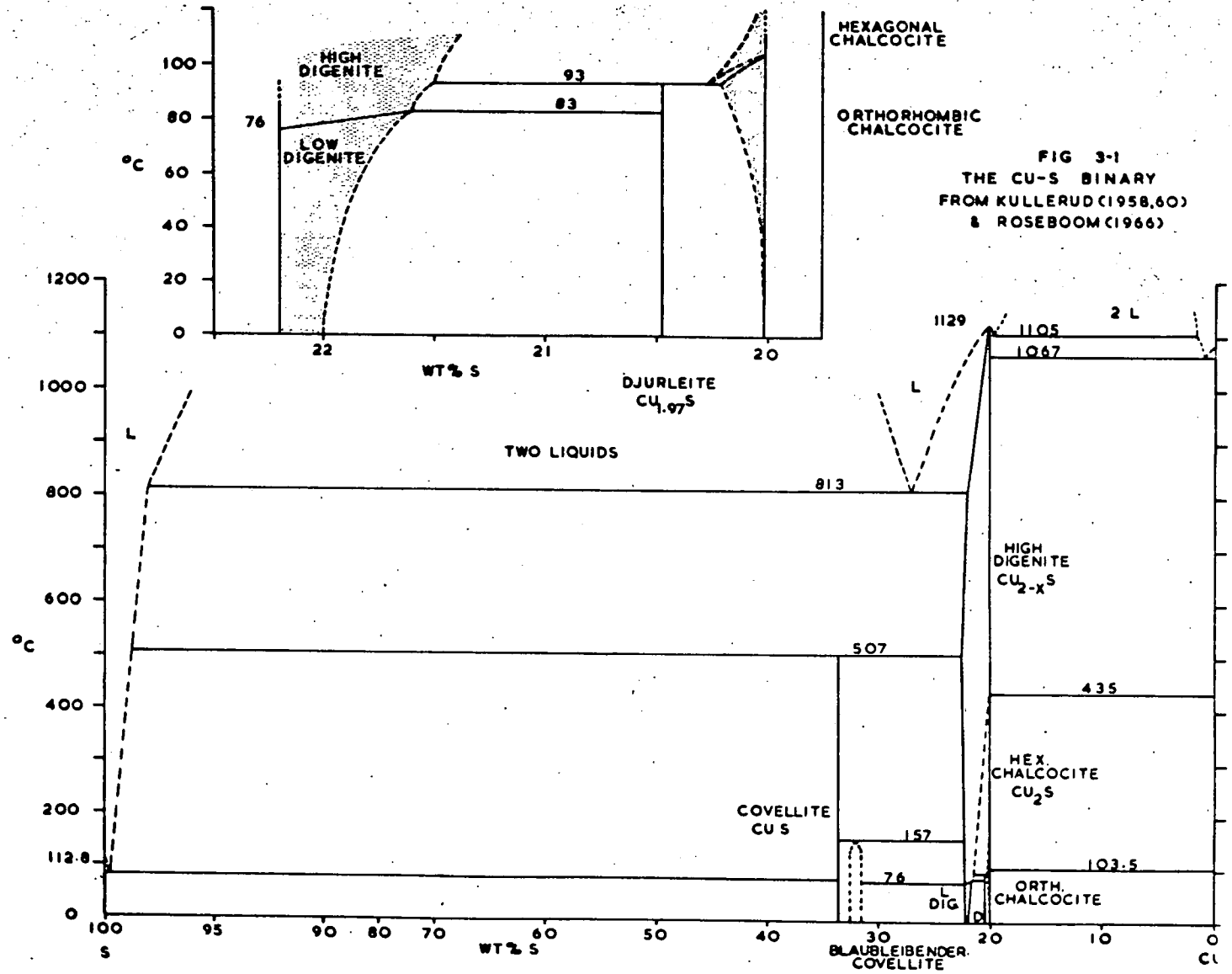

FIG 3-1
THE CU-S BINARY
FROM KULLERUD (1958,60)
& ROSEBOOM (1966)

FIG 3-2
THE SB-S BINARY
HANSEN & ANDERKO 1958

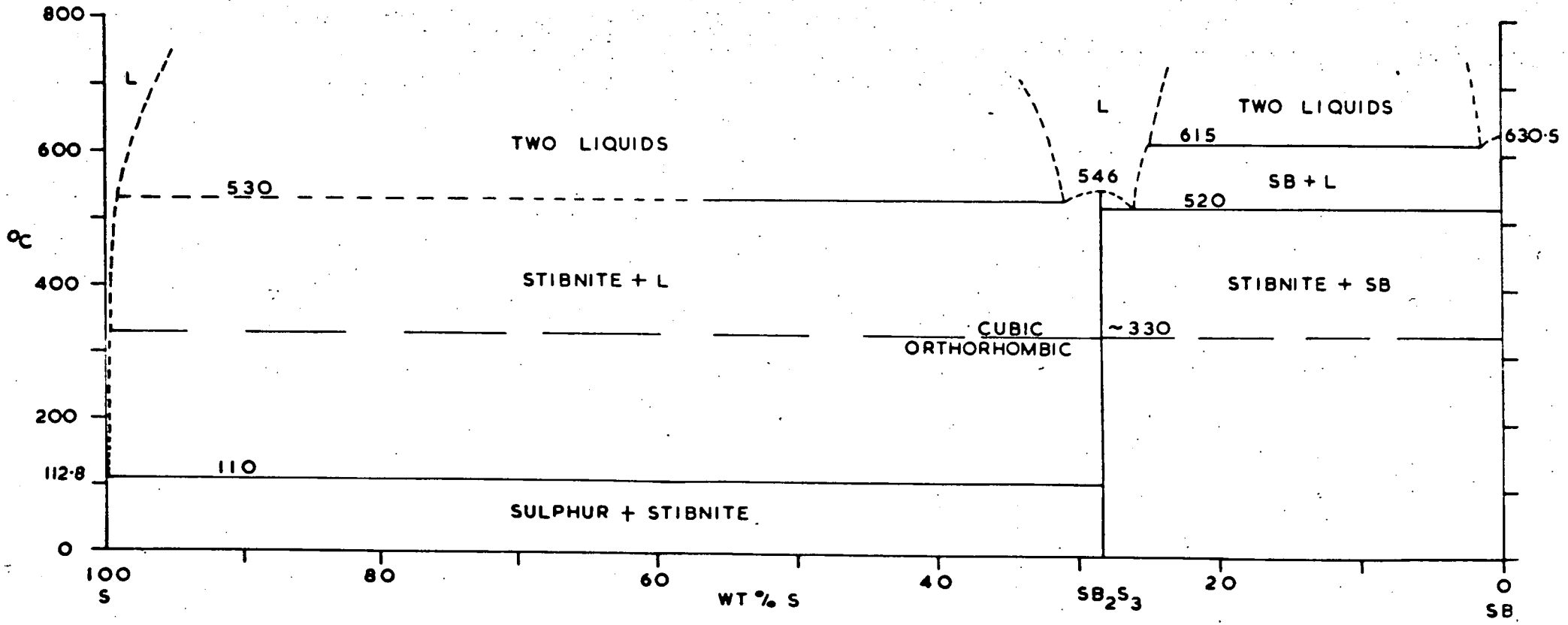

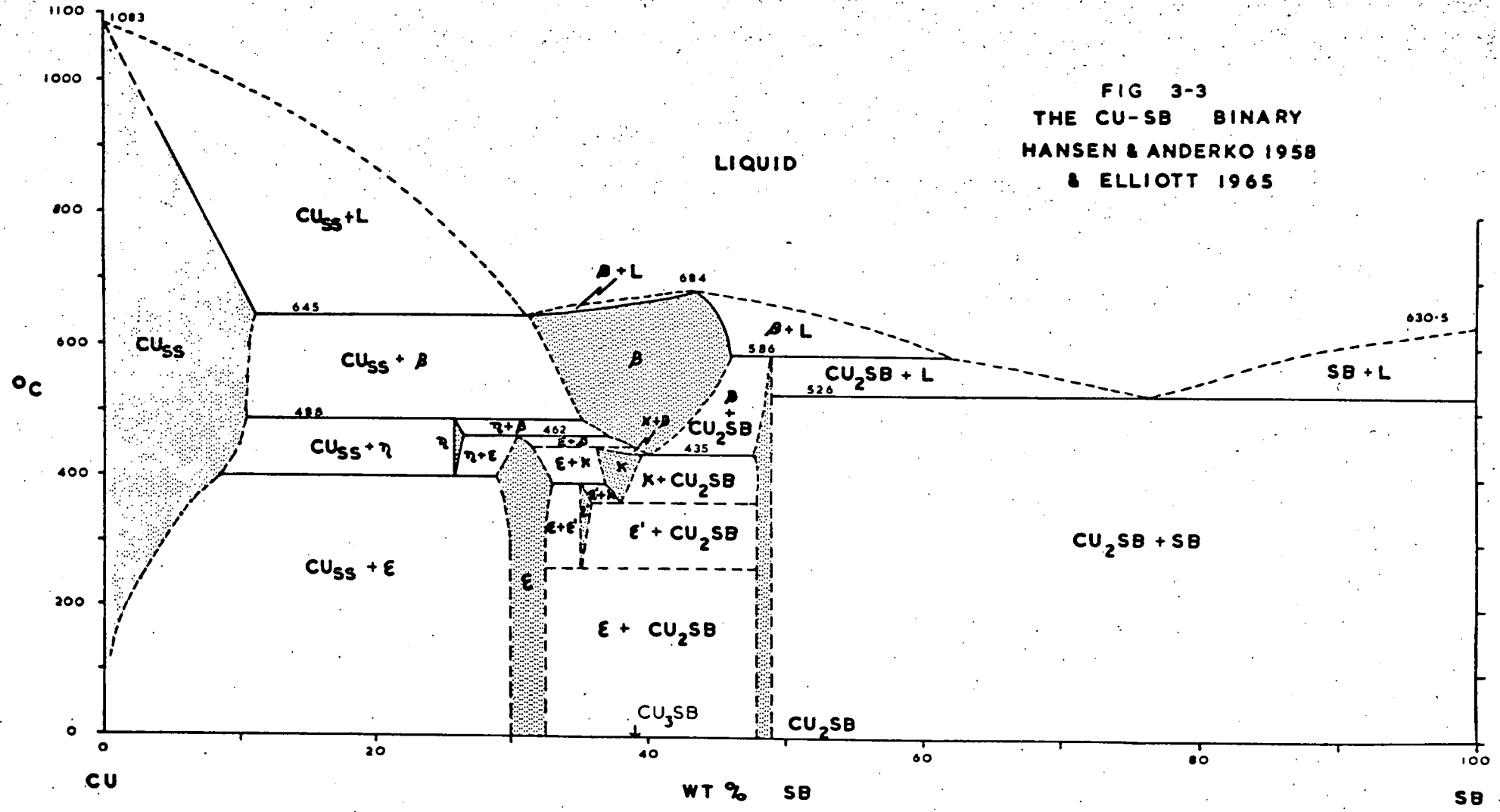

FIG 3-3
THE CU-SB BINARY
HANSEN & ANDERKO 1958
& ELLIOTT 1965

FIG 3-4
THE CU_2S - SB JOIN
GUERTLER & MEISSNER 1921

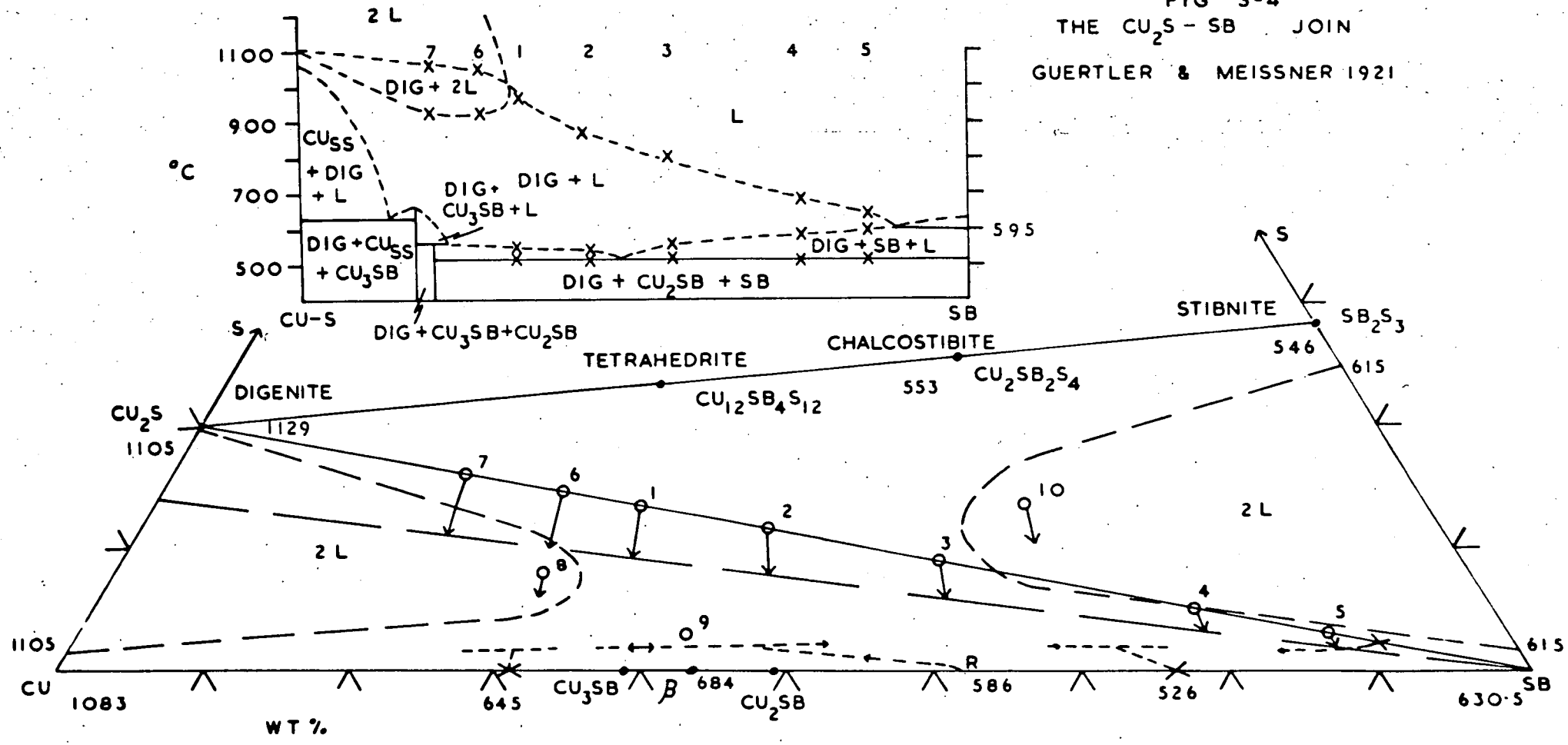

FIG 3-5
THE $Cu_2S - Sb_2S_3$ JOIN
CAMBI & ELLI 1965

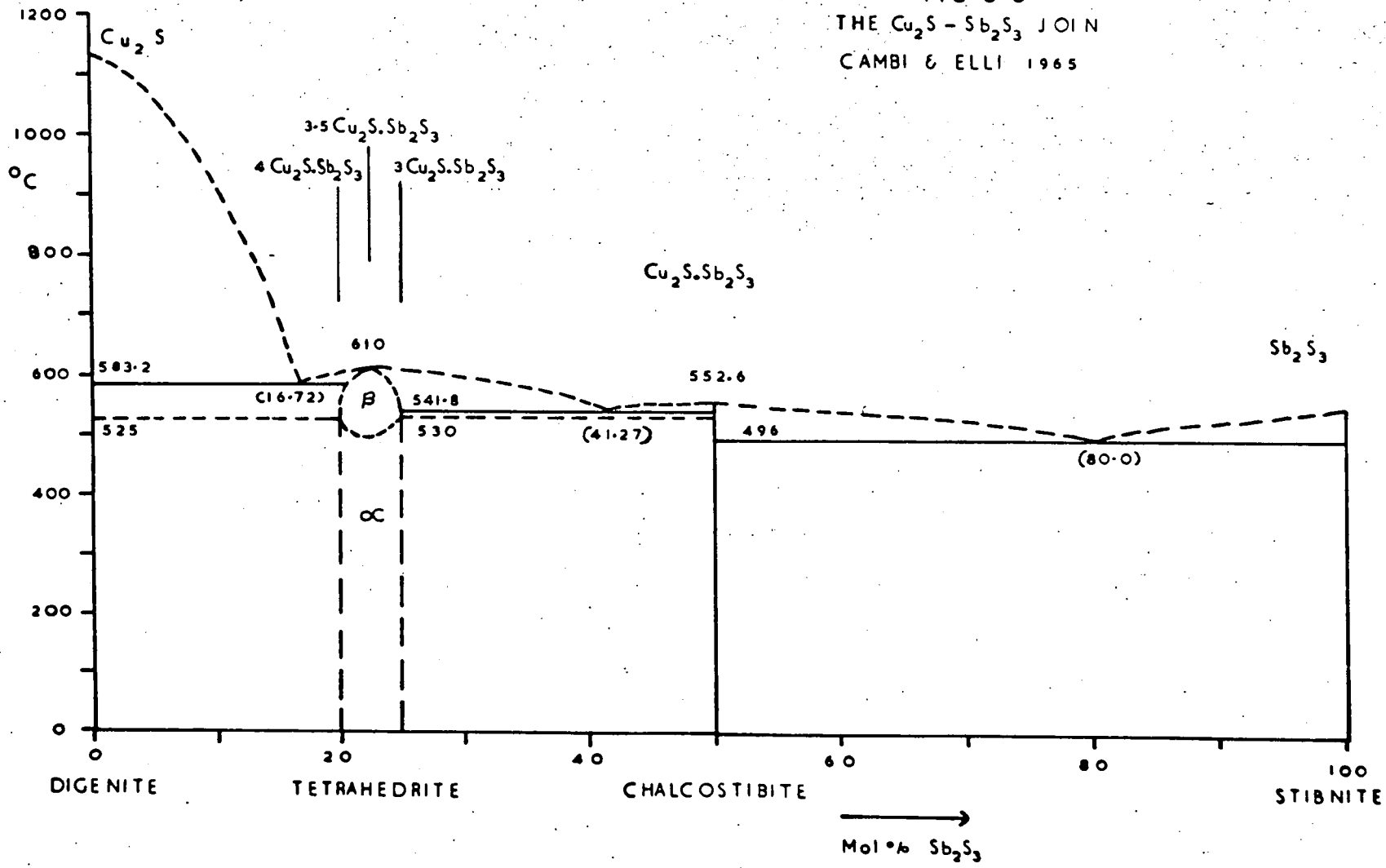

FIG 3-6 THE CU-SB-S SYSTEM — 600°C ISOTHERMAL SECTION

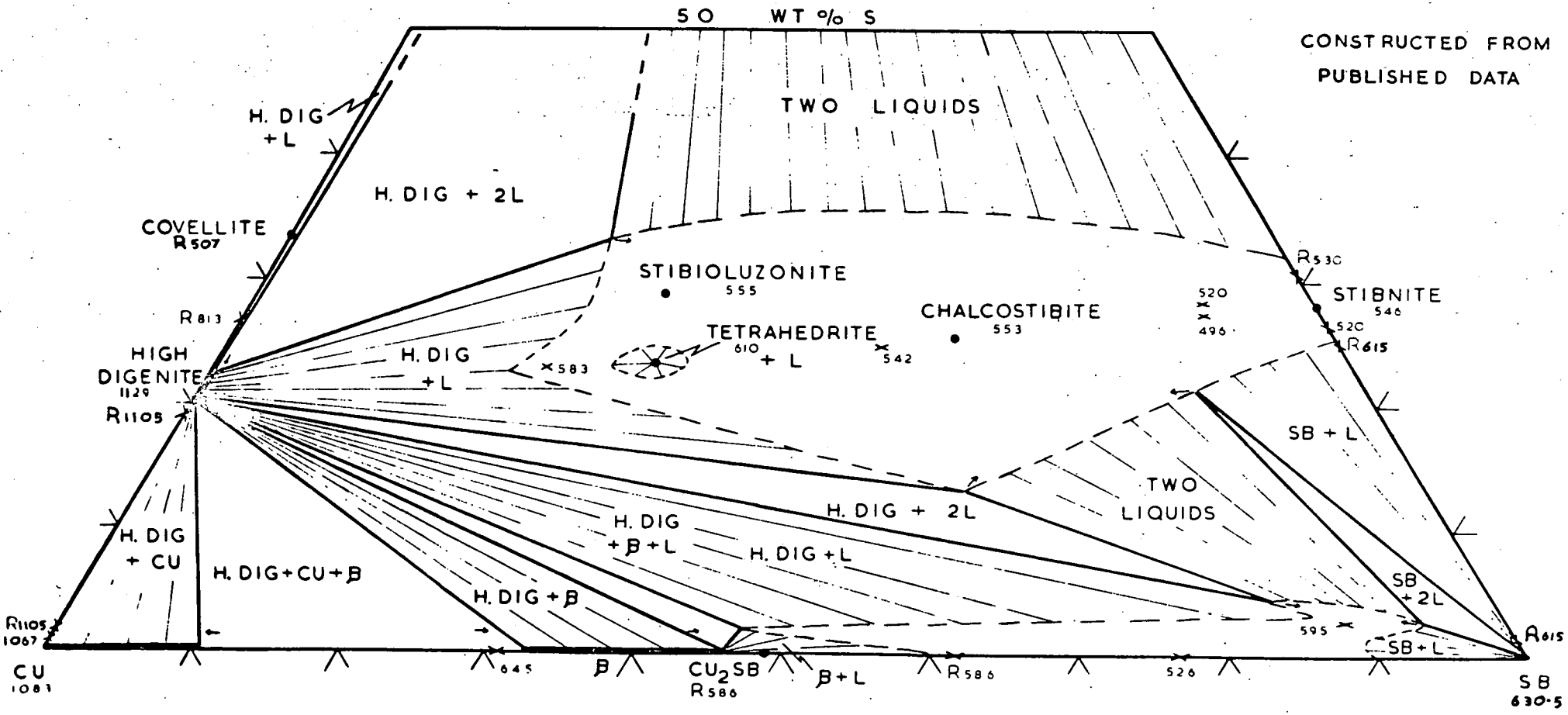

The Central Area of the Cu-Sb-S System

The high purity chemicals used are given in Table 1-1b. The technique of synthesis is described in Chapter 2. The starting compositions are listed in Table 3-1 and plotted in Fig.3-7. The three phases being investigated were stibiolu-zonite, tetrahedrite and Cu_3SbS_3, a new phase, which had been synthesised in early experiments before the work of Godovikov et al.(1970) was known to the author. The specimens were run in two batches with similar temperature histories which are given in Table 3-2. Polished specimens were prepared for phase identification and textural inter-pretation. Identification of the phases obtained was confirmed by microprobe analysis.

Temperature History

The specimen temperature was raised slowly to 600°C, lowered slowly to 500°C and maintained at this temperature for 43 hours before removing the specimens from the furnace. This sequence was chosen in order to obtain information on the subsolidus phase relations of tetrahedrite. Attempts at synthesis of tetrahedrite by crystallisation from the melt had proved unsatisfactory because of the incomplete reaction on cooling of primary digenite in the tetrahedrite composi-tion melt.

Polished Specimen Examination

The phases obtained and their textural relationships are given in Table 3-3. The three main phases Cu_3SbS_4, $Cu_{12}Sb_4S_{13}$ and Cu_3SbS_3 were well defined, there being little variation in their microscopic character. The $Cu_{2-x}S$ phase varied in colour, internal texture and relationship with other phases as expected from its complexity in the Cu-S binary.

Microprobe Analysis

The major phases obtained from each polished specimen were analysed for Sb and S. Cu was computed by difference using TIM. The conditions of analyses and the results are given in Table 3-4. Phases unsuitable for analysis because of inclusions, intergrowths, etc., include all those in specimen 71 and tetrahedrite in specimen 65.

There was no significant variation in composition noted for tetrahedrite, stibioluzonite and Cu_3SbS_3 in all the specimens analysed. All analyses were Cu deficient in relation to the expected stoichiometric compositions but this was because of the 'Cu by difference' analytical technique used. The analyses have been plotted in Fig.3-8.

Full analyses of tetrahedrite (Spec.63), stibioluzonite (spec.64) and Cu_3SbS_3 (spec.65) were undertaken. The conditions of analyses and the results are given in Table 3-5. The results confirm the formulae of the phases - Cu_3SbS_4 (stibioluzonite), $Cu_{12}Sb_4S_{13}$ (tetrahedrite) and Cu_3SbS_3.

Phase Relations

The significant facts obtained are - $Cu_{2-x}S$ co-exists with stibioluzonite, tetrahedrite and Cu_3SbS_3. Stibioluzonite co-exists with tetrahedrite, blaubleibender covellite and chalcostibite. Tetrahedrite co-exists with chalcostibite. Cu_3SbS_3 co-exists with Cu_2S, inverted tetrahedrite, Sb and chalcostibite. Chalcostibite co-exists with Sb.

Cu_{2-x}, often rimmed by stibioluzonite, formed ovoid dendrites in tetrahedrite. The texture of Sb in Cu_3SbS_3 suggested independent crystallisation - a two liquid phenomenon. Oriented blebs and rods of Cu_2S and $Cu_{2-x}S$ in Cu_3SbS_3 suggested a high temperature range in composition of Cu_3SbS_3 towards $Cu_{2-x}S$.

A tentative phase diagram for the central part of the Cu-Sb-S system at 450°C is given in Fig.3-9. Information from several early selected composition runs in the Cu-Sb-S system has supported the conclusions. 450°C has been chosen to represent subsolidus phase relations in the system. With decreasing temperature only changes in tie lines coming from the Cu-S binary are expected to occur.

TABLE 3-1

The Central Area of the Cu-Sb-S System
Starting Compositions - see Fig.3-7

Specimen number	Composition	Furnace Batch Number
63	$Cu_{12}Sb_4S_{13}$	1971C
64	Cu_3SbS_4	1971C
65	Cu_3SbS_3	1971C
69	$Cu_{12}Sb_4S_{14}$	1971C
70	$Cu_{12}Sb_4S_{15}$	1971C
71	$Cu_{12}Sb_4S_{11}$	1971D
72	$3.5Cu_2S.Sb_2S_3$	1971D
73	$2.5Cu_2S.Sb_2S_3$	1971D
75	$Cu\,0.39Sb\,0.16S\,0.45$	1971D
76	$Cu0.43Sb\,0.13S\,0.44$	1971D

TABLE 3-2

The Central Area of the Cu-Sb-S System
Temperature Histories

Batch	Hours to max.	Max. Temp.	Hours at Max.	Hours to Min.	Min. Temp.	Hours at Min.	Hours to Room Temp.
1971C	24	600°C	16	8	500°C	43	< 1
1971D	29	600°C	14	12	500°C	43	< 1

TABLE 3-3

The Central Area of the Cu-Sb-S System
Phases Obtained and Textural Relationships

Specimen No.63

Main phases - tet 90-95%, stblz 5-10%

Texture - Large tet crystals with fractured welded rims. In tet, blue $Cu_{2-x}S$ spheroids with narrow stblz rims. Chst interstitial. Tet weak anisotropy.

Specimen No.64

Main phases - stblz 90-100%

Texture - Large Interlocking crystals of stblz. Scarce interstitial $Cu_{2-x}S$, and blaubleibender cov with lamellae of cov.

Specimen No.65 Plate 3-1, 2

Main phases - Cu_3SbS_3 80%, inv tet 10%, chst 10%.

Texture - Interlocking crystals of Cu_3SbS_3 occasionally full of oriented minute $Cu_{2-x}S$ blebs and rods (when grey = Cu_2S ?) Skeletal tet (idioblastic?) enclosing Cu_3SbS_3 and sometimes also contains $Cu_{2-x}S$ blebs. Chst interstitial in eutectic intergrowth with Cu_3SbS_3.

Specimen No.69

Main phases - Stblz 45%, tet 40%, chst 10%, $Cu_{2-x}S$ 5%.

Texture - Large intergrown tet and stblz (mutual boundary). $Cu_{2-x}S$ ovoid dendrites with stblz rims in tet. Chst interstitial.

Specimen No.70

Main phases - Stblz 75%, tet 20%, chst>5%, $Cu_{2-x}S$>5%.

Texture - Large proeutectic stblz crystals with interstitial tet and scarce chst. $Cu_{2-x}S$ ovoids in stblz and ovoidal dendrites with stblz rims in tet.

Specimen No.71

Main phases - Cu_3SbS_3 60%, $Cu_{2-x}S$ 20%, Sb 20%.

Texture - Anhedral grains of $Cu_{2-x}S$, some intergrown with Sb, some including Cu_3SbS_3, in Cu_3SbS_3. Large interlocking crystals of Cu_3SbS_3 full of minute orientated blebs of Cu_2S; also contains dendritic stockworks of Sb which are independent of Cu_3SbS_3 crystal margins (- two liquid texture?).

Specimen No.72

Main phases - Cu_3SbS_3 70%, $Cu_{2-x}S$ 30%.

Texture - Large interlocking Cu_3SbS_3 many full of orientated $Cu_{2-x}S$ blebs and rods. Ovoidal dendritic $Cu_{2-x}S$.
Scarce tetrahedrite patches.

Specimen No.73

Main phases - Cu_3SbS_3 75%, chst 20%, Sb 5%.

Texture - Subhedral Cu_3SbS_3 crystals with interstitial chst and Sb.

Specimen No.75

Main phases - Tet 70%, stblz 15%, chst 15%.

Texture - Stblz laths with marginal chst blebs in tet.
Chst intergrown with tet and interstitial.

Specimen No.76

Main phases - Tet 75-85%, stblz 10-15%. chst <5%, $Cu_{2-x}S$ 10%. Texture - $Cu_{2-x}S$ ovoidal dendrites, blue and white, with stblz rims, in tet. Stblz laths in tet. Scarce interstitial chst.

where tet = tetrahedrite
stblz = stibioluzonite
chst = chalcostibite
cov = covellite
inv = inverted

TABLE 3-4

Microprobe Analysis of Ternary Phases in the Cu-Sb-S System

Element	Line	KV	Standard
Cu	-------- by difference using TIM		
Sb	L_α	15	Sb_2S_3
S	K_α	15	Sb_2S_3

	uwt%	cwt%	at%	uwt%	cwt%	at%
	63TET			64STBLZ		
Cu	-	44.78	40.58	-	42.09	36.38
Sb	28.44	30.05	14.21	26.25	28.20	12.72
S	23.25	25.18	45.21	27.35	29.72	50.90
	65W			70STBLZ		
Cu	-	45.80	42.01	-	42.35	36.61
Sb	28.76	30.26	14.48	26.07	28.00	12.63
S	22.12	23.94	43.51	27.26	29.64	50.76
	70TET			72TET		
Cu	-	45.08	40.84	-	45.09	40.72
Sb	28.24	29.84	14.11	27.96	29.57	13.94
S	23.16	25.09	45.05	23.38	25.34	45.35
	72W			73W		
Cu	-	45.69	42.03	-	45.45	41.87
Sb	29.08	30.56	14.67	29.34	30.82	14.82
S	21.98	23.75	43.30	21.95	23.73	43.32
	73CHST			75STBLZ		
Cu	-	24.97	24.53	-	42.38	36.76
Sb	47.87	49.23	25.24	26.36	28.28	12.80
S	24.78	25.80	50.23	27.00	29.34	50.43
	75TET			75CHST		
Cu	-	44.86	40.63	-	25.26	24.81
Sb	28.33	29.94	14.15	47.66	49.02	25.13
S	23.27	25.20	45.22	24.69	25.72	50.06
	76 STBLZ			76TET		
Cu	-	42.80	37.05	-	44.78	40.48
Sb	25.93	27.84	12.58	28.23	29.85	14.08
S	26.99	29.36	50.37	23.42	25.37	45.44
	69STBLZ			69TET		
Cu	-	42.63	36.86	-	44.36	40.17
Sb	25.94	27.86	12.57	28.63	30.26	14.30
S	27.13	29.51	50.56	23.45	25.38	45.54

where TET = tetrahedrite, $Cu_{12}Sb_4S_{13}$

STBLZ = stibioluzonite, Cu_3SbS_4

W = Cu_3SbS_3

CHST = chalcostibite, $CuSbS_2$

FIG 3-7 SPECIMEN LOCALITIES IN THE CENTRAL PART OF THE CU-SB-S TERNARY

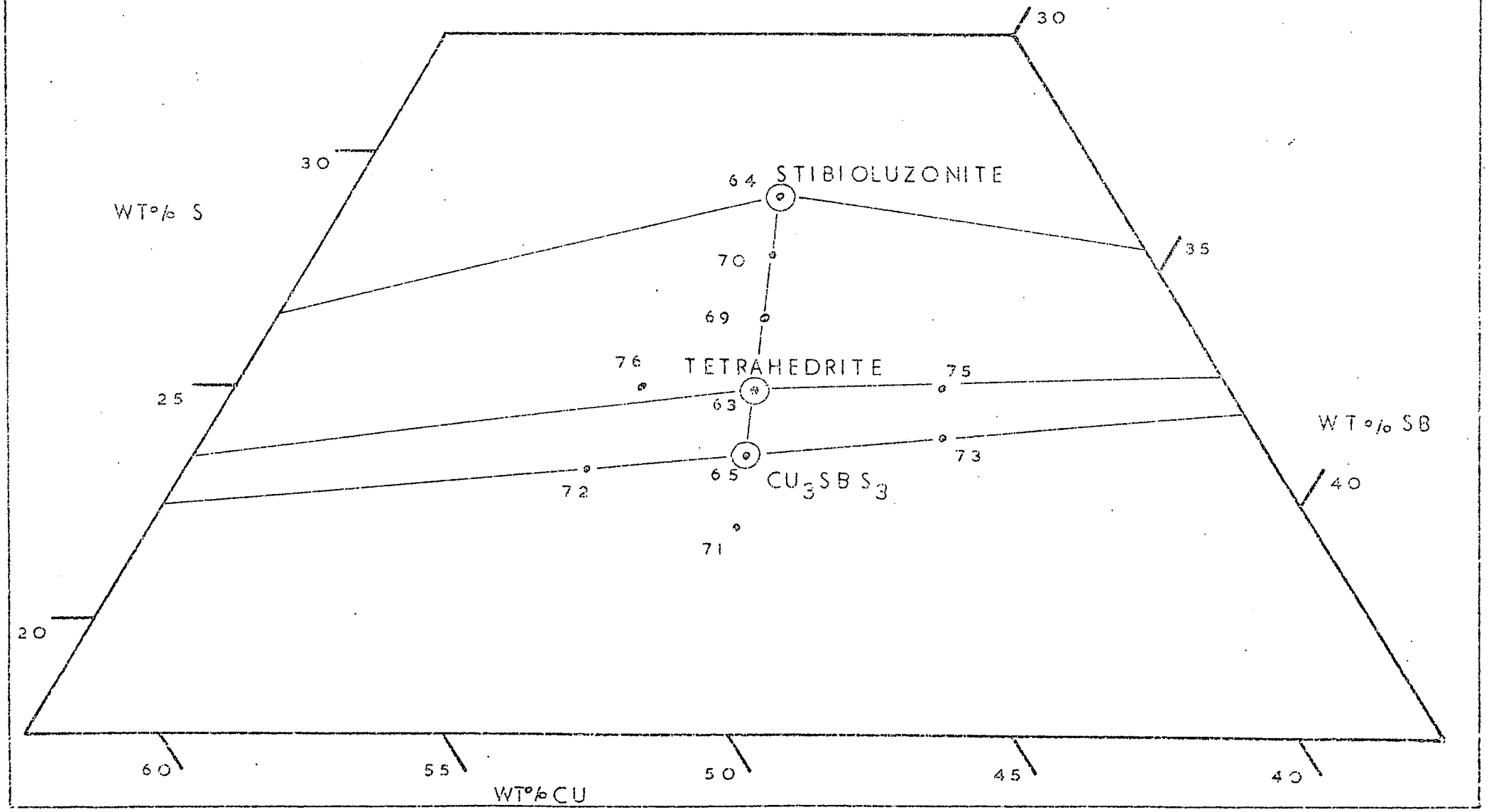

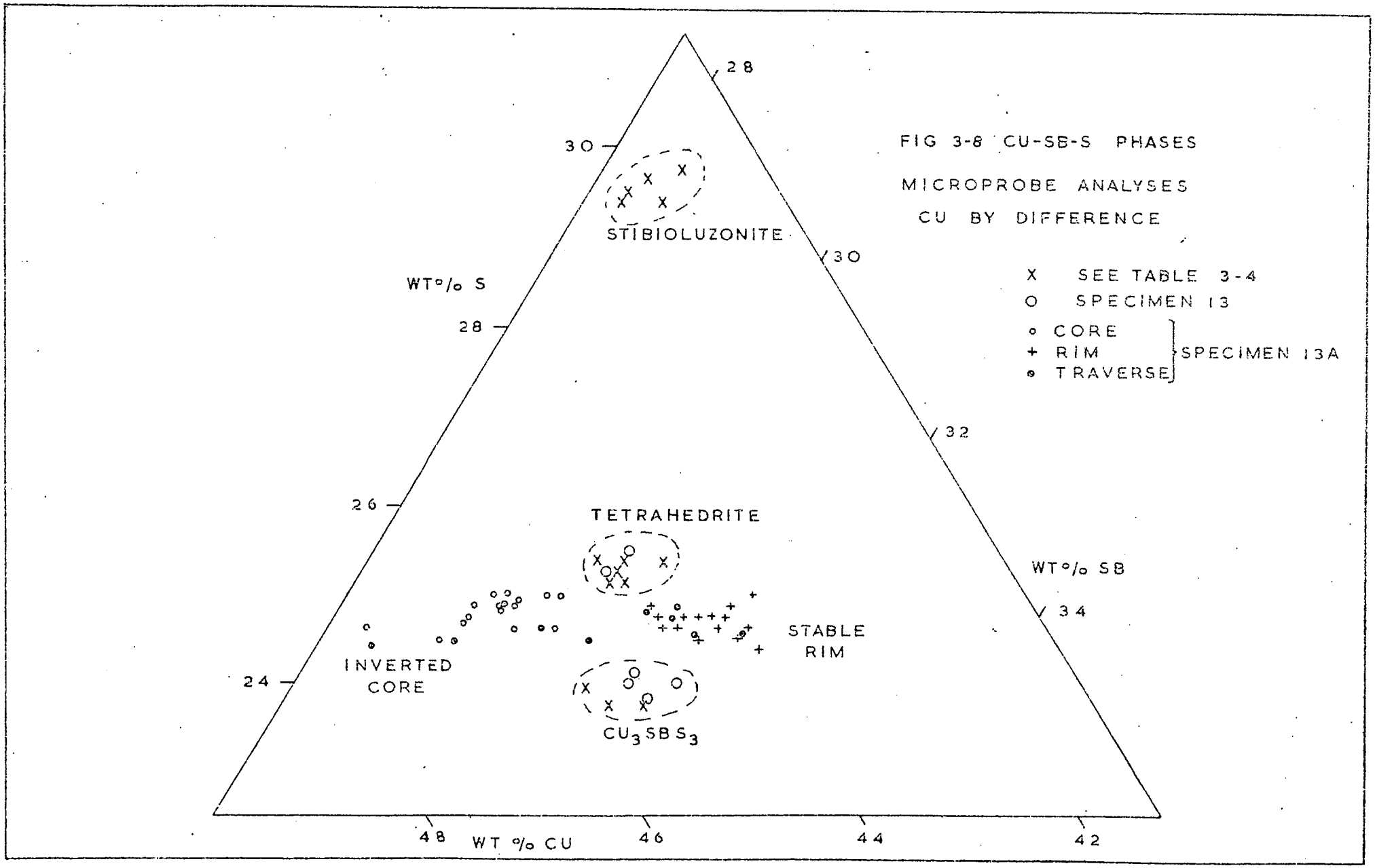

FIG 3-8 CU-SB-S PHASES

MICROPROBE ANALYSES

CU BY DIFFERENCE

X SEE TABLE 3-4

O SPECIMEN 13

∘ CORE
\+ RIM
⊙ TRAVERSE
} SPECIMEN 13A

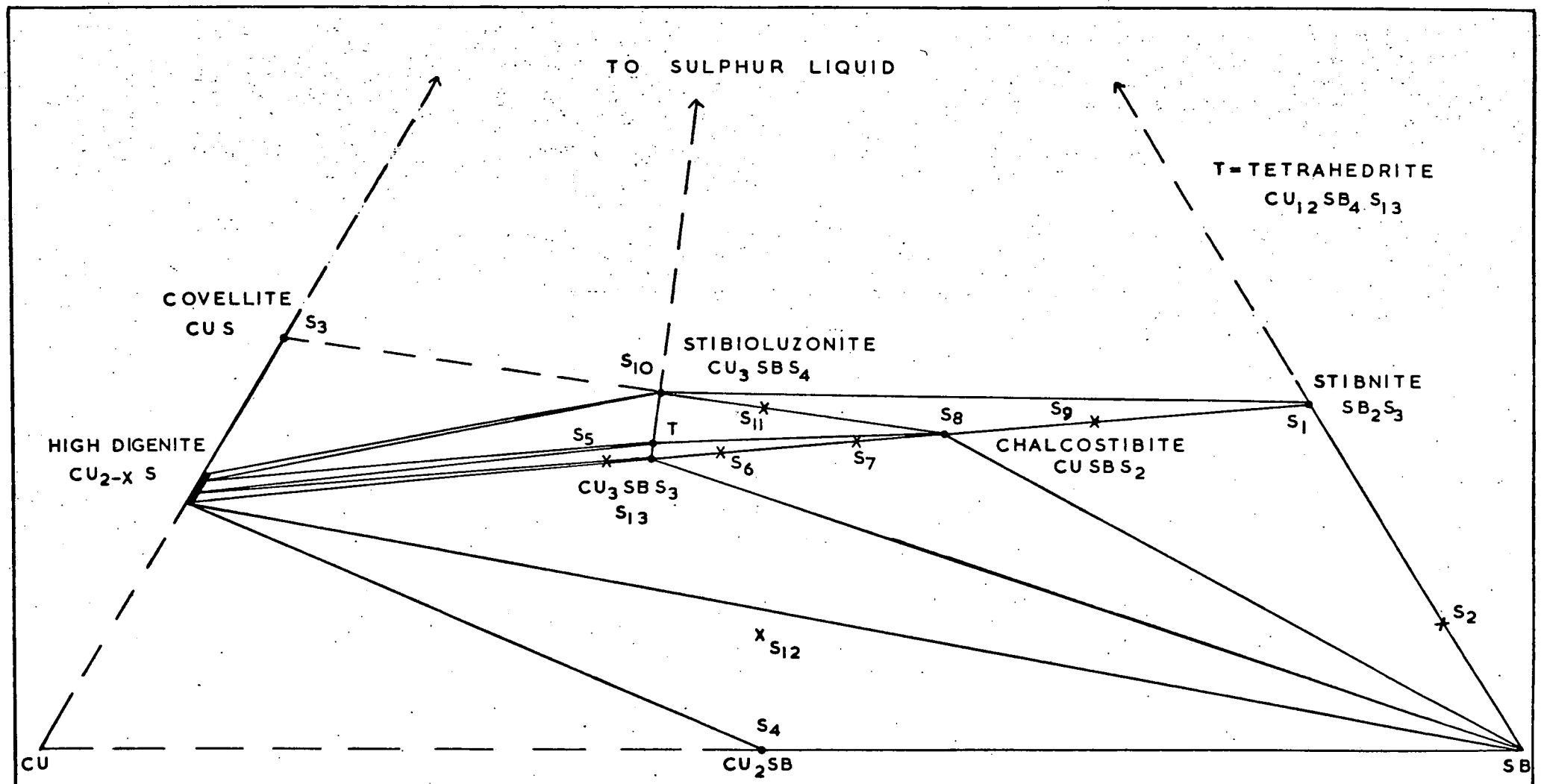

FIG 3-9 TENTATIVE PHASE RELATIONS IN THE CU-SB-S SYSTEM AT 450°C
ALSO LOCALITIES OF SELECTED COMPOSITIONS SYNTHESISED

(WT %)

PLATE 3-1

Spec. No.65 x 220

Skeletal tetrahedrite (dark grey) in Cu_3SbS_3 (grey). Pitting of tetrahedrite indicates structural inversion - fragments lost due to conchoidal fracturing developed as cell size changes (see text).

PLATE 3-2

Spec. No.65 x polars x 220

(As Plate 3-1) Skeletal tetrahedrite (isotropic) in Cu_3SbS_3 (anisotropic).

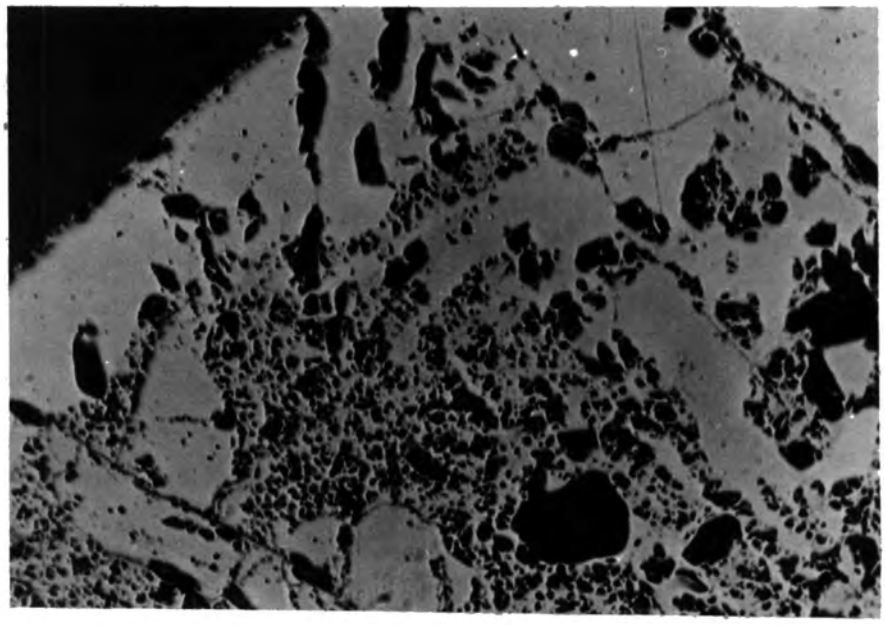

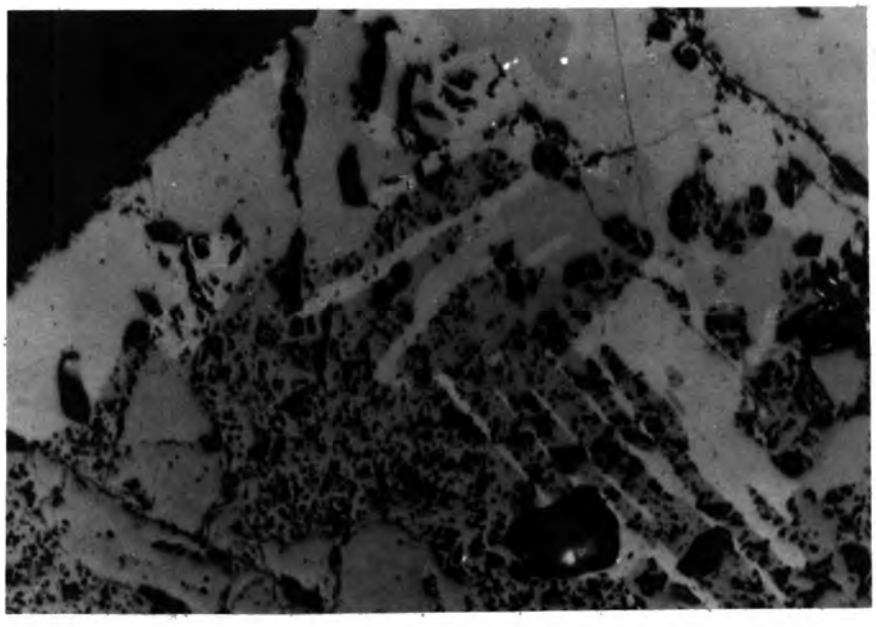

PLATE 3-3

Spec.No.73 x 220

Cu_3SbS_3 (grey) with interstitial chalcostibite, $CuSbS_2$ (light grey) and Sb (white).

PLATE 3-4

Spec.No.73 x polars x 220

(As Plate 3-3) Cu_3SbS_3 (weak anisotropy) with interstitial chalcostibite (strong anisotropy) and Sb.

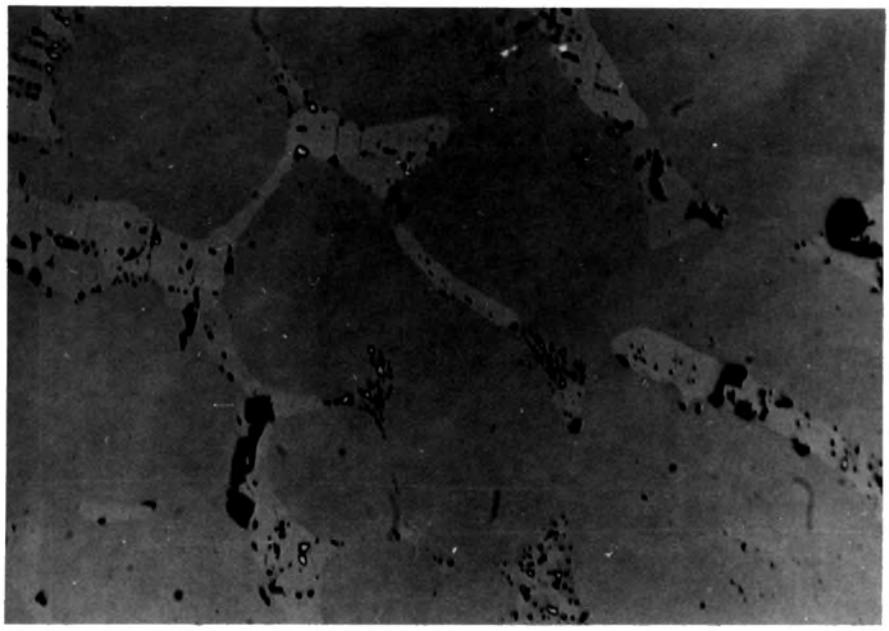

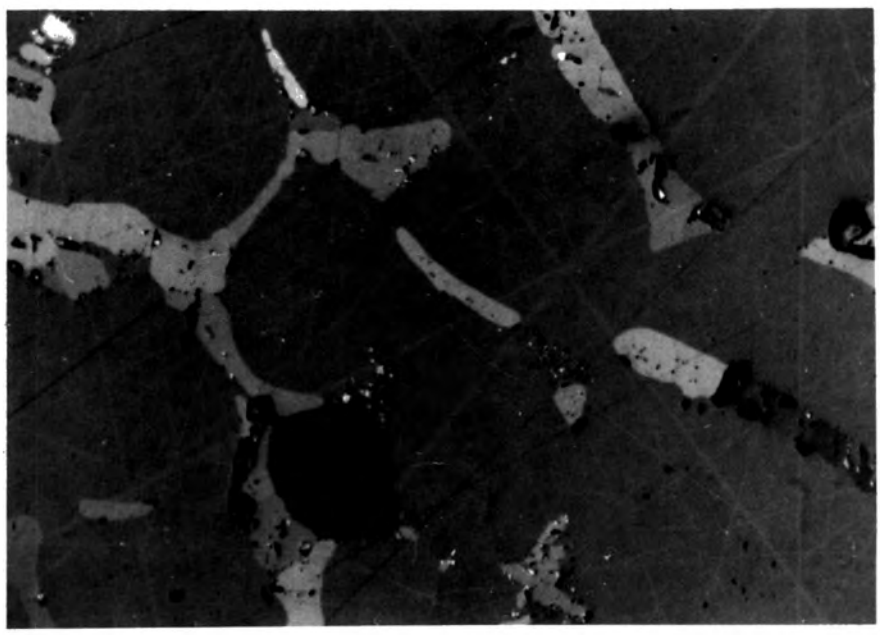

Selected Compositions in the Cu-Sb-S System

During the development of the technique of synthesis and throughout the present work, non-systematic syntheses have contributed to the understanding of phase relations in the Cu-Sb-S system. The locations of the starting compositions are shown in Fig.3-9.

Spec.No. - S1 Plates 3-5, 6

Comp.- Sb_2S_3 Chemicals - High Purity

Significance - Stibnite

Temp. History - Heated to 720°C over 24 hours. Cooled slowly to room temperature over 110 hours.

Result - Large acicular and elongate crystals of stibnite.

Conclusion - Suitable for microprobe standard.

Spec.No. - S2 Plates 3-7, 8

Comp. - Sb_7S_3 Chemicals - Low Purity

Significance - in two liquid field.

Temp. History - Heated to 650°C over 75 hours, maintained for 22 hours, cooled slowly over 50 hours to 620°C then removed.

Result - Two liquid texture. Sb spheroids with minor stibnite, in stibnite with minor Sb.

Sepc.No. -S3

Comp. - CuS Chemicals - High Purity

Temp. History - Heated to 720°C over 24 hours. Cooled slowly to room temperature over 110 hours.

Result - Texturally complex. Small interlocking crystals of covellite with curved lamellae - blaubleibender covellite (?).

Conclusion - Unsuitable as microprobe standard.

Spec.No. - S4

Comp. - Cu_2Sb Chemicals - High Purity

Significance - Possible microprobe standard.

Temp.History - Heated to 720°C over 24 hours. Cooled slowly to room temperature over 110 hours.

Result - Large interlocking crystals of Cu_2Sb, some with very fine lamellae. Interstitial Cu_3Sb (confirmed by microprobe analysis).

Conclusion - Slight range in composition noted on probe therefore limited use as standard.

Spec.No. - S5 Plates 3-9, 10

Comp. - $3.5Cu_2S.Sb_2S_3$ Chemicals - Low Purity

Significance - The tetrahedrite of Cambi and Elli (1965).

Temp. History - Heated to 700°C over 58 hours. Cooled to room temperature over 6 hours.

Result - $Cu_{2-x}S$ dendrites at top of charge (and ovoids at base), in tetrahedrite with interstitial chalcostibite.

Conclusion - Primary crystallisation of $Cu_{2-x}S$.

Spec.No. - S6 Plates 3-11, 12

Comp. - $Cu_7Sb_3S_8$ Chemicals - Low Purity

Significance - Close to tetrahedrite on Cu_2S - Sb_2S_3 join.

Temp. History - Heated to 595°C over 48 hours, maintained for 18 hours, cooled slowly over 6 hours to 550°C then removed.

Result - Isolated euhedral stibioluzonite rimmed by tetra-

hedrite. Tetrahedrite interstitial with chalcostibite. Euhedral tetrahedrite, with rim of tetrahedrite-chalcostibite intergrowth, in Cu_3SbS_3. Anisotropic subhedral Cu_3SbS_3. Compositions confirmed by microprobe analysis.

Conclusion - The phase relations in this part of the diagram are more complex than indicated by Cambi and Elli (1965).

Spec.No. - S7 Plate 3-13

Comp. - $Cu_{1.175}Sb_{0.825}S_{1.825}$ Chemicals - Low Purity

Significance - Chalcostibite-tetrahedrite eutectic (Cambi and Elli 1965)

Temp. History - Heated to 560°C over 30 hours, maintained for 116 hours, cooled slowly over 4 hours to 500°C then removed.

Result - Eutectic intergrowth of tetrahedrite and chalcostibite. Cu_3SbS_3 also present (anisotropic).

Conclusion - Tetrahedrite and anisotropic Cu_3SbS_3 are difficult to distinguish when intergrown with chalcostibite. This eutectic involves more phases than observed by Cambi and Elli (1965).

Spec.No. - S8 Plate 3-14

Comp.- $CuSbS_2$ Chemicals - Low Purity

Significance - Chalcostibite

Temp. History - Heated to 580°C over 70 hours, maintained for 28 hours, cooled slowly over 74 hours to 510°C then removed.

Result - Large subhedral chalcostibite crystals with interstitial stibnite and some stibioluzonite.

Conclusion - Confirms the congruent melting of chalcostibite. Slower cooling across the melting point required in order to obtain larger crystals.

Spec.No. - S9 Plates 3-15, 16

Comp. - $Cu_2Sb_4S_7$ Chemicals - Low Purity

Significance - The chalcostibite-stibnite eutectic of Cambi and Elli (1965).

Temp. History - Heated to 580°C over 70 hours, maintained for 28 hours, cooled slowly over 74 hours to 510°C then removed.

Result - Acicular dendritic chalcostibite with ophitic interstitial stibnite.

Conclusion - Confirms the chalcostibite-stibnite eutectic.

Spec.No. - S10 Plates 3-17, 18

Comp. - Cu_3SbS_4 Chemicals - Low Purity

Significance - Stibioluzonite.

Temp. History - Heated to 600°C over 12 hours. Maintained for 13 hours, cooled slowly over 7 hours to 380°C then removed.

Result - Mainly large stibioluzonite crystals in mutual boundary texture with large subhedral tetrahedrite crystals. Interstitial chalcostibite.

Conclusion - Co-existence of stibioluzonite - tetrahedrite - chalcostibite established. Temperature history unsatisfactory for monophasal tetrahedrite.

Spec.No. - S11 Plates 3-19, 20

Comp. - Cu_2SbS_3 Chemicals - Low Purity

Significance - On the stibioluzonite-chalcostibite join.

Temp. History - Heated to 606°C over 49 hours, maintained for 17 hours, cooled slowly over 27 hours to 538°C then removed.

Result - Subhedral to euhedral proeutectic stibioluzonite crystals with anhedral chalcostibite in a ternary eutectic of stibioluzonite + chalcostibite + stibnite. Scarce small euhedral Cu_2Sb crystals in the intergrowth.

Conclusion - The stibioluzonite-chalcostibite and stibioluzonite-stibnite tie lines and the eutectic nature of stibioluzonite-chalcostibite-stibnite confirmed.

Spec.No. - S12 Plates 3-21, 22

Comp. - $Cu_2SbS_{0.8}$ Chemicals - Low Purity

Significance - Between the two two-liquid fields of Guertler and Meissner (1921).

Temp. History - Heated to 740°C over 48 hours, maintained for 48 hours, cooled slowly to 260°C over 96 hours then removed.

Result - The specimen separated into two portions - dark grey granular material (mainly Cu_2S with interstitial Sb and Cu_2Sb + Sb) and bright metallic spheroids (primary Sb with interstitial Cu_2Sb + Sb eutectic intergrowth).

Conclusion - in the condensed Cu-Sb-S system the two two-liquid field probably extends across the diagram from the Cu-S to the Sb-S binary. The Cu_2S-Sb and Cu_2S-Cu_2Sb tie lines were established.

Spec.No. - S13 Plate 3-23

Comp. - Cu_3SbS_3 ($Cu_{12}Sb_4S_{12}$) Chemicals - Low Purity

Significance - Tetrahedrite without the '13th' sulphur atom.

Temp. History - Heated to 600°C over 45 hours, maintained for 25 hours, cooled slowly over 25 hours to 570°C then removed.

Result - Interlocking crystals of anisotropic Cu_3SbS_3(90%). Some crystals with inversion twinning. Interstitial chalcostibite. Euhedral tetrahedrite, interstitial and included by Cu_3SbS_3, rimmed by tetrahedrite + chalcostibite intergrowth which is replacing(?) Cu_3SbS_3. Microprobe analyses, Fig.3-8, confirm Cu_3SbS_3 and euhedral tetrahedrite, $Cu_{12}Sb_4S_{13}$. Powder photograph data of Cu_3SbS_3 are given in Table 3-6. The diffraction lines were indexed by comparison with wittichenite and the cell parameters were obtained using COHEN -

a_o = 7.782Å stnd. dev. 0.026Å

b_o = 10.344Å stnd. dev. 0.030Å

c_o = 6.672Å stnd. dev. 0.021Å

Conclusion - Cu_3SbS_3 is a distinct non-cubic phase possibly with a high temperature polymorph.

Spec.No. - S13a Plates 3-24, 25, 26

Comp. Reground S13 (Cu_3SbS_3)

Temp. History - Heated to 625°C over 43 hours, maintained for 25 hours, cooled slowly over 5 hours to 585°C, then removed.

Result - Skeletal tetrahedrite with interstitial chalcostibite and Sb. The tetrahedrite cores are bluish (isotropic) and the rims increasingly pinkish

(isotropic). The tetrahedrite cores are conchoidally fractured. Polishing scratch marks have caused inversion from the pink to the blue phase with the development of conchoidal fractures. There is an increase in stability in the pinkish phase towards the margin of the crystal. The metastability of the pink phase is demonstrated by inversion induced by diamond indentation (Plates 3-25, 26).

Microprobe analyses of the blue cores, the pink rims and a traverse from core to rim, for Sb and S (computing Cu by difference using TIM) have been plotted in Fig.3-8. Microprobe analyses of tetrahedrite, stibioluzonite and Cu_3SbS_3 (synthesised in the study of the central portion of the Cu-Sb-S system), and, Cu_3SbS_3 and tetrahedrite in S13, using the same technique of analyses are also plotted in Fig.3-8. All analyses are Cu deficient with respect to the stoichiometric compositions but the compositional relationship of the phases remains. This technique was employed for the zoned tetrahedrite because the precision was found to be greater when Cu was not determined.

Specimens of the inverted blue cores and stable pink rims were picked out from the polished specimen and powder photographs obtained (Table 3-7).

Conclusion - Cu_3SbS_3 melts incongruently to a non-stoichiometric tetrahedrite which has a range in composition and is sulphur deficient relative to normal tetrahedrite, $Cu_{12}Sb_4S_{13}$. Non-stoichiometric tetrahedrite co-exists with chalcostibite + Sb indicating a

change in tie lines in the Cu-Sb-S system above about 600°C. The blue cores of non-stoichiometric tetrahedrite are Cu rich and the pink rims Sb rich. The approximate corrected formulae of the two end-members of the series obtained by projecting the compositions in Fig.3-8 towards Cu are $Cu_{12.12}Sb_{3.34}S_{13}$ to $Cu_{13.04}Sb_{3.86}S_{13}$.

There are high and low temperature polymorphs of non-stoichiometric tetrahedrite. Cu rich members invert readily and the low temperature polymorph has a cell size of 10.3196Å, stnd. err. 0.0006. With increasing Sb content, stability increases, and the Sb end-member high temperature polymorph has a cell edge of 10.428Å stnd. err. 0.012. The powder pattern of the Cu rich member, low temperature polymorph is indistinguishable from that of normal tetrahedrite. Only poor films with impurity lines could be obtained for the Sb rich phase.

PLATE 3-5

Spec.No.S1 x 3

Acicular crystals of stibnite, Sb_2S_3.

(True colour is grey with metallic lustre).

PLATE 3-6

Spec.No.S1 x 220

Stibnite, Sb_2S_3. Note strong bireflectance. Deformation of crystals has resulted in curved cleavage traces.

PLATE 3-7

Spec.No.S2 x 220

Two liquid texture. Spheroids of Sb (white) with stibnite, Sb_2S_3 (grey) in stibnite (grey) with Sb.

PLATE 3-8

Spec.No.S2 (Oil) x 1340

(As Plate 3-7) Two liquid texture. Sb (white) with stibnite (grey) in stibnite (grey) with Sb.

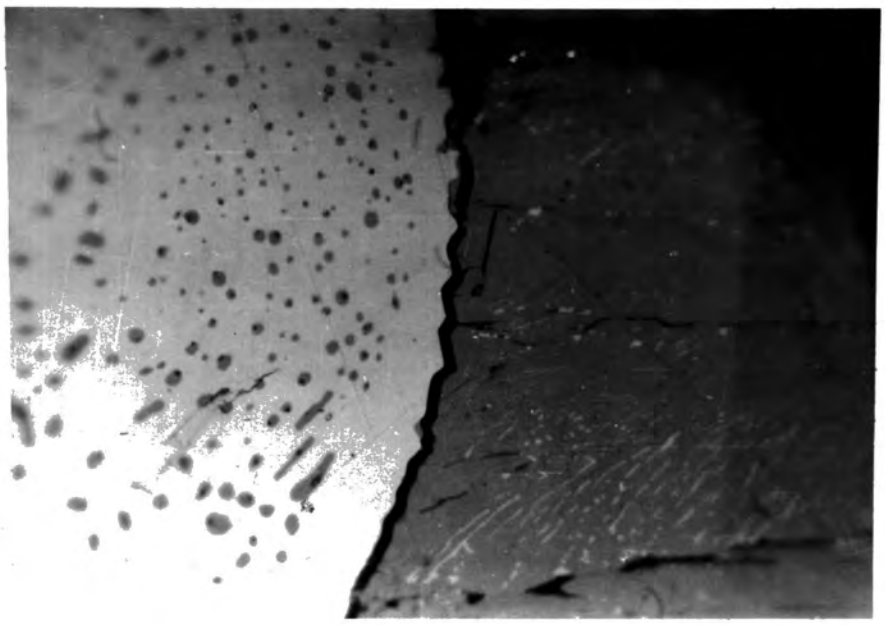

PLATE 3-9

Spec.No.S5 x 220

Top of specimen. Cu_{2-x} dendrites (two phase, dark grey and grey) in tetrahedrite (grey) with interstitial chalcostibite (light grey).

PLATE 3-10

Spec.No.S5 x 220

Base of specimen. $Cu_{2-x}S$ spheroids in tetrahedrite with interstitial chalcostibite.

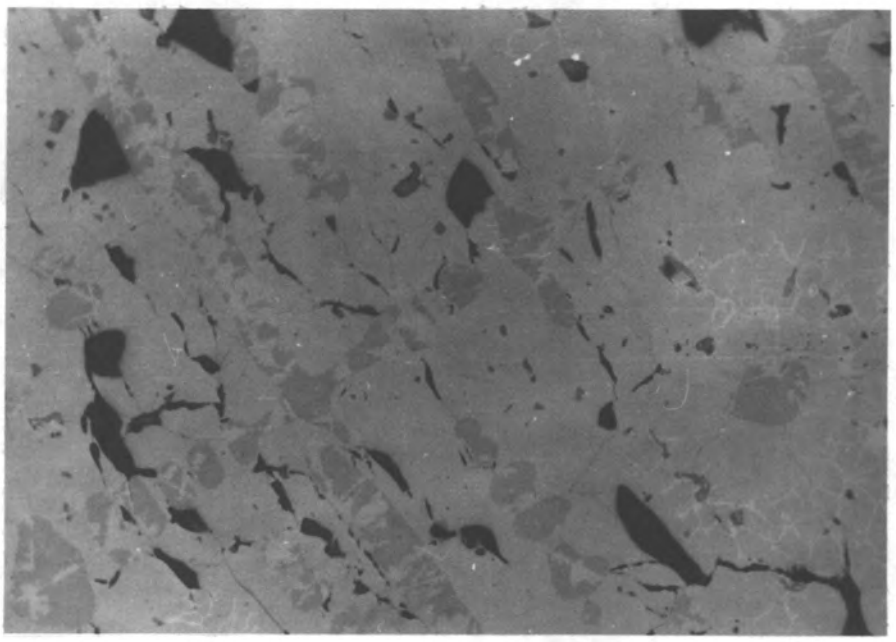

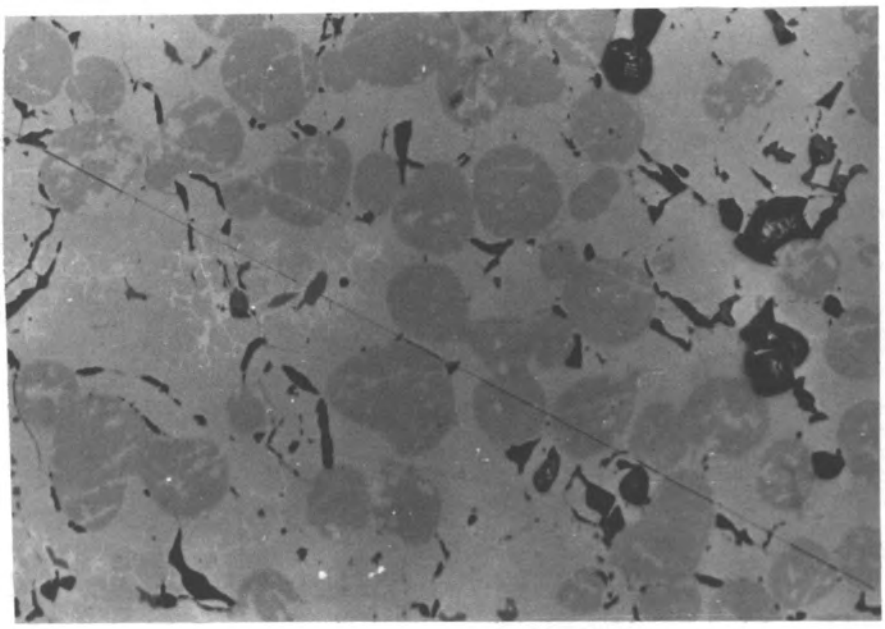

PLATE 3-11

Spec.No.S6 x 220

Stibioluzonite Cu_3SbS_4, twin (reddish brown). Euhedral tetrahedrite, $Cu_{12}Sb_4S_{13}$ (brown). Cu_3SbS_3 (grey). Interstitial chalcostibite, $CuSbS_2$ (light grey). Note narrow rim of tetrahedrite around stibioluzonite. Note tetrahedrite + chalcostibite intergrowth, often around euhedral tetrahedrite, replacing Cu_3SbS_3.

PLATE 3-12

Spec.No.S6 x Polars x 220

(As Plate 3-11) Stibioluzonite strongly anisotropic. Tetrahedrite isotropic. Cu_3SbS_3 weakly anisotropic, red internal reflections. Chalcostibite strongly anisotropic.

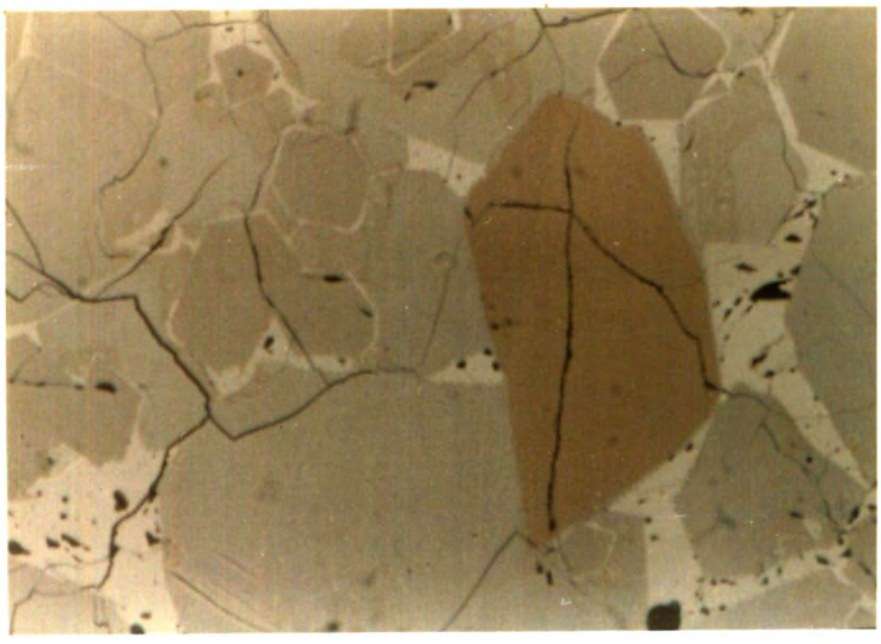

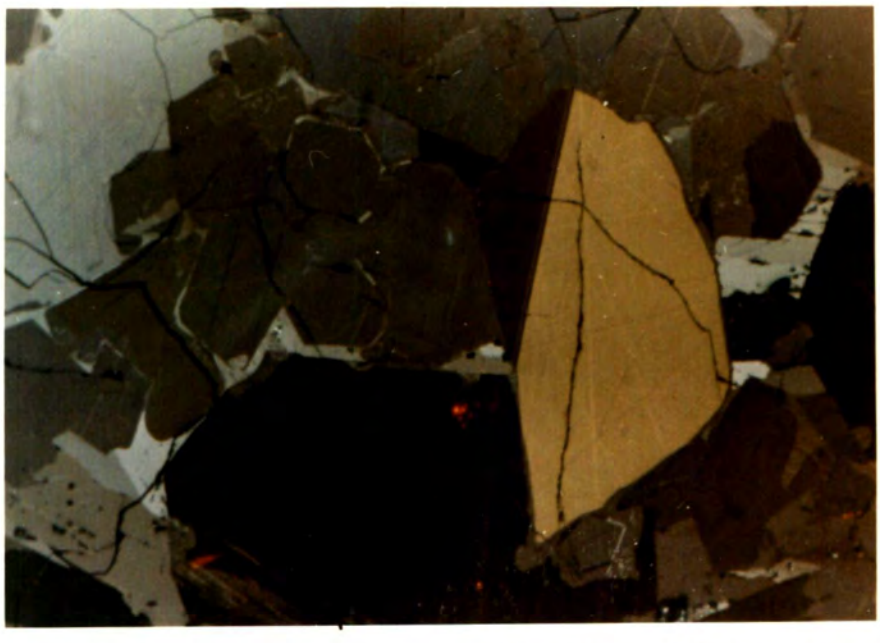

PLATE 3-13

Spec.No.S7 x Polars x 220

Eutectic intergrowth of tetrahedrite (isotropic) and chalcostibite (strongly anisotropic). Note optical continuity of chalcostibite.

PLATE 3-14

Spec.No.S8 x Polars x 220

Chalcostibite (dark grey, anisotropic) with interstitial stibnite (light grey, strongly anisotropic) and stibioluzonite (dark grey, anisotropic).

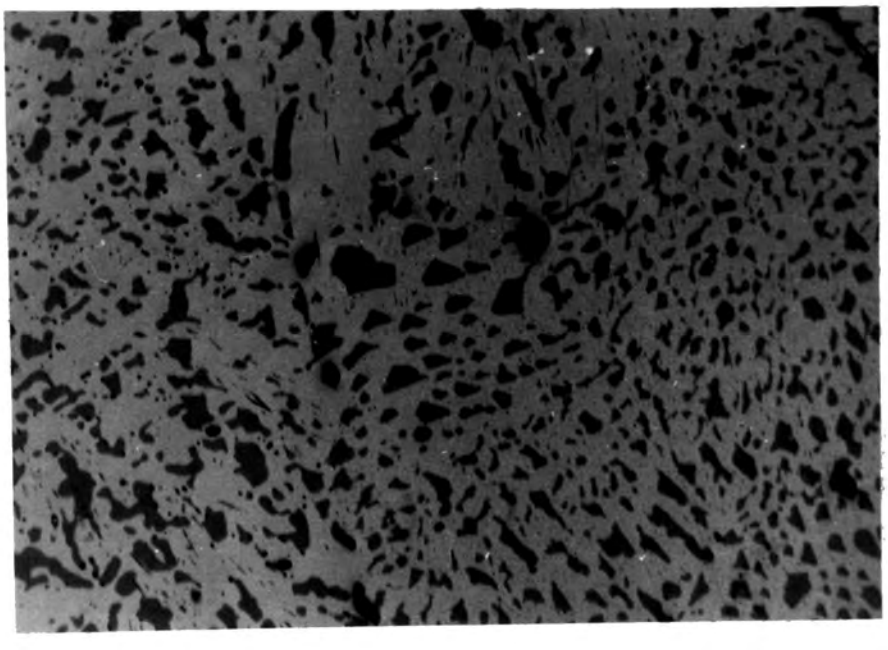

PLATE 3-15

Spec.No.S9 x 220

The chalcostibite - stibnite eutectic. Proeutectic dendritic chalcostibite (dark grey) with interstitial patches of stibnite (grey).

PLATE 3-16

Spec.No.S9 x polars x 220

(As Plate 3-15). Dendritic chalcostibite (anisotropic). Stibnite patches (strongly anisotropic).

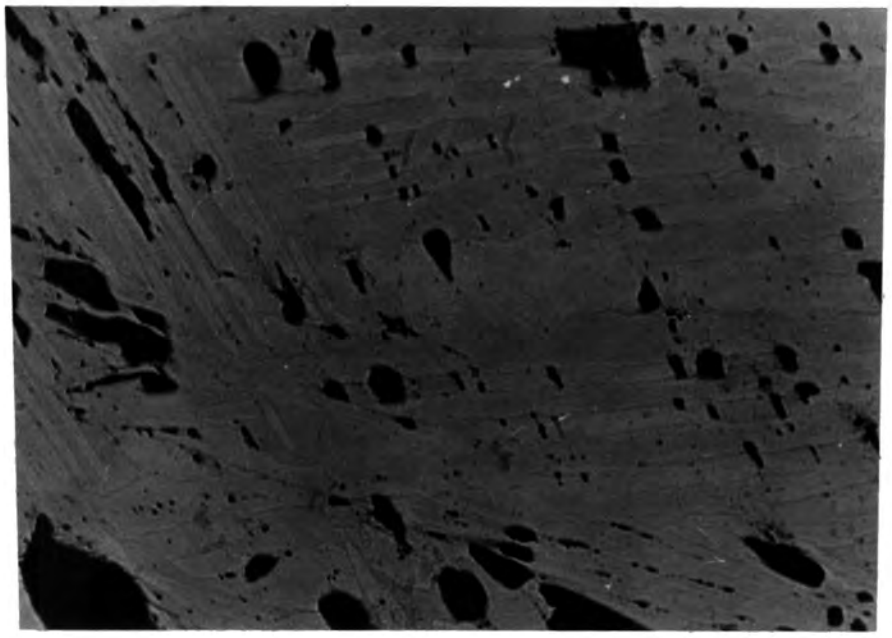

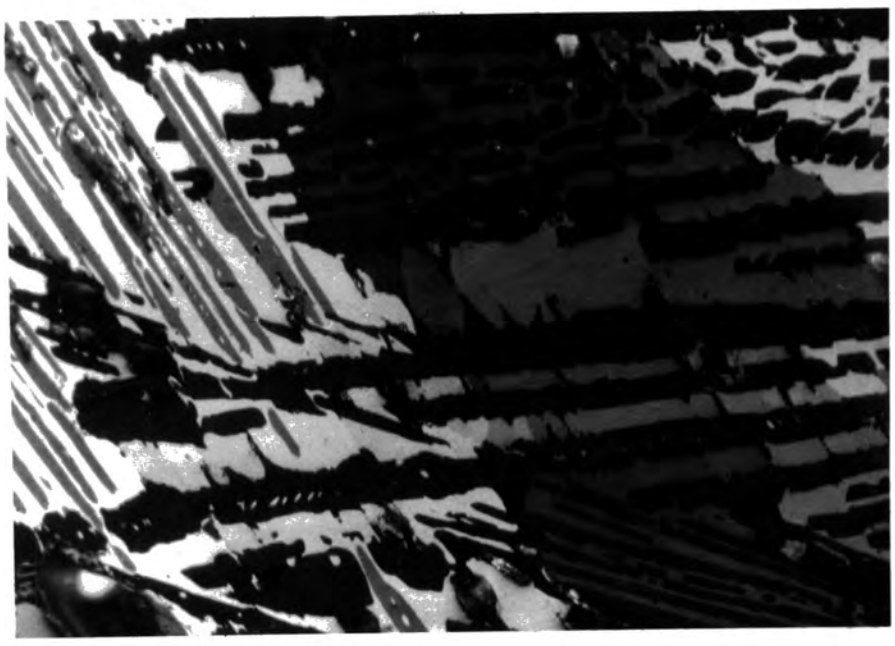

PLATE 3-17

Spec.No.S10 low x 220

Co-existing stibioluzonite, Cu_3SbS_4 (dark grey), tetrahedrite, $Cu_{12}Sb_4S_{13}$ (grey) and chalcostibite, $CuSbS_2$ (light grey). Mutual boundary texture.

PLATE 3-18

Spec.No.S10 x 540

(As Plate 3-17). Note three phase intergrowths indicating stibioluzonite - tetrahedrite-chalcostibite ternary eutectic.

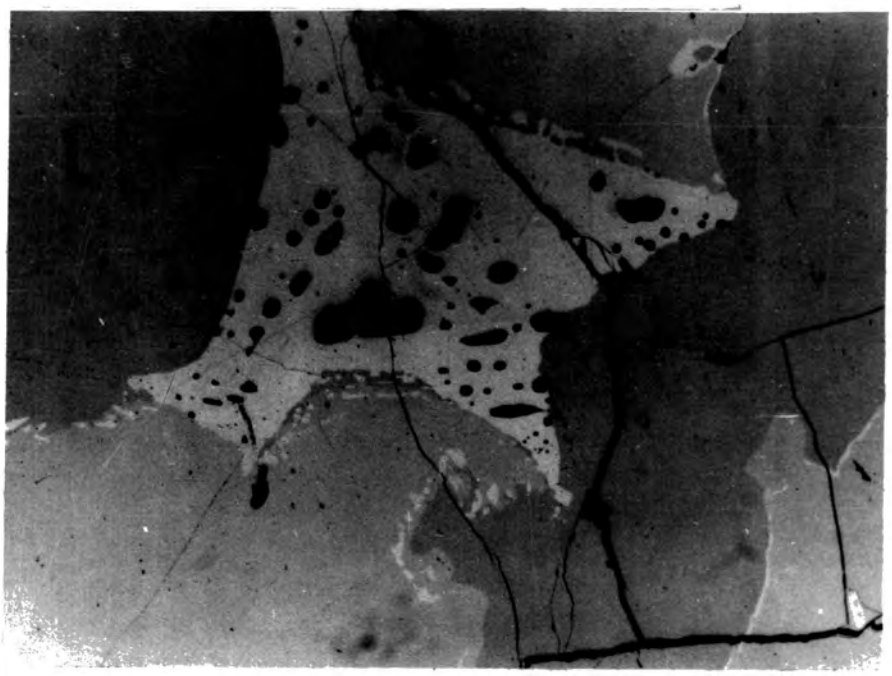

PLATE 3-19

Spec.No.S11 x 220

Euhedral twinned stibioluzonite (pinkish brown) in chalcostibite (white).

PLATE 3-20

Spec.No.S11 x Polars x 220

(As Plate 3-19) stibioluzonite, strongly anisotropic (yellow brown) in chalcostibite, strongly anisotropic (grey blue).

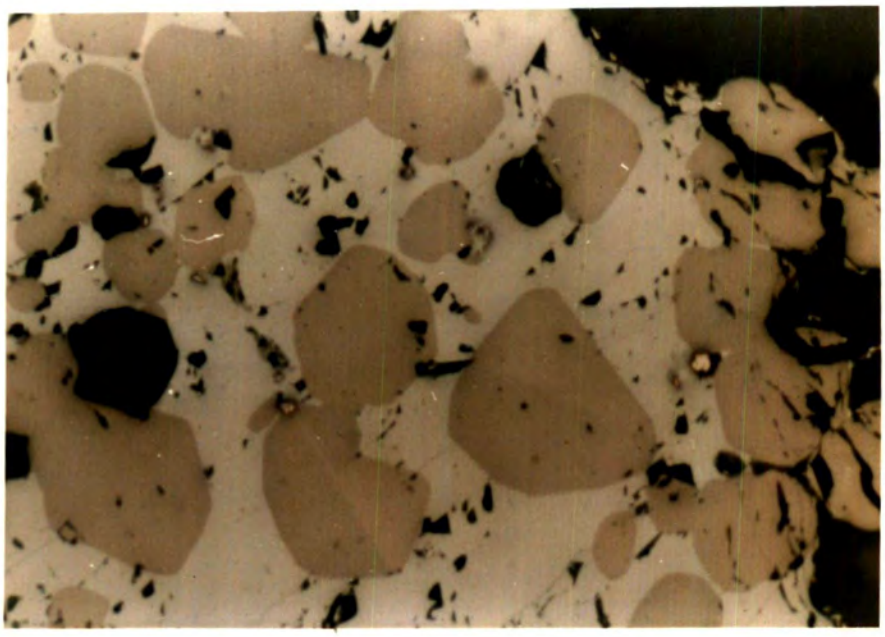

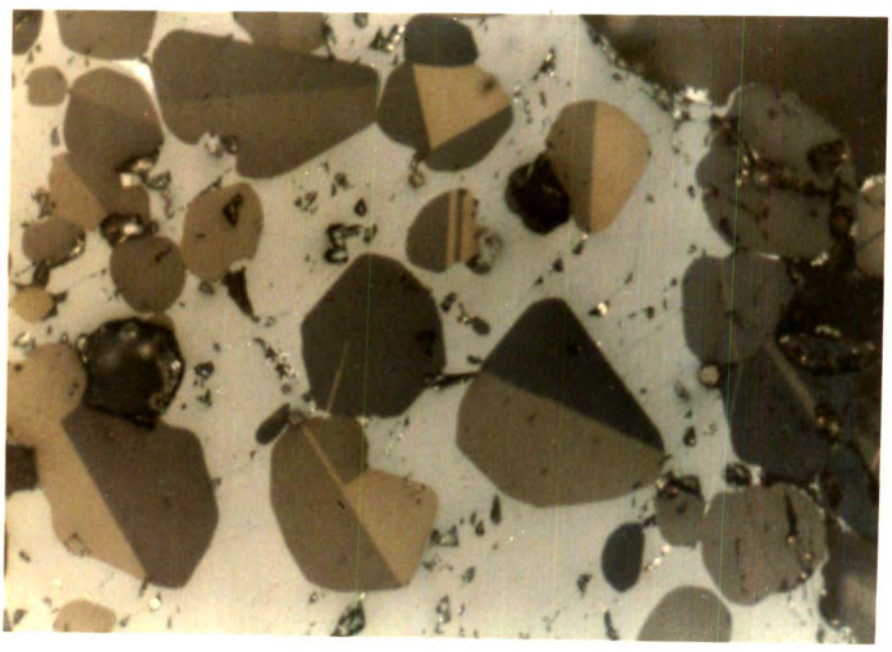

PLATE 3-21

Spec.No.S12 x 220

Contact of granular material - chalcocite, Cu_2S (dark grey) with metallic spheroid - primary Sb (light grey) with interstitial eutectic intergrowth of Sb (light grey) and Cu_2Sb (grey).

PLATE 3-22

Spec.No.S12 x 220

Metallic spheroid. Primary Sb (light grey). Eutectic colony of Sb + Cu_2Sb (grey). Note increase in grain size outwards from centre of colony.

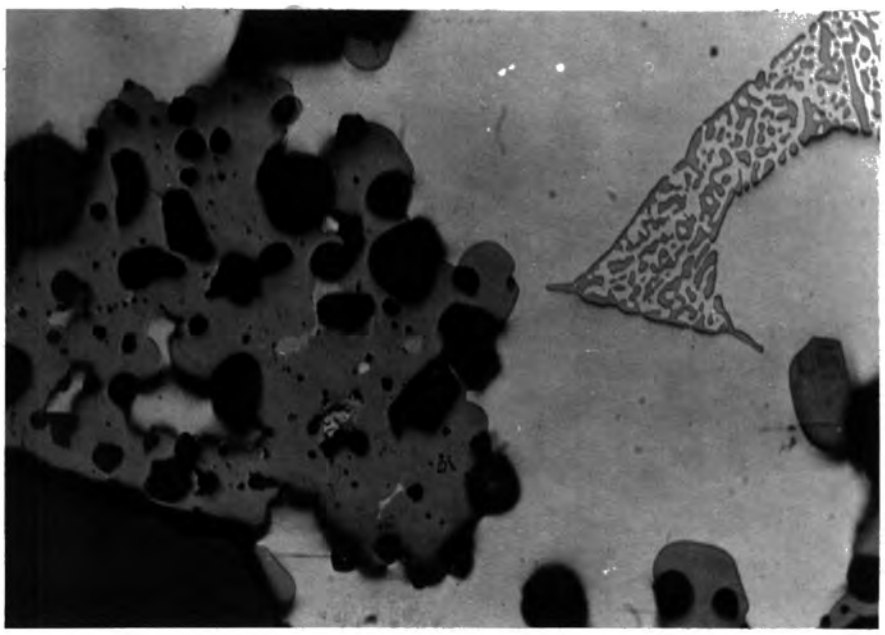

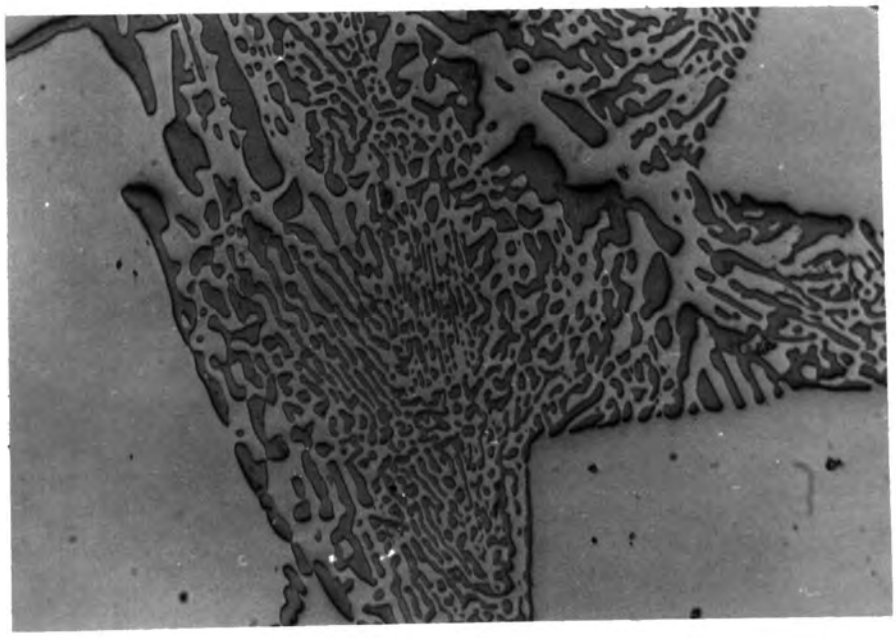

PLATE 3-23

Spec.No.S13 (oil) x 1340

Euhedral tetrahedrite (dark grey) rimmed by chalcostibite (light grey) and a fine tetrahedrite + chalcostibite intergrowth in Cu_3SbS_3 (grey).

PLATE 3-24

Spec.No.S13a x 220

Skeletal zoned non-stoichiometric tetrahedrite (grey) with interstitial chalcostibite (light grey) and Sb (small black grains). Cores of tetrahedrite have inverted causing fractures and pitting.

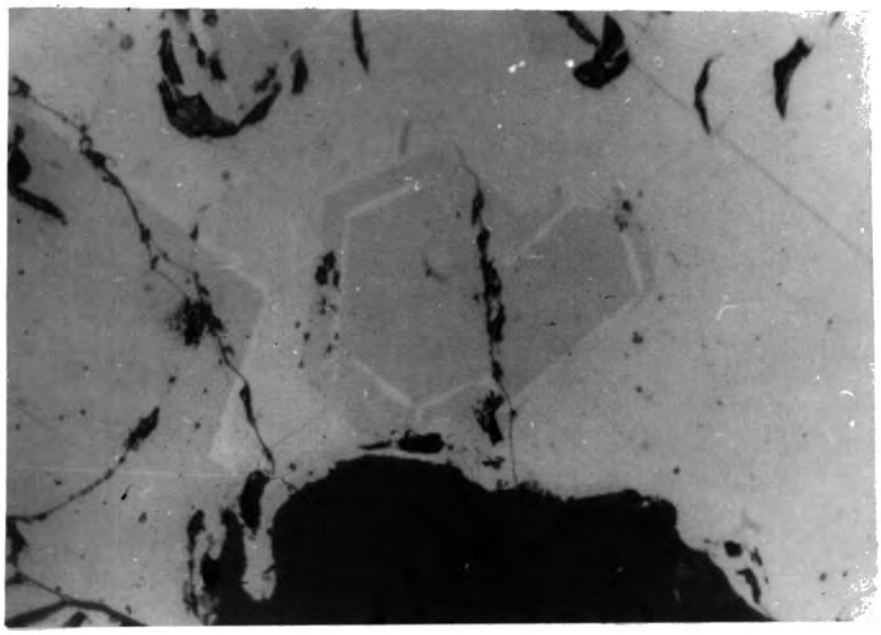

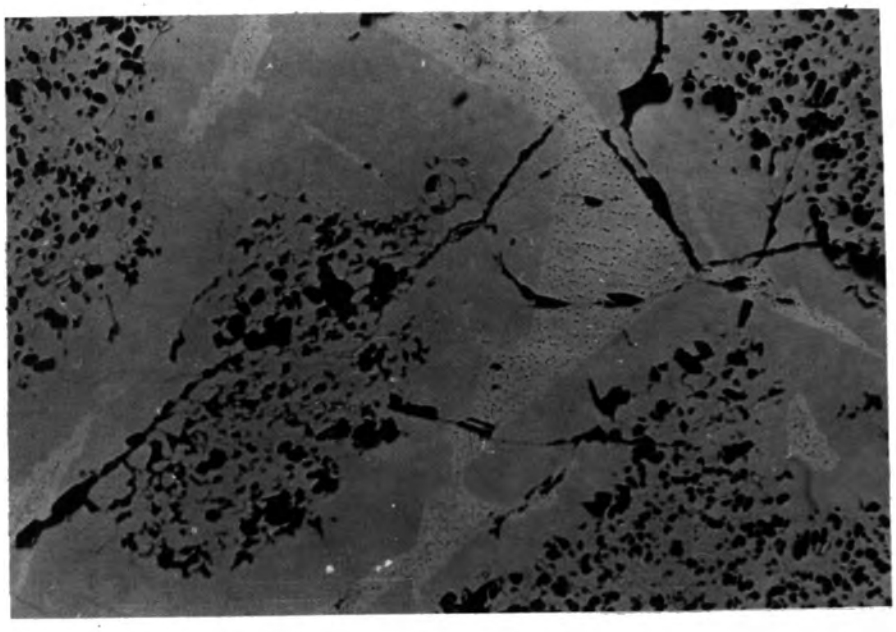

PLATE 3-25

Spec.No.S13a x 220

Zoned non-stoichiometric tetrahedrite with interstitial chalcostibite (white). Cu rich tetrahedrite has inverted to the blue polymorph. Pink Sb richer tetrahedrite is metastable and diamond microhardness indentation has caused inversion.

PLATE 3-26

Spec.No.S13a (oil) x 1340

Note conchoidal fracturing due to unit cell contraction in blue tetrahedrite. Diamond indentation causes inversion from the pink to the blue polymorph - note the increase in stability of the pink tetrahedrite towards the crystal margin.

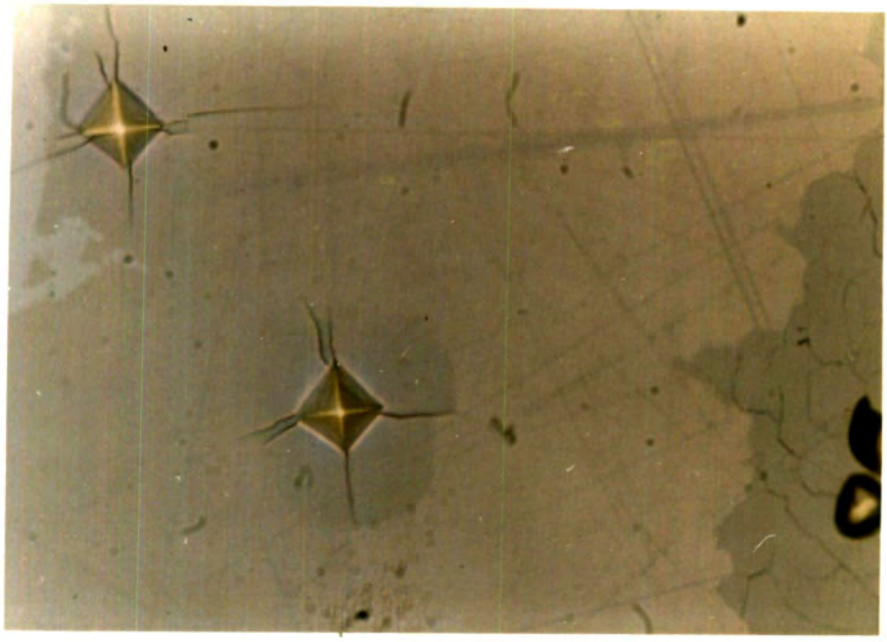

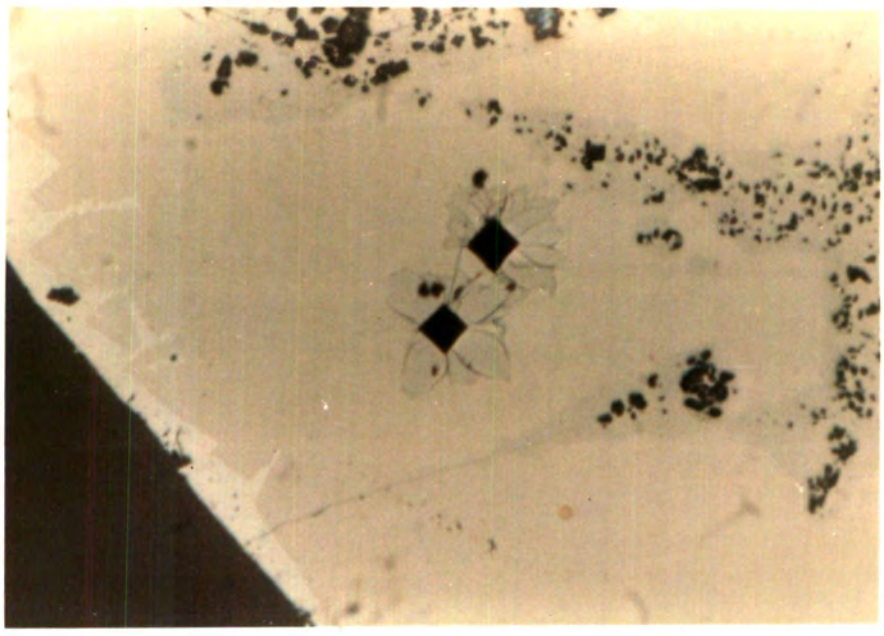

PLATE 3-27

x 220

Dendrite of $Cu_{2-x}S$ (two phases, blue and pale blue) rimmed by stibioluzonite, Cu_3SbS_4 (pinkish brown) in tetrahedrite, $Cu_{12}Sb_4S_{13}$ (brownish grey). Obtained from $Cu_{12}Sb_4S_{13}$ composition melt.

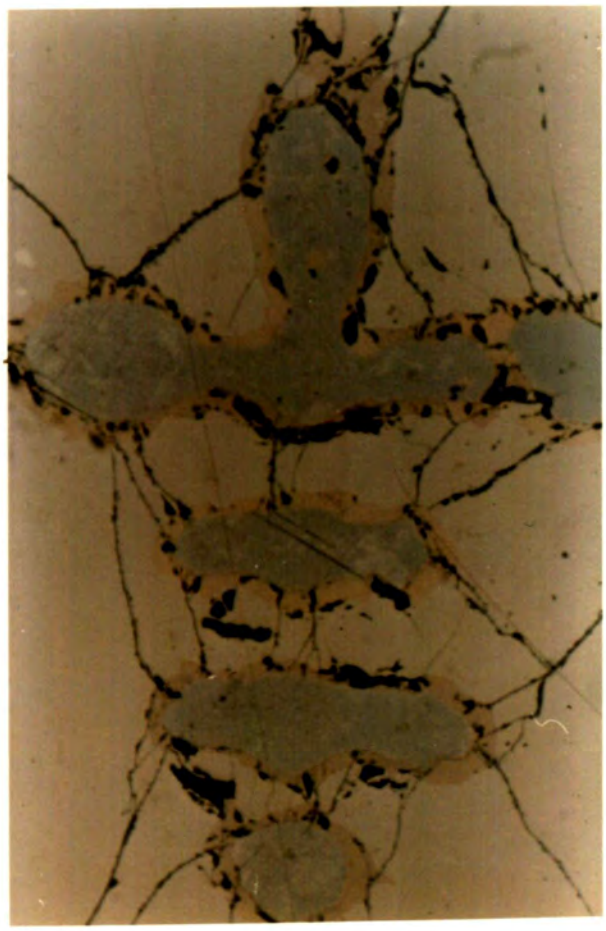

Cu-Sb-S System - Ternary Phases

Appearance in Polished Specimen and X-ray Diffraction Data

Tetrahedrite, $Cu_{12}Sb_4S_{13}$

Tetrahedrite appeared brownish-grey against other Cu-Sb-S phases. It was usually isotropic but occasionally had a very weak anisotropy. Symmetrical six-sided sections were typical. Tetrahedrite readily formed euhedral or skeletal crystals when there was interstitial melt. No cleavage traces were observed and fracturing tended to be conchoidal.

Microprobe analysis of tetrahedrite (spec. 63) is given in Table 3-5. The formula derived from the analysis is $Cu_{12.18}Sb_{4.05}S_{13}$.

X-ray diffraction data from powder photographs (spec. 63) are given in Table 3-8. The cubic unit cell edge, obtained using selected high angle lines in NELRIL (Chapter 2), is $a_o = 10.31907\text{Å}$ stnd. err. 0.00048.

This is the 'normal tetrahedrite' obtained in most of the experiments.

Stibioluzonite, Cu_3SbS_4

In polished specimen stibioluzonite appeared strongly coloured brownish-pink, strongly bireflecting and strongly anisotropic (yellow-brown or bronze). Rounded subhedral crystals were common but sometimes laths were developed. Growth twinning was common and was usually simple. No colour zoning nor cleavage traces were observed.

Microprobe analysis of stibioluzonite (spec. 64) is given in Table 3-5. The formula derived from the analysis is $Cu_{3.03}Sb_{1.02}S_4$.

X-ray diffraction data from powder photographs (spec.64) are listed in Table 3-9. The tetragonal cell parameters obtained using COHEN (Chapter 2) are -

a_o = 5.38305Å stnd.dev. = 0.00040

c_o = 10.76594Å stnd.dev. = 0.00124

Chalcostibite, $CuSbS_2$

Chalcostibite was prepared, using high purity chemicals, by slow cooling from the melt.

In polished specimen chalcostibite appeared cream or greyish-white, was strongly bireflecting and strongly anisotropic (greys and blues). Platy crystals were typical.

X-ray diffraction data from powder photographs are given in Table 3-10. The orthorhombic unit cell parameters obtained using COHEN (Chapter 2) are -

a_o = 6.01600Å stnd. dev. = 0.00538

b_o = 14.50545Å stnd. dev. = 0.01112

c_o = 3.80001Å stnd. dev. = 0.00234

Cu_3SbS_3

In polished specimen Cu_3SbS_3 was pinkish grey, weakly bireflecting and weakly anisotropic (dark greys). Against chalcostibite, Cu_3SbS_3 appeared pink and resembled tetrahedrite. Strong blood-red internal reflections were typical. Inversion twinning was observed occasionally. Polishing scratch marks were yellowish on the grey surface. The crystals commonly occurred as laths or as a matrix of interlocking crystals. Orientated rods and blebs of Cu_2S and $Cu_{2-x}S$ in Cu_3SbS_3 have been observed and indicated a high temperature range in composition towards $Cu_{2-x}S$.

Microprobe analysis of Cu_3SbS_3 (spec. 65) is given in Table 3-5. The formula derived from the analysis is - $Cu_{2.99}Sb_{1.01}S_{3.00}$.

Powder photographs were obtained and the diffraction data are listed in Table 3-11. The orthorhombic unit cell parameters obtained using COHEN (Chapter 2) are -

a_o = 7.67291Å stnd. dev. = 0.00547
b_o = 10.34198Å stnd. dev. = 0.00893
c_o = 6.69280Å stnd. dev. = 0.00762

Cu_3SbS_3, specimen 13 (Table 3-6) was cooled more slowly than Cu_3SbS_3, specimen 65 (Table 3-11) and this may account for the better 'fit' of spec.13 to the wittichenite structure (Table 3-6). The cell parameters of wittichenite, spec.13 and spec.65 are given for comparison in Table 3-13.

Non-Stoichiometric Tetrahedrite

Non-stoichiometric tetrahedrite exhibits a range in composition and high and low temperature polymorphism.

By melting Cu_3SbS_3 (spec. 13) zoned tetrahedrites were obtained ranging in composition from $Cu_{13.04}Sb_{3.86}S_{13}$ to $Cu_{12.12}Sb_{4.34}S_{13}$ (spec. 13a). The compositional range was sulphur deficient relative to normal tetrahedrite, $Cu_{12}Sb_4S_{13}$ (see Fig.3-8). In polished specimen euhedral crystals which tended to become skeletal at corners of faces were observed. The copper rich cores readily inverted to blue low temperature non-stoichiometric tetrahedrite with the development of characteristic conchoidal fractures, evidently due to contraction. The cell edge was a_o = 10.3196Å stnd. err. 0.00016. Intermediate compositional members were metastable and inverted from the pink high temperature form to the blue

low temperature form on scratching. The antimony rich rims were stable and the cell edge, a_o = 10.428Å stnd. err. 0.012, was obtained for the pink high temperature polymorph of the antimony end-member. Diffraction data for these phases is given in Table 3-7.

Quenched $Cu_{12}Sb_4S_{12.5}$ ($Cu_{12.48}Sb_{4.16}S_{13}$) (spec.30b) yielded inverted tetrahedrite (Plate 4-4). The diffraction profile showing peak doubling over a range in 2θ is given in Fig.4-11. Using ground material, powder photographs with line doubling were obtained (Table 3-12). Cell edges obtained were a_o = 10.435Å stnd. err. 0.003 and a_o = 10.3289Å stnd. err. 0.0006. Picked tetrahedrite grains gave single lines and the cell edge a_o = 10.3179Å stnd. err. 0.003 was obtained.

Slowly cooled $Cu_{12}Sb_4S_{12.5}$ ($Cu_{12.48}Sb_{4.16}S_{13}$) (spec.40) yielded normal tetrahedrite with fractured grain margins (Plate 4-1). The diffraction profile, showing slight peak doubling, over a range in 2θ is given in Fig.4-4. Powder photographs using ground material gave a cell edge of a_o = 10.3313Å stnd. err. 0.0004 from the strong lines. Picked tetrahedrite grains (Table 4-12) gave 10.3206Å stnd. err. 0.0003.

It is therefore concluded that there is a range in cell edges of the high temperature and low temperature polymorphs of non-stoichiometric tetrahedrite. Three 'types' of tetrahedrite were obtained; the Cu rich low temperature polymorph, a_o = 10.32Å; the Sb rich high temperature polymorph, a_o = 10.43Å; and low temperature intermediate or Sb rich compositions (which rim normal tetrahedrite), a_o = 10.33Å.

The preparation of material for x-ray diffraction in different ways has led to anomalous results because of

zoning and metastability.

The acquisition of diffraction data and its interpretation therefore requires care in the case of synthetic tetrahedrite - polished specimen and microprobe examination being necessary.

Discussion of the Cu-Sb-S System

Digenite, $Cu_{2-x}S$, is the most refractory phase in the ternary and its primary phase field dominates the Cu-S side of the diagram. Copper has a stronger affinity for sulphur than has antimony thus controlling the direction of the tie lines. There will therefore be a tendency to obtain $Cu_{2-x}S$, either due to non-equilibrium in low temperature runs, or by primary crystallisation in high temperature runs, and this has proved to be the case in starting compositions near tetrahedrite.

The appearance of $Cu_{2-x}S$ obtained in polished specimen depends on the starting composition and the temperature history. On cooling, the cubic, high digenite ($Cu_{2-x}S$) field contracts slightly and high digenite breaks down progressively into a number of low temperature phases. Although high temperature digenite cannot be quenched, as far as x-ray determination of the structure is concerned (Roseboom 1966), in polished section a rapidly cooled $Cu_{2-x}S$ appears isotropic (or with a weak anisotropy) and the colour varies from deep blue to white. Metastable phases have been preserved in lamellar and herringbone intergrowths. Scratch induced inversion has caused colour changes of pink to white and blue (isotropic) to white (anisotropic). In sulphur-poor ternary compositions grey Cu_2S is obtained.

Reaction rims around $Cu_{2-x}S$ have been observed in ternary starting compositions (Plate 3-27). The following reactions may occur due to changing orientation of tie lines as $Cu_{2-x}S$ is cooled and the sulphur content is reduced -

$$Cu_{2-x}S + \text{tetrahedrite} \rightarrow Cu_2S + \text{stibioluzonite}$$

$$Cu_{2-x}S + Cu_3SbS_3 \longrightarrow Cu_2S + \text{tetrahedrite}$$

Ternary compositions in the system are stibioluzonite (Cu_3SbS_4), chalcostibite ($CuSbS_2$), tetrahedrite ($Cu_{12}Sb_4S_{13}$), and the new compositions Cu_3SbS_3 and non-stoichiometric tetrahedrite.

Tetrahedrite-chalcostibite, stibioluzonite-chalcostibite, chalcostibite-stibnite and stibioluzonite-stibnite have eutectic melting relationships.

Stibioluzonite and chalcostibite have simple phase relationships and no inversion phenomena have been observed in them.

Cu_3SbS_3 may have a range in composition which extends towards Cu_2S at high temperatures. Inversion twinning indicates the existence of a high temperature polymorph of Cu_3SbS_3. Cu_3SbS_3 melts incongruently to a sulphur deficient 'non-stoichiometric' tetrahedrite at about 600°C. The non-stoichiometric tetrahedrite has a range in Cu:Sb ratio. On cooling Cu rich members invert to a blue cubic tetrahedrite but Sb rich pink members are stable. Although normal tetrahedrites and non-stoichiometric tetrahedrite obtained in this study are quite distinct detailed phase equilibrium studies are required to obtain the variation in the compositional range of tetrahedrite and its structural polymorphs with temperature.

Low temperature tie lines ($<500^{o}C$) have been established and are shown in Fig.3-9. High temperature tie lines ($>600^{o}C$) have been established between non-stoichiometric tetrahedrite and chalcostibite and non-stoichiometric tetrahedrite and antimony.

The two liquid field in the metal rich part of the system probably extends from the Cu-S to the Sb-S binary.

In conclusion the phase relations of tetrahedrite are more complex than indicated in previous work on the system. A 'normal' tetrahedrite, $Cu_{12}Sb_4S_{13}$ (composition from spec. 63), can however, be identified and characterised. This is the basic composition of natural substituted tetrahedrites (Springer 1969). $Cu_{12}Sb_4S_{13}$ was therefore used as the basic starting composition in the experiments on substitution of Cu in tetrahedrite, described in Chapter 5.

TABLE 3-5

Microprobe Analysis

Element	Line	KV	Standard
Cu	K_α	15	Cu
Sb	L_α	15	Sb_2S_3
S	K_α	15	Sb_2S_3

Corrected using TIM

63 Tetrahedrite

	uwt%	cwt%	nwt%	at%	(stoichiometric formula wt%)
Cu	45.25	46.49	45.96	41.67	45.76
Sb	28.05	29.63	29.29	13.86	29.23
S	23.09	25.04	24.75	44.47	25.02
		101.16			

64 Stibioluzonite

Cu	42.22	43.93	43.31	37.66	43.26
Sb	26.35	28.24	27.84	12.63	27.63
S	26.90	29.26	28.85	49.71	29.11
		101.43			

65 Cu_3SbS_3

Cu	45.79	46.84	46.48	42.76	46.65
Sb	28.81	30.28	30.05	14.43	29.80
S	21.86	23.67	23.49	42.82	23.54
		100.78			

TABLE 3-6

Powder Diffraction Data for Cu_3SbS_3

	Wittichenite, Cu_3BiS_3 (Nuffield 1947)		Cu_3SbS_3 Specimen S13	
hKl	dÅ	I	dÅ	I
011	5.68	10	5.588	10 *
020	5.22	10	5.096	10 *
111	4.55	40	4.532	40 *
200	3.83	30	3.901	60 *
121, 210	3.62	10		
002, 201	3.34	10	3.265	30 *
012, 211	3.19	30	3.196	50
			3.108	40
220, 102, 031	3.08	80	3.046	70
			2.975	70
112	2.96	10	2.918	30
131	2.85	100	2.821	100 *
022	2.81	5		
122	2.66	40	2.616	50 *
040, 230	2.58	20	2.567	20 *
310	2.49	5	2.476	20 *
032, 231	2.39	30	2.390	30 *
311	2.34	5	2.357	20 *
141, 320	2.28	5	2.297	20 *
013, 321	2.17	20	2.192	30 *
113	2.10	5		
330, 023	2.05	20	2.035	20 *
312, 150, 123	1.989	20	1.968	20 *
151	1.910	5	1.918	30
322	1.895	30	1.896	40 *
133, 250, 340	1.821	30	1.822	60 *
052	1.762	30	1.758	40 *
421	1.734	20	1.749	40
303, 160, 430	1.681	30	1.674	30

Contd.

TABLE 3-6 (Contd.)

hKl	dÅ	I	dÅ	I
323, 252, 342	1.600	10	1.596	30
	1.585	55		
	1.542	5	1.557	40
	1.506	10	1.503	20
	1.453	10	1.488	20
	1.443	5		
	1.408	10		
	1.382	10		

(* lines used in cell size computation).

TABLE 3-7

Powder Diffraction Data for
Non-stoichiometric Tetrahedrite (Spec.13a)

	Blue Core		Pink Rim	
N	dÅ	I	dÅ	I
2			7.240	40
4	5.151	40	5.192	40
6	4.207	30	4.239	20
8	3.643	50	3.667	50
10	3.285	30	3.309	20
12	2.972	100	2.992	100
14	2.753	60	2.770	50
16	2.575	70	2.595	60
18	2.428	50	2.446	40
20	2.303	30	2.304	40
22	2.196	10	2.243	30
24	2.105	20	2.119	50
26	2.020	60	2.034	50
30	1.881	50	1.896	60
32	1.822	90	1.834	90
34	1.766	30	1.780	20
36	1.718	20	1.732	10
38	1.671	60	1.683	40
40	1.629	20	1.644	10
42	1.590	10	1.604	10
44	1.554	80	1.568	70
46	1.520	20	1.523	10
48	1.487	30	1.496	10
50	1.458	30	1.469	10
54	1.402	20		
56	1.379	20		
62	1.310	30		
64	1.289	40		
66	1.270	40		
70	1.233	40		
74	1.198	40		
76	1.184	40		
78	1.168	10		
80	1.154	10		
82	1.139	10		
84				
86	1.113	30		
90	1.087	40		
94	1.064	30		
96	1.053	50		
98	1.042	10		
102	1.022	30		
106				
108	0.993	40		
110	0.984	50		
114	0.966	30		
118	0.950	30		

Contd.

TABLE 3-7 (Contd.)

N	dÅ	I	dÅ	I
122	0.934	40		
126	0.919	50		
128	0.912	30		
130	0.905	30		

Cell edge
a_o = 10.31962
Stnd.err. = 0.00061

Cell edge
a_o = 10.42840
Stnd.err. = 0.01235

TABLE 3-8

Powder Diffraction Data for
Tetrahedrite, $Cu_{12}Sb_4S_{13}$ (Spec.63)
(mean of two photographs)

N	dÅ	I	hkl
4	5.145	35	200
6	4.200	20	211
8	3.638	45	220
9	3.460	5	300 (?)
12	2.971	100	222
14	2.754	40	321
16	2.572	65	400
18	2.428	55	411, 330
20	2.302	35	420
22	2.196	10	332
24	2.103	25	422
26	2.020	50	510, 431
30	1.8795	45	521
32	1.8208	90	440
34	1.7668	35	530, 433
36	1.7167	15	600, 442
38	1.6717	55	611, 532
40	1.6290	20	620
42	1.5913	10	541
44	1.5531	75	622
46	1.5195	25	631
48	1.4879	25	444
50	1.4581	30	710, 550, 543
54	1.4033	10	721, 633, 552
56	1.3780	10	642
62	1.3094	20	732, 651
64	1.2886	25	800
66	1.2687	30	811, 741, 554
70	1.2320	30	653
74	1.1979	40	831, 750, 743
76	1.1820	40	662
78	1.1670	10	752
80	1.1521	10	840
82	1.1383	10	910, 833
86	1.1117	20	921, 761, 655
90	1.0868	35	930, 851, 754
94	1.0639	30	932, 763
96	1.0527	45	844
98	1.0418	10	941, 853, 770
102	1.0212	20	
106	1.0018	10	
108	0.9927	35	
110	0.9836	45	
114	0.9662	30	
118	0.9498	35	
122	0.9342	45	
126	0.9193	50	
128	0.9121	40	
130	0.9051	25	

Cell edge 10.31907
Stnd.err. 0.00048

TABLE 3-9

Powder Diffraction Data for
Stibioluzonite, Cu_3SbS_4 (Spec.64)

dÅ	I	hKl (GENSTRUK)
5.363	40	002
4.810	50	101
3.804	40	110
3.107	100	112
2.981	40	103
2.689	60	004, 200
2.403	40	202
2.346	40	211
2.196	30	114
1.9968	40	105, 213
1.9017	90	204, 220
1.7907	20	006, 222
1.7713	20	301
1.7017	10	310
1.6218	80	116, 312
1.6052	20	215
1.5527	40	224
1.4781	20	107, 321
1.4375	20	314
1.3778	20	305, 323
1.3451	50	008, 400
1.3039	20	226, 402
1.2952	20	217, 411
1.2343	60	316, 332
1.2309	10	413
1.2026	40	208, 404, 420
1.1740	10	422
1.1664	10	109, 307
1.0982	60	228, 424
1.0702	20	219, 327, 501, 431
1.0542	10	318, 510
1.0358	60	336, 512, 1110
0.9953	10	309, 417, 521
0.9633	20	523, 1011, 435, 505
0.9514	50	408, 440
0.9099	60	516, 3110, 532
0.9080	50	
0.8975	30	

Tetragonal unit cell parameters (COHEN)

a_o = 5.38305 Stnd. Dev. 0.00040

C_o = 10.76594 Stnd. Dev. 0.00124

TABLE 3-10

Powder Diffraction Data for Chalcostibite, $CuSbS_2$

(Mean of two photographs)

dÅ	I	hkl (GENSTRUK)
7.336	10	020
4.582	30	120
3.612	30	011,040
3.112	100	111
3.091	90	140
2.988	90	200
2.973	90	031
2.934	30	210,121
2.765	20	220
2.541	30	230
2.295	70	240,051
2.231	50	160,221
2.111	60	231
1.8932	60	002,260
1.8234	60	251,071
1.8080	40	080
1.7538	80	122,340
1.7366	30	171,180
1.6831	30	261,042
1.6018	30	202,212
1.5912	10	341
1.5487	40	280,360
1.4453	20	162,370
1.4380	50	191,281,430
1.3716	10	421,312
1.3442	30	380,431
1.3093	30	082,2100
1.2884	50	342, 1110
1.2583	20	
1.2328	20	
1.2232	20	
1.2009	40	
1.1920	30	
1.1844	10	
1.1589	20	
1.1431	40	
1.1337	40	
1.0962	10	
1.0820	30	
1.0762	10	
1.0690	40	
1.0356	20	
1.0207	10	
1.0086	40	

Contd.

TABLE 3-10 (Contd.)

dÅ	I	hkl
1.0054	40	
0.9888	10	
0.9825	40	
0.9793	50	
0.9597	30	
0.9512	30	
0.9349	40	
0.9256	20	
0.9203	20	
0.9152	20	
0.9090	20	
0.9001	20	

TABLE 3-11

Powder Diffraction Data for Cu_3SbS_3 (Spec.65)

(mean of three photographs)

dÅ	I	hkl(Genstruk)
5.575	20	011
5.067	20	101, 020
4.527	60	111
4.056	10	021
3.896	70	200
3.606	10	121, 210
3.349	20	002
3.310	40	201
3.190	70	012, 211
3.099	30	220
3.042	80	102, 031
2.918	50	112
2.824	100	131
2.781	30	221, 022
2.615	60	122
2.559	40	230
2.539	20	202
2.471	30	310
2.441	20	212, 140
2.393	30	231, 032, 301
2.358	20	311
2.283	30	132, 320
2.249	20	222
2.192	30	013
2.148	10	240
2.037	40	302, 241, 232
2.013	20	150, ...
1.9709	20	123, 142, 051
1.9558	20	331
1.9138	20	151, 400
1.8973	40	213, 322
1.8533	30	401
1.8212	30	250, 340, 133
1.8029	50	242, 223, 420
1.7553	40	341, 251, 052
1.7495	50	332, ...
1.7006	30	
1.6935	20	
1.6753	30	
1.6568	30	
1.5951	30	
1.5759	20	
1.5617	30	
1.5535	20	
1.5227	10	
1.5030	30	
1.4899	20	
1.4531	10	

TABLE 3-11 (Contd.)

dÅ	I	hkl (Genstruk)
1.4115	10	
1.3984	20	
1.3095	10	
1.2979	10	
1.2752	20	
1.2181	20	
1.1965	20	
1.1886	30	
1.1802	30	
1.1626	20	
1.1353	10	
1.1101	10	
1.1022	10	
1.0856	20	
1.0708	10	
1.0550	10	
1.0234	10	
1.0116	30	
0.9961	10	
0.9828	30	
0.9735	10	
0.9388	30	
0.9218	20	
0.9157	20	

TABLE 3-12

Powder Diffraction Data for Quenched Tetrahedrite, Starting Composition $Cu_{12}Sb_4S_{12.5}$ (Spec.30b)

	Ground sample		Picked sample	
N	dÅ	I	dÅ	I
4	5.152	30	5.155	40
6	4.208	20	4.206	20
8	3.644	40	3.643	50
10			3.288	30
12	2.998	75		
12	2.969	100	2.975	100
14	2.766	15		
14	2.748	30	2.755	40
16	2.596	35		
16	2.571	40	2.576	60
18	2.441	15		
18	2.422	30	2.429	50
20	2.328	5		
20	2.302	30	2.304	30
22	2.235	10		
22	2.198	10	2.199	10
24	2.120	15		
24	2.101	20	2.105	20
26	2.037	15		
26	2.019	40	2.021	50
30	1.900	35		
30	1.882	40	1.881	40
32	1.842	65		
32	1.821	90	1.821	90
34	1.768	10	1.767	30
36	1.717	10	1.719	10
38	1.688	15		
38	1.671	50	1.672	50
40	1.629	10	1.630	20
42	1.591	10	1.589	10
44	1.569	25		
44	1.555	80	1.554	80
46	1.520	20	1.521	20
48	1.489	20	1.488	20
50	1.459	30	1.458	30
54	1.404	20	1.403	10
56	1.378	10	1.378	10
62	1.312	20	1.310	30
64	1.290	20	1.289	30
66	1.272	20	1.268	30
70	1.235	30	1.233	30
74	1.200	40	1.199	20
76	1.184	40	1.183	30
78	1.168	10		
80	1.154	10		
82	1.141	10		

Contd.

TABLE 3-12 (Contd.)

	dÅ	I	dÅ	I
86	1.113	20	1.112	20
90	1.100	10		
90	1.088	30	1.087	30
94	1.065	30	1.064	20
96	1.054	50	1.053	40
98	1.043	10	1.042	10
102	1.023	20	1.021	10
106	1.003	10		
108	0.994	30	0.993	20
110	0.985	40	0.984	30
114	0.967	30	0.966	20
118	0.951	30	0.950	30
122	0.945	15		
122	0.935	40	0.934	40
126	0.930	15		
126	0.920	40	0.919	40
128	0.913	30	0.912	30
130	0.906	30	0.905	20

Cubic Cell Edges (NELRIL)

a_o = 10.43571 Stnd.Err. .00296	
a_o = 10.32888 Stnd.Err. .00060	a_o = 10.31792 Stnd.err. = .00028

TABLE 3-13

Comparison of the Orthorhombic Unit Cell Parameters of Phases with the Wittichenite Structure

	a_o	b_o	c_o
Cu_3BiS_3, Wittichenite (Nuffield 1947)	7.68	10.33	6.70
Cu_3SbS_3, Spec.13	7.782	10.344	6.672
(stnd. dev. =)	(0.026)	(0.029)	(0.021)
Cu_3SbS_3, Spec.65	7.673	10.342	6.693
(stnd. dev. =)	(0.005)	(0.009)	(0.008)

CHAPTER 4

Substitution of Sb by As in Tetrahedrite - The Tetrahedrite-Tennantite Series

Introduction

Tetrahedrite and tennantite appear to form an isomorphous series in nature and although discussed in several publications no systematic investigation of the series has been published. The tetrahedrite-tennantite series was therefore selected for synthesis in the hope that variations in mineralogical properties along the series could be related to changing composition.

The formula of the series was the subject of a continuing controversy in the literature so, since the main dispute was over the presence of the thirteenth sulphur atom in the formula $Cu_{12}(SbAs)_4S_{13}$, it was decided to use a starting composition corresponding to the formula $Cu_{12}(SbAs)_4S_{12.5}$.

Microprobe analysis of tetrahedrite synthesised during experiments on the Cu-Sb-S system had been proving difficult because of the lack of suitable standards but the synthesis of orthorhombic Cu_3SbS_3, which had not previously been reported in the Cu-Sb-S system made it more probable that $Cu_{12}Sb_4S_{13}$ was the correct formula of tetrahedrite. Even if this proved to be the case the compromise formula chosen for the experiments was still acceptable because the resultant sulphur deficiency would only result in an increase in the amount of impurities obtained.

During early experiments in the Cu-Sb-S system it was realised that the phase relations of tetrahedrite were

resulting in difficulties in the synthesis of large pure crystals. It was hoped that the addition of arsenic to the system would result in more successful crystal growth.

Nine compositions from tetrahedrite to tennantite were prepared and two capsules, labelled 'a' and 'b', were filled for each (Table 4-1). The duplicate capsules ('b') were prepared primarily as substitutes in case of damage to the 'a' capsules but also served as a check on the mixing technique (i.e. runs 31a and 31b). After a preliminary run the products were examined ('series 30' results) and excess material reground and rerun in an attempt to homogenise the specimens ('series 40' results).

Sample Preparation and Synthesis

The technique of capsule preparation is outlined in Chapter 2. Details of the impure chemicals used are given in Table 1-1a. The 'a' capsules and one 'b' capsule (31b) were run in three batches with similar temperature histories (Fig. 4-1). A 'run' consisted of loading the capsules into the furnace and leaving overnight at about 400°C for reaction to take place. The temperature was then raised slowly to about 670°C and left for about sixty hours. The temperature was then lowered gradually through the liquidus of tetrahedrite-tennantite (610-640°C approx.) to below 500°C before removal from the furnace. The capsules reached room temperature after about one hour. In each case the charge melted and solidified to form a grey button. Most buttons were vesicular, some with interfering triangular crystal faces (characteristic of tetrahedrite-tennantite) developed on the surface. Each specimen was broken into fragments and cleavage faces with a strong metallic lustre were observed. Several fragments of

each charge were polished, several ground for diffraction and the remainder ground under acetone for reheating ('series 40'). The ground specimens were resealed in capsules and run in two batches with similar temperature histories (Fig.4-2). The temperature was raised to just above the liquidus and cooling was slow to below 400°C before removal from the furnace. Again the specimens were broken into fragments for polishing and diffraction.

Examination of Polished Specimens

Notes on each specimen of series 30 and 40 are given in Table 4-2. The mineral phases present and their relative abundances varied from fragment to fragment in some specimens though the phase relationships, as indicated by textural features, remained the same. The second run (series 40) made little difference to the nature of the phases present but 'welded grain boundaries' which were a result of the grinding and reheating process were obtained (Plate 4-1). The antimony rich end-member yielded the most $Cu_{2-x}S$, occurring as ovoidal dendrites within tetrahedrite, and the most chalcostibite, occurring as orientated laths in tetrahedrite and interstitially between tetrahedrite crystals which became skeletal marginally. With increasing As:Sb ratio the $Cu_{2-x}S$ phase disappeared with an associated decrease in interstitial chalcostibite while a sulphur rich impurity, stibioluzonite-luzonite ($Cu_3(SbAs)S_4$), increased. This occurred as irregular patches or irregular dendrites within tetrahedrite-tennantite grains. The nomenclature of these minerals is as suggested by Levy (1966) -

orthorhombic isotypes	enargite Cu_3AsS_4
	stibioenargite Cu_3SbS_4
tetragonal isotypes	luzonite Cu_3AsS_4
	stibioluzonite Cu_3SbS_4

The transition temperature of Cu_3AsS_4 from the low temperature tetragonal form (luzonite) to the high temperature orthorhombic form (enargite) is 320°C. No attempt has been made to distinguish luzonite and enargite in this study and 'luzonite' is used exclusively for $Cu_3As\ S_4$.

Starting composition 32 was the only member to yield tetrahedrite-tennantite co-existing with native Sb.

Two $Cu_3(SbAs)S_4$ phases could be distinguished in specimen '34.' One of the phases had orange-pink bireflectance, bronze-yellow anisotropy and was twinned while the other had purple-pink bireflectance, brown-green anisotropy and was untwinned. The orange-pink phase dominated in Sb rich members of the series whereas the purple-pink phase dominated in As rich members.

Conclusions from Examination of Polished Specimens

The solidification of a tetrahedrite composition liquid resulted in the crystallisation of $Cu_{2-x}S$ dendrites. Complete reaction with the liquid was not achieved resulting in an Sb enriched liquid and subsequent crystallisation of interstitial chalcostibite and stibnite (see Chapter 3). The laths of chalcostibite in tetrahedrite resemble an exsolution feature but they were more likely to have been included during skeletal growth of the tetrahedrite (Plate 4-2).

With the increase in As:Sb ratio the Sb enrichment effect was reduced, chalcostibite and tetrahedrite crystallising in eutectic intergrowth in specimen 31. (Plate 4-3).

With further increase in As:Sb ratio the $Cu_{2-x}S$ primary phase volume continued to contract in the Cu-Sb-As-S quaternary and no longer controlled the texture of the specimens. The co-existence of As rich members with a sulphur rich impurity, $Cu_3(SbAs)S_4$, was unexpected because of the low sulphur content of the starting composition. It can only be concluded that tennantite and As rich tetrahedrite have a lower sulphur content than the formula $Cu_{12}(AsSb)_4S_{13}$ (see microprobe analysis Table 4-5).

The fact that tetrahedrite-tennantite co-exists with Sb in specimen 32 indicates that there is no extensive solid-solution from Cu_3SbS_3 to an As counterpart, Cu_3AsS_3.

A discontinuity in the Cu_3SbS_4 - Cu_3AsS_4 system has been reported by Springer (1969) and this explains the co-existence of two phases, stibioluzonite ($Cu_3(SbAs)S_4$) and luzonite ($Cu_3(AsSb)S_4$) in specimen 34.

Electron Microprobe Analysis

A preliminary survey of intermediate members of the series indicated that the specimens were inhomogenous with a large variation in the Sb:As ratio existing within single grains. Using the standard technique of microprobe analysis two elements can be determined simultaneously but the compositions determined would be quite inaccurate if four elements were present and varied over small distances. The fixed stoichiometry option of EMPADR VII (see Chapter 2) was therefore used to determine the variation in Sb:As ratio in the tetrahedrite-tennantite series. The greater the difference in concentration, associated elements and bonding type between the element in the unknown, which is being analysed, and in the standard used, the greater the correction required. The synthetic end-members, tetrahedrite

and tennantite, were therefore assumed to be $Cu_{12}Sb_4S_{13}$ and $Cu_{12}As_4S_{13}$ respectively and used as standards. The Sb and As concentrations were corrected for the presence of Cu and S by EMPADR. If the formulae assumed for the standards was slightly incorrect this would make little difference to the correction applied.

The conditions of analyses and the results for the means of each specimen are given in Tables 4-3 and 4-4. The large standard deviations of the mean analyses indicates the inhomogeneity of the specimens. All the points analysed have been plotted in Fig.4-3. Although each specimen is inhomogenous there is an effectively linear relationship between Sb and As content. The line of points is however rather broad and analyses of starting composition Sb_3As (specimens 32 and 42) have a high Sb+As content. There is a deficiency of probable points in the vicinity of starting compositions $Sb_{2.5}As_{1.5}$ and $Sb_{1.5}As_{2.5}$. The best fit straight line indicates an Sb enriched end-member of the solid solution series compared with the synthesised end-member. For series 40, excluding specimen 42, the extrapolated end-member has $3.51 \pm 0.43\%$ more Sb than the end-member tetrahedrite synthesised.

The end-member tetrahedrite synthesised (spec.40a) was analysed fully using different standards (Table 4-5). The results indicate that tetrahedrite (spec. 40a) is close in composition to that of the stoichiometric formula $Cu_{12}Sb_4S_{13}$. The end-member tennantite synthesised (spec. 48a) was also analysed fully (Table 4-5). The composition obtained is lower in sulphur than in the stoichiometric formula $Cu_{12}As_4S_{13}$. The analyses of tetrahedrite and tennantite

have been plotted in Fig.4-12.

Complete analysis of tennantite (spec. 48a) has shown it to be slightly As poor compared with $Cu_{12}As_4S_{13}$. (48a = 13.60 at% As, $Cu_{12}As_4S_{13}$ = 13.79 at% As). This means that the weight % arsenic values of members of the tetrahedrite-tennantite series (Tables 4-3, 4) are high. The '% of end-member values' are, however, still valid because the difference between the true and assumed As contents of the standard (tennantite) will have little effect on the small correction factor. Only '% of end-member values' have been used in deriving conclusions on the range in composition of the tetrahedrite-tennantite series.

Conclusions from Microprobe Analysis

The results obtained are inconsistent with tetrahedrite-tennantite being a simple isomorphous series. There is evidence of non-stoichiometry but from the microprobe results obtained it is not possible to define the range in non-stoichiometry or how it changes from the Cu-Sb-S system to the Cu-As-S system. Because of the non-stoichiometry of the series and the lack of complete analysis of individual members of the series, measurements of physical properties of the series have been plotted against Sb : As ratio of the starting composition. The discontinuities in the series are indicative of miscibility gaps and will be discussed later.

X-ray Diffraction

Smear mounts were prepared for each member of the series but the diffraction results obtained were, in most cases, difficult to interpret because of the lack of published information on synthetic phases in the Cu-Sb-As-S system. The major peaks of the tetrahedrite-tennantite series were identified, however, and a range in 2θ for several specimens

has been given in Fig.4-4, illustrating the general dependance of peak position on Sb:As ratio.

Debye-Scherrer powder photographs were obtained using ground specimen or material picked out from the polished specimen. Difficulty was experienced in obtaining sharp diffraction lines, especially in the back reflection region. Satisfactory photographs were measured and d-spacings computed and indexed. The cubic unit cell edge was computed using selected back reflections (see Chapter 2). The results are given in Table 4-6 and the cell edges are plotted against starting composition in Fig.4-5.

The powder photograph obtained for specimen 40a using ground material (40a3) gave a cell edge of 10.33Å whereas the photograph obtained using material picked from the polished specimen (40a5) gave a cell edge of 10.32Å. Also, the low angle lines on the photograph prepared from the ground specimen were split indicating the presence of a larger unit cell tetrahedrite. Slight peak doubling can also be seen in the diffraction chart prepared for specimen 40a (Fig.4-4).

Conclusions from x-ray Diffraction Results

It was concluded that in the investigation of synthetic sulphides a study of polished sections is more satisfactory for identification of minor phases present than using diffraction charts and that using material picked out from the polished specimen for powder photographs is a more satisfactory means of obtaining diffraction data and cell parameters.

The broadening of lines in the powder photographs was due to the range in composition of the tetrahedrite-tennantite specimens.

From Fig.4-5 it is apparent that there is a general increase in cell edge with increasing Sb:As ratio but the points do not lie on a straight line. Another factor must be affecting the cell edge and this factor has probably resulted in the large cell edge of specimen 32. The evidence suggests, therefore, that the cell edge varies with non-stoichiometry in tetrahedrite-tennantite as well as with Sb:As ratio.

The dependance of the variation in diffraction profile on specimen preparation, noted for specimen 40, must be due to the presence of the several varieties of tetrahedrite noted during experiments in the Cu-Sb-S system. No inversion phenomena were noted in the grain cores in the polished specimens. It is concluded that the bulk of the grains examined were normal tetrahedrite ($Cu_{12}Sb_4S_{13}$) but the grain boundaries were sulphur deficient non-stoichiometric tetrahedrite.

Microhardness Measurements

The technique employed is described in Chapter 2. The results for the tetrahedrite-tennantite series are given in Table 4-7 and plotted in Fig.4-6. Measurements were only made on series 40. Microhardness is a relatively crude technique and only the general increase in microhardness with increasing As:Sb ratio is apparent in Fig.4-6.

Reflectivity Measurements

The technique employed is described in Chapter 2. Spectral reflectivities were obtained for each member of series 40. The results are given in Table 4-8 and plotted in Fig.4-7. There is a general decrease in reflectivity with increasing As:Sb ratio but the change is different at

different wavelengths. Specimen 42 has an exceptionally high reflectivity. The variation in reflectivity is therefore dependant on another factor, apart from Sb:As ratio, and as in the case of the diffraction experiments, it is concluded that non-stoichiometry must be the factor.

Colour Measurements

There is little change in the form of the spectral reflectivity curve of members of the tetrahedrite-tennantite series with changing Sb:As ratio but, since a colour difference between tetrahedrite and tennantite was evident from optical examination, the colour changes were determined quantitatively using the spectral reflectivity values. The technique of colour measurement is outlined in Chapter 2.

For each member of series 40 the tristimulus values, X, Y, and Z, were computed for standard sources A (tungsten light), B (direct sunlight) and C (average daylight) (Table 4-9). For standard source A the chromaticity co-ordinates, x, y and z (Table 4-10), were computed from the tristimulus values permitting the calculation of the dominant wavelength and excitation purity of the colour of each member (Table 4-11). An enlarged area of the chromaticity diagram (see Fig.2-4) illustrates the colour relationships of the phases (Fig.4-8). Plots of starting composition versus dominant wavelength and % excitation purity are given in Fig.4-9. The colour discrimination (threshold) ellipse is shown in Fig.4-8 for specimen 41. The human eye is incapable of distinguishing colour differences of phases which plot inside this ellipse.

% purity is plotted against dominant wavelength in Fig.4-10. Anisotropic pyrolusite is also plotted in Fig.4-10 to give an indication of the colour of the synthetic phases.

The brightness (Y) of pyrolusite is 32.4-33.7, slightly higher than that of the synthetic tetrahedrite-tennantite series. Galena and sphalerite are common associates of natural tetrahedrites and are also plotted in Fig.4-10.

Conclusions from Colour Measurements

For the tetrahedrite-tennantite series 40 there is little change in colour although the dominant wavelength and excitation purity do increase slightly with increasing As:Sb ratio (Figs. 4-8, 9). Two members of the series, 40 (tetrahedrite) and 42, do however have significant differences in dominant wavelengths and excitation purities (Figs.4-8, 9, 10). The human eye is capable of distinguishing the colour difference between specimens 40 and 42 and the rest of the series and should be able to detect the change in colour from the Sb end (specimen 41) to the As end (specimen 48) of the normal members of the series. The colour difference observed will be in intensity of colour (% purity) as the wavelength change (Fig.4-9) is less than the minimum detectable ($\pm$ 1.5 nm) in this region of the spectrum (Wright and Pitt 1934).

These conclusions are supported by optical examination of the specimens but the colour of tetrahedrite (specimen 40) appears brownish against chalcostibite. Tennantite has the expected greyish colour.

Further Experiments

In order to investigate further the possible high temperature polymorphism of tetrahedrite, indicated by the line splitting of powder photographs prepared for specimen 40, and to ascertain whether tennantite behaved similarly, the two compositions, $Cu_{12}Sb_4S_{12.5}$ (spec.30b) and $Cu_{12}As_4S_{12.5}$ (spec.38b), (representing tetrahedrite and

tennantite respectively) were synthesised and quenched at 600°C.

Inversion phenomena were observed in the polished specimen of tetrahedrite (Plate 4-4) and diffraction lines were observed to be split in powder photographs prepared from ground material (Table 3-12). No inversion phenomena nor line splitting were observed for tennantite.

X-ray diffraction charts were obtained for the quenched tetrahedrite and tennantite and a range in 2θ has been selected which illustrates the diffraction line splitting of tetrahedrite in contrast to the single lines of tennantite (Fig.4-11).

TABLE 4-1 TETRAHEDRITE-TENNANTITES

Starting Compositions and Furnace Batch Number

Starting composition	Series 30 Spec.No.	Batch No.	Series 40 Spec.No.	Batch No.
$Cu_{12}Sb_4S_{12.5}$	30a	1	40a	1
	30b			
$Cu_{12}Sb_{3.5}As_{0.5}S_{12.5}$	31a	3	41a	2
	31b	2	41b	2
$Cu_{12}Sb_3AsS_{12.5}$	32a	2	42a	1
	32b			
$Cu_{12}Sb_{2.5}As_{1.5}S_{12.5}$	33a	1	43a	2
	33b			
$Cu_{12}Sb_2As_2S_{12.5}$	34a	2	44a	1
	34b			
$Cu_{12}Sb_{1.5}As_{2.5}S_{12.5}$	35a	3	45a	2
	35b			
$Cu_{12}SbAs_3S_{12.5}$	36a	1	46a	1
	36b			
$Cu_{12}Sb_{0.5}As_{3.5}S_{12.5}$	37a	3	47a	2
	37b			
$Cu_{12}As_4S_{12.5}$	38a	2	48a	1
	38b			

TABLE 4-2 SERIES 30 + 40 - PHASES OBTAINED

Polished Spec. No.	$Cu_{2-x}S$	% Concentration (Visual Estimate) $Cu_{12}(SbAs)_4S_{13}$	$Cu_3(SbAs)S_4$	$CuSbS_2$	Sb_2S_3	Sb	Other
30a	1	80	-	18	2	-	-
31a	1	85	4	10	1	-	-
31b	1	95	-	5	-	-	--
32a	-	95	-	4	-	1	-
33a	-	100	-	-	-	-	-
34a	-	94	4	2	-	-	-
35a	-	90	8	-	-	-	2
36a	-	98	-	-	-	-	2
37a	-	99	-	-	-	-	1
38a	-	95	4	-	-	-	1
40a	2	93	-	4	1	-	-
41a	1	97	1	1	-	-	-
41b	1	80	-	19	-	-	-
42a	-	98	-	1	-	1	-
43a	1	98	-	1	-	-	-
44a	-	95	4	-	-	-	1
45a	-	90	6	-	-	-	4
46a	-	99	-	-	-	-	1
47a	-	98	-	-	-	-	2
48a	-	99	1	-	-	-	-

TABLE 4-3 - Series 30 Microprobe Analysis

Instrumental Conditions

Elem.	Stnd.	Line	KV	Crystal	Angle	E	ΔE	Counter
Sb	TET(30a)	L_α	15	Quartz	61°55"	3.70	2.53	Flow
As	TEN(38a)	K_α	15	LiF	33°57"	4.30	1.42	Sealed

Corrected using EMPADR VII

Assumed Stoichiometry - $Cu_{12}(SbAs)_4S_{13}$

Results - Mean of each specimen given.

Spec. No.	Elem.	Points	uwt%	cwt%	% of end member	Stnd. Dev.
31a	Sb	18	25.42	25.61	87.62	3.35
	As	18	3.30	3.17	15.65	3.16
31b	Sb	18	26.24	26.41	90.35	2.67
	As	18	2.82	2.71	13.38	2.62
32a	Sb	18	22.82	23.10	79.03	3.22
	As	18	5.28	5.10	25.17	2.91
33a	Sb	18	19.96	20.27	69.35	5.78
	As	18	6.63	6.42	31.96	5.87
34a	Sb	18	13.63	13.99	47.86	4.76
	As	18	11.22	10.98	54.20	5.38
35a	Sb	18	15.17	15.54	53.16	5.92
	As	18	10.39	10.15	50.10	6.12
36a	Sb	18	7.81	8.10	27.17	4.79
	As	18	14.63	14.48	71.47	4.79
37a	Sb	18	4.42	4.61	15.77	3.28
	As	18	17.42	17.29	85.34	3.95

TABLE 4-4 - Series 40 Microprobe Analysis

Instrumental Conditions

Elem.	Stnd.	Line	KV	Crystal	Angle	E	ΔE	Counter
Sb	TET(40a)	L_α	20	Quartz	61°55"	3.70	2.53	Flow
As	TEN(48a)	K_α	20	LiF	33°57"	4.30	1.42	Sealed

Corrected using EMPADR VII

Assumed Stoichiometry - $Cu_{12}(SbAs)_4S_{13}$

Results - Mean of each specimen given.

Spec. No.	Elem.	Points	uwt%	cwt%	% of end member	Stnd. Dev.
41a	Sb	10	25.86	26.04	89.09	3.32
	As	10	2.73	2.65	13.08	3.49
41b	Sb	10	24.98	25.21	86.25	2.90
	As	10	3.65	3.54	17.47	2.75
42a	Sb	10	22.92	23.23	79.47	3.15
	As	10	5.46	5.32	26.26	3.31
43a	Sb	10	17.73	18.10	61.92	3.89
	As	10	8.15	7.97	39.34	4.16
44a	Sb	10	14.58	14.98	51.25	3.87
	As	10	10.63	10.44	51.53	4.33
45a	Sb	10	15.25	15.64	53.51	5.53
	As	10	9.85	9.67	47.73	6.09
46a	Sb	10	7.04	7.33	25.08	4.29
	As	10	15.44	15.31	75.75	4.89
47a	Sb	10	2.37	2.49	8.52	2.47
	As	10	18.55	18.50	91.31	3.31

TABLE 4-5

Microprobe Analysis (corrected using TIM)

Element	Line	kv
Cu	K_α	15
As	K_α	20
Sb	L_α	15
S	K_α	15

Tetrahedrite, spec.No.40a

(standard = $Cu_{12}Sb_4S_{13}$, spec.63) (Standards = Cu and Sb_2S_3)

	uwt%	cwt%	nwt%	at%	uwt%	cwt%	nwt%	at%
Cu	45.73	45.72	45.79	41.52	44.75	46.01	45.54	41.20
Sb	29.38	29.37	29.41	13.92	28.11	29.71	29.40	13.88
S	24.78	24.77	24.80	44.56	23.35	25.32	25.06	44.92
		99.86				101.04		

Tennantite, spec.No.48a

(standards = Cu, As, ZnS)

	(Grain 1)				(Grain 2)			
	uwt%	cwt%	nwt%	at%	uwt%	cwt%	nwt%	at%
Cu	51.38	53.97	52.93	42.74	50.56	53.09	52.71	42.58
As	17.66	20.11	19.72	13.51	17.66	20.10	19.96	13.68
S	27.98	27.88	27.34	43.75	27.63	27.53	27.33	43.75
		101.96				100.72		

(The means of each pair of analyses are plotted in Fig.4-12).

TABLE 4-6

Tetrahedrite-Tennantite Unit Cell Parameters
obtained by NELRIL using selected high angle lines

Specimen number	Powder preparation	Cell edge in Å	Stnd. Err. on intcpt.
Series 30			
30b(1)	ground	10.32888	0.00060 (quenched)
		also 10.43571	0.00296
30b(2)	picked	10.31792	0.00028 (quenched)
31a(1)	ground	10.30817	0.00047
32a(4)	ground	10.33643	0.00078
35a(3)	ground	10.21289	0.00069
36a(2)	ground	10.19312	0.00033
36a(5)	ground	10.19639	0.00038
37a(3)	ground	10.18851	0.00035
38a(1)	picked	10.16984	0.00041
38b(1)	ground	10.17305	0.00017 (quenched)
Series 40			
40a(3)	ground	10.33129	0.00036
40a(5)	picked	10.32061	0.00034
41a(1)	ground	10.30720	0.00023
43a(3)	ground	10.26665	0.00045
44a(1)	ground	10.24474	0.00041
46a(1)	ground	10.19527	0.00064
47a(2)	ground	10.18539	0.00028
48a(2)	ground	10.16471	0.00020

TABLE 4-7 SERIES 40

Microhardness Measurements

Vickers Microhardness
Diamond Indentation, 100g Load.

Specimen number	Number of indentations	Mean Hardness	Standard Deviation
40a	10	243	14
41a	5	258	26
42a	5	280	5
43a	5	308	30
44a	5	311	19
45a	5	332	31
46a	5	328	24
47a	5	351	15
48a	10	352	33

TABLE 4-8 - SERIES 40

Spectral reflectivity measurements

Spec.No.	wavelength 440	460	480	500	520	540	560	580	600	620	640	660
40a	31.5	31.7	30.8	30.3	29.9	29.6	29.5	29.5	29.4	29.0	28.4	27.1
41a	30.6	30.0	29.5	29.1	29.5	29.2	28.7	28.6	28.2	27.6	26.7	26.0
42a	33.3	32.7	32.3	31.1	32.2	31.5	31.5	31.2	31.1	31.0	30.3	30.1
43a	31.4	30.9	30.5	30.0	29.8	29.7	29.7	29.5	28.8	28.3	27.4	26.5
44a	30.8	30.5	30.0	29.6	29.8	29.2	29.2	28.9	28.5	27.7	27.0	25.8
45a	29.6	29.3	28.8	28.5	28.3	28.2	28.1	27.9	27.3	26.6	25.9	24.9
46a	30.5	30.1	29.4	29.1	29.2	29.0	28.8	28.3	27.7	26.8	25.8	25.1
47a	29.6	29.3	28.9	28.6	28.5	28.3	28.0	27.6	26.9	26.2	25.0	24.3
48a	29.9	29.4	29.1	28.7	28.7	28.2	28.2	27.5	26.7	26.0	24.9	23.9

TABLE 4-9 - Series 40

Tristimulus values for standard sources
A (tungsten light), B (direct sunlight), D (average daylight)

Specimen No.		X	Y	Z
40a	A	31.9909	29.4088	11.0945
	C	29.0396	29.6057	37.0022
	B	29.1768	29.5477	26.6808
41a	A	30.7494	28.4873	10.6851
	C	27.9823	28.7334	35.6927
	B	28.0945	28.6703	25.7227
42a	A	34.1342	31.2929	11.6281
	C	30.8636	31.4272	38.8567
	B	31.0475	31.3970	28.0019
43a	A	31.5304	29.2021	10.9872
	C	28.7202	29.4504	36.6926
	B	28.8260	29.3855	26.4455
44a	A	30.9929	28.7544	10.8105
	C	28.2290	29.0247	36.0694
	B	28.3361	28.9529	26.0042
45a	A	29.7882	27.6389	10.3840
	C	27.1394	27.8939	34.6516
	B	27.2403	27.8256	24.9800
46a	A	30.1919	28.1603	10.6645
	C	27.6133	28.4854	35.6163
	B	27.6798	28.4004	25.6696
47a	A	29.3827	27.4404	10.3976
	C	26.8741	27.7753	34.6823
	B	26.9385	27.6886	25.0051
48a	A	29.2523	27.4024	10.4729
	C	26.8393	27.7786	34.9621
	B	26.8738	27.6812	25.2014

TABLE 4-10 - Series 40

Chromaticity co-ordinates for standard sources
A (tungsten light), B (direct sunlight), C (average daylight)

Specimen No.		x	y	z
40a	A	0.4413	0.4057	0.1530
	C	0.3036	0.3095	0.3869
	B	0.3416	0.3460	0.3124
41a	A	0.4398	0.4074	0.1528
	C	0.3028	0.3109	0.3862
	B	0.3406	0.3476	0.3118
42a	A	0.4430	0.4061	0.1509
	C	0.3051	0.3107	0.3842
	B	0.3433	0.3471	0.3096
43a	A	0.4396	0.4072	0.1532
	C	0.3028	0.3105	0.3868
	B	0.3405	0.3471	0.3124
44a	A	0.4393	0.4075	0.1532
	C	0.3025	0.3110	0.3865
	B	0.3402	0.3476	0.3122
45a	A	0.4393	0.4076	0.1531
	C	0.3206	0.3110	0.3864
	B	0.3403	0.3476	0.3121
46a	A	0.4375	0.4080	0.1545
	C	0.3011	0.3106	0.3883
	B	0.3386	0.3474	0.3140
47a	A	0.4371	0.4082	0.1547
	C	0.3008	0.3109	0.3882
	B	0.3383	0.3477	0.3140
48a	A	0.4358	0.4082	0.1560
	C	0.2996	0.3101	0.3903
	B	0.3369	0.3471	0.3160

TABLE 4-11 - SERIES 40

Dominant wavelength and excitation purity for standard source A (tungsten light)

Specimen No.	Dominant wavelength	Excitation purity
40a	489.89	1.57
41a	494.57	1.85
42a	489.56	1.15
43a	494.15	1.90
44a	494.79	1.96
45a	495.00	1.96
46a	495.64	2.37
47a	495.93	2.46
48a	495.80	2.76

TABLE 4-12

Powder Diffraction Data

(see Table 4-5 for microprobe analyses)

	Tetrahedrite, spec.No.40a(5) Starting comp. $Cu_{12}Sb_4S_{12.5}$		Tennantite, spec.No.48a Starting comp. $Cu_{12}As_4S_{12.5}$	
N	dÅ	I	dÅ	I
2			7.144	40
4	5.148	40		
6	4.206	30	4.153	50
8	3.647	50	3.591	30
12	2.976	100	2.931	100
14	2.754	40	2.711	30
16	2.577	60	2.537	60
18	2.430	40	2.391	50
20	2.304	30		
22	2.199	20		
24	2.105	30	2.071	10
26	2.021	40	1.9901	40
30	1.8824	40	1.8519	50
32	1.8224	90	1.7941	90
34	1.7680	30	1.7390	30
36	1.7179	10	1.6902	10
38	1.6722	50	1.6456	40
40	1.6298	20	1.6068	20
42	1.5910	10		
44	1.5539	80	1.5297	90
46	1.5198	20		
48	1.4879	20	1.4653	30
50	1.4590	30	1.4359	30
54	1.4022	20	1.3807	20
56	1.3767	20	1.3559	10
62	1.3103	30	1.2873	10
64	1.2889	30	1.2697	30
66	1.2695	30	1.2490	20
70	1.2323	30	1.2136	30
74	1.1987	40	1.1807	40
76	1.1826	40	1.1647	50
78	1.1677	10		
80	1.1529	10	1.1355	30
82	1.1391	10	1.1217	20
84			1.1089	10
86	1.1119	20	1.0950	30
90	1.0874	30	1.0705	20
94	1.0640	20	1.0477	20
96	1.0529	40	1.0367	50
98	1.0420	10	1.0263	10
102	1.0216	20		
104			0.9962	10
106	1.0018	5		
108	0.9927	30	0.9779	40
110	0.9837	40	0.9688	40
114	0.9665	30	0.9517	30
118	0.9502	30	0.9355	30
120			0.9277	30
122	0.9343	40	0.9202	40
126	0.9194	50	0.9055	50
128	0.9123	30	0.8984	50
130	0.9052	20		

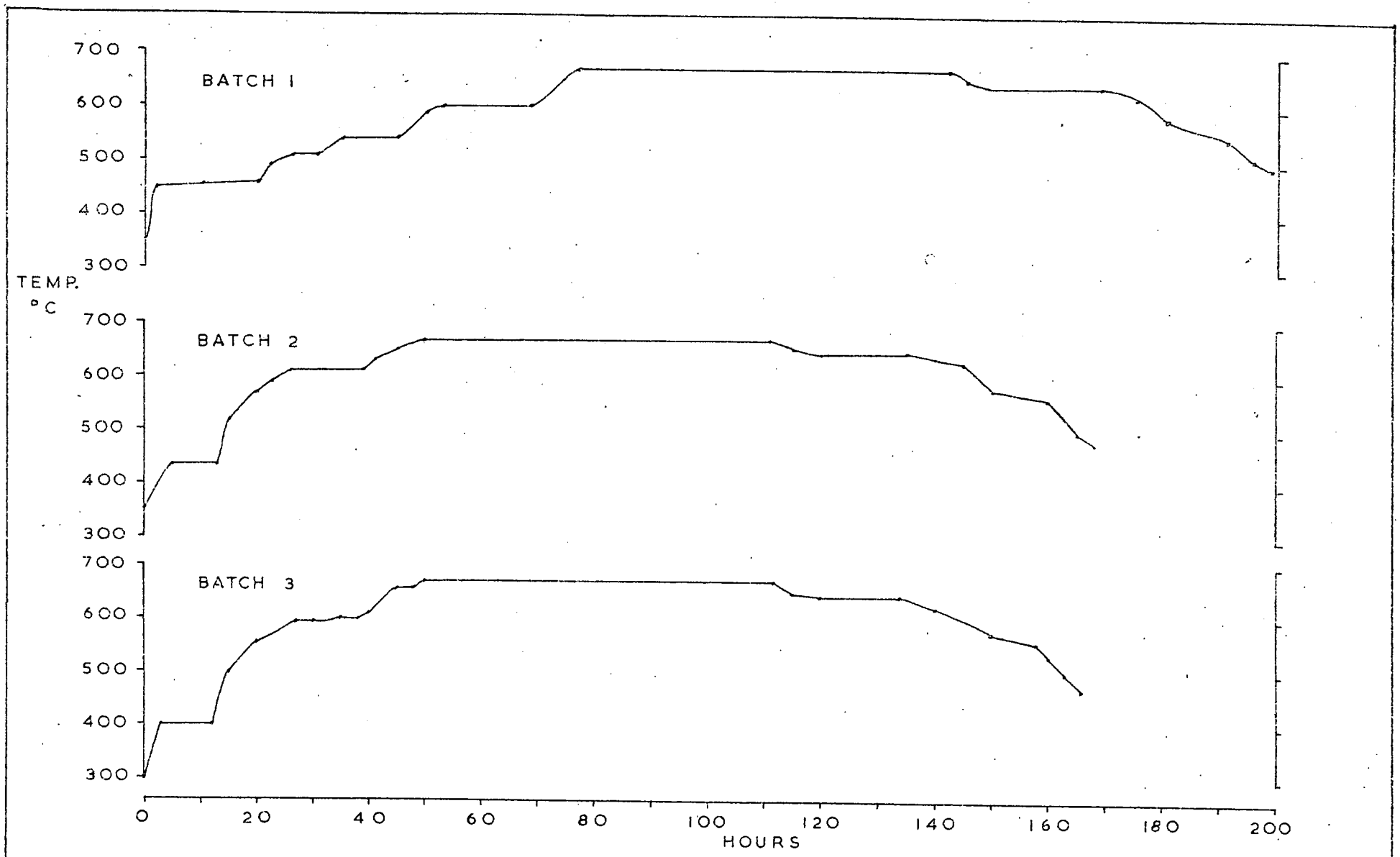

FIG · 4-1 SERIES 30, $CU_{12}(CSBAS)_4S_{12.5}$ TEMPERATURE RECORD

FIG 4-2
TEMPERATURE RECORD
SERIES 40 $CU_{12}(SBAS)_4S_{12.5}$

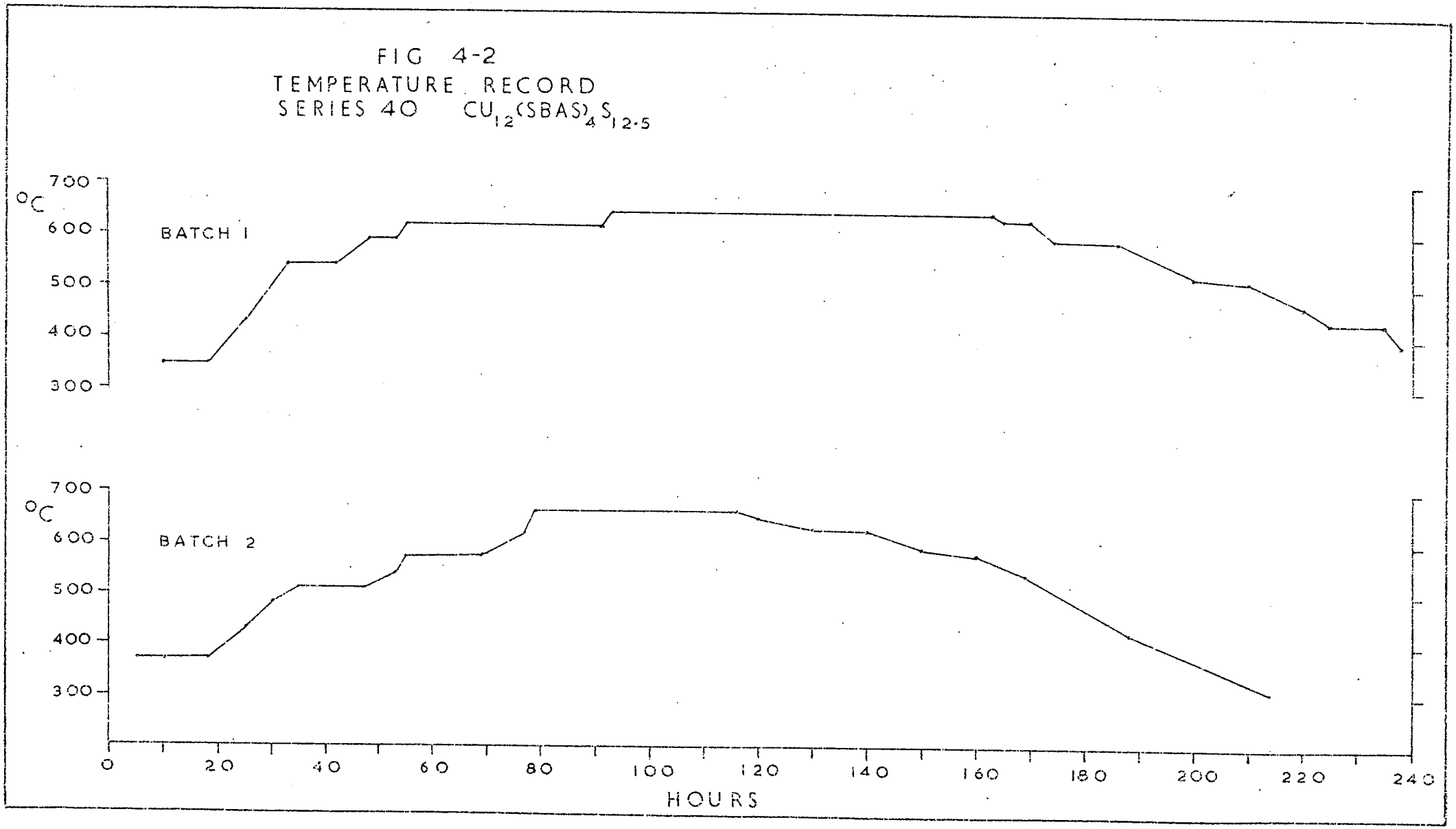

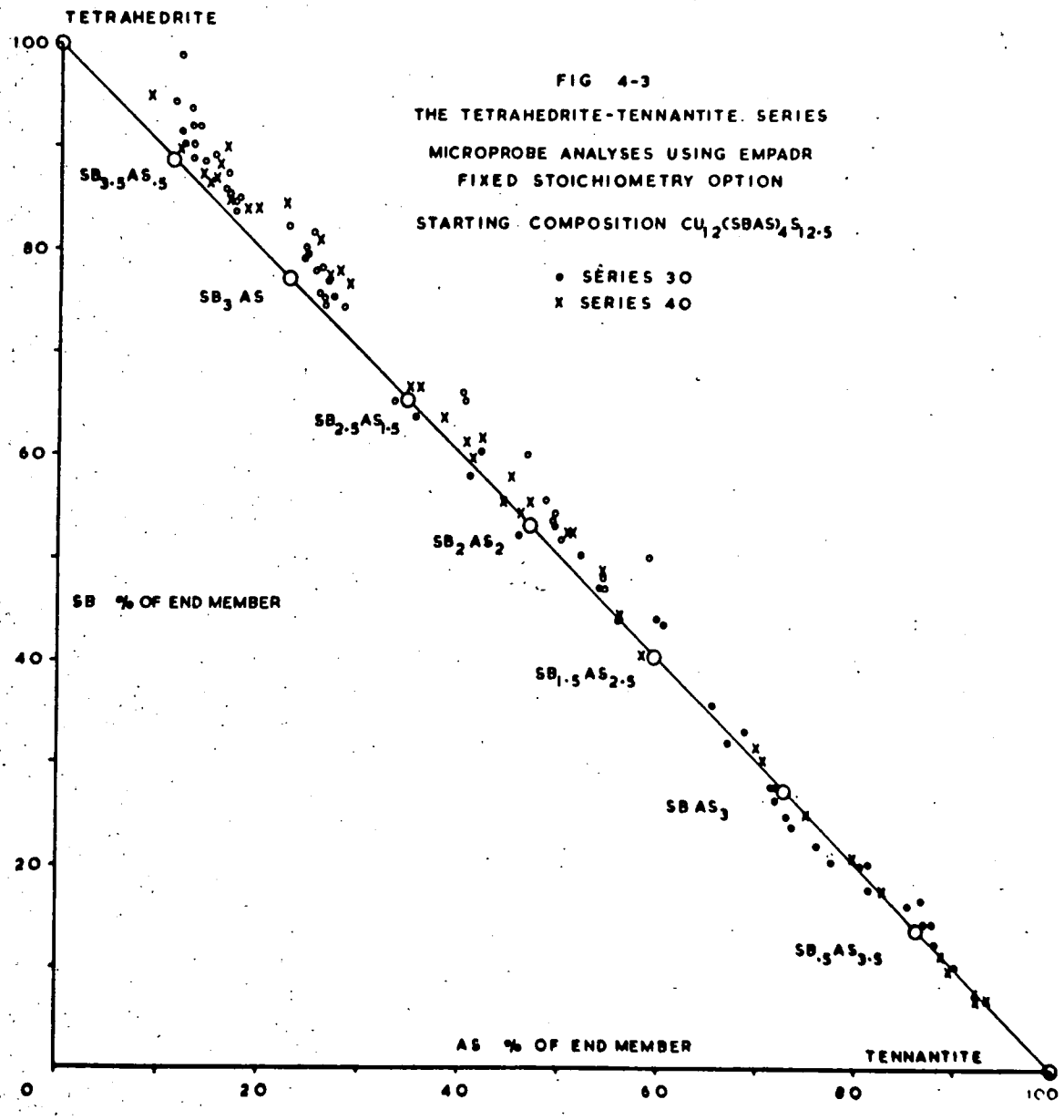

FIG 4-3

THE TETRAHEDRITE-TENNANTITE SERIES

MICROPROBE ANALYSES USING EMPADR
FIXED STOICHIOMETRY OPTION

STARTING COMPOSITION $Cu_{12}(SBAS)_4S_{12.5}$

• SERIES 30
x SERIES 40

FIG 4-4
DIFFRACTION PROFILES OF
TETRAHEDRITE-TENNANTITES

NO.	STARTING COMPOSITION
40	$Cu_{12}Sb_4S_{12.5}$
43	$Cu_{12}Sb_{2.5}As_{1.5}S_{12.5}$
46	$Cu_{12}SbAs_3S_{12.5}$
48	$Cu_{12}As_4S_{12.5}$

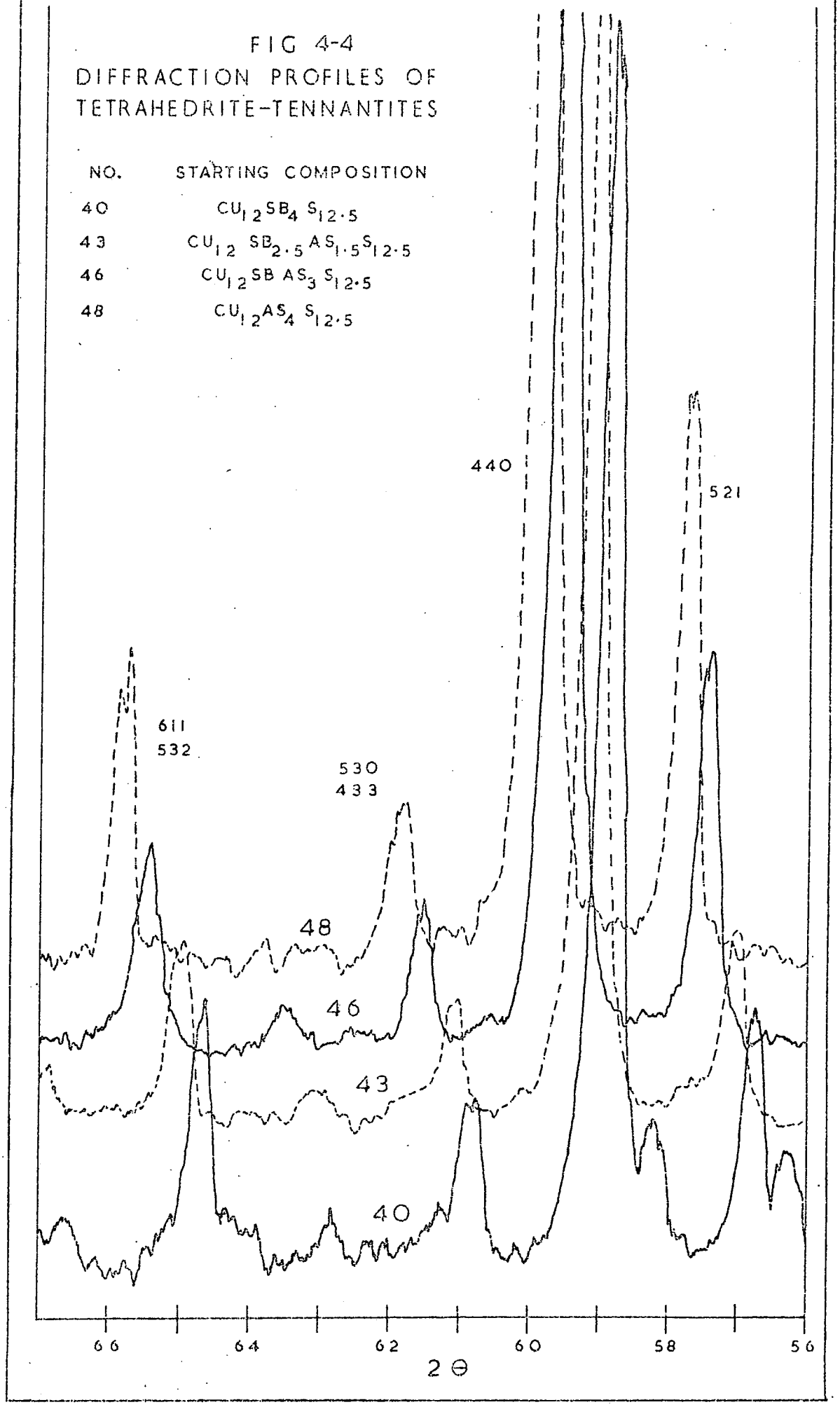

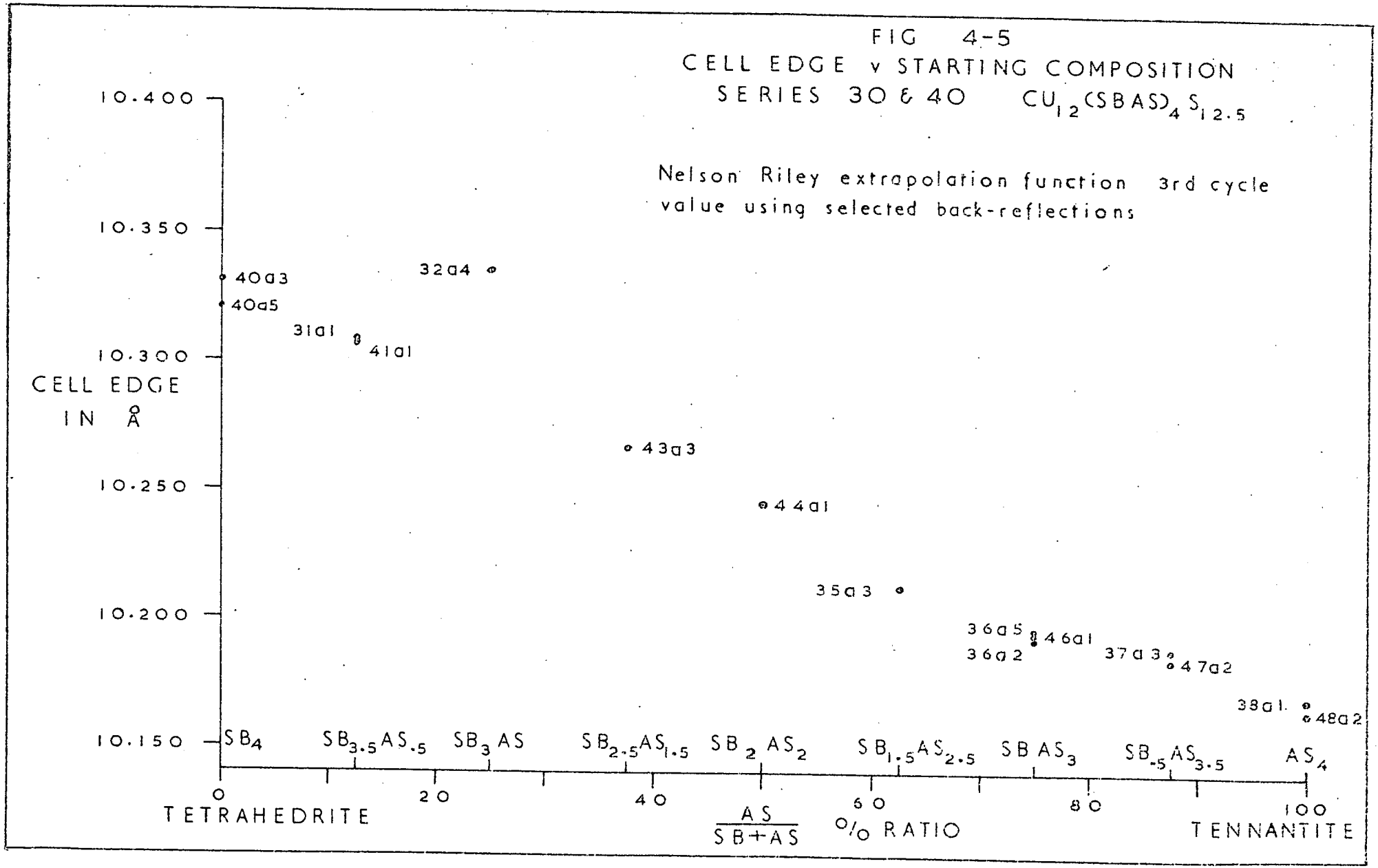
FIG 4-5
CELL EDGE v STARTING COMPOSITION
SERIES 30 & 40 $Cu_{12}(SbAs)_4S_{12.5}$
Nelson Riley extrapolation function 3rd cycle value using selected back-reflections
10.400
10.350
10.300
10.250
10.200
10.150
CELL EDGE IN Å
40a3
40a5
32a4
31a1
41a1
43a3
44a1
35a3
36a5
36a2
46a1
37a3
47a2
38a1
48a2
Sb_4
$Sb_{3.5}As_{.5}$
Sb_3As
$Sb_{2.5}As_{1.5}$
Sb_2As_2
$Sb_{1.5}As_{2.5}$
$SbAs_3$
$Sb_{.5}As_{3.5}$
As_4
0
20
40
60
80
100
TETRAHEDRITE
$\frac{As}{Sb+As}$ % RATIO
TENNANTITE

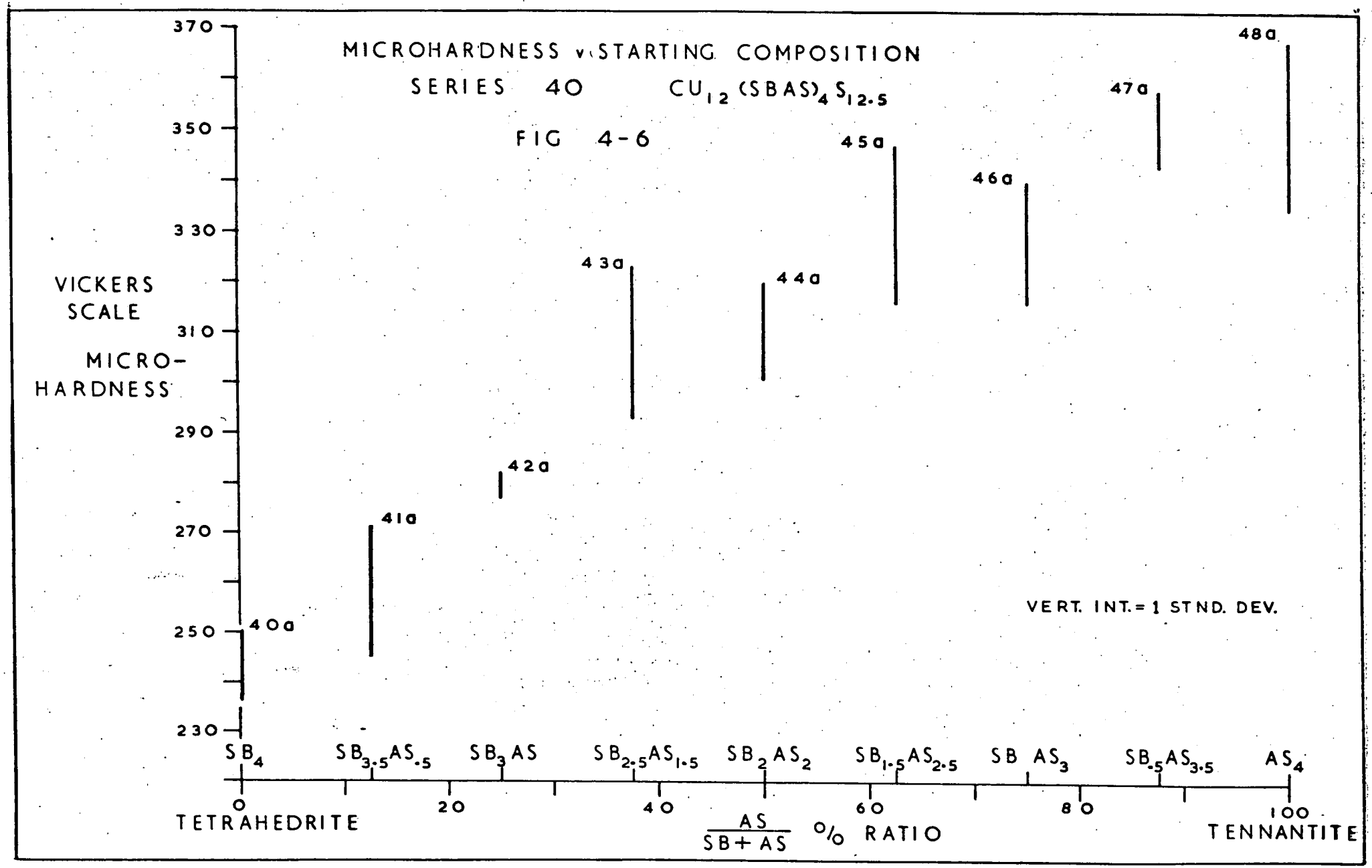
MICROHARDNESS v. STARTING COMPOSITION
SERIES 40 $CU_{12}(SBAS)_4S_{12.5}$
FIG 4-6
VICKERS SCALE MICRO-HARDNESS
370
350
330
310
290
270
250
230
40a
41a
42a
43a
44a
45a
46a
47a
48a
VERT. INT. = 1 STND. DEV.
SB_4
$SB_{3.5}AS_{.5}$
SB_3AS
$SB_{2.5}AS_{1.5}$
SB_2AS_2
$SB_{1.5}AS_{2.5}$
$SBAS_3$
$SB_{.5}AS_{3.5}$
AS_4
0
20
40
60
80
100
TETRAHEDRITE
$\frac{AS}{SB+AS}$ % RATIO
TENNANTITE

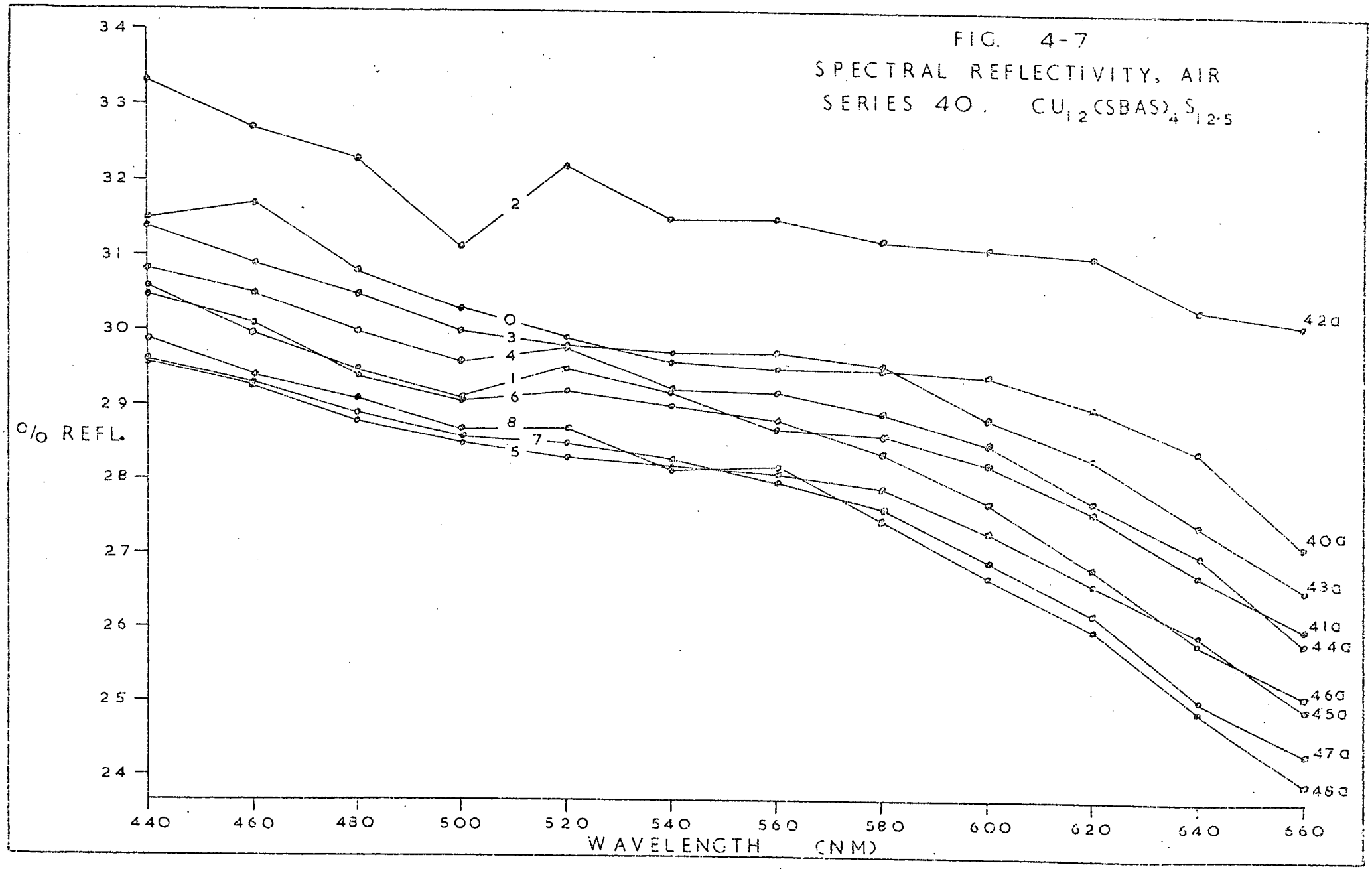
FIG. 4-7
SPECTRAL REFLECTIVITY, AIR
SERIES 40. $CU_{12}(SBAS)_4S_{12.5}$
% REFL.
WAVELENGTH (NM)
34
33
32
31
30
29
28
27
26
25
24
440
460
480
500
520
540
560
580
600
620
640
660
2
0
3
4
1
6
8
7
5
42a
40a
43a
41a
44a
46a
45a
47a
48a

FIG. 4-8 SERIES 40 $CU_{12}(SBAS)_4 S_{12\cdot5}$

ENLARGED AREA OF THE CHROMATICITY DIAGRAM
WITH COLOUR DISCRIMINATION (THRESHOLD) ELLIPSE

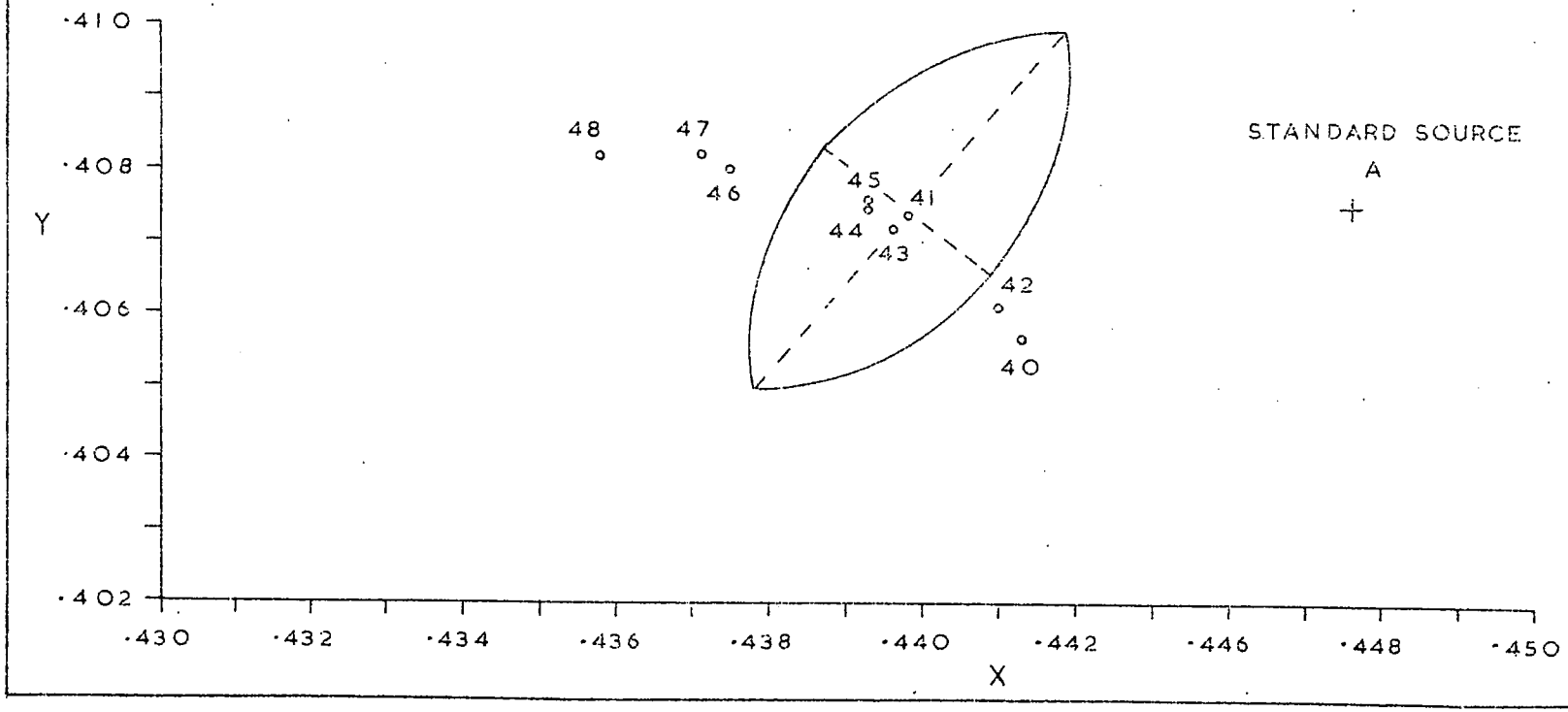

FIG 4-9 SERIES 40 $CU_{12}(SB\,AS)_4S_{12\cdot5}$

COLOUR MEASUREMENT FOR STANDARD SOURCE A

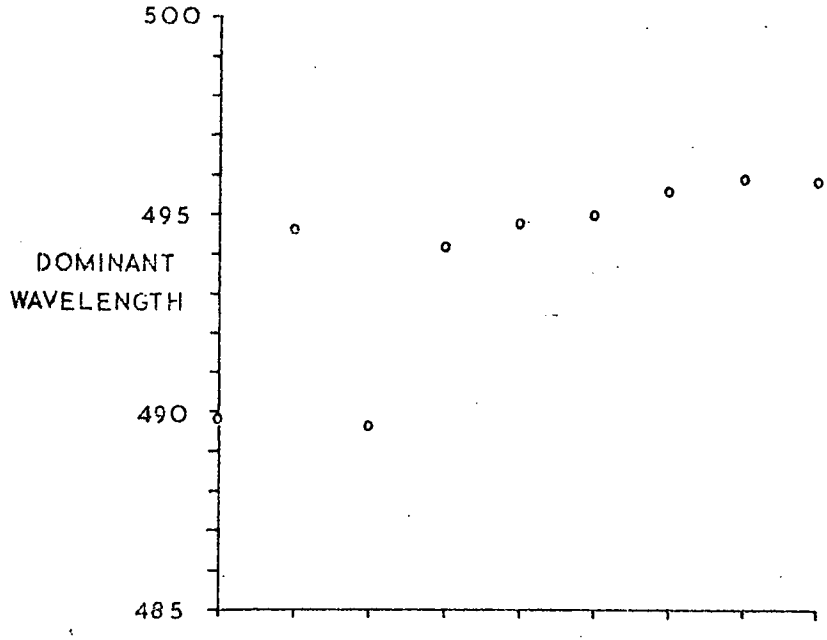

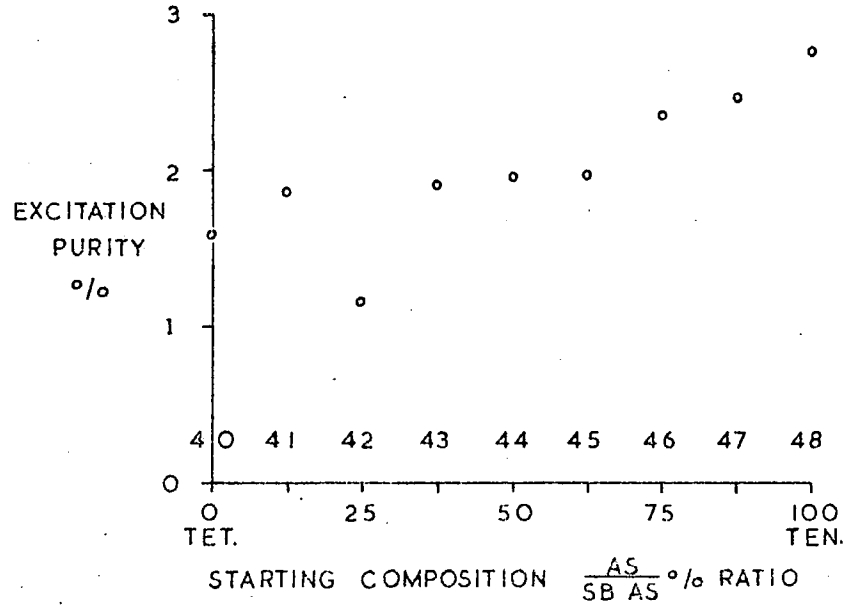

FIG.4-10 SERIES 40 $CU_{12}(CSBAS)_4S_{12.5}$

COLOUR MEASUREMENT FOR STANDARD SOURCE A

(Y = VISUAL BRIGHTNESS)

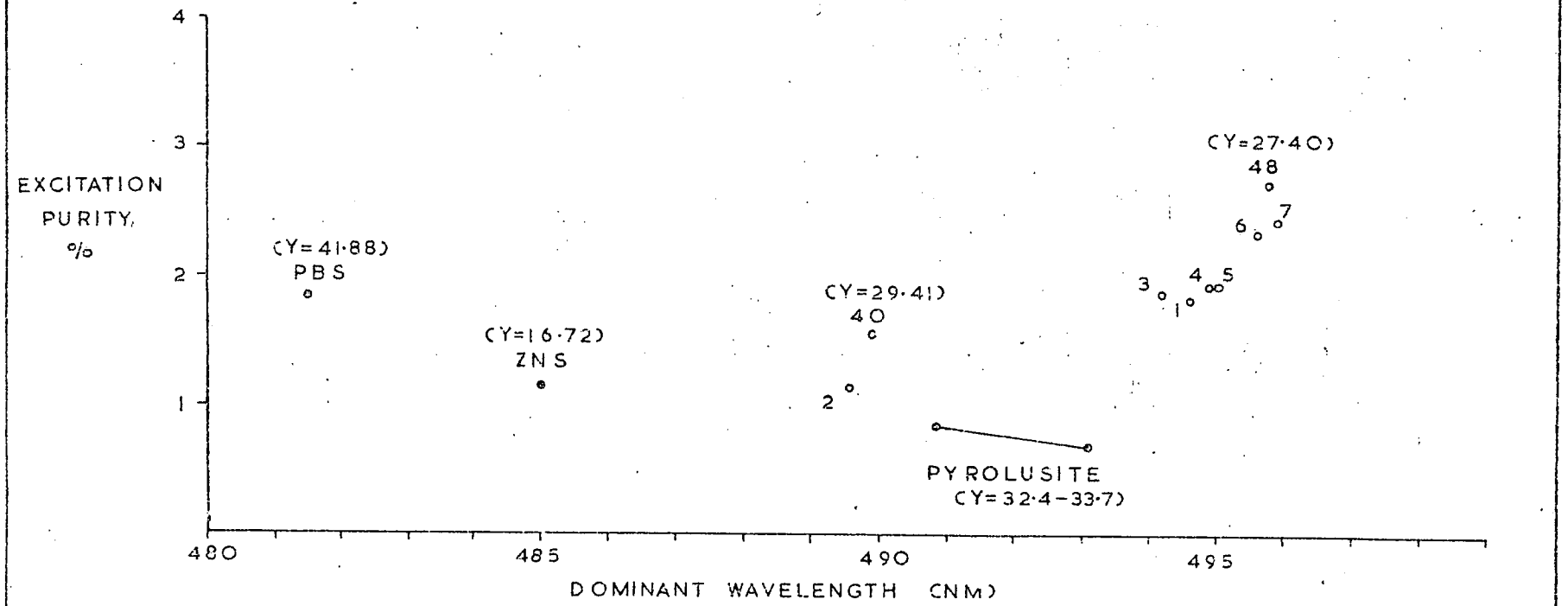

FIG 4-11 DIFFRACTION PROFILES OF QUENCHED TETRAHEDRITE AND TENNANTITE

STARTING COMPOSITIONS		PROFILE
TETRAHEDRITE	$Cu_{12}Sb_4S_{12.5}$	SOLID
TENNANTITE	$Cu_{12}As_4S_{12.5}$	DASHED

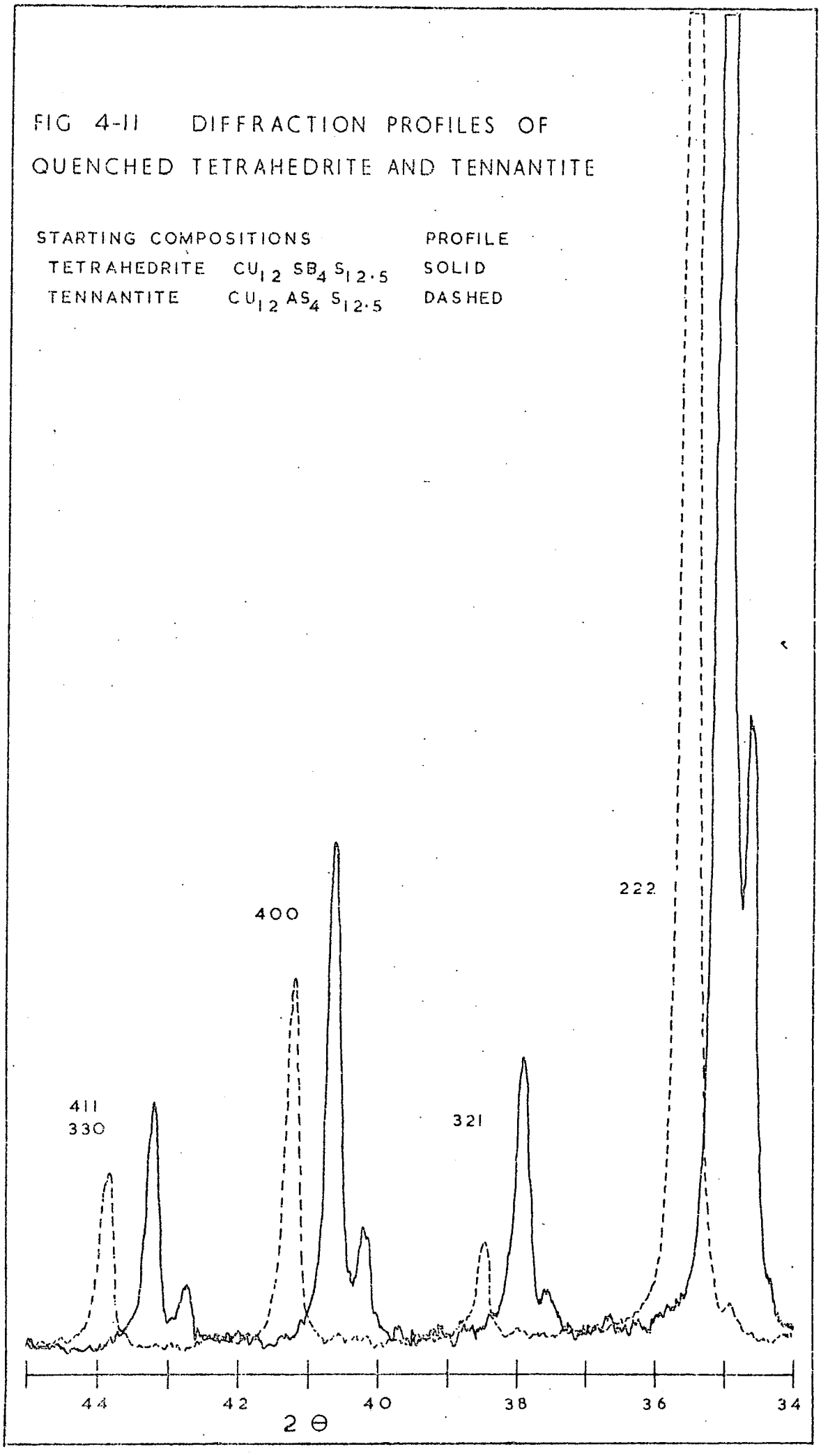

PLATE 4-1

Spec.No.40a x 220

Starting composition - $Cu_{12}Sb_4S_{12.5}$

$Cu_{2-x}S$ ovoids (two phases) rimmed by stibioluzonite, Cu_3SbS_4 (dark grey) in tetrahedrite, $Cu_{12}Sb_4S_{13}$. Note pitted and fractured grain margins of tetrahedrite - (non-stoichiometric tetrahedrite?).

PLATE 4-2

Spec.No.30a x polars x 220

Starting composition - $Cu_{12}Sb_4S_{12.5}$

Tetrahedrite (isotropic) with enechelon lamellae of chalcostibite, $CuSbS_2$ (anisotropic). Interstitial chalcostibite (anisotropic) and stibnite, Sb_2S_3 (strongly anisotropic, white).

PLATE 4-3

Spec.No.31a x 220

Starting composition - $Cu_{12}Sb_{3.5}As_{0.5}S_{12.5}$
Tetrahedrite-tennantite (grey) with interstitial tetrahedrite-tennantite and chalcostibite, $CuSbS_2$ (light grey).

PLATE 4-4

Spec.No.30b x 220

Starting composition - $Cu_{12}Sb_4S_{12.5}$(quenched)
Inverted tetrahedrite with interstitial intergrowth of pink tetrahedrite (grey) and chalcostibite (light grey). The euhedral bluish grey tetrahedrite crystal has a narrow rim of pink tetrahedrite.

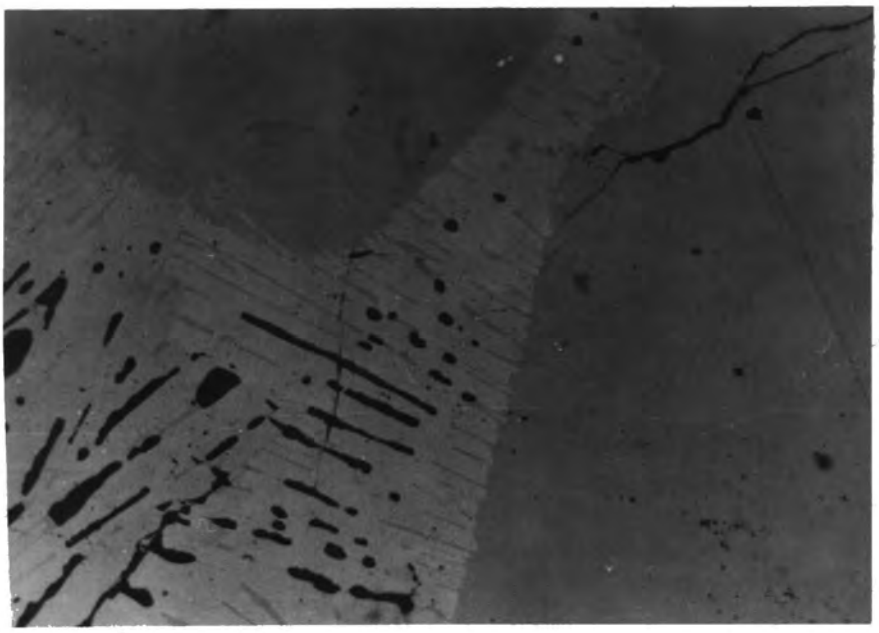

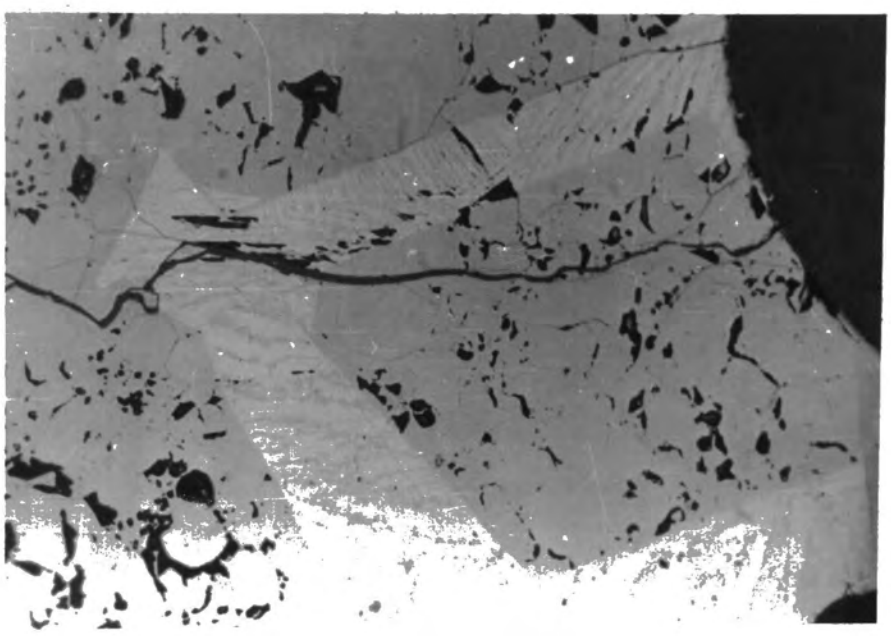

Summary of Conclusions and Discussion

It is concluded that the tetrahedrite-tennantite series in the Cu-Sb-As-S system is not a simple stoichiometric isomorphous seriesand that, although the results obtained contribute to the understanding of the complexity of the series, much more detailed experimental work, which is beyond the capabilities of the apparatus available for this study, is required.

From the examination of the synthesised tetrahedrite-tennantite series, starting composition $Cu_{12}(SbAs)_4S_{12.5}$, it was concluded that with increasing As:Sb ratio there is a general decrease in cubic cell edge, increase in microhardness, decrease in reflectivity and increase in colour intensity (excitation purity).

The mineralogical properties of two of the members of the series deviate in magnitude from the general trend of the series. These are the synthesised end-member tetrahedrite, $Cu_{12}Sb_4S_{13}$ (specimen 40), which is relatively Sb deficient, and specimen 42 which is Sb+As enriched. There is a continuity in the series with increasing Sb:As ratio from tennantite almost to an Sb end-member. If this series is extrapolated the hypothetical Sb end-member has 3.51% more Sb than the synthesised tetrahedrite, $Cu_{12}Sb_4S_{13}$ (specimen 40). The synthesised tennantite end-member was sulphur deficient relative to the stoichiometric composition - $Cu_{12}As_4S_{13}$.

Maske and Skinner (1971) have shown that synthetic tennantite has a range in composition along a line from $Cu_{12}As_4S_{13}$ towards Cu in the Cu-As-S system and that the tennantite field approaches the stoichiometric composition with decreasing temperature. The stoichiometric composition

was not attained in the experiments which were above 300°C. The cell edge of non-stoichiometric tennantites decreased with decreasing Cu content. No high temperature polymorph of tennantite was noted by Maske and Skinner nor in quench experiments in the present study.

Experiments in the Cu-Sb-S system in the present study (Chapter 2) have shown the existence of a range in Cu:Sb ratio for a non-stoichiometric (sulphur deficient) tetrahedrite. The stoichiometric tetrahedrite, $Cu_{12}Sb_4S_{13}$, was however obtained in most experiments. The cell edge of the non-stoichiometric tetrahedrite increases with increasing Sb:Cu ratio. There is a high temperature cubic polymorph of non-stoichiometric tetrahedrite and its stability increases with increasing Sb:Cu ratio. The possible entire range in composition of tetrahedrite in the Cu-Sb-S system and its variation with temperature has not been defined but the possible extent at high temperatures is shown in Fig.4-12.

The features of the synthesised tetrahedrite-tennantite series, starting composition $Cu_{12}(SbAs)_4S_{12.5}$, can now be understood. The data relevant to this discussion are summarised in Fig.4-12. The continuity in the series, from the synthetic tennantite, almost to an Sb end-member represents a movement from 48a to B (Fig.4-12). Cell size increases due to increasing Sb:As ratio but specimen 32, probably due to an error in specimen preparation, is Sb+As rich, has a large cell size, and lies close to point D. Cell size will also be increasing due to changing stoichiometry of the series. The end-member tetrahedrite obtained has a low cell edge compared to the projected end-member of the series which therefore lies between B and 13a. The point D has

3.51% more Sb than $Cu_{12}Sb_4S_{13}$ and therefore is the extrapolated end-member of the series.

From the microprobe analyses given in Fig.4-3 it was concluded that there are two possible miscibility gaps in the tetrahedrite-tennantite series. The structure of tetrahedrite-tennantite, $Cu_{12}(SbAs)_4S_{13}$, (Wuensch 1964, 66) is illustrated in Fig.6-1. In the unit cell there are eight semi-metal (Sb+As) atoms in trigonal pyramidal co-ordination with sulphur atoms. Four of the pyramids point inwards towards the octahedrally co-ordinated sulphur atom at the centre of the unit cell and four point outwards (Fig.4-13). Ordering of the Sb and As atoms in these sites in the $Cu_{12}Sb_2As_2S_{13}$ composition is therefore suggested as a model which results in increased stability of the Sb:As $\simeq$ 1:1 ratio (Fig.4-13). The resultant solvi would therefore be expected to peak at Sb_3As and $SbAs_3$. Series 30 and 40 give observed gaps with approximate centres at $Sb_{2.25}As_{1.75}$ and $Sb_{1.25}As_{2.75}$, slightly closer to Sb_2As_2 than expected.

The miscibility gaps may be associated with discontinuous changes in phase relations of tetrahedrite-tennantite between the Cu-Sb-S and the Cu-As-S systems.

There is little point in speculating further on the nature of the tetrahedrite-tennantite series because much more detailed work is obviously required. A complete determination of the Cu-Sb-As-S system is required. The nature of the tetrahedrite-tennantite series, i.e. its range in Cu:(SbAs):S ratio with changing Sb:As ratio and temperature, makes it too complex for satisfactory study with the apparatus available for this present study. Both quench experiments and, because of the metastable phases, D.T.A.

experiments are required. Verification of the miscibility gaps could be achieved by very slow cooling of starting compositions corresponding to the centre of the miscibility gaps. The splitting into two compositions could then be shown by microprobe analyses of random points on the polished specimen and possibly by x-ray diffraction.

The change in physical properties with changing Sb:As ratio will be discussed further in Chapter 6 on aspects of substitution in tetrahedrite.

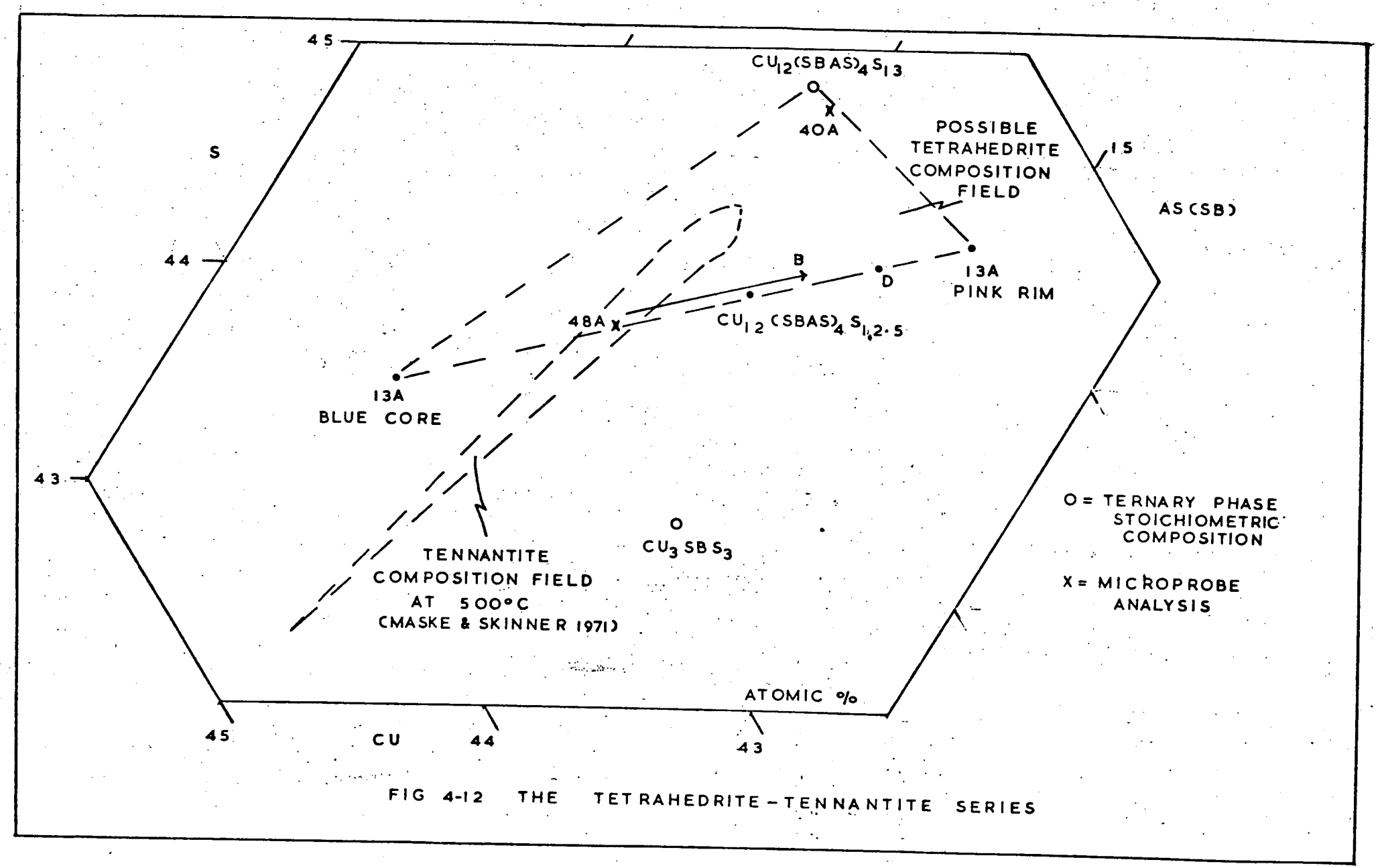

FIG 4-12 THE TETRAHEDRITE – TENNANTITE SERIES

FIG 4-13 SEMI-METAL ORDERING

IN $CU_{12}SB_2AS_2S_{13}$

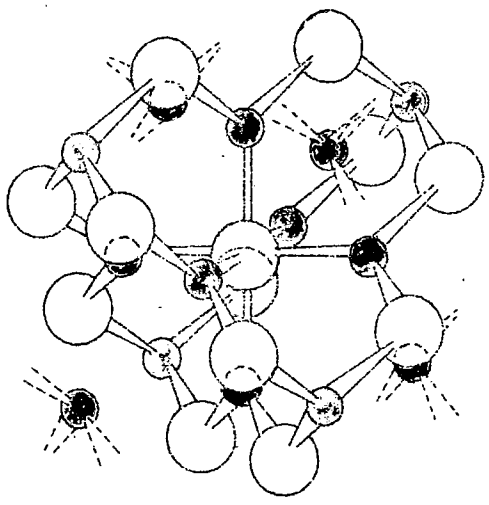

S NON-METAL

CU METAL

SB, AS } SEMI-METAL

CHAPTER 5

Substitution of Cu by Zn, Fe and Ag in Synthetic Sulphosalts

Introduction

Silver, zinc and iron are the main elements found substituting for copper in natural tetrahedrites. In order to determine the limits of substitution of these elements in tetrahedrite and to ascertain the resultant changes in the mineralogical properties of tetrahedrite, several substituted tetrahedrites have been synthesised. Silver, zinc and iron are an appropriate choice in elements because silver is always univalent, zinc always divalent and iron divalent or trivalent in their salts whereas copper is univalent or divalent.

Synthesis of one silver+zinc substituted tetrahedrite, one silver substituted stibioluzonite and one zinc substituted stibioluzonite was also attempted in order to obtain information useful in the discussion on theoretical aspects of substitution.

Substituted tetrahedrite starting compositions will first be described. Substitution in other phases will then be described in two sections - one on the substituted stibioluzonite starting compositions and the other on solid solutions in the Cu-Ag-Sb-S system obtained in the attempt to synthesise Ag-tetrahedrite. A summary of the conclusions reached will then be followed by a discussion of the results.

Substituted Tetrahedrite ($Cu_{12}Sb_4S_{13}$) Starting Compositions

Sample Preparation and Synthesis

Details of the high purity elements used for synthesis are given in Table 1-1b. The technique of sample preparation and synthesis was as described in Chapter 2. The specimens were run in several batches. The temperature history of each batch is given in Table 5-1a. All the specimens had similar heating histories which were planned to yield large crystals of substituted tetrahedrite by slow cooling of the melt. The melting point of pure tetrahedrite is about 610°C. The specimens were therefore heated to about 680°C and cooled slowly to 400°C. Cooling from 400°C to room temperature was moderately rapid in order to obtain textural evidence of any temperature dependant substitution.

Examination of Polished Specimens

For each substituting element, the phases obtained and observed in the polished specimens have been tabulated with the starting composition in Tables 5-2 to 5-5. Substituted tetrahedrites suitable for the determination of mineralogical properties using microanalytical techniques were obtained.

In zinc starting compositions ZnS was obtained as an impurity in tetrahedrite and chalcostibite with native Sb was interstitial (Plate 5-3).

In the low iron starting composition bornite was obtained as an impurity, rimmed by stibioluzonite, in tetrahedrite. Chalcostibite was interstitial (Plate 5-1). In the high iron starting composition chalcopyrite, usually intergrown with bornite, was obtained in tetrahedrite. Chalcostibite and native Sb were interstitial (Plate 5-2).

Ag-tetrahedrites were only obtained from the two starting compositions with the lowest initial silver content and were veined and pseudomorphed by a fine grained intergrowth of stibioluzonite and $(CuAg)_3SbS_3$ (Plates 5-4, 5, 6). A similar coarse grained intergrowth was interstitial. In starting compositions with higher initial silver content, stibioluzonite and $(AgCu)_3SbS_3$ were the two main co-existing phases obtained. Primary laths of stibioluzonite were in a matrix of $(AgCu)_3SbS_3$ or $(AgCu)_3SbS_3$ + stibioluzonite.

Substituted ZnAg-tetrahedrite was obtained from the zinc+silver starting composition. ZnS was obtained as an impurity in tetrahedrite. $(CuAg)_3SbS_3$ intergrown with stibioluzonite and chalcostibite was interstitial. Large impurity-free tetrahedrites were obtained as well as some tetrahedrites which were replaced, marginally, by a $(CuAg)_3SbS_3$ + stibioluzonite intergrowth.

There was no evidence of exsolution, nor for a phase change (structural inversion) in any of the substituted tetrahedrites obtained.

Conclusions from Polished Specimen Study

Only a small amount of ZnS was obtained in the low zinc starting composition indicating that most of the zinc had entered the tetrahedrite structure. The large amount of ZnS obtained from the high zinc starting composition indicated that the tetrahedrite should be saturated in zinc.

In the texture obtained from the low iron starting composition, bornite played the role of $Cu_{2-x}S$ in pure tetrahedrite starting compositions. A reaction relationship is evident -

Fe-tetrahedrite $\longrightarrow$ bornite + Sb-rich liquid

The stibioluzonite rim around bornite (Plate 5-1) indicates decreasing sulphur content of bornite solid solution with decreasing temperature (as $Cu_{2-x}S$). The excess sulphur reacts with tetrahedrite to give stibioluzonite.

Chalcopyrite was obtained from the iron rich starting composition. The serrated rims of the grains indicate incomplete reaction and, from the appearance of the charge (Table 5-3), complete melting was not achieved. The chalcopyrite-bornite intergrowth (Plate 5-2) is due to decreasing solid solution in the Cu-Fe-S system with decreasing temperature.

In iron and zinc starting compositions no evidence of exsolution was observed indicating that the substitution of Zn and Fe in tetrahedrite is independent of temperature. In iron and zinc rich starting compositions the co-existence of substituted tetrahedrite and native metal (or native metal + chalcostibite) indicates that there is probably no $(CuFe)_3SbS_3$ nor $(CuZn)_3SbS_3$ solid solution extending into the Cu-Fe-Sb-S or Cu-Zn-Sb-S system respectively (Plates 5-2, 3).

The stability of Ag-tetrahedrite is obviously temperature dependant. Cooling results in a eutectoid type breakdown -

$$(CuAg)_{12}Sb_4S_{13} \longrightarrow 3(AgCu)_3SbS_3 + (CuAg)_3SbS_4$$

The breakdown products form irregular veins within tetrahedrites and pseudomorph tetrahedrite (Plates 5-4, 5, 6). The Ag-tetrahedrites preserved are therefore probably metastable, the breakdown process having been 'frozen' on cooling.

The co-existence of stibioluzonite and $(AgCu)_3SbS_3$ at

higher initial silver contents indicates that Ag-tetrahedrite solid solution does not extend far into the Cu-Ag-Sb-S quaternary. Substitution in this system will be discussed below.

In the zinc+silver starting composition the divalent cation excess was again located in phases within tetrahedrite and the excess Ag was located in interstitial phases.

General Character of Substituted Tetrahedrites in Polished Specimen

Changes in the appearance of the tetrahedrites due to substitution were difficult to observe because of the illusionary effects of different adjacent impurity grains. Several Zn-tetrahedrites were weakly anisotropic. This was difficult to observe but quite definite. This phenomenon may be related to ordering in substituted tetrahedrites. Changes in the powder x-ray diffraction pattern would be small (e.g. superlattice lines) and completely monophasal samples would be necessary for their detection.

The hardness of Ag- and Zn,Fe-tetrahedrites differs significantly; scratching with a needle distinguishes the hard, brittle Zn,Fe-tetrahedrites from Ag-tetrahedrite.

Electron Microprobe Analysis

The analytical conditions are given in Table 5-1b. The substituted tetrahedrites and some of the other phases obtained were analysed completely (Tables 5-2 to 5-5). Corrections were made using EMPADR VII (Chapter 2).

The substituted element content obtained is plotted against starting composition in Fig.5-1. The 'starting composition join' (Fig.5-1) indicates the element content which would have been obtained if equilibrium had been attained and the starting composition represented a possible

substituted tetrahedrite composition. The 'expected divalent max' indicates the limit of substitution of divalent cations if tetrahedrite is a normal valence compound (see Chapter 6). The variation in copper to substituted element ratio of the substituted tetrahedrites was obtained using the fixed stoichiometry option of EMPADR VII (Fig.5-2). Impurity phases which were not fully analysed were partially analysed on the microprobe in order to confirm optical identification.

Conclusions from Microprobe Analysis

The limits of substitution of zinc and iron in tetrahedrite were reached in the experiments (Figs.5-1, 2) and are the limits expected if tetrahedrite is a normal valence compound, i.e. the elements have their normal valencies and the charges of the electropositive and electronegative elements balance.

Silver substitution in the Ag-tetrahedrite did not reach such a definite saturation value (Figs.5-1, 2) and the silver content was low compared to that expected from the starting composition (Fig.5-1).

The variation in the ratio of copper to substituted element in any one specimen was small (Fig.5-2).

The zinc+silver starting composition yielded a tetrahedrite with the expected zinc content and silver was only low by 1 at%. The high Zn+Ag at% total in tetrahedrite indicates that zinc and silver do not compete for copper sites. If zinc and silver did compete for copper sites the maximum at% Zn+Ag content possible would equal the maximum at% Zn content found (6.90 at%).

The analyses confirm the general formula of substituted tetrahedrite -$(CuAg)_{10}(CuZnFe)_2Sb_4S_{13}$.

X-ray Diffraction

Debye-Scherrer powder photographs were obtained by picking out material from the polished specimen. The d-spacings were measured and indexed (Table 5-6). The unit cell edge of each substituted tetrahedrite was computed (Table 5-7) using NELRIL (Chapter 2) and plotted against substituted element content in Fig.5-3.

Only poor powder photographs of Ag-tetrahedrite could be obtained due to the admixture of impurity. The standard error on the intercept obtained during the Nelson-Riley extrapolation procedure (NELRIL) is therefore large and is shown in Fig.5-3.

Conclusions from X-ray Diffraction

There is no detectable departure from the pure tetrahedrite cubic powder pattern as Cu is substituted apart from an increase in d-spacing values. The lines missing in some substituted tetrahedrites are of low intensity or have been superimposed by impurity lines.

The cell edges of tetrahedrite increased in every case of substitution (Fig.5-3). The cell edge of substituted tetrahedrite is dependant on the at% Cu substituted but independent of the substituting cation. The cell edge of zinc and iron substituted tetrahedrite reaches a maximum of about 10.385Å corresponding to substitution of 6.90 at% Cu. This cell edge value is exceeded by Zn+Ag substituted tetrahedrite. The accumulative effect of Zn+Ag substitution on the cell edge therefore confirms the conclusion that Zn and Ag do not compete for Cu sites in tetrahedrite and confirms the general formula of substituted tetrahedrite - $(CuAg)_{10}(CuZnFe)_2Sb_4S_{13}$.

The cell edge of tetrahedrite saturated in substituted divalent element, $Cu_{10}(ZnFe)_2Sb_4S_{13}$, can be obtained from Fig.5-3 and is 10.385 Å.

Microhardness Measurements

The Vickers Microhardness of each substituted tetrahedrite was measured (Table 5-8) using the technique described in Chapter 2. Conchoidal fractures and splintering were common in zinc and iron substituted tetrahedrites but Ag-tetrahedrites were less brittle.

Microhardness was plotted against substituted element content in Fig.5-4. In the case of ZnAg-tetrahedrite the microhardness has been plotted against the zinc content.

Conclusions from Microhardness Measurements

The microhardness of substituted tetrahedrite increases with substitution of Cu by Fe and Zn but decreases with substitution of Cu by Ag. The ZnAg-tetrahedrite has a lower microhardness than expected from its Zn content and this is due to the Ag content (Fig.5-4).

The microhardness of tetrahedrite saturated in substituted divalent elements, $Cu_{10}(ZnFe)_2Sb_4S_{13}$, can be obtained from Fig.5-4 and is 390.

Reflectivity Measurements

The reflectivities of the substituted tetrahedrites were measured at three wavelengths using the technique described in Chapter 2. The results are given in Table 5-9 and plotted in Fig.5-5. The reflectivities at wavelength = 540nm are plotted against substituting element content in Fig.5-6.

Conclusions from Reflectivity Measurements

Reflectivities at the three wavelengths increase with

Zn and Fe substitution of Cu in tetrahedrite (Fig.5-5). The increase in reflectivity differs at different wavelengths and, with increasing content of substituted Zn and Fe, a peak develops at 540nm. With substitution of Cu by Ag, reflectivities decrease, and the decrease is greater at greater wavelengths. The reflectivity of the ZnAg-tetrahedrite is less than expected from its Zn content, the reduction in reflectivity being due to its Ag content (Figs. 5-5, 6).

The results indicated that changes in the spectral reflectivity curve of substituted tetrahedrite will be sensitive to compositional changes but the lack of strong correlation of reflectivity with substituted element content at high zinc contents (Fig.5-6) indicates that non-stoichiometry of substituted tetrahedrite can have an effect.

Substitution in Other Phases

Substituted Stibioluzonite Starting Compositions

Sample Preparation and Synthesis

Details of the high purity elements used for synthesis are given in Table 1-1b. The sample preparation and technique of synthesis was as described in Chapter 2. Starting compositions representing a silver substituted stibioluzonite and a zinc substituted stibioluzonite were prepared. The specimens were run with specimens of the substituted tetrahedrite starting compositions and therefore had the same temperature history.

Examination of Polished Specimens

The phases observed in the polished specimens prepared have been tabulated with each starting composition (Table 5-10).

Large anhedral stibioluzonite crystals with interstitial silver rich sulphosalts (pyrargyrite and miargyrite) were obtained from the silver starting composition. There was no textural evidence of temperature dependance of silver substitution in stibioluzonite.

The zinc starting composition produced a great deal of ZnS and this was entirely associated with tetrahedrite. Stibioluzonite was obtained and this had a mutual boundary texture with tetrahedrite (Plate 5-7). Tetrahedrite was observed to contain lamellae of stibioluzonite, with associated studs of a native metal, in three orientations (Plates 5-7, 8).

Conclusions from Polished Specimen Study

In the silver starting composition the presence of interstitial silver rich sulphosalts indicated that only a limited amount of silver entered the stibioluzonite structure.

In the zinc starting composition stibioluzonite was obtained, but the association of ZnS with tetrahedrite only, indicated the improbability of zinc substitution in stibioluzonite.

The tetrahedrite-stibioluzonite texture (Plates 5-7, 8) was not observed in runs in the Cu-Sb-S system. The presence of zinc is therefore the key to the explanation of this texture. Zn-tetrahedrite must be capable of dissolving excess sulphur at high temperatures. On cooling, the sulphur is expelled from the structure (in the 111 orientation), resulting in lamellae of stibioluzonite. A close structural relationship between stibioluzonite and the 111 orientation in tetrahedrite is indicated. Stibioluzonite cannot accept zinc into the structure (see microprobe analysis) and zinc is therefore rejected from the areas of sulphur accumulation. The white studs are tentatively identified as being zinc rejected during this process.

Electron Microprobe Analysis and Conclusions

The analytical conditions are given in Table 5-1b. The main phases obtained were analysed fully (Table 5-10). Corrections were made using EMPADR VII (Chapter 2).

Only a small amount of silver entered the stibioluzonite structure. The interstitial silver rich phases were confirmed to be pyrargyrite, $(AgCu)_3SbS_3$, and miargyrite, $(AgCu)SbS_2$.

Zinc did not enter the stibioluzonite structure but tetrahedrite containing a high concentration of zinc was formed.

X-ray Diffraction and Conclusions

A specimen of Ag-stibioluzonite was picked from the polished specimen and a powder photograph obtained. The d-spacings were measured, indexed using GENSTRUK, and the tetragonal unit cell parameters calculated using COHEN (Chapter 2). The diffraction data for this Ag-stibioluzonite are given in Table 5-11 and the cell parameters, given in Table 5-12, plotted in Fig.5-10.

The effects of silver on the structure of stibioluzonite are discussed below.

Solid Solutions in the Cu-Ag-Sb-S System

The attempt to synthesise Ag-tetrahedrites resulted in the recognition of the following solid solutions in the Cu-Ag-Sb-S system - $(CuAg)_{12}Sb_4S_{13}$, $(CuAg)_3SbS_3$ and $(CuAg)_3SbS_4$.

Microprobe analyses of the co-existing phases obtained from each starting composition (Table 5-4) are plotted in the Cu_3SbS_3 - Cu_3SbS_4 - Ag_3SbS_4 - Ag_3SbS_3 plane (Fig.5-7). The location of this plane in the Cu-Ag-Sb-S quaternary is given in Fig.5-8.

The $(CuAg)_{12}Sb_4S_{13}$ and $(CuAg)_3SbS_4$ solid solutions are limited but there is extensive Cu_3SbS_3 - Ag_3SbS_3 solid solution. The possibility remains, however, of a miscibility gap in Cu_3SbS_3 - Ag_3SbS_3 between 30 and 75 mol% Cu_3SbS_3. The fact that Cu_3SbS_3 is orthorhombic (wittichenite structure) and Ag_3SbS_3 (pyrargyrite) is hexagonal increases this possibility.

The softness of the phases obtained along the Cu_3SbS_3 - Ag_3SbS_3 series compared with the harder co-existing

stibioluzonite made it impossible to obtain satisfactory powder photographs by picking material from the polished specimens. On impact by the electron microprobe beam the Cu rich members fractured readily and this may be related to low totals for some of the analyses. In polished specimen this series is characterised by strong blood red internal reflections.

Using the fixed stoichiometry option of EMPADR VII (Chapter 2) the variation in Cu:Ag ratio of the Ag-stibioluzonites was obtained and the microprobe analyses are plotted in Fig.5-9.

Several Ag-stibioluzonites were picked out from the polished specimens, powder photographs obtained and the diffraction lines measured and indexed (Table 5-11). The tetragonal cell parameters, given in Table 5-12, were computed using COHEN (Chapter 2) and plotted against silver content in Fig.5-10. Silver causes a shortening of the unit cell in the direction of the 'c' axis and an expansion of the 'a' axes. The change from a 'c':'a' ratio of 2:1 in pure stibioluzonite results in a splitting of certain lines which is seen clearly in the powder photographs (Table 5-11).

CONCLUSIONS

(A) - Substitution of Zn, Fe, Ag and Zn+Ag for Cu in synthetic tetrahedrite.

(1) The general formula of substituted tetrahedrite is confirmed to be $(CuAg)_{10}(CuZnFe)_2Sb_4S_{13}$.

(2) Substitution of Zn and Fe for Cu in stoichiometric tetrahedrite has a limit (6.90 at%) which is independent of temperature whereas the substitution of Ag for Cu is temperature dependant.

(3) The cubic unit cell edge of substituted tetrahedrite increases with increase in the at% of Cu which is substituted but is independent of the type of substituting element.

(4) The microhardness of substituted tetrahedrite increases with Zn and Fe substitution of Cu but decreases with Ag substitution of Cu.

(5) The reflectivity of substituted tetrahedrite increases with Zn and Fe substitution of Cu but decreases with Ag substitution of Cu. The magnitude of change in reflectivity differs at different wavelengths.

(6) Tetrahedrite containing substituted Zn is capable of dissolving excess sulphur which is exsolved on cooling.

(7) Silver rich tetrahedrite starting compositions are represented by $(AgCu)_3SbS_3$ and $(CuAg)_3SbS_4$ which are also the low temperature breakdown products of Ag-tetrahedrite.

(B) - Substitution in other phases.

(1) In stibioluzonite, Cu can be substituted to a limited extent by Ag but not at all by Zn.

(2) Substitution of silver for copper in stibioluzonite causes a decrease in 'c' and an increase in 'a' of the tetragonal unit cell and the resultant change in 'c':'a' ratio from 2:1 causes a splitting of certain lines on the X-ray powder photograph.

(3) There is extensive Cu_3SbS_3 - Ag_3SbS_3 solid solution but the possibility remains of a miscibility gap between 30 and 75 mol% Cu_3SbS_3.

Discussion of Results

The limit of substitution of Zn and Fe in tetrahedrite, $Cu_{12}Sb_4S_{13}$, was established. Exsolution lamellae of stibioluzonite in Zn-tetrahedrite and the slight variation in physical properties of Zn rich tetrahedrites indicate that non-stoichiometry of tetrahedrite is possible, especially at high temperatures. As in the case of the tetrahedrite-tennantite series, non-stoichiometry necessitates caution when reaching conclusions on the relation of physical properties to concentration of substituting elements. Quantitative conclusions on the physical properties of zinc and iron saturated tetrahedrite must therefore remain tentative until verified by further experiment.

The limits of substitution obtained for Zn and Fe are in excellent agreement with the contents of Zn+Fe+Hg observed in natural substituted tetrahedrite-tennantites (Fig.1-2). The postulate that silver substitution in natural tetrahedrite is related to a Cu : Fe+Zn+Hg ratio of 5:1 (Chapter 1) has not been verified by the present experimental work but the low concentration of Ag alone entering tetrahedrite, and its temperature dependance, is strong negative supporting evidence.

In natural tetrahedrites, relating the variation in physical properties to substitution of Cu, is hindered by variations due to semi-metal substitution. Conclusions on correlations are of little value without complete analyses which are necessary to obtain atomic % concentrations. Few workers on natural tetrahedrites have realised the importance of relating physical properties to atomic % concentration.

The unexpected conclusion that the cell size of

substituted tetrahedrite is dependant on the atomic % Cu substituted and independent of the type of substituting element requires verification as the silver, which is normally a large atom in sulphides, is contained in metastable Ag-tetrahedrite. This verification is an important prerequisite of any attempt to devise a means of determining chemical composition of natural tetrahedrites from their mineralogical properties.

The subtractive effect of silver substitution on the microhardness and reflectivity of Zn-tetrahedrite and the accumulative effect on the cell edge of Zn-tetrahedrite are important because differing effects by different substituting elements are essential if the compositions of complex sulphosalts are to be determined from mineralogical properties.

The reflectivities of the substituted tetrahedrites were only determined at three wavelengths. From the results it is concluded that spectral reflectivity will be sensitive to compositional changes in tetrahedrite but precise compositional control of synthetic substituted tetrahedrites will be required before measurement of spectral reflectivities is worthwhile. This is because of the variations in reflectivities of zinc rich tetrahedrites which are probably due to non-stoichiometry.

The variation in physical properties of the substituted tetrahedrites will be discussed in Chapter 6 on the crystal chemistry of tetrahedrite.

The conclusion that Zn does not substitute for Cu in stibioluzonite is as expected if the elements in Cu_3SbS_4 have their normal valencies : Cu = +1 ; Sb = +3; S = -2. There are

two types of Cu site in stibioluzonite - tetrahedral and distorted tetrahedral (Marumo and Nowacki, 1967). It is most likely that Ag enters the distorted site and, since complex low co-ordination is characteristic of silver in silver sulphides (Jellinek 1968), increasing distortion should stabilise the structure. The distortion is evident from the change in 'c' and 'a' parameters. If substitution had been simple cation substitution the cell parameters would simply have increased due to the large Ag atom. The effect observed indicates the directional nature of covalent bonds in Ag-stibioluzonite.

From a study of irridescent filming of stibioluzonite synthesised in a study of the Cu-Ag-Sb-S system, Gaudin and McGlashan (1939) suggested silver solid solution, of the addition type, in stibioluzonite. In the present study silver solid solution in stibioluzonite has been shown to be the substitutional type - Ag in place of Cu (Fig.5-9).

The extensive Cu_3SbS_3 -Ag_3SbS_3 solid solution has not previously been reported. Further study of this series is important because Ag_3SbS_3 (pyrargyrite) has special optical properties (Hulme et al. 1967) and is being manufactured commercially. The 'ruby silvers' pyrargyrite and prousite (Ag_3AsS_3) are so called because they transmit long wave-length red light and this results in characteristic blood red internal reflections which are also found in Cu_3SbS_3. Synthesis of the Cu_3SbS_3 end-member may prove difficult because of its phase relations in the Cu-Sb-S system but Cu substituted Ag_3SbS_3 should be readily obtainable by crystallisation from the melt as Ag_3SbS_3 melts congruently at 485°C (Keighin and Honea 1969).

The crystal structures of the two end-members differ and a limit of 30 mol% Cu_3SbS_3 in Ag_3SbS_3 is indicated.

TABLE 5-1a

Substituted Tetrahedrites

Temperature Histories

Batch	Hours to max.	Max. temp.	Hours at max.	Hours to min.	Min. Temp.	Hours at min.	Hours to room temp.
1971A	25	670°C	11	30	400°C	21	< 1
1971B	26	680°C	11	36	400°C	17	< 1
1971E	28	690°C	12	33	400°C	19	< 1

TABLE 5-1b

Substituted Tetrahedrites

Microprobe Analysis: Operating Conditions

Elem.	Line	Stnd.	KV	Cryst.	2θ angle	Bck-gnd.	E(int)	Counter
Cu	K_α	Cu	15	LiF	44°59'	±2°	2.5v	sealed
Zn	K_α	ZnS	15	LiF	41°41'	±2°	2.5v	sealed
Ag	L_α	Ag	15	Quartz	76°49'	±2°	1.5v	flow
Fe	K_α	Fe	15	LiF	57°28'	±2°	1.0v	sealed
Sb	L_α	Sb_2S_3	15	Quartz	61°55'	±2°	2.5v	flow
S	K_α	Sb_2S_3	15	Quartz	106°55'	±2°	2.5v	flow

TABLE 5-2

Zinc Starting Compositions

Starting composition A=Zn	Batch History	Result	%Tet.	Major impurities
$Cu_{11}A\ Sb_4S_{13}$	1971B	button	85-99	Stblz, ZnS, $Cu_{2-x}S$, Chst
$Cu_{10}A_2Sb_4S_{13}$	1971B	sponge	95	ZnS, $Cu_{2-x}S$
$Cu_9A_3Sb_4S_{13}$	1971B	granular	80	ZnS, Sb
$Cu_8A_4Sb_4S_{13}$	1971B	granular	50	ZnS, $Cu_{2-x}S$, Chst, Sb

Microprobe Analyses of Tetrahedrites

Starting composition	Element	uwt%	cwt%	nwt%	at%	(Tet)
$Cu_{11}A\ Sb_4S_{13}$	Cu	41.93	43.22	42.19	38.13	(41.38)
	Zn	3.74	3.53	3.45	3.03	
	Sb	28.30	29.92	29.21	13.77	(13.79)
	S	23.49	25.78	25.16	45.07	(44.83)
			102.45			
$Cu_{10}A_2Sb_4S_{13}$	Cu	38.51	39.70	38.60	34.93	
	Zn	7.95	7.51	7.30	6.42	
	Sb	28.26	29.89	29.06	13.73	
	S	23.43	25.76	25.04	44.92	
			102.85			
$Cu_9A_3Sb_4S_{13}$	Cu	37.79	38.99	37.98	34.26	
	Zn	8.48	8.02	7.81	6.85	
	Sb	27.99	29.65	28.88	13.60	
	S	23.65	26.01	25.34	45.29	
			102.66			
$Cu_8A_4Sb_4S_{13}$	Cu	38.35	39.55	38.53	34.82	
	Zn	8.18	7.73	7.54	6.61	
	Sb	27.95	29.59	38.83	13.60	
	S	23.43	25.77	25.11	44.96	
			102.64			

TABLE 5-3

Iron Starting Compositions

Starting Composition A=Fe	Batch History	Result	%Tet.	Major Impurities
$Cu_{11}ASB_4S_{13}$	1971E	Button	65	Bornite, Chst
$Cu_9A_3Sb_4S_{13}$	1971E	Granular	60	Chpy,Chst,Sb,Bornite

Microprobe Analyses of Tetradrites

Starting composition	Element	uwt%	cwt%	nwt%	at%
$Cu_{11}ASb_4S_{13}$	Cu	41.74	43.17	42.10	37.77
	Fe	3.40	3.28	3.20	3.26
	Sb	28.31	29.96	29.22	13.68
	S	23.86	26.12	25.48	45.28
			102.53		
$Cu_9A_3Sb_4S_{13}$	Cu	38.13	39.53	38.71	34.59
	Fe	6.51	6.32	6.19	6.29
	Sb	28.42	30.09	29.47	13.74
	S	23.95	26.17	25.63	45.38
			102.10		

Microprobe Analyses of impurities

Bornite in $Cu_{11}ASb_4S_{13}$	Cu	59.88	64.79	62.96	49.12
	Fe	10.61	9.97	9.69	8.60
	Sb	0.01	0.01	0.01	0.00
	S	24.35	28.14	27.34	42.28
			102.90		
Chalcopyrite in $Cu_9A_3Sb_4S_{13}$	Cu	29.18	32.71	31.96	22.95
	Fe	32.24	33.13	32.38	26.44
	Sb	0.08	0.09	0.09	0.00
	S	31.96	36.40	35.57	50.61
			102.33		
Chalcostibite in $Cu_9A_3Sb_4S_{13}$	Cu	25.52	26.08	26.90	25.83
	Fe	0.09	0.09	0.10	0.10
	Sb	42.96	44.82	46.24	23.16
	S	24.37	25.94	26.76	50.91
			96.92		

TABLE 5-4

Silver Starting Compositions

Starting Composition A=Ag	Batch History	Result	% Tet.	Major impurities
$Cu_{10}A_2Sb_4S_{13}$	1971A	button	40	Stblz, $(CuAg)_3SbS_3$
$Cu_8A_4Sb_4S_{13}$	1971A	button	40	Stblz, $(CuAg)_3SbS_3$, Sb
$Cu_6A_6Sb_4S_{13}$	1971A	button	-	Stblz(25%), $(CuAg)_3SbS_3$(75%)
$Cu_4A_8Sb_4S_{13}$	1971A	button	-	Stblz(25%), $(CuAg)_3SbS_3$(75%)
$Cu_2A_{10}Sb_4S_{13}$	1971A	button	-	Stblz(30%), $(CuAg)_3SbS_3$(70%)

Microprobe Analyses of Tetrahedrites

Element	In $Cu_{10}A_2Sb_4S_{13}$				In $Cu_8A_4Sb_4S_{13}$			
	uwt%	cwt%	nwt%	at%	uwt%	cwt.	nwt%	at%
Cu	41.64	42.68	42.19	38.82	40.28	41.15	40.68	37.82
Ag	3.85	4.68	4.43	2.51	5.55	6.71	6.64	3.63
Sb	27.06	28.73	28.39	13.47	27.02	28.71	28.38	13.77
S	23.13	25.08	24.79	45.20	22.79	24.59	24.30	44.78
		101.81				101.17		

TABLE 5-4 (Contd.)

Microprobe Analyses of impurities

Stibioluzonites

Element	$(CuAg)_3SbS_4$ in $Cu_{10}A_2Sb_4S_{13}$ uwt%	cwt%	nwt%	at%	$(CuAg)_3SbS_3$ in $Cu_{10}A_2Sb_4S_{13}$ uwt%	cwt.	nwt%	at%
Cu	42.04	43.83	42.62	37.07	32.73	33.19	34.20	33.90
Ag	0.77	0.95	0.93	0.47	15.73	18.71	19.28	11.25
Sb	26.29	28.22	27.44	12.46	22.71	24.50	25.24	13.06
S	27.18	29.83	29.01	50.00	19.53	20.65	21.28	41.79
		102.83				97.04		
	in $Cu_8A_4Sb_4S_{13}$				in $Cu_8A_4Sb_4S_{13}$			
Cu	41.87	43.63	42.44	36.97	11.91	11.52	11.48	13.14
Ag	1.02	1.26	1.23	0.63	42.68	47.99	47.85	32.23
Sb	26.25	28.18	27.41	12.46	20.63	22.55	22.48	13.42
S	27.12	29.75	28.93	49.95	18.67	18.24	18.19	41.21
		102.82				100.30		
	in $Cu_6A_6Sb_4S_{13}$				in $Cu_6A_6Sb_4S_{13}$			
Cu	40.59	42.30	41.52	36.22	8.09	7.78	7.61	8.89
Ag	1.64	2.04	2.00	1.03	47.06	52.52	51.36	35.37
Sb	25.94	27.89	27.38	12.46	21.53	23.56	23.04	14.06
S	27.07	29.64	29.10	50.29	19.05	18.40	18.00	41.68
		101.86				102.26		
	in $Cu_4A_8Sb_4S_{13}$				in $Cu_4A_8Sb_4S_{13}$			
Cu	40.00	41.60	40.74	35.80	2.66	2.53	22.50	3.01
Ag	2.79	3.45	3.38	1.75	52.60	58.08	57.28	40.73
Sb	25.77	27.72	27.15	12.45	20.92	22.97	22.66	14.27
S	26.87	29.33	28.73	50.01	18.73	17.80	17.56	41.99
		102.10				101.39		
	in $Cu_2A_{10}Sb_4S_{13}$				in $Cu_2A_{10}Sb_4S_{13}$			
Cu	37.20	38.56	37.89	33.68	1.08	1.03	1.01	1.23
Ag	5.41	6.67	6.55	3.43	53.98	59.39	58.28	41.86
Sb	25.38	27.41	26.94	12.49	21.66	23.76	23.31	14.84
S	26.88	29.12	28.62	50.40	18.75	17.74	17.40	42.07
		101.76				101.92		

TABLE 5-5

Zinc + Silver Starting Composition

Starting composition	Batch history	Result	%Tet.	Major impurities
A_2=Zn A_1=Ag				
$Cu_9A_{2+1}Sb_4S_{13}$	1971	Button	50	Stbiz, ZnS, $(CuAg)_3SbS_3$, Chst.

Microprobe Analysis

ZnAg-tetrahedrite

Element	uwt%	cwt%	nwt%	at%
Cu	33.84	34.71	34.27	31.49
Zn	8.13	7.63	7.54	6.73
Ag	3.76	4.57	4.52	2.44
Sb	27.28	29.00	28.63	13.73
S	23.35	25.37	25.05	45.61
		101.28		

TABLE 5-6 Substituted Tetrahedrites

Starting Composition $Cu_{12-n}Zn_nSb_4S_{13}$

N	$Cu_{12}Sb_4S_{13}$		Zn		Zn_2		Zn_3		Zn_4	
	dÅ	Int	dÅ	Int	dÅ	Int	dÅ	Int	dÅ	Int
2										
4	5.145	35	5.162	40	5.186	40	5.164	40	5.185	40
6	4.200	20	4.216	20	4.236	30	4.238	30	4.235	20
8	3.638	45	3.644	50	3.665	50	3.663	50	3.661	50
10										
12	2.971	100	2.976	100	2.996	100	2.991	100	2.992	100
14	2.754	40	2.760	40	2.771	40	2.772	40	2.771	40
16	2.572	65	2.582	60	2.593	60	2.623	60	2.590	60
18	2.428	55	2.436	50	2.442	50	2.445	50	2.443	50
20	2.302	35	2.312	30	2.318	30	2.317	20	2.321	30
22	2.196	10	2.202	30	2.213	20	2.209	20	2.210	20
24	2.103	25	2.111	30	2.117	30	2.115	20	2.117	30
26	2.020	50	2.025	50	2.033	50	2.034	50	2.033	50
30	1.880	45	1.885	40	1.892	40	1.893	40	1.893	50
32	1.821	90	1.826	90	1.832	90	1.832	90	1.833	90
34	1.767	35	1.769	30	1.779	30	1.778	30	1.778	40
36	1.717	15	1.719	10	1.728	20	1.729	5	1.729	5
38	1.672	55	1.676	50	1.682	40	1.681	50	1.682	50
40	1.629	20	1.632	20	1.640	20	1.639	5	1.640	5
42	1.591	10	1.595	10	1.601	10	1.599	5		
44	1.553	75	1.558	80	1.563	80	1.563	80	1.563	80
46	1.520	25	1.522	20	1.529	30	1.529	10	1.530	20
48	1.488	25	1.491	20	1.497	30	1.496	20	1.497	20
50	1.458	30	1.461	30	1.467	30	1.467	30	1.467	20
54	1.403	10	1.407	20	1.411	20	1.410	10	1.413	10
56	1.378	10	1.382	20	1.387	20	1.386	10	1.386	10
62	1.309	20	1.313	30	1.318	30	1.317	20	1.317	20
64	1.289	25	1.293	30	1.297	30	1.297	20	1.297	30
66	1.269	30	1.273	30	1.278	30	1.276	20	1.278	30
70	1.232	30	1.236	40	1.240	40	1.241	30	1.240	50
74	1.198	40	1.201	50	1.205	50	1.206	40	1.206	40
76	1.182	40	1.186	50	1.190	50	1.190	40	1.190	40
78	1.167	10	1.170	20	1.174	10	1.174	10	1.175	10
80	1.152	10	1.156	20	1.159	10	1.161	10	1.161	10
82	1.138	10	1.143	20	1.145	10	1.147	10	1.146	10
86	1.112	30	1.115	30	1.118	40	1.119	30	1.119	20
90	1.087	35	1.090	40	1.094	40	1.094	30	1.094	30
94	1.064	30	1.067	30	1.070	30	1.071	30	1.070	20
96	1.053	45	1.055	50	1.059	50	1.060	40	1.059	40
98	1.042	10	1.045	10	1.048	20	1.049	5	1.048	5
102	1.021	20	1.024	30	1.027	20	1.028	20	1.028	5
106	1.002	10	1.005	10	1.008	10	1.008	5	1.008	5
108	0.993	35	0.995	40	0.998	40	0.999	40	0.999	30
110	0.984	45	0.986	50	0.989	50	0.990	50	0.990	40
114	0.966	30	0.969	20	0.972	30	0.972	30	0.972	30
118	0.950	35	0.953	30	0.955	40	0.956	40	0.956	40
122	0.934	45	0.937	40	0.940	50	0.940	40	0.940	40
126	0.919	50	0.922	50	0.925	50	0.925	50	0.925	50
128	0.912	40	0.915	30	0.917	40	0.918	30	0.918	30
130	0.905	25	0.908	20	0.910	20	0.911	20	0.911	20

TABLE 5-6 (Contd.)

Starting composition = $Cu_{12-n}A_nSb_4S_{13}$

	$A_n=Fe_1$		$A_n=Fe_3$		$A_n=Ag_2$		$A_n=Ag_4$		$A_n=Zn_2Ag$	
N	dÅ	I	dÅ	I	dÅ	I	dÅ	I	dÅ	I
2	7.232	40	7.292	25					7.362	30
4	5.163	20	5.192	45	5.168	25			5.190	40
6	4.230	10	4.235	20	4.217	20			4.242	30
8	3.644	50	3.664	50	3.656	40	3.660	50	3.673	50
10			3.283	5						
12	2.980	100	2.990	100	2.987	100	2.986	100	2.997	100
14	2.758	40	2.770	40	2.768	20	2.767	30	2.775	40
16	2.581	50	2.594	60	2.583	45	2.576	60	2.598	60
18	2.438	40	2.443	45	2.437	35	2.434	50	2.448	50
20			2.316	30	2.310	15	2.311	30	2.322	30
22			2.209	20	2.209	25	2.209	30	2.216	30
24			2.117	30	2.107	10	2.112	30	2.121	30
26	2.025	40	2.034	35	2.031	30	2.024	50	2.037	50
30	1.889	30	1.893	30			1.889	40	1.898	40
32	1.825	90	1.833	90	1.830	85	1.831	90	1.837	90
34			1.779	25	1.773	20	1.773	30	1.782	30
36			1.730	10	1.730	5	1.727	10	1.733	20
38	1.678	30	1.682	45	1.677	25	1.673	40	1.686	50
40			1.639	15			1.626	10	1.644	10
42					1.580	10	1.579	10	1.605	10
44	1.557	50	1.564	75	1.558	70	1.556	80	1.567	70
46	1.524	20	1.529	15	1.522	10	1.524	20	1.532	20
48	1.492	10	1.498	15			1.494	20	1.502	20
50	1.463	10	1.467	25	1.463	20	1.463	20	1.471	30
54			1.412	10					1.416	20
56			1.387	10					1.391	10
62	1.311	20	1.318	25	1.314	15	1.314	10	1.320	30
64	1.289	30	1.298	30	1.292	15	1.292	10	1.300	30
66	1.273	10	1.277	30	1.274	15	1.274	10	1.281	30
70	1.236	20	1.240	35	1.236	35	1.235	30	1.243	30
74	1.202	30	1.205	45	1.202	25	1.203	20	1.209	40
76	1.186	30	1.189	45	1.186	25	1.187	20	1.193	40
78									1.176	10
80	1.159	10	1.159	10					1.163	10
82	1.143	20	1.146	10					1.149	10
86	1.115	20	1.119	30			1.116	20	1.121	30
90	1.090	20	1.094	35	1.090	30	1.091	20	1.096	30
94	1.067	30	1.070	30	1.067	20	1.065	10	1.073	20
96	1.055	30	1.059	45	1.055	30	1.056	40	1.062	40
98			1.047	10					1.051	5
102			1.027	10					1.030	20
106										
108	0.996	10	0.999	25	0.996	20			1.001	30
110	0.986	30	0.990	35	0.986	20			0.992	30
114			0.972	20					0.975	10
118			0.956	20	0.952	25			0.958	20
122	0.937	30	0.940	30	0.937	20			0.942	20
126	0.922	30	0.925	40	0.921	20				
128			0.918	30						
130			0.911	10						

TABLE 5-7

Substituted Tetrahedrites-Cell Parameters
obtained using selected high angle lines in NELRIL

Starting composition*	Cell Edge in Å	Stnd. Err.
$Cu_{12}Sb_4S_{13}$	10.31907	0.00048
$Cu_{11}ZnSb_4S_{13}$	10.34944	0.00028
$Cu_{10}Zn_2Sb_4S_{13}$	10.37919	0.00021
$Cu_9Zn_3Sb_4S_{13}$	10.38195	0.00056
$Cu_8Zn_4Sb_4S_{13}$	10.38237	0.00068
$Cu_{11}FeSb_4S_{13}$	10.34718	0.00098
$Cu_9Fe_3Sb_4S_{13}$	10.38314	0.00066
$Cu_{10}Ag_2Sb_4S_{13}$	10.34191	0.00127
$Cu_8Ag_4Sb_4S_{13}$	10.35238	0.00384
$Cu_9Zn_2AgSb_4S_{13}$	10.40692	0.00052

*N.B. Microprobe analyses given in Tables 5-2,3,4,5.

TABLE 5-8

Substituted Tetrahedrites
Vickers Microhardness Results

Diamond Indentation.

100g. load.

Starting composition	Number of points	Mean Vickers hardness	Standard deviation
$Cu_{12}SB_4S_{13}$	10	262	7
$Cu_{11}ZnSb_4S_{13}$	10	343	21
$Cu_{10}Zn_2Sb_4S_{13}$	10	392	23
$Cu_9Zn_3Sb_4S_{13}$	10	395	23
$Cu_8Zn_4Sb_4S_{13}$	10	357	18
$Cu_{11}FeSb_4S_{13}$	10	328	26
$Cu_9Fe_3Sb_4S_{13}$	10	371	18
$Cu_{10}Ag_2Sb_4S_{13}$	10	225	12
$Cu_8Ag_4Sb_4S_{13}$	10	238	9
$Cu_9Zn_2AgSb_4S_{13}$	10	278	19

TABLE 5-9 Substituted Tetrahedrites Reflectivity Measurements (Air)

Wavelength		460			540			640	
Starting composition	No. of points	Mean	Stnd.Dev.	No. of points	Mean	Stnd.Dev.	No. of points	Mean	Stnd.Dev.
$Cu_{12}Sb_4S_{13}$	4	29.72	0.17	9	28.46	0.27	8	27.49	0.29
$Cu_{11}ZnSb_4S_{13}$	4	30.20	0.11	4	30.00	0.19	4	28.71	0.31
$Cu_{10}Zn_2Sb_4S_{13}$	4	30.71	0.14	4	31.14	0.28	4	29.60	0.10
$Cu_9Zn_3Sb_4S_{13}$	4	30.34	0.11	4	31.23	0.20	4	29.23	0.15
$Cu_8Zn_4Sb_4S_{13}$	4	30.71	0.24	4	30.54	0.21	4	29.52	0.10
$Cu_{11}FeSb_4S_{13}$	4	29.74	0.12	4	29.53	0.10	4	27.99	0.26
$Cu_9Fe_3Sb_4S_{13}$	5	30.79	0.30	4	31.20	0.28	4	30.48	0.12
$Cu_{10}Ag_2Sb_4S_{13}$	4	29.74	0.11	4	27.93	0.17	4	26.36	0.48
$Cu_8Ag_4Sb_4S_{13}$	4	29.75	0.10	4	28.14	0.14	4	25.98	0.55
$Cu_9Zn_2AgSb_4S_{13}$	4	30.11	0.30	4	29.69	0.26	4	28.90	0.41

TABLE 5-10

Substitution in Stibioluzonite

Starting Composition	Batch History	Result	% Stblz.	Major impurities
$Cu_{2.5}Zn_{0.5}SbS_4$	1971E	Button	50	Tet, ZnS, Chst
$Cu_{2.5}Ag_{0.5}SbS_4$	1971E	Button	75	$(AgCu)_3SbS_3$, Miagy

Microprobe Analyses

	Elem.	uwt%	cwt%	nwt%	at%
Starting composition $Cu_{2.5}Ag_{0.5}SbS_4$					
Stibioluzonite $(CuAg)_3SbS_4$	Cu	40.99	42.69	41.69	36.41
	Ag	1.59	1.98	1.93	0.99
	Sb	26.16	28.10	27.44	12.51
	S	27.06	29.63	28.94	50.08
			102.40		
Pyrargyrite $(AgCu)_3SbS_3$	Cu	2.21	2.11	2.08	2.53
	Ag	53.59	59.03	58.22	41.68
	Sb	20.76	22.79	22.47	14.26
	S	18.43	17.48	17.23	41.53
			101.40		
Miargyrite $(AgCu)SbS_2$	Cu	2.22	2.13	2.11	2.43
	Ag	34.28	38.27	37.83	25.82
	Sb	37.17	39.58	39.13	23.66
	S	21.85	21.18	20.93	48.08
			101.15		
Starting composition $Cu_{2.5}Zn_{0.5}SbS_4$					
Tetrahedrite $(CuZn)_{12}Sb_4S_{13}$	Cu	37.91	39.10	38.05	34.35
	Zn	8.39	7.93	7.72	6.77
	Sb	28.11	29.76	28.59	13.64
	S	23.63	25.98	25.28	45.23
			102.77		
Stibioluzonite Cu_3SbS_4	Cu	42.49	44.38	43.15	37.32
	Zn	0.06	0.06	0.06	0.00
	Sb	26.33	28.25	27.46	12.40
	S	27.43	30.18	29.34	50.29
			102.87		

TABLE 5-11

Powder Diffraction Data of Substituted Stibioluzonites

Starting Composition (see Tables 5-4 and 5-10 for Microprobe Analysis)

hkl	Cu_3SbS_4		$Cu_6Ag_6Sb_4S_{13}$		$Cu_4Ag_8Sb_4S_{13}$		$Cu_{2.5}Ag_{0.5}SbS_4$	
	dÅ	I	dÅ	I	dÅ	I	dÅ	I
002	5.363	40	5.343	30	5.370	30	5.374	30
101	4.810	50	4.807	40	4.812	50	4.827	40
110	3.804	40	3.809	20	3.819	30	3.817	30
112	3.107	100	3.107	100	3.109	100	3.120	100
103	2.981	40	2.976	20	2.988	30	2.985	20
200	2.689	60	2.686	50	2.701	50	2.697	40
004	2.689		2.686		2.683	40	2.697	
202	2.403	40	2.412	30	2.411	30	2.412	30
211	2.346	40	2.353	30	2.356	30	2.355	30
114	2.196	30	2.191	20	2.197	20	2.199	10
105,213	1.997	40	1.996	30	1.998	40	2.001	20
220,204	1.902	90	1.903	90	1.905	80	1.906	90
006,222	1.791	20					1.798	10
301	1.771	20					1.776	10
310	1.702	10					1.709	5
312	1.623	80	1.622	80	1.628	70	1.629	60
116	1.623		1.622		1.620	70	1.623	60
215	1.605	20	1.604	10	1.605	10	1.609	20
224	1.553	40	1.555	30	1.555	40	1.556	30
107,321	1.478	20			1.485	10	1.483	5
314	1.438	20	1.439	10	1.442	10	1.440	10
305,323	1.378	20	1.380	10	1.384	20	1.381	10
400	1.345	50	1.348	30	1.352	50	1.351	30
008	1.345		1.343	30	1.341	50	1.344	30
226,402	1.304	20			1.304	20		
217,411	1.295	20			1.293	10		
332	1.234	60	1.235	60	1.240	20	1.236	50
316	1.234		1.235		1.236	50	1.236	
413	1.231	10						
420	1.203	40	1.204	30	1.207	20	1.205	20
208,404	1.203		1.204		1.202	20	1.205	
422	1.174	10						
109,307	1.166	10						
424	1.098	60	1.100	50	1.103	50	1.101	30
228	1.098		1.098	50	1.100	30	1.099	30
219,327	1.070	20						
501,431								
510,318	1.054	10	1.056	10				
512	1.036	60	1.038	30	1.041	30	1.039	20
336	1.036		1.034	30	1.038	30	1.034	30
309,417, 521	0.995	10	0.998	10	0.998	5		
523,435, 505	0.963	20	0.964	10	0.967	10		
440	0.951	50	0.954	20	0.956	20		
408	0.951		0.952	40	0.953	40	0.952	40
532	0.910	60	0.912	40	0.913	50		
516	0.910							
3110	0.910		0.909	50	0.910	40	0.910	50

TABLE 5-12

Substituted Stibioluzonites - Tetragonal Cell Parameters obtained using selected lines in COHEN

Starting composition*	Parameter	Stnd.Dev.
Cu_3SbS_4	A_o = 5.38305	0.0004
	C_o = 10.76594	0.0012
$Cu_{2.5}Ag_{0.5}SbS_4$	A_o = 5.39186	0.0015
	C_o = 10.76180	0.0049
$Cu_6Ag_6Sb_4S_{13}$	A_o = 5.39419	0.0010
	C_o = 10.75807	0.0037
$Cu_4Ag_8Sb_4S_{13}$	A_o = 5.40521	0.0015
	C_o = 10.74242	0.0059

*Microprobe analyses given in Tables 5-4 and 5-10.

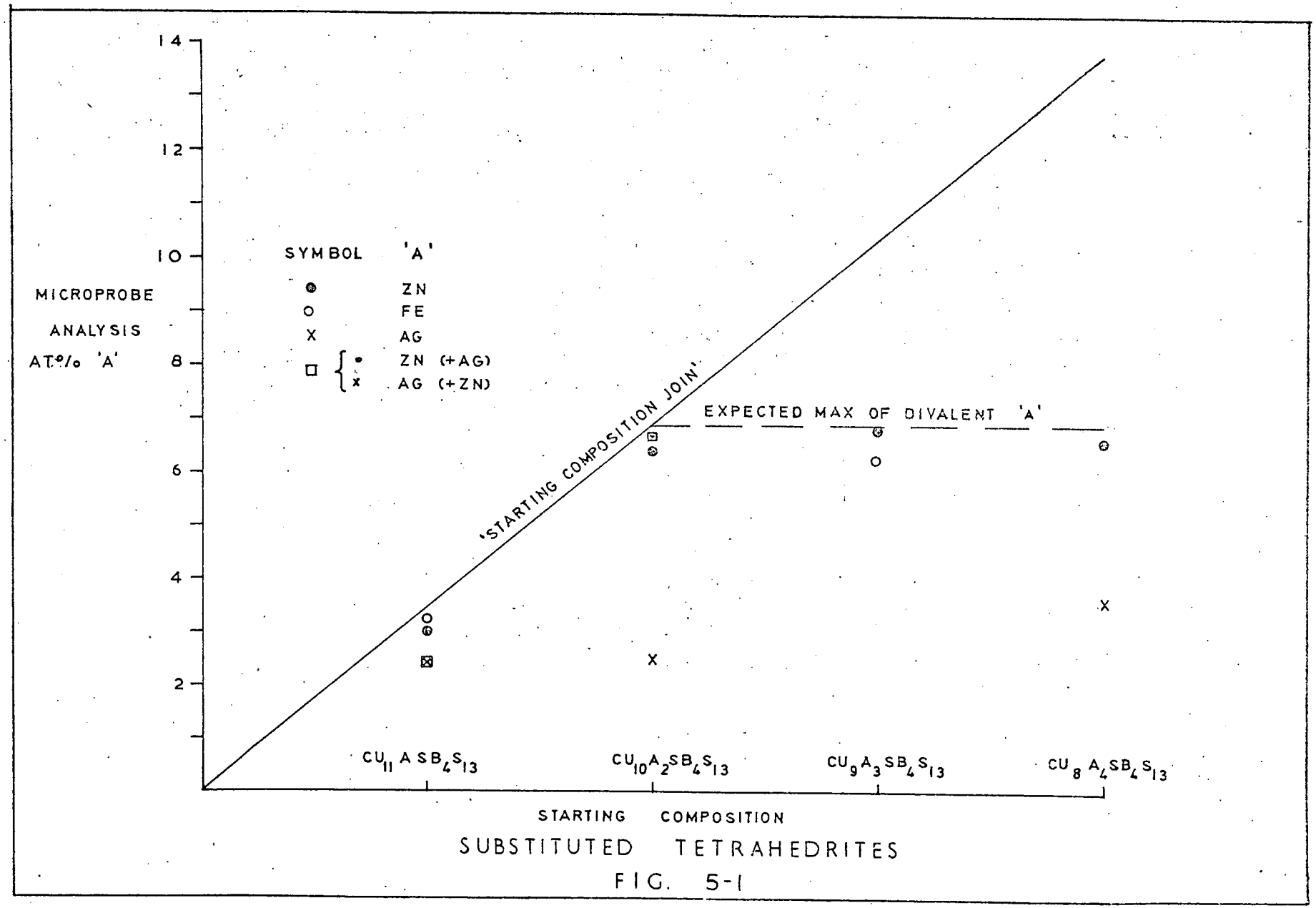

SUBSTITUTED TETRAHEDRITES

FIG. 5-1

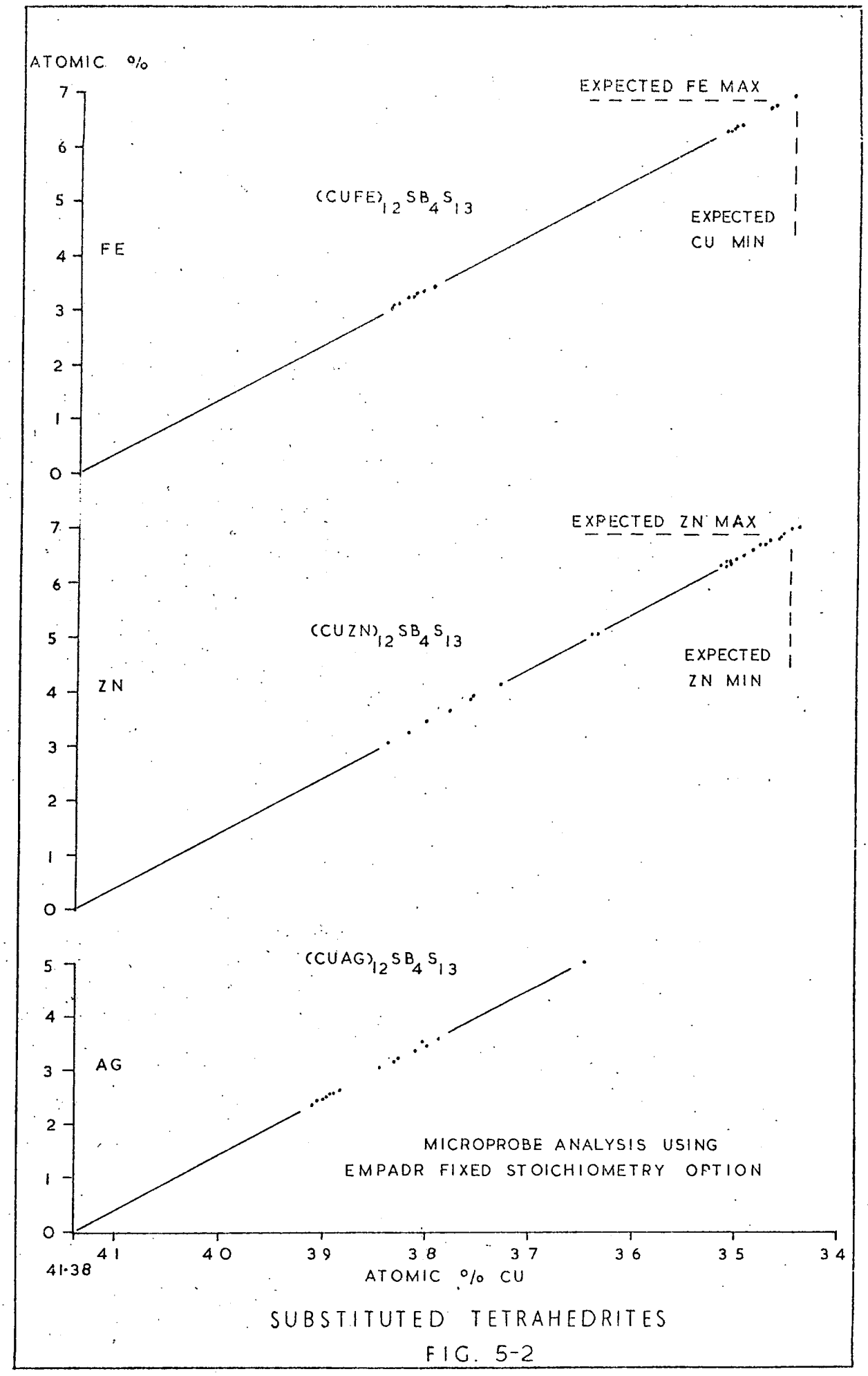

SUBSTITUTED TETRAHEDRITES

FIG. 5-2

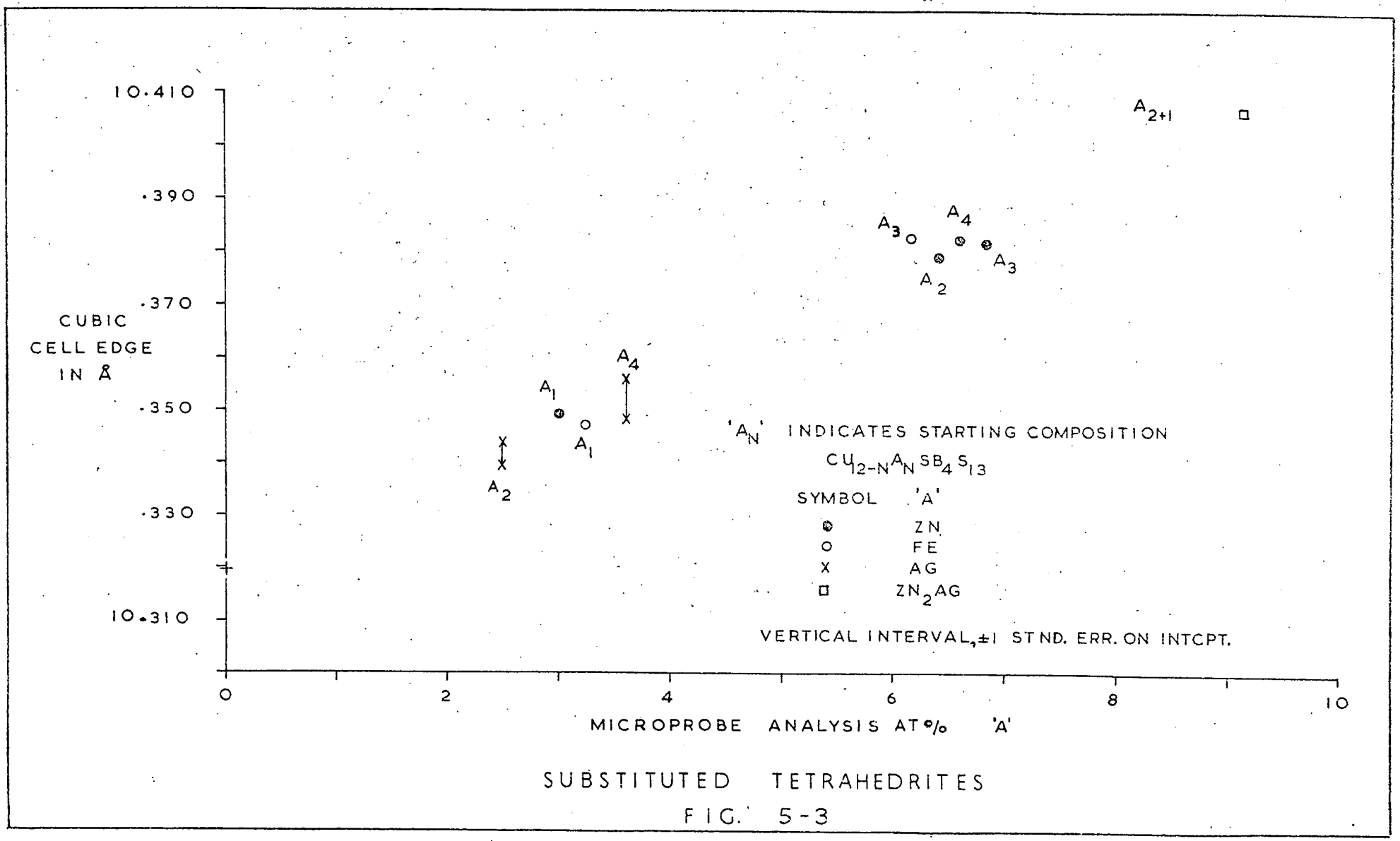

SUBSTITUTED TETRAHEDRITES

FIG. 5-3

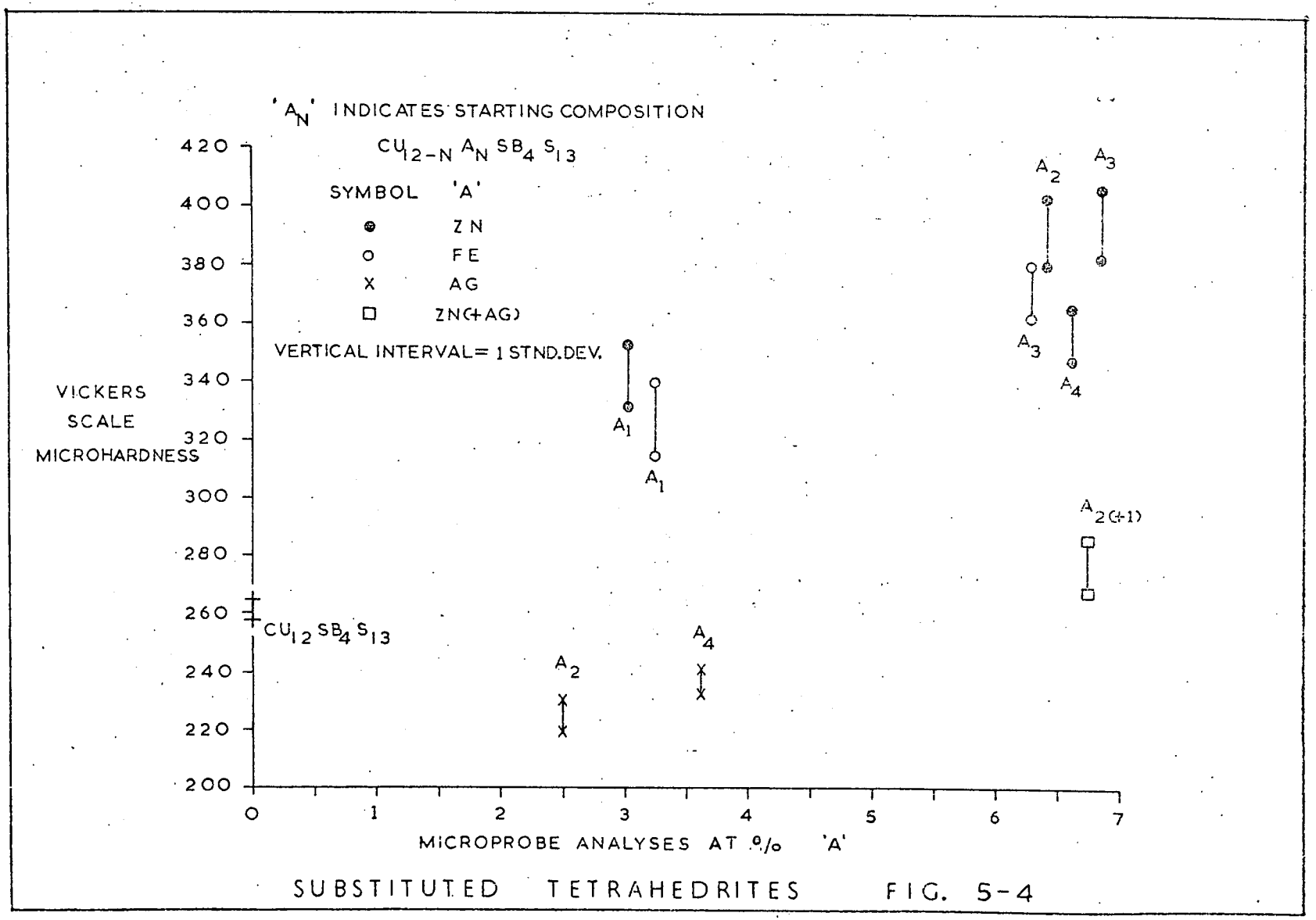

SUBSTITUTED TETRAHEDRITES FIG. 5-4

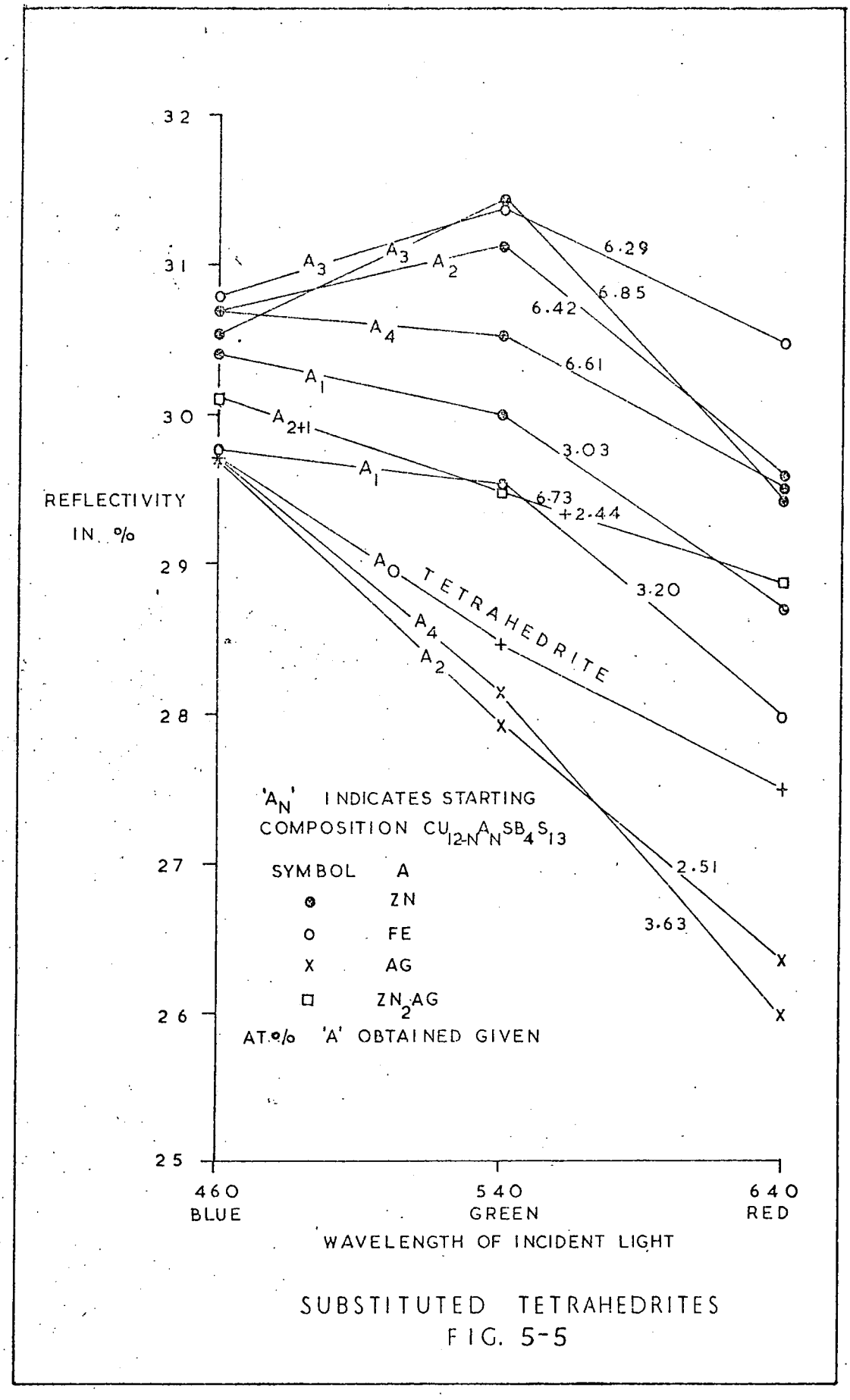

SUBSTITUTED TETRAHEDRITES

FIG. 5-5

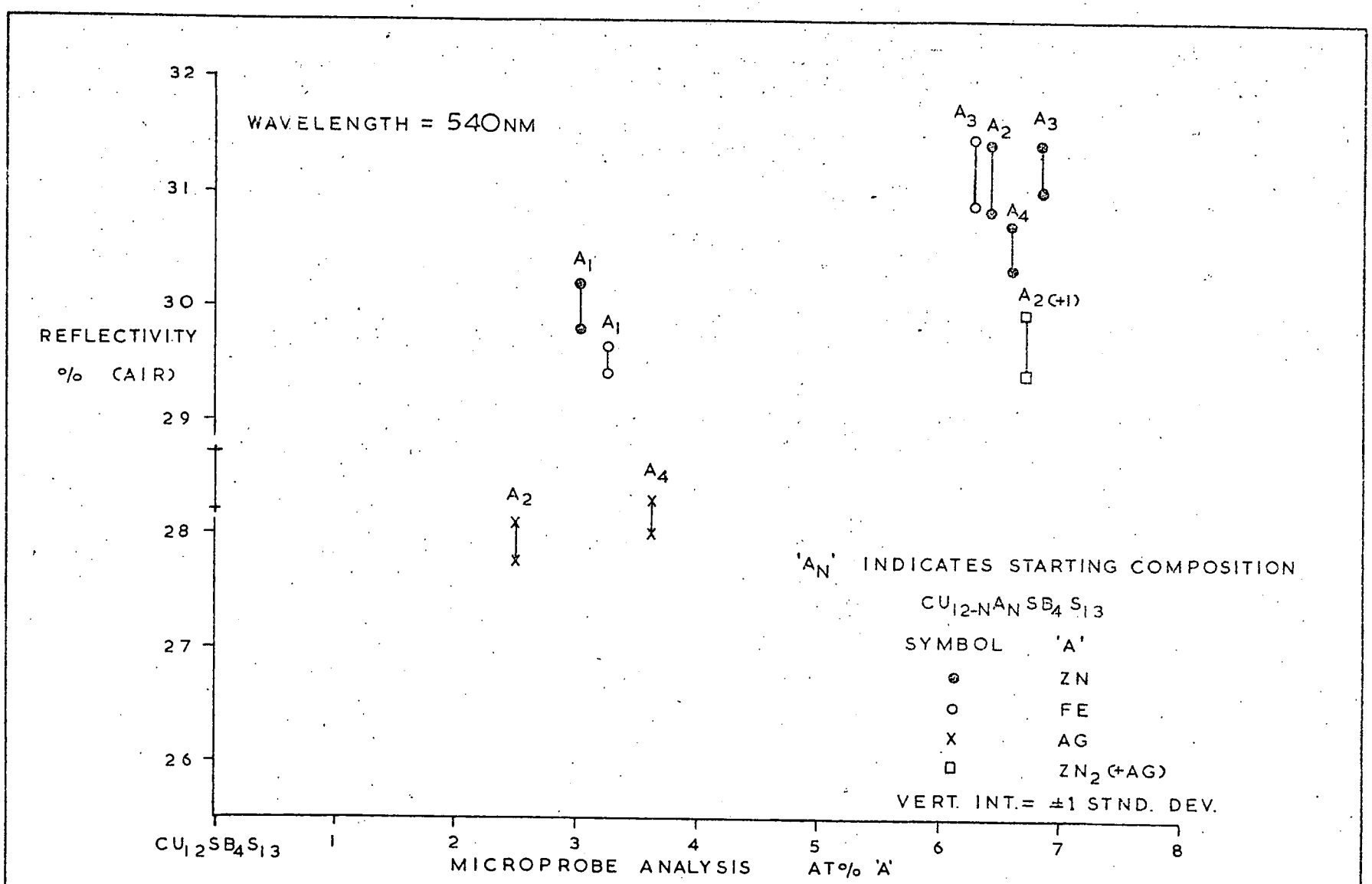

FIG 5-6 REFLECTIVITIES OF SUBSTITUTED TETRAHEDRITES

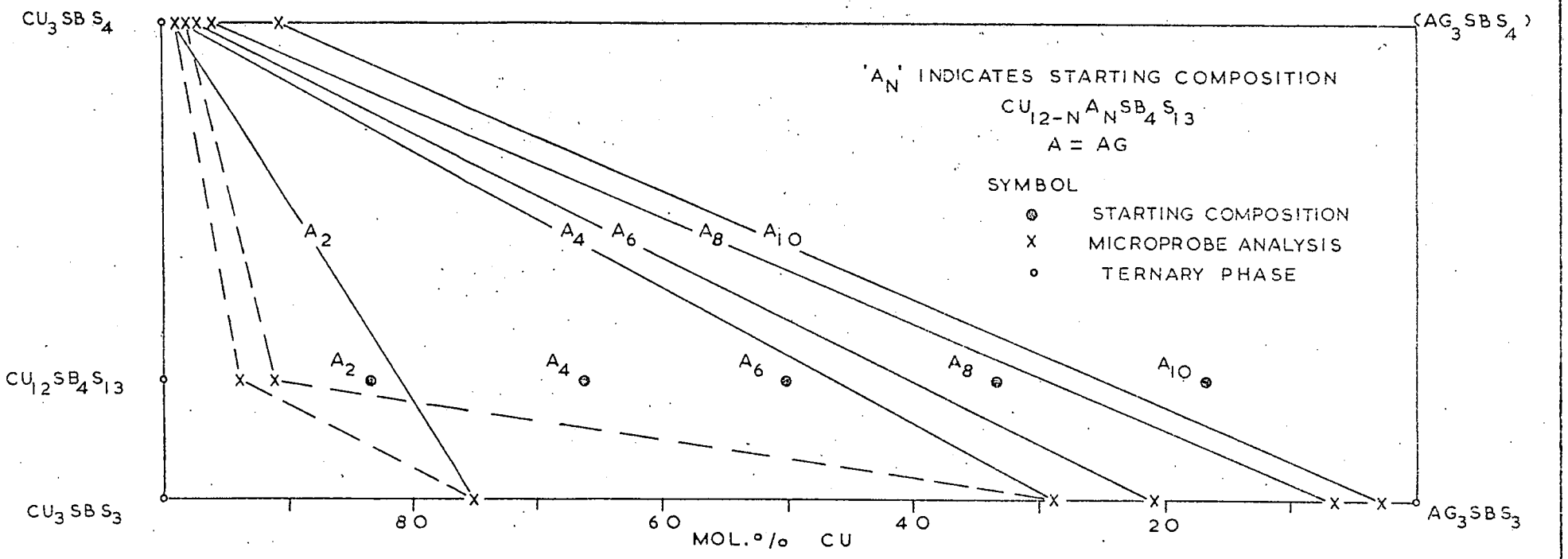

CO-EXISTING CU-AG-SB-S PHASES

FIG. 5-7

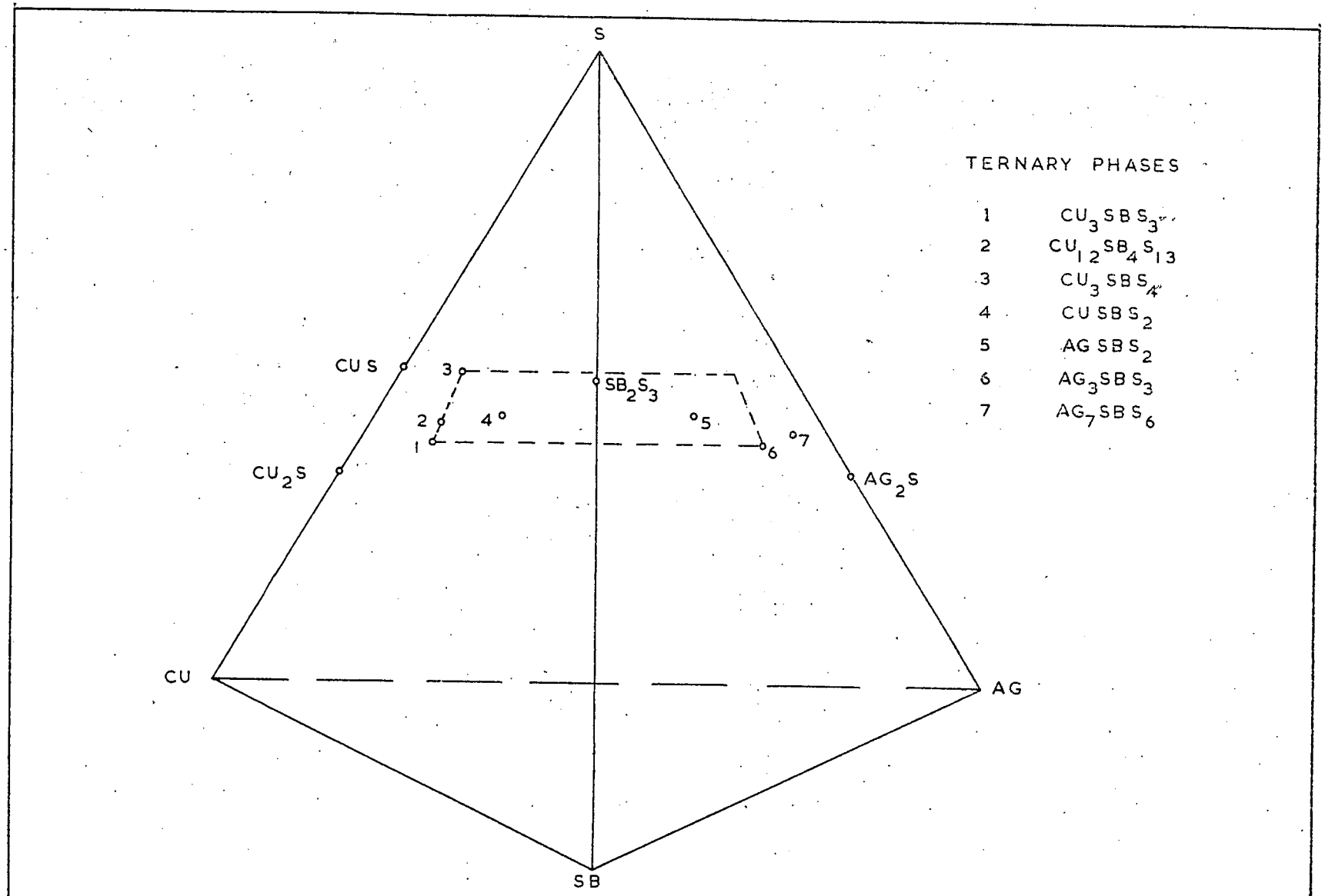

FIG. 5-8 LOCATION OF THE CU_3SBS_3-CU_3SBS_4-AG_3SBS_4-AG_3SBS_3 PLANE

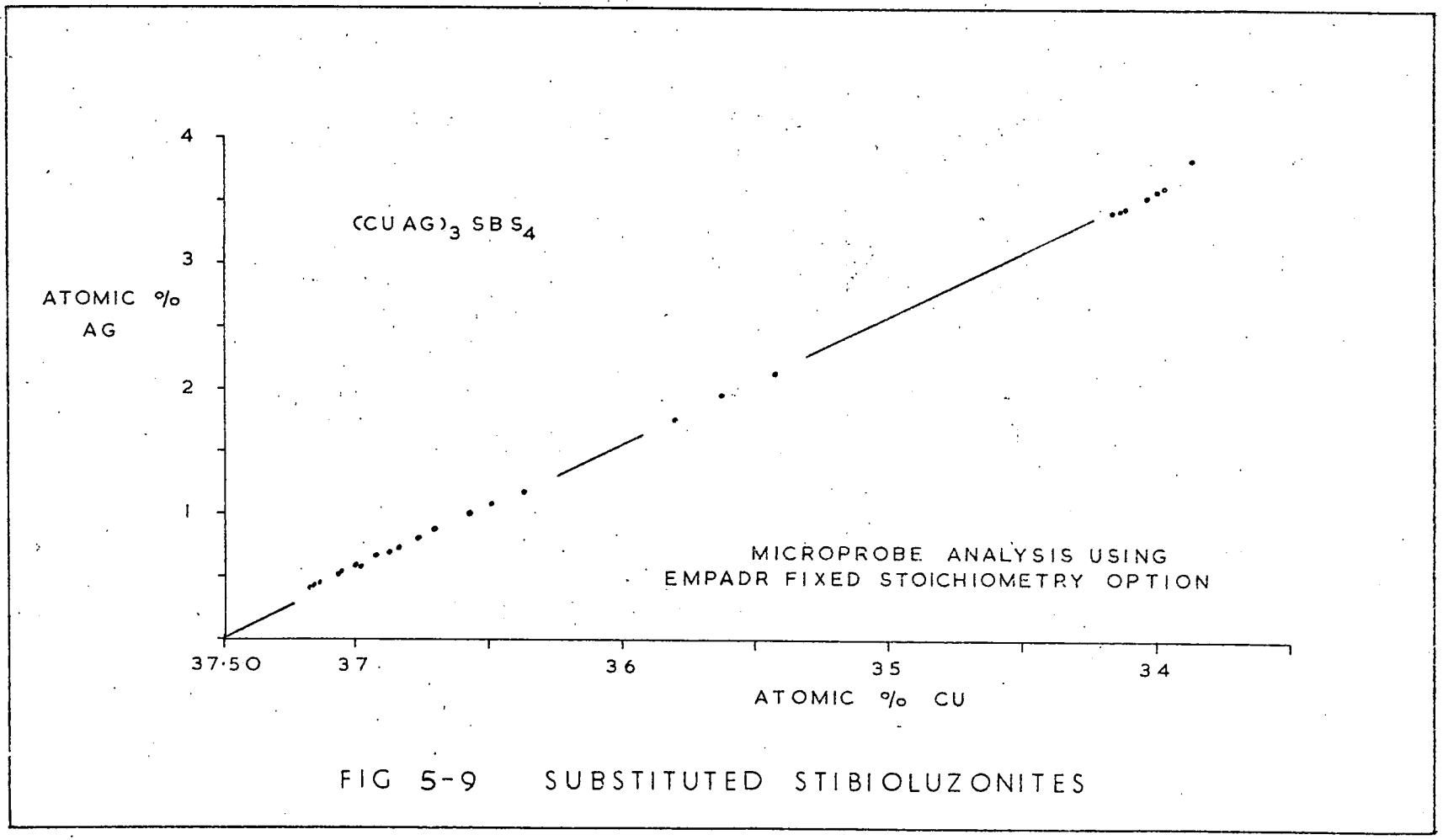

FIG 5-9 SUBSTITUTED STIBIOLUZONITES

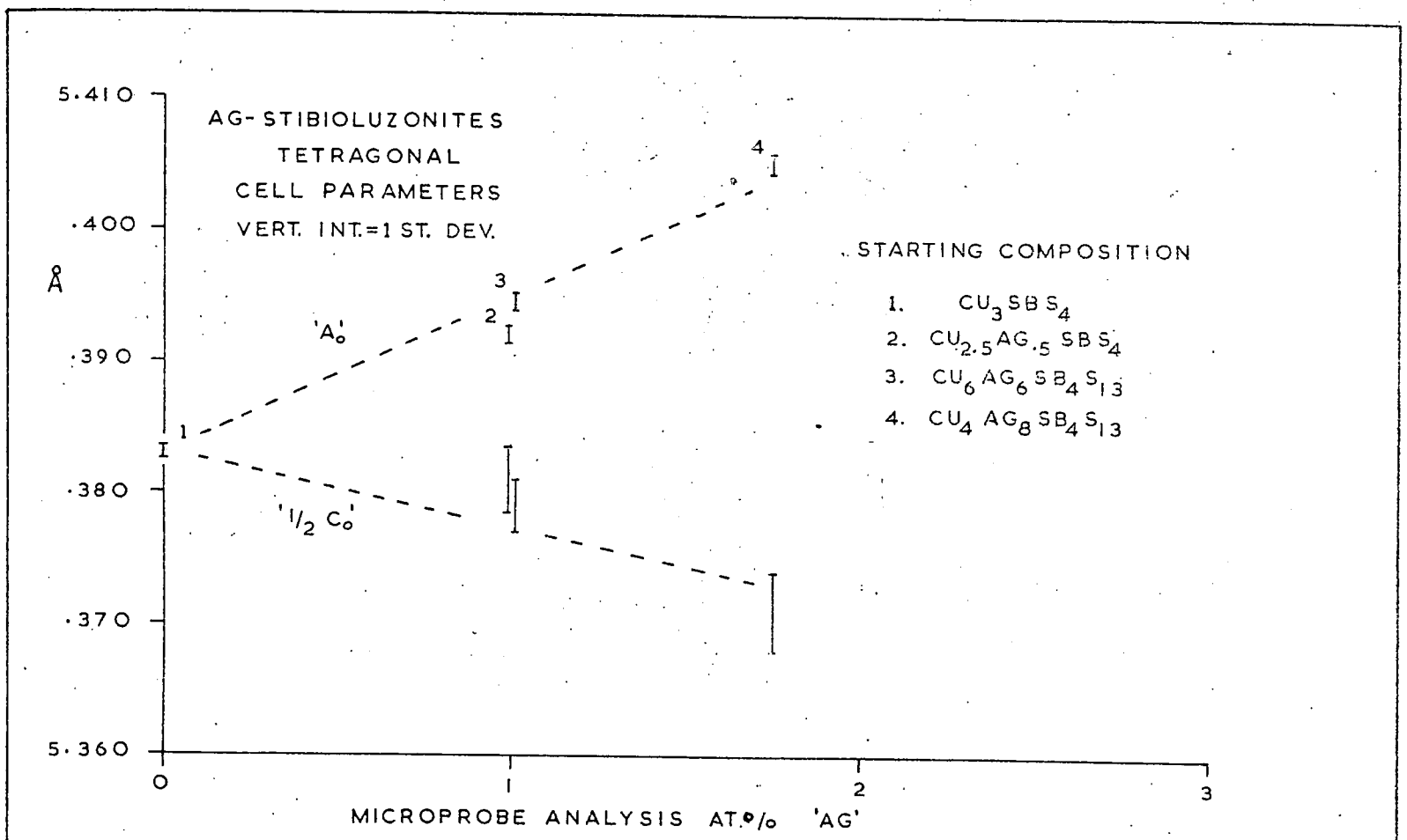

SUBSTITUTED STIBIOLUZONITES FIG 5-10

PLATE 5-1

Starting comp. $Cu_{11}FeSb_4S_{13}$ x 220

Ovoid dendritic bornite (dark grey) with a narrow rim of stibioluzonite in Fe-tetrahedrite (grey). Chalcostibite (light grey) is interstitial.

PLATE 5-2

Starting comp. $Cu_9Fe_3Sb_4S_{13}$ x 220

Grains of chalcopyrite (light grey) with bornite (dark grey) in Fe-tetrahedrite (grey). Chalcostibite (light grey) and antimony (white) are interstitial.

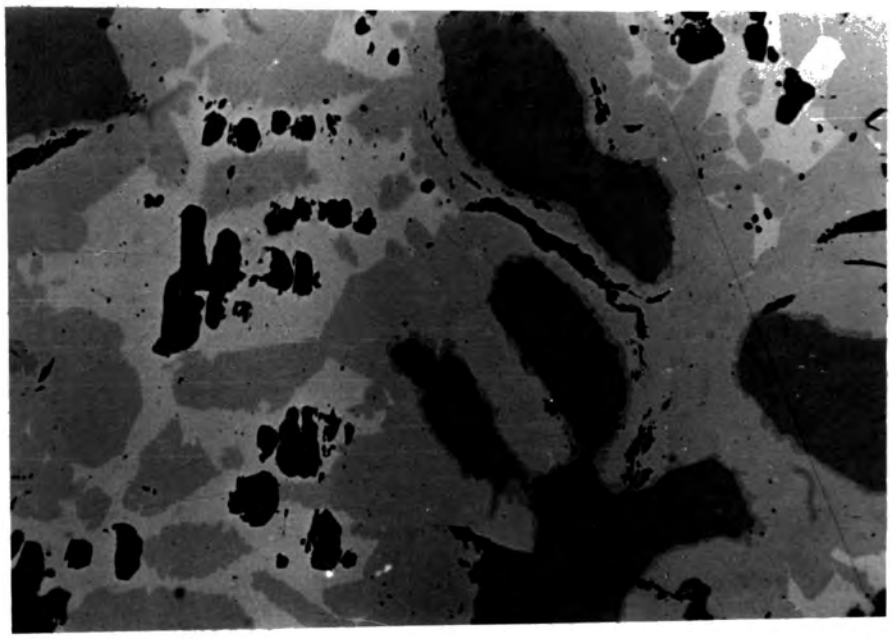

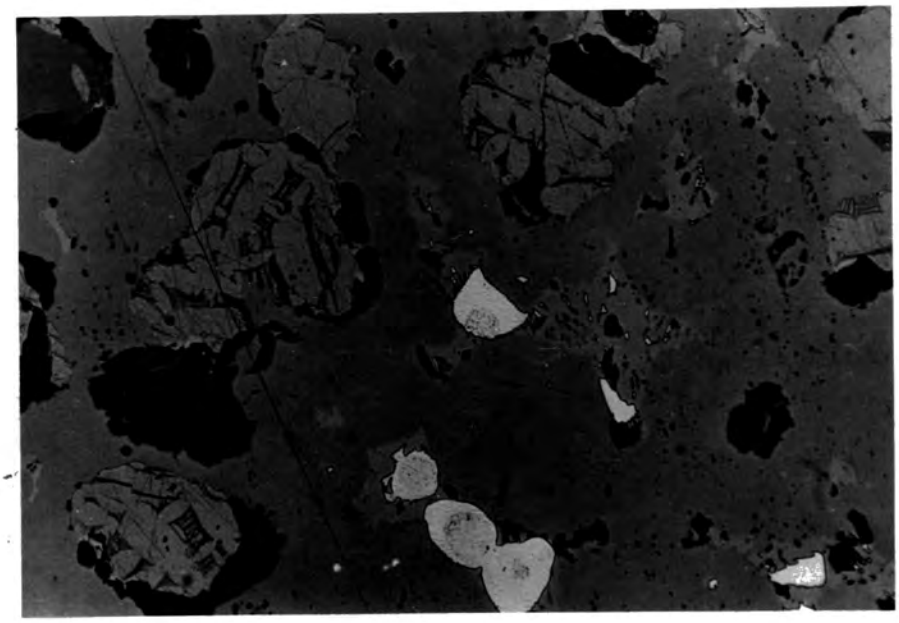

PLATE 5-3

Starting comp. $Cu_8Zn_4Sb_4S_{13}$ x 220

Subhedral ZnS (dark grey) in Zn-tetrahedrite (grey). Chalcostibite (light grey) and antimony (white) are interstitial.

PLATE 5-4

Starting comp. $Cu_{10}Ag_2Sb_4S_{13}$ x 220

Ag-tetrahedrite (grey) veined by $(CuAg)_3SbS_3$ (light grey) with blebs of stibioluzonite (grey). Eutectoid-type breakdown of Ag-tetrahedrite.

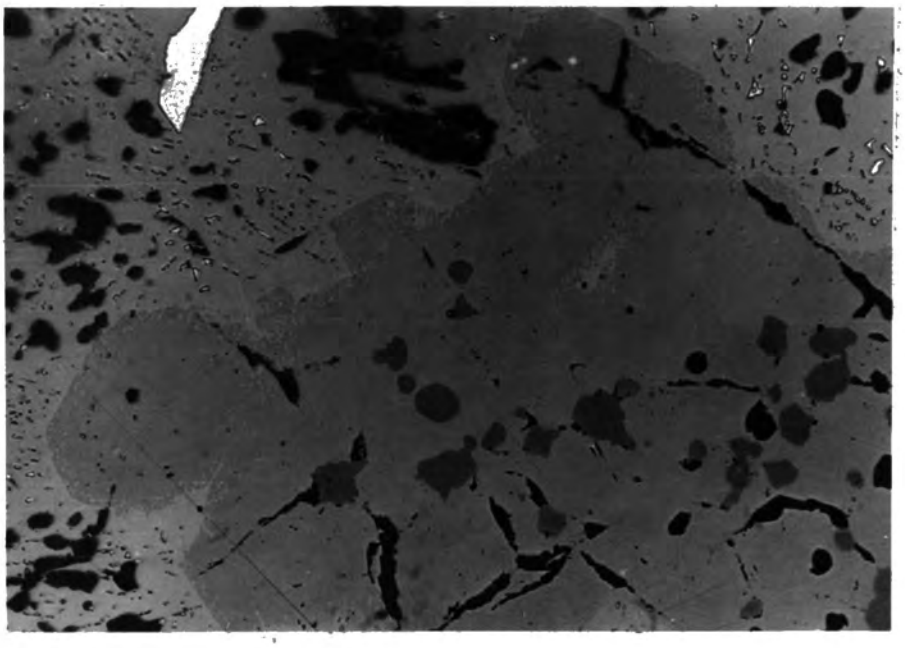

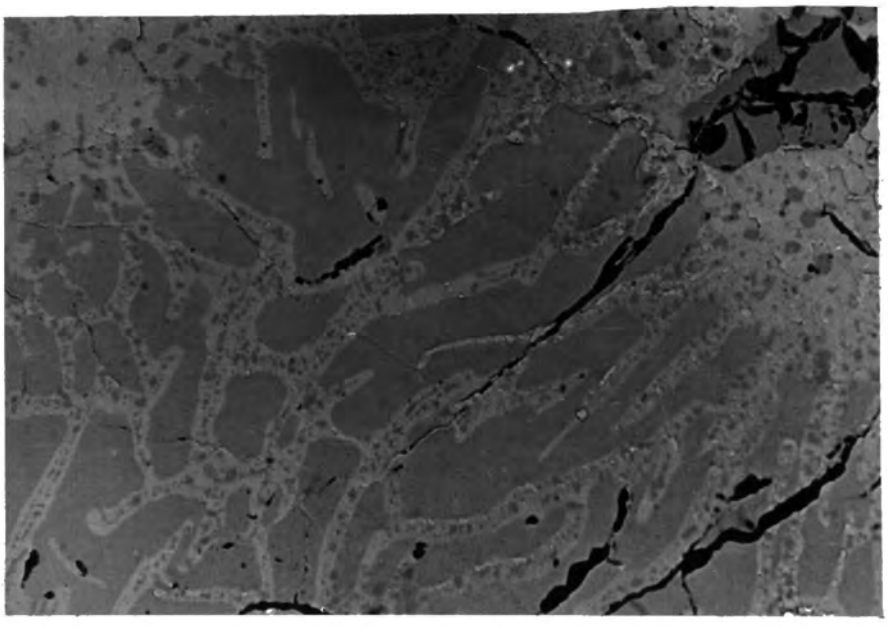

PLATE 5-5

Starting comp. $Cu_8Ag_4Sb_4S_{13}$ x 220

Ag-tetrahedrite (grey) veined and pseudomorphed by a fine $(CuAg)_3SbS_3$ (light grey) and stibioluzonite (grey) intergrowth.

Coarse interstitial $(CuAg)_3SbS_3$ and stibioluzonite.

Note preservation of original crystal boundary of tetrahedrite.

PLATE 5-6

Starting comp. $Cu_8Ag_4Sb_4S_{13}$ (oil) x 1340

(As Plate 5-5) Note the preservation in the $(CuAg)_3SbS_3$ and stibioluzonite intergrowth of an original tetrahedrite contact boundary (arrowed).

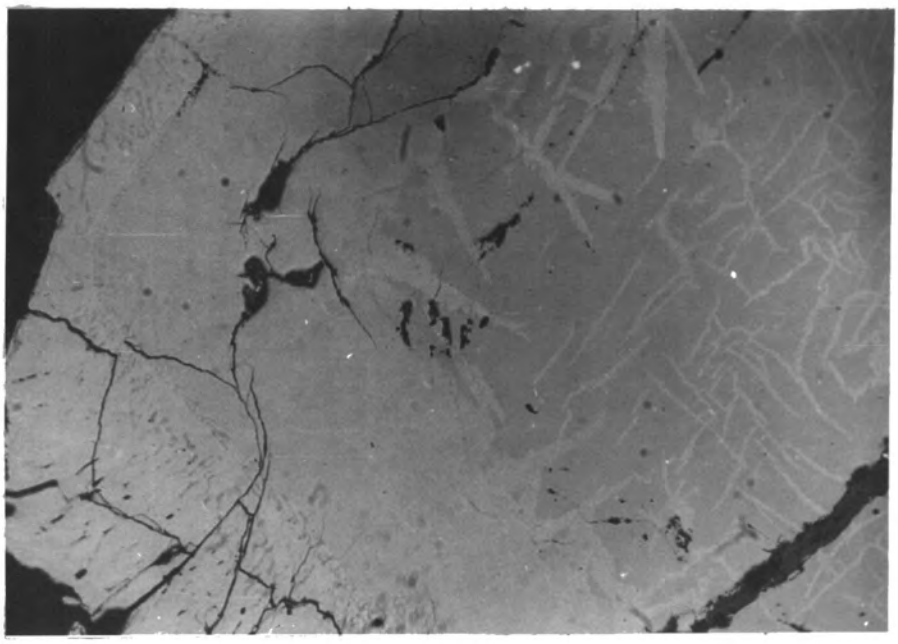

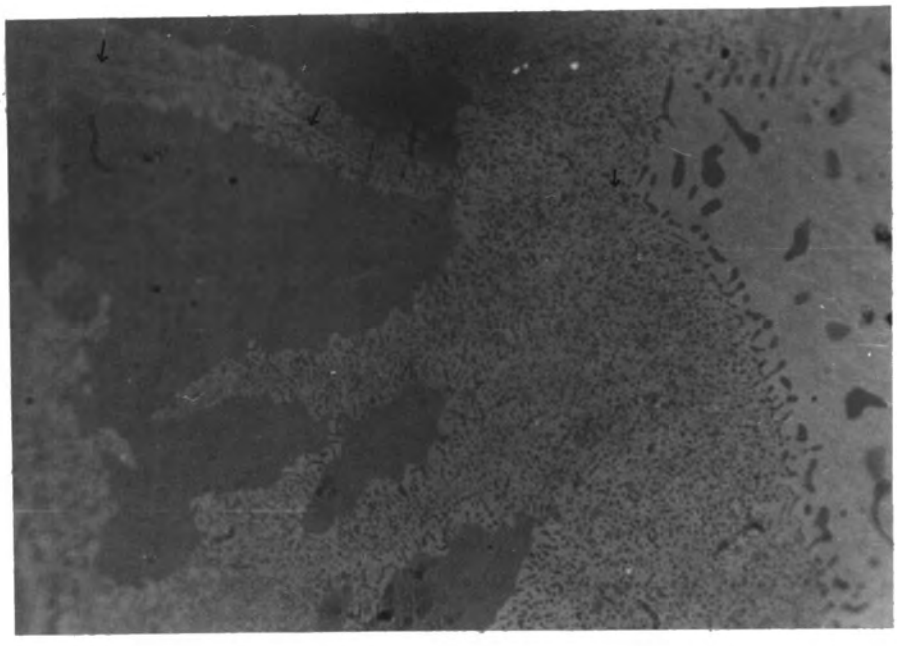

PLATE 5-7

Starting comp. $Cu_{2.5}Zn_{0.5}SbS_4$ (oil) x 220

ZnS (dark grey) in Zn-tetrahedrite (light grey).
Stibioluzonite (grey) in mutual boundary texture with Zn-tetrahedrite.
Note lamellae of stibioluzonite in tetrahedrite.

PLATE 5-8

Starting comp. $Cu_{2.5}Zn_{0.5}SbS_4$ (oil) x 1340

(As Plate 5-7) Stibioluzonite lamellae (grey) in three orientations in Zn-tetrahedrite (light grey). Studs of metal (white) associated with the lamellae.

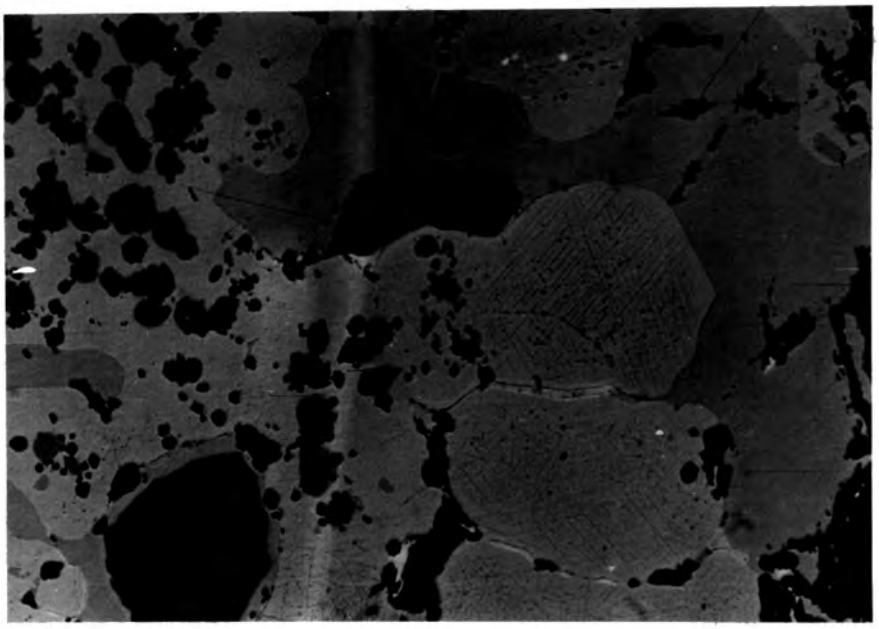

CHAPTER 6

Crystal Chemistry

Introduction

Crystal chemistry is a study of the interactions between atoms in the solid state. There are three well established major types of atomic bonding - ionic, covalent and metallic. Discussions of their nature and how they relate to the physical properties of materials are available in many texts (Pauling, 1960; Brown, 1967; Companion 1964; Seel, 1965).

In considering crystal structures, the most important aspects of atomic character are: (i) the valency properties (valency, bond-orbital symmetry and perhaps electron concentration), (ii) atomic size (although this cannot be rigorously defined, there are two empirical scales - ionic and covalent-metallic - either one or the other of which may be applicable to a particular compound, and (iii) effective atomic charge, resulting from the balance of the ionization potentials and electron affinities of the component atoms (Pearson 1964).

Sulphides, and tetrahedrite is a typical example, have physical properties which indicate that the chemical bonding between atoms in their structures is of an intermediate type. A theory of bonding, which can explain the chemical and physical features of sulphides, has not been developed to the same extent as has been possible for the end-member types of bonding. The principles determining the structure of the sulphide minerals, therefore, have not as yet been

formulated in a comprehensive way and this is the reason for this lengthy introduction.

Progress in the understanding of bonding in sulphides has come mainly from semiconductor research. Unlike metals, the conductivity of semiconductors increases with temperature, and this is because thermally excited electrons are transferred across an energy gap from the valence energy band to the conduction band. The 'band model' is proving to have its limitations as a theory of metals (Rundle 1967) but nevertheless is a valuable concept when relating the crystal chemistry to the physical properties of crystalline materials. Bragg scattering of electron waves in a regular lattice results in allowed and forbidden energy bands. Normally only the outer, higher energy bands involving the valence electrons are important.

A semiconductor is stabilised when its valence band is exactly filled and this means that all the valence electrons contributed by the component elements are used in forming bonds. Pearson (1964) concludes, therefore, that valency is the most important criterion in considering the crystal structures of semiconductors. It is the presence of anions with filled valence subshells that prevent arrays of 'metallic' orbitals from running continuously throughout the structure. Substitution into the structure, of a cation which donates an excess of valence electrons, leads to instability but this can be prevented by cation site vacancies. The polarizability of the sulphur atom permits such vacancies in sulphides (Jellinek 1968). In this way, extensive solid solution in the Cu-Fe-S system occurring in lines along which compositions have their valence energy band exactly filled, has been explained by Frueh (1954).

Using this same rule of stability adamantine (sphalerite) type structures require an average of four valence electrons per atom in order to fill the valence band exactly. A formula enabling the prediction of sphalerite-type structures has been determined by Parthé (1967), which takes lattice vacancies into account -

$$\text{for } X_mY_nZ_o(\ )_s \qquad \frac{m.e_x + n.e_y + o.e_z}{m + n + o + s} = 4$$

where e_x is the valence electron contribution of x.

A general valence rule for semiconductors, if they contain anions lying to the right of the Zintl border (Group iv-vii atoms excluding the transition metals), has been established by Pearson (1964) -

$$(n_e + b_a - b_c)/n_a = 8$$

where n_e is the total number of valence electrons,

n_a is the number of anions,

b_a is the number of electrons involved in forming anion-anion bonds,

b_c is the number of electrons involved in forming cation-cation bonds and including any 'unshared' valence electrons on the cations.

All these values are calculated per formula unit of the compound. 'Anion' and 'cation' are used to designate respectively the most electronegative atoms and the remaining atoms in compound semiconductors.

The valence rule expresses the bonding requirements for the anions to attain a filled valence subshell of eight (atomic) s and p electrons. The rule applies to polyanionic valence compounds ($n_e/n_a < 8$), polycationic valence compounds

($n_e/n_a > 8$) and normal valence compounds ($n_a/n_e = 8$). The discussion on tetrahedrite will mainly be concerned with the latter class.

The valence electron contribution in a compound can be determined by balancing the cation-anion charges in the unit formula but ambiguous results can be obtained when a selection of variable valence atoms are involved. A knowledge of the co-ordinations of the atoms in the structure can contribute to the assessment of the valence electron contribution of individual atoms. This is because co-ordination in directed-bond compounds is intimately related to molecular orbital symmetry. Linear combinations of s, p and d atomic orbitals (Fig.6-1) result in directional molecular orbitals (Pauling 1931). The strength of the directional bonds between atoms depends on the degree of overlap of their orbitals. Only certain combinations of atomic orbitals can lead to a given molecular orbital and associated co-ordination. The problem of defining the co-ordinations possible from combinations of atomic orbitals has been tackled using group theory by Kimball (1940).

Since the electronic configurations and the normal valencies of the elements are established, for a given atom the atomic orbitals which contain the likely valence electrons are known (from the ground state configuration), and those required for a given co-ordination can therefore be deduced. This method will be utilised in the discussion of bonding in tetrahedrite.

Pearson (1964) considers that the directional nature of the chemical bonds is the second most important criterion in considering the crystal structures of semiconductors. The

chemical bonds in characteristically ionic and metallic compounds are essentially non-directional. Compounds of the various bond types, nevertheless, frequently adopt the same structural types because regular co-ordination polyhedra such as tetrahedra and octahedra can satisfy the stability requirements though in different ways.

The investigations of bonding in complex molecules has contributed a great deal to the understanding of the directional nature of covalent bonding (Brown 1967). The localised electron-pair covalent bond theory has been important in this field. Each single bond between two atoms requires a pair of electrons for stability. This is because in molecular orbitals as in atomic orbitals only two electrons of opposing spin can occupy the same energy level. In molecules the structure usually only extends over very short distances and it is a simple matter to establish the distribution and source of the valence electrons. Progress has therefore been made in the detailed study of bonding and the distortions in complexes involving transition metals have been investigated (Mingos 1971).

The electron pair valence bond theory can be applied to crystal structures as well as finite molecules. In sulphides the theory becomes less appropriate. In sphalerite, for example, electron pair bonds can form by the donation of two outer shell (s) electrons by zinc and six outer shell (s+p) electrons by sulphur. Both atoms are in tetrahedral co-ordination and sp^3 hybridisation of the atomic orbitals can account for this (Kimball 1940). In order to form electron pair bonds sulphur must contribute $1.5e^-$ and zinc $0.5e^-$ to each of the four bonds per atom. Although it must be an unrealistic model of the actual situation, the concept of

fractional contributions of electrons by atoms to electron pair bonds is useful, because it is a convenient means of verifying the likely valence electron contribution of the atoms. This approach has therefore been used in the discussion on tetrahedrite.

The close relationship between co-ordination and valence electron contribution has not been utilised by authors discussing crystal chemistry. Tetrahedral co-ordination is implicit in the general formula of adamantine compounds established by Parthé (1967).

Assuming that the stability requirement for a sulphide is that its valence band is exactly filled, that each σ bonding molecular orbital can only contain the same number of electrons as its constitutent atomic orbitals and that the co-ordination polyhedra are directly related to molecular orbital symmetry then the paired electron bond concept is applicable and for stability the number of bonds per formula unit equals half the total valence electron contribution. Usually the number of electron pair bonds around an atom will equal its co-ordination number.

In some sulphides, however, the ligancy of atoms is greater than the covalence. This means that there are insufficient valence electrons to satisfy all the electron pair bonds suggested by the co-ordination polyhedra. Pauling (1970) explains this phenomenon as being due to a small number of bonds resonating between a large number of positions and quotes galena (PbS) as an example. This same concept was used by Pauling (1938) to account for bonding in metals where again the electrons are too few to form electron pair bonds between the atoms of a metal and are delocalised (resonate) over the atom pairs (Rundle 1967). The resonance concept of

an electron pair bond alternating between different positions appears to have arisen, in the case of sulphides, because the directional nature of the atomic orbitals has not been taken completely into account. In galena the p orbitals of Pb and S are directed along the cartesian axes of the atoms (Fig.6-1). Pb has two, and S four, p electrons. Octahedral co-ordination will result in overlap of the S and Pb p orbitals forming three bonding orbitals (filled by the six contributed valence electrons) and three empty antibonding orbitals. Although three electron pairs have been formed they are delocalised. Although resonance is not necessary in the explanation of octahedral co-ordination of galena the concept will be required for tetrahedrite.

The number of electron pair bonds is therefore not necessarily equal to the co-ordination number. The number of electron pairs formed is equal to half the number of atomic orbitals used in the bonding and it is the symmetry of the bonding orbitals (atomic or hybrid) which is related to co-ordination: -

$$\text{No. of electron pairs/formula unit} = \frac{\sum_{1}^{n}(N_n \times A_n)}{2} = \frac{\text{total valence electron contribution}}{2}$$

where N_n is the number of atoms of one type (element-valency-co-ordination) in the formula,

A_n is the number of atomic orbitals of that atom which contribute to the bonding,

n is the number of types of atom in the formula.

Therefore for stability (i.e. a full valence band) -

$$\sum_{1}^{n}(N_n \times A_n) = \text{the total valence electron contribution}$$

In many sulphides (as in ionic compounds) the sum of the valence electrons contributed by the electropositive element (i.e. the normal cation valency) will equal the number of electrons accepted by the electronegative element (i.e. the normal anion valency). This, however, need not always be readily apparent in covalent sulphides because of S-S and M-M bonds. The use of the above formula in describing pyrite indicates the value of considering co-ordination as well as valency when charge balancing is difficult.

In pyrite, FeS_2, the octahedral co-ordination of iron means that two outer shell (d) valence electrons are contributed to the d^2sp^3 hybrid orbital. The tetrahedral co-ordination of sulphur means that six electrons are contributed to the sp^3 hybrid orbital. This is well established (Burns 1970). For pyrite, therefore, the formula ${}^{6}Fe^{2}\,{}^{4}S_{2}^{6}$ applies where the right hand superscript is the valence electron contribution and the left hand superscript the number of atomic orbitals involved in bonding. In this case the number of atomic orbitals involved in bonding equals the co-ordination number.

For pyrite -

$$\sum_{1}^{n}(N_n \times A_n) = (1 \times 6) + (2 \times 4) = 14$$

$$\text{valence electron contribution} = (2 \times 1) + (6 \times 2) = 14$$

Any other permutation of co-ordination = 4 or 6 and valence electron contribution = 2 or 3 which are common for iron, or co-ordination = 4 or 6 and valence electron contribution = 4 or 6 which are possible for sulphur, will not give this result of stability for FeS_2. The structure of pyrite can therefore be deduced from a knowledge of the

atomic configurations of iron and sulphur. The use of the above formula will be demonstrated again in the discussion on tetrahedrite.

Tetrahedrite

The nature of bonding in sulphides is of variable complexity and since as yet there is no real theory of sulphides several approaches will be utilised in the discussion on tetrahedrite.

Tetrahedrite and tennantite are isostructural. The structure of binnite, $(CuFe)_{12}As_4S_{13}$, a variety of tennantite, was determined by Pauling and Neuman (1934). The structure of tetrahedrite, $Cu_{12}Sb_4S_{13}$, was refined by Wuensch (1964) and of binnite (tennantite), $Cu_{12}As_4S_{13}$, by Wuensch, Takéuchi and Nowacki (1966).

Tetrahedrite has a cubic superstructure based on the sphalerite arrangement. The unit cell formula is $2(Cu_{12}Sb_4S_{13})$ and the space group $I\bar{4}3m$. The unit cell edge of 10.319Å (this study), indicates that there are eight sphalerite cells (a_o = 5.4Å) per unit cell of tetrahedrite. The co-ordinations of copper (two sites), antimony (one site) and sulphur (two sites) have been established (Fig.6-3) (Wuensch 1964, 66).

The structural formula can be written -

$$2(^{3}Cu_6\,^{4}Cu_6\,^{3}Sb_4\,^{4}S_{12}\,^{6}S)$$

where the superscript is co-ordination number. The half unit cell is shown in Fig.6-2.

The limit of substitution of divalent cations, Zn+Fe (synthetic) and Zn+Fe+Hg (natural) is important when considering bonding in tetrahedrite. The general formula of substituted tetrahedrite, $(CuAg)_{10}(CuFeZn)_2(SbAs)_4S_{13}$,

established by Springer (1969) for natural specimens and for synthetic specimens in this study indicates that tetrahedrite is a normal valence compound - $Cu_{10}^{+1}\ Zn_{2}^{+2}\ Sb_{4}^{+3}\ S_{13}^{-2}$

During this discussion Zn^{+2} will be used to represent the divalent cations in tetrahedrite.

There is a contradiction between the structural formula of tetrahedrite and the valency distribution. Since zinc normally, and iron often, occur in tetrahedral sites, it is most likely that they will replace one third of the tetrahedrally co-ordinated Cu atoms in tetrahedrite. If this takes place randomly the structure will remain isometric.

A molecular orbital theory approach permits the co-ordinations of the atoms to be explained by σ bonding. The electron pair bond concept using fractional distributions of electrons is valid for most of the atoms where the number of atomic orbitals involved in bonding equals the co-ordination number.

Description of individual atoms (Figs.6-2, 3)

Antimony co-ord. No.3: Threefold co-ordination is common for antimony. The Sb atom is displaced outwards from an S atom triangle-trigonal pyramidal co-ordination. The Sb ground state is $4d^{10}5s^{2}5p^{3}$. Sb can therefore contribute $5e^{-}$ to four sp^{3} hybrid orbitals directed tetrahedrally. One bonding direction is occupied by a 'lone pair' of electrons. Sb therefore contributes one electron to each of the three electron pair $^{3}Sb\text{-}^{4}S$ bonds (superscript is co-ordination no.) and is trivalent.

Zinc and Copper co-ord. No.4: Fourfold co-ordination of copper and zinc can be explained by sp^{3} hybridisation yielding four tetrahedrally directed bonds.

The Cu ground state is $3d^{10}4s^{1}$. Cu can therefore contribute one electron to the sp^3 bonding. In tetrahedrite the Cu tetrahedra are slightly distorted (Wuensch 1964). In sulphides copper is often in distorted tetrahedral sites - approaching triangular or linear co-ordination. This may be due to (excited) configurations e.g. $d^9(d,s)^1$ or $d^8(d,s)^2$. These hybrids are stabilised by lowering the symmetry of the cation (Jellinek 1968). In pure tetrahedrite, therefore, the divalency of copper, which requires that one d electron is involved in the bonding, may result simply in increased distortion of the Cu polyhedra.

The Zn ground state is $3d^{10}4s^{2}$. Zn can therefore contribute $2e^-$ to the sp^3 bonding.

One third of the cation (Cu) tetrahedral sites in substituted tetrahedrite contain divalent cations. The average contribution to the $^4(CuZn)-^4S$ bond will therefore be $^1/_3e^-$.

Sulphur co-ord. No.4: Fourfold co-ordination of sulphur is normal and is due to sp^3 hybridisation. The S ground state is $3s^23p^4$. S can therefore contribute $6e^-$ to the bonds but since the four bonds already contain differing numbers of electrons the distribution will be as shown in Fig.6-3. This irregular distribution may be related to the distortion of the S tetrahedra reported by Wuensch (1964).

Sulphur co-ord. No.6: Sixfold co-ordination of sulphur can arise by utilisation of the p electrons resulting in octahedral co-ordination but only requiring three electron pairs in the molecular orbital bond. The S ground state is $3s^23p^4$. S can therefore contribute $4e^-$ to the molecular orbital and only requires $2e^-$ to satisfy electron spin pairing.

Copper co-ord. No.3: Threefold co-ordination of copper can arise by sp^2 hybridisation. The Cu ground state is $3d^{10}4s^1$. Cu can therefore contribute a total of one electron to its three bonds. But $^2/_3e^-$ is required by the ^3Cu-^4S bond leaving $^1/_3e^-$ for each ^3Cu-^6S bond. There are six ^3Cu atoms around the ^6S atom. A total of $2e^-$ is therefore donated by the coppers to sulphur and satisfies the requirements of sulphur.

Only σ bonding has so far been considered but π bonding could contribute and would result in a decrease in cation-anion interatomic distances (Burns 1970). Because of the greater co-ordination, the ^6S-^3Cu bond length would be expected to be greater than the ^4S-^3Cu bond length and the structural determination of tetrahedrite by Pauling and Neuman (1934) showed this to be the case (Pauling 1970). The refinement of the structures of tetrahedrite and tennantite by Wuensch (1964, 66), however, indicated a decrease in bond length in the higher co-ordination case - the ^3Cu-^6S distance being 2.234Å and the ^3Cu-^4S distance being 2.272Å in tetrahedrite.

The greater symmetry of the atomic orbitals around the Cu-S bonds in sixfold co-ordinated sulphur than in fourfold co-ordinated sulphur in tetrahedrite must permit extensive π bonding which decreases the Cu-S distance. The π bonding can take place between full Cu d orbitals and empty S d orbitals provided the symmetry requirements are met. In Fig.6-3, for example, the full Cu $d_{x_2-y_2}$ orbital can bond with the empty S d_{zx} orbital by sideways overlap (π bonding). Similarly the full Cu d_{xy} orbital could form π bonds with the S d_z2 orbital.

In this bonding model described for tetrahedrite the elements have their normal valencies, Cu = +1, Zn = +2, Sb = +3 and S = -2. The thirteenth sulphur atom in the formula $Cu_{10}Zn_2Sb_4S_{13}$ has the normal valency, i.e. it accepts two electrons. If the p electrons only contribute to the bonding this means that the formula of Pearson (1964), which requires that sulphur attains an octet of outer shell electrons by contributing all its outer shell electrons (6) to the valence band is invalid.

$$(n_e + b_a - b_c)/n_a = 8$$

$$110 + 0 - 8 / 13 \neq 8$$

The two missing valence electrons are the two s electrons of the thirteenth sulphur atom.

Octahedral co-ordination of sulphur may be explained by sp^3d^2 hybridisation. This is probably the case in SF_6 where sulphur is the electropositive atom. If this was the case, in tetrahedrite, then the formula of Pearson (1964) would be valid. However, for electron spin pairing, the six atomic orbitals would require an additional six electrons. This means that another four cations in $Cu_{10}Zn_2Sb_4S_{13}$ would have to be divalent and this is evidently not the case as no more zinc can be substituted into the $Cu_{12}Sb_4S_{13}$ structure.

The formula for stability -

$$\sum_1^n(N_n + A_n) = \text{total valence electron contribution}$$

can be satisfied for the bonding model of tetrahedrite described. The delocalised nature of the bonding (in some parts of the structure) requires that for description the electrons must be frozen (localised) and a resonance concept introduced.

Since the octahedrally co-ordinated sulphur atom has three atomic orbitals involved in bonding and has four valence electrons then it can be imagined that only three of the surrounding copper atoms are contributing electrons to satisfy sulphur's requirements. Only three Cu atoms are therefore in trigonal co-ordination (bonding) and the other three are in angular twofold co-ordination with tetrahedrally co-ordinated sulphur. This situation resonates between all the Cu atoms which are in trigonal sites.

The bonding formula can be stated -

$$({}^{3}Cu_{3}^{1}\ {}^{2}Cu_{3}^{1})\ {}^{4}Cu_{4}^{1}\ {}^{4}Zn_{2}^{2}\ 3(+1)Sb_{4}^{3}(+2)\ {}^{4}S_{12}^{6}\ {}^{3}S^{4}$$

	sp^2	sp	sp^3	sp^3	sp^3	sp^3	p^3		
$A_n \times N_n$	9	6	16	8	12	48	3	=	102
V.E.C.	3	3	4	4	12	72	4	=	102

where N_n is the number of atoms of one type, A_n is the number of atomic orbitals which contribute to the bonding and V.E.C. is the valence electron contribution. The left hand superscript is the number of atomic orbitals contributed to the valence band of the structure, the number in brackets being atomic orbitals filled by electron pairs from that atom. The total number of atomic orbitals for each atom is the number which dictates the co-ordination symmetry of the atom. The right hand superscript is the valence electron contribution to the valence band of the structure, the number in brackets being atomic orbitals filled by electron pairs from that atom. The bracketed parts of the formula are involved in resonance.

Stibioluzonite

Stibioluzonite, Cu_3SbS_4, is isostructural with the low temperature polymorph of Cu_3AsS_4, luzonite. There is only limited miscibility between the two compositions (Skinner 1969). The high temperature polymorph (transition temperature = 320°C) of Cu_3AsS_4, enargite, has limited Sb miscibility. The nomenclature has been in a state of confusion in the past (Harcourt 1937) and the nomenclature recommended by Levy (1966) is used in this study. Use of the term 'Famatinite' which is of uncertain definition has been avoided in this study except in references to earlier work where the term has been used.

The structure of stibioluzonite-luzonite was determined by Gaines (1957) and the structure of natural luzonite, $Cu_3(As_{0.64}Sb_{0.36})S_4$, refined by Marumo and Nowacki (1967).

Stibioluzonite-luzonite is tetragonal, space group D_{2d}^{11} - $I\bar{4}2m$ and the cell parameters (synthetic stibioluzonite, this study) a_o = 5.383 and c_o = 10.766 Å.

The co-ordinations of copper (tetrahedral), Sb (and As) (tetrahedral) and sulphur (tetrahedral) were established by Marumo and Nowacki (1967) and the unit cell described as consisting of two 'sphalerite type' (a_o = 5.41 Å) cells. The copper and antimony atoms occupy zinc positions.

The structural formula of stibioluzonite can be written -

$$2(^{4}Cu_3{}^{4}Sb{}^{4}S_4)$$

where the superscript is co-ordination number.

In the present study it was noted that zinc does not enter the stibioluzonite lattice but there is limited substitution of Cu by Ag. There is no extensive substitution of Cu by divalent cations reported in natural specimens of

stibioluzonite (famatinite) or enargite in Dana (1944).

The valence formula for stibioluzonite can therefore be written - $Cu_3^{+1}Sb^{+5}S_4^{-2}$

The fourfold co-ordination of each atom is due to sp^3 hybridisation therefore Cu (ground state $3d^{10}4s^1$) can contribute $1e^-$, Sb (ground state $4d^{10}5s^25p^3$) can contribute $5e^-$ and S (ground state $3s^23p^4$) can contribute $6e^-$ to the valence band.

The rule for stability of adamantine structures (Parthé 1967) is obeyed.

$$\frac{m.e_x + n.e_y + o.e_z}{m + n + o + s} = \frac{(3x1) + (1x5) + (4x6)}{3 + 4 + 1} = 4$$

The general valence rule for semiconductors (Pearson 1964) is obeyed.

$$(n_e + b_a - b_c)/n_a = (32 + 0 - 0)/4 = 8$$

The formula for stability (this study) is obeyed and the bonding formula can be written -

$$^4Cu_3^1\ ^4Sb^5\ ^4S_4^6$$

$$sp^3 \quad sp^3 \quad sp^3$$

$N_n \times A_n$	12	4	16	= 32
V.E.C.	3	5	24	= 32

The formula format is described in the section on tetrahedrite.

It is reported by Marumo and Nowacki (1967) that half of the Cu atoms in luzonite, $Cu_3(AsSb)S_4$, are in distorted tetrahedral sites. The high temperature polymorph of Cu_3AsS_4, enargite, is a wurtzite derivative structure but there is no Cu_3SbS_4 equivalent reported. These observations indicate

that non-bonding electrons (probably Cu d-electrons) or interactions between second-nearest neighbours can influence the structure.

$\underline{Cu_3SbS_3}$

The structure of this phase has not been determined but it is isostructural with wittichenite, Cu_3BiS_3, is orthorhombic and has the unit cell parameters $a_o = 7.673$ $b_o = 10.342$ and $c_o = 6.693$Å (This study).

The structure of wittichenite is not available but the space group D_2^4 - $P2_12_12_1$ was given by Nuffield (1947). Hellner (1958) reports that a preliminary structural determination of wittichenite indicated that the structure could be derived from that of tetrahedrite.

In the present study it was noted that silver substitutes for copper in Cu_3SbS_3 and that divalent cation substitution was unlikely.

The valence formula of Cu_3SbS_3 is therefore -

$$Cu_3^{+1}Sb^{+3}S_3^{-2}$$

The general valence rule for semiconductors (Pearson 1964) is obeyed -

$$(n_e + b_a - b_c)/n_a = (26 + 0 - 2)/3 = 8$$

Chalcostibite

The structure of chalcostibite (wolfsbergite), $CuSbS_2$, has been described by Hofmann (1933). Chalcostibite (natural) was found to be orthorhombic, space group D_{2H}^{16} - PNAM. The unit cell parameters of synthetic chalcostibite are $a_o = 6.016$ $b_o = 14.505$ and $c_o = 3.800$Å (This study).

The co-ordinations of the atoms were determined by

Hofmann (1933). The Cu atom is in tetrahedral co-ordination with four S atoms, the Sb atom is in the usual trigonal pyramidal co-ordination with three S atoms, one S atom is in tetrahedral co-ordination with two Cu atoms and two Sb atoms, and the other S atom is in octahedral co-ordination with four Sb and two Cu atoms.

The structural formula of chalcostibite is therefore -

$$4(^{4}Cu^{3}Sb^{4}S^{6}S)$$

where the superscript is co-ordination number.

No information on substitution in synthetic chalcostibite was obtained in this study. No extensive substitution of Cu by divalent cations in natural chalcostibite is reported by Dana (1944) but up to 1,000 ppm Ag content has been reported (Boyle 1968).

The valence formula for chalcostibite can therefore be written - $Cu^{+1}Sb^{+3}S_2^{-2}$

Octahedral co-ordination of sulphur can be explained by the utilisation of p orbitals only. Three electron pairs are therefore needed for stability. The general formula for semiconductors (Pearson 1964) is therefore invalid.

The formula for stability (this study) is obeyed and the bonding formula can be written -

$$4_{Cu}{}^{1}\ 3(+1)_{Sb}{}^{3}(+2)\ 4_{S}{}^{6}\ 3_{S}{}^{4}$$

	sp^3	sp^3	sp^3	p^3	
$N_n \times A_n$	4	3	4	3	= 14
V.E.C.	1	3	6	4	= 14

The formula format is described in the section discussing tetrahedrite.

Substitution in Tetrahedrite, $Cu_{12}Sb_4S_{13}$

In this section the crystallochemical factors affecting substitution in tetrahedrite and the effects of substitution on the physical properties of tetrahedrites will be discussed.

The formula of substituted tetrahedrite is -

$$(CuAg)_{10}(ZnFeCu)_2(SbAs)_4S_{13}$$

Substitution of Sb by As extends from tetrahedrite to the As end-member, tennantite. Possible ordering of Sb and As resulting in increased stability of the intermediate member with Sb:As = 1:1 has been discussed in Chapter 4. Substitution of Cu by Zn and Fe has a limit, indicated in the general formula, of 6.90 at%. Substitution of Cu by Ag is restricted and temperature dependant. The effects of substitution on the physical properties of tetrahedrite are summarised below -

substituting element	cell edge	microhardness	reflectivity
As	-	+	-
Zn	+	+	+
Fe	+	+	+
Ag	+	-	-

where '+' indicates an increase and '-' a decrease.

Arsenic

There is one type of Sb site in tetrahedrite. The ground state configuration of As, $3d^{10}4s^24p^3$, is similar to that of Sb, $4d^{10}5s^25p^3$. The As atom, in sp^3 hybridisation, can therefore contribute the same number of electrons to the structure as Sb and this is the reason for their extensive interchange in tetrahedrite-tennantite. Arsenic is more electronegative than antimony and the covalency of the As-S

bond is therefore greater (Table 6-1). The values of the various types of radii (Table 6-1) are smaller for arsenic than for antimony. The decrease in cell edge from tetrahedrite to tennantite is therefore due to the smaller size of the As atom and to increasing covalency of the semi-metal - sulphur bond.

The increase in microhardness of tetrahedrite as Sb is substituted by As indicates an increase in the minimum bond strength of bonds in tetrahedrite. This can be explained by the greater covalency of the As-S bond. An increase in minimum bond strength is also apparent from the higher melting point of tennantite. There must be a limit of compressability of the Cu-S bonds and the range in composition of tennantite, towards Cu, with an associated increase in cell edge (Maske and Skinner 1971) may be a compensatory effect which increases stability.

Zinc and Iron

Substitution of Cu by Zn and Fe in tetrahedrite reaches a maximum when the valence formula is -

$$Cu_{10}^{+1}(ZnFe)_{2}^{+2}Sb_{4}^{+3}S_{13}^{-2}$$

The limit of substitution (6.90 at%) corresponds to the filling of 1/3 of the available Cu tetrahedral sites. The controlling factor is the valence electron contribution of Zn and Fe in tetrahedral co-ordination.

Tetrahedral (fourfold) co-ordination of Zn, ground state $3d^{10}4s^{2}$, can be explained by sp^{3} hybridisation, Zn contributing $2e^{-}$ to the valence band. In the case of univalent Cu, sp^{3} hybridisation means that only $1e^{-}$ is contributed to the valence band. Further replacement of Cu by Zn would, therefore, result in an excess of valence electrons in the structure

and instability.

The ground state configuration of Fe is $4s^2 3d^6$. Minster (1964), in a study of isomorphism in sphalerite, concluded from the semiconducting properties of the tetrahedral phases discussed, that the tetrahedral bonds of Fe form by sp^3 and not d^3s hybridisation. As in the case of Zn, sp^3 hybridisation will result in the contribution of $2e^-$ by Fe to the valence electron band and the limit of substitution of Fe in tetrahedrite is therefore the same as that of Zn.

Substitution of Cu by both Fe and Zn resulted in an increase in the unit cell edge and the microhardness of tetrahedrite and no difference in magnitude of change was detected. Both Fe and Zn are less electronegative than Cu (Table 6-1) and a decrease in covalency and associated increase in M-S bond length in tetrahedrite is to be expected. This is also the case in other sulphides (Table 6-1).

The reason for the increase in microhardness is not obvious. Nickel et al. (1971) have noted that microhardness values decrease and M-S bond lengths increase in the sequence $FeS_2 > CoS_2 > NiS_2$ though S-S bond lengths decrease. In the case of tetrahedrite, therefore, although the (ZnFe)-S bond strength is less (less covalent) the minimum M-S bond strength in the structure may be greater.

Silver

Substitution of Cu by Ag in tetrahedrite was found to be temperature dependant (Chapter 5). Ag-tetrahedrites synthesised were probably metastable. The ground state configuration of the Ag atom is $4d^{10}5s^1$ which is similar to that of Cu, $3d^{10}4s^1$. There is, therefore, no valency restriction on substitution of Cu by Ag within the limits indicated in the

general formula above. The large size of the Ag atom (Table 6-1) and the resultant(?) preference for a small co-ordination number in sulphides (Jellinek 1968) is probably the cause of the temperature dependance of substitution of Cu by Ag in tetrahedrite. On cooling Ag-tetrahedrite, Ag is not simply rejected as silver metal but a eutectoid-type breakdown occurs and Ag enters the $(AgCu)_3SbS_3$ phase (Chapter 5). Ag has a low co-ordination number (2) in Ag_3SbS_3 (Engel and Nowacki 1966) and probably has a low co-ordination number in Cu_3SbS_3 but the structure has not been determined.

Although the Ag atom is larger than atoms of Zn or Fe (Table 6-1) substitution of Cu by an equivalent atomic% of Zn, Fe or Ag results in a similar increase in the cell edge of tetrahedrite (Fig.5-3). The reason for this is not known.

The decrease in microhardness of tetrahedrite due to Ag substitution maybe related to the metastability of Ag-tetrahedrite. Nickel et al. (1971) explain the decrease in microhardness in the sequence $FeS_2 > CoS_2 > NiS_2$ as being due to the extra d-electrons of Co and Ni, which cannot be accommodated in the valence band, and which decrease the M-S bond stability. In Ag-tetrahedrites a small co-ordination (bonding) number of Ag, although it may be held in a tetrahedral (or trigonal) site, will result in an excess of electrons in the tetrahedrite structure. The excess electrons are those which would have contributed to the bonds with Ag. As in the case of the pyrite structures, the excess electrons result in instability, a decrease in microhardness and an increase in cell size.

Reflectivity

Reflectivity has not been discussed above. There is no simple relationship between reflectivity and microhardness or

unit cell edge of tetrahedrites nor between reflectivity and the properties of the substituting atoms listed in Table 6-1.

Bither et al. (1968) and Burns and Vaughan (1970) conclude that reflectivity is dependant on the number of energy levels available to electrons excited by light from the valence band to the conduction band and that the excess d-electrons, in antibonding molecular orbitals, (i.e. the conduction band) results in a decrease in stability, reflectivity, microhardness and increase in cell edge in the sequence $FeS_2 > CoS_2 > NiS_2 > CuS_2$. Vaughan, Burns and Burns (1971) conclude that the composition ranges, geochemistry, and variations of cell parameters, microhardness, reflectivities and relative stabilities of thiospinels are directly related to the number of electrons in antibonding molecular orbitals.

In Ag-tetrahedrite, the decrease in reflectivity, therefore, may be related to the instability of the Ag atom in the tetrahedrite structure at low temperatures, and as discussed above, this may also result in a decrease in microhardness and increase in cell edge.

The interpretation of the relationships between reflectivity and other properties of substituted tetrahedrite not only requires the collection of more systematic data but an advance in the theory of reflectivity.

TABLE 6-1

Elem.	At.No.	Single bond covalent radius	Metallic radius	Ions	Ionic Radius	Pauling Electronegativity	M-S bond length in 4-fold co-ordination
S	16	1.04	1.27	S^{2-}	1.84	2.5	
Cu	29	1.173	1.28	Cu^{+}	0.93	1.8	2.31 (covellite)
				Cu^{++}	0.72	2.0	2.19 (covellite)
Fe	26	1.165	1.26	Fe^{++}	0.76	1.65	2.36 (stannite)
				Fe^{3+}	0.64	1.8	2.20,2.30 (chalcopyrite)
Zn	30	1.249	1.37	Zn^{++}	0.72	1.5	2.35 (sphalerite)
Ag	47	1.339	1.44	Ag^{+}	1.21	1.8	2.644 (average)
Sb	51	1.41	1.59	Sb^{3+}	0.92	1.8	2.536 (average)
				Sb^{5+}	0.63	2.1	2.494 (average)
As	33	1.21	1.39	As^{3+}	0.69	2.0	2.273 (average)
				As^{5+}	0.46	-	2.245 (average)

(Data from Fyfe (1964), Minster (1964) and Nowacki (1964)).

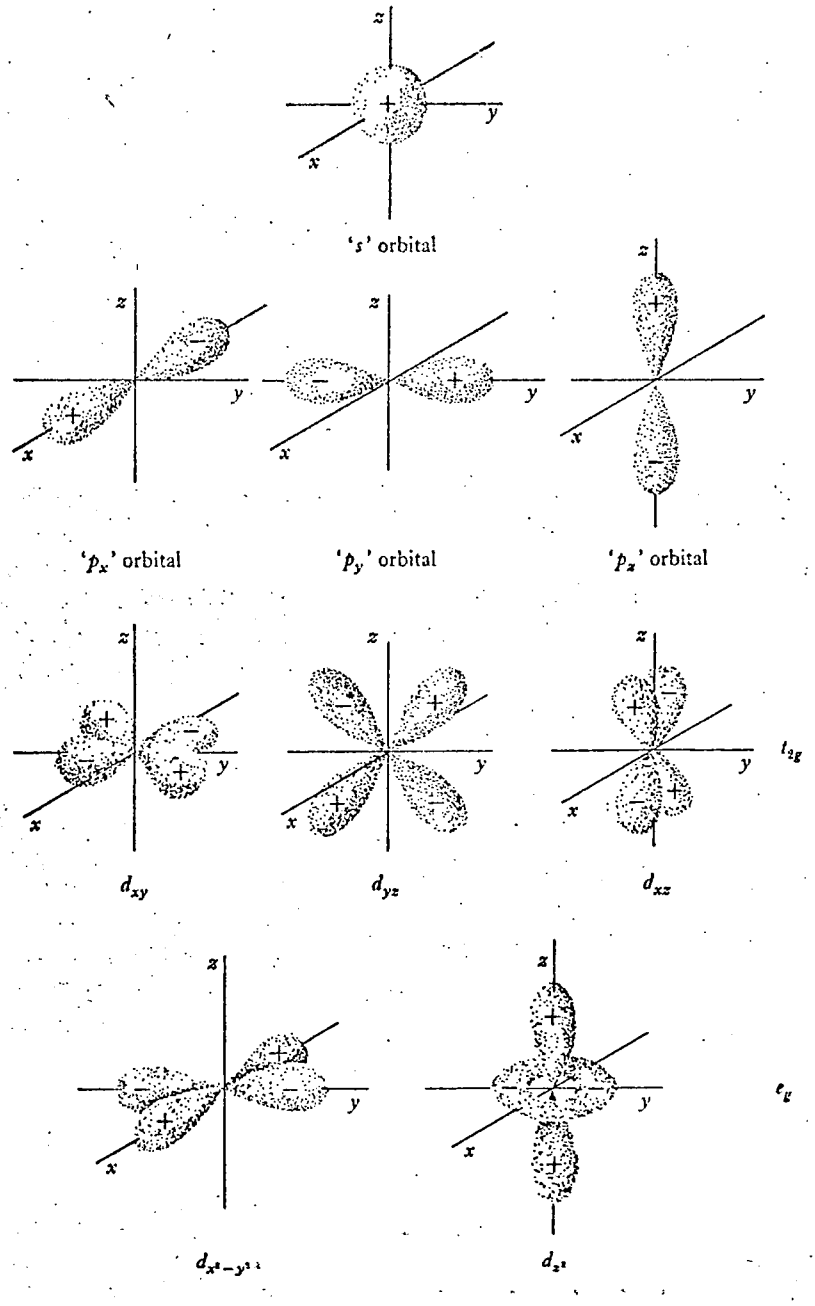

FIG 6-1

BOUNDARY SURFACES OF ATOMIC ORBITALS

(FROM BURNS 1970)

FIG 6-2

TETRAHEDRITE 1/2 CELL

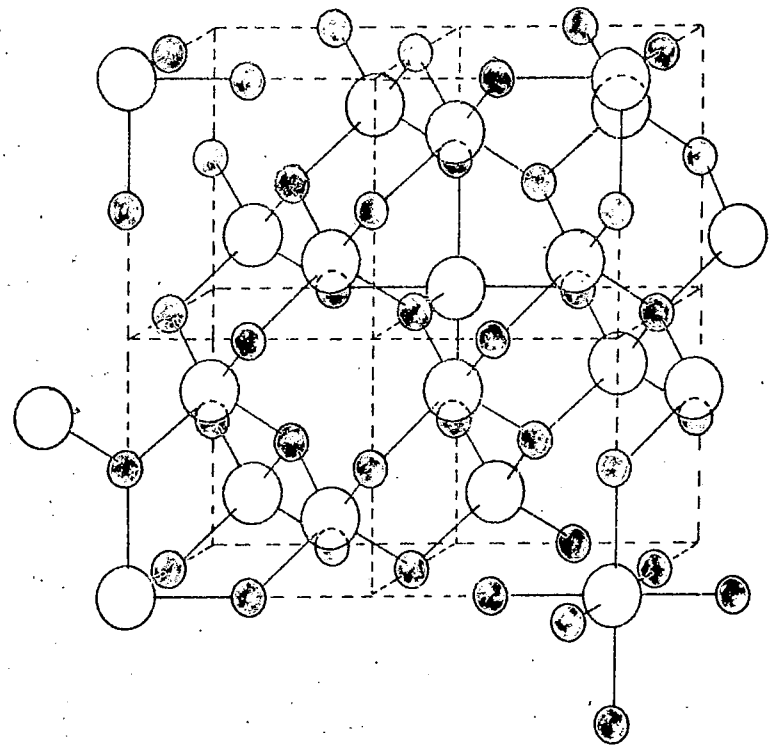

S

CU

SB

AFTER
PAULING & NEUMAN(1934)

FIG 6-3 TETRAHEDRITE

ATOM CO-ORDINATIONS AND ELECTRON DISTRIBUTION

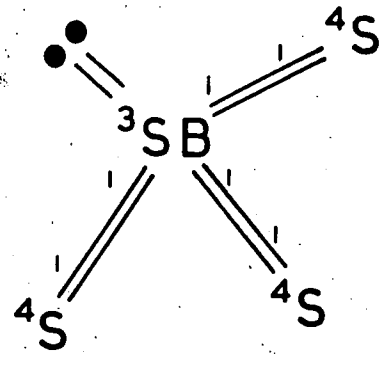

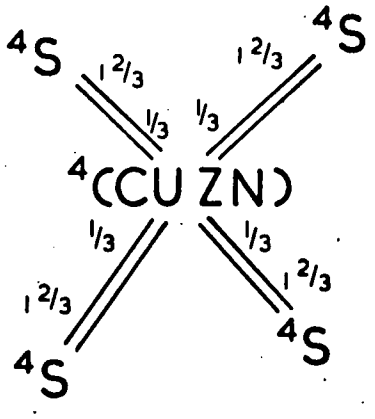

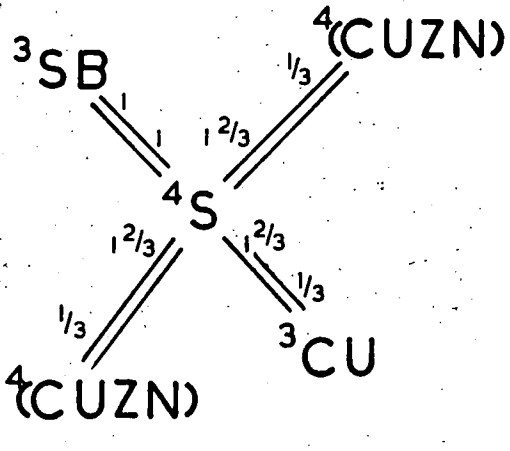

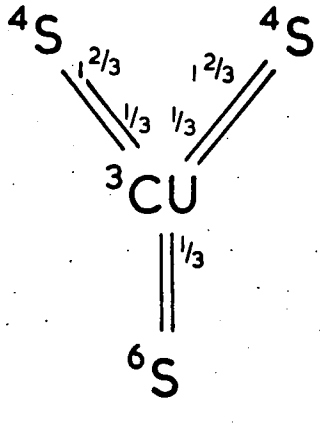

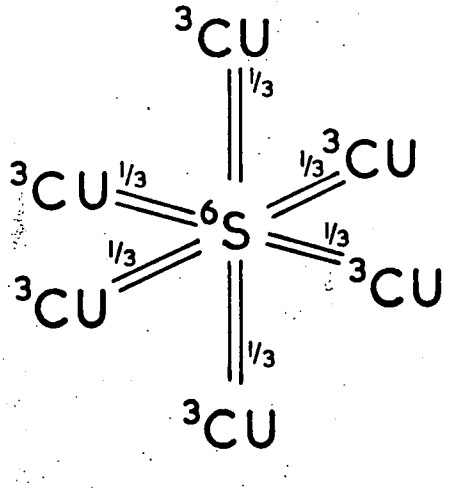

FIG. 6-4

TT BONDING IN TETRAHEDRITE

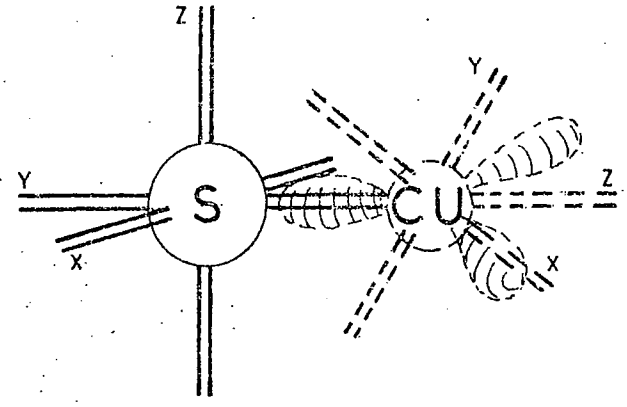

PERSPECTIVE VIEW OF THE $^{6}S-^{3}CU$ BOND

CU SP^2 ORBITAL IN THE Z-Y PLANE

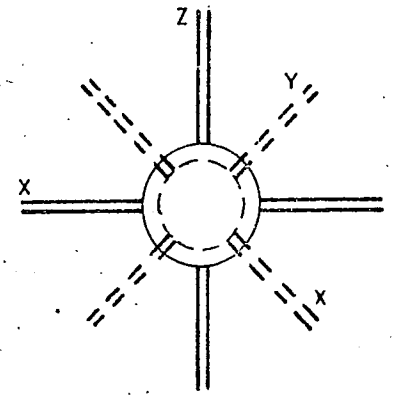

VIEW ALONG THE $^{6}S-^{3}CU$ BOND

CHAPTER 7

Suggestions of Possible Further Work and Conclusions

Further Work

Suggestions of possible further work on various aspects of sulphide mineralogy have been made throughout this study. The major topics requiring further study are -

(a) The Cu-Sb binary which requires revision.

(b) The Cu-Sb-S system which requires detailed study using D.T.A. and high temperature x-ray diffraction techniques in order to investigate the high temperature phase relations of tetrahedrite and Cu_3SbS_3.

(c) The Cu-Sb-As-S system which requires study in order to understand the phase relations of the tetrahedrite-tennantite series. The series is non-stoichiometric ans possibly contains miscibility gaps.

(d) The Cu-Ag-Sb-S system which contains several quaternary solid solutions, e.g. $(CuAg)_3SbS_4$, $(CuAg)_{12}Sb_4S_{13}$, and $(CuAg)_3SbS_3$. The latter series is important because its ability to transmit long wavelength red light means that it may have applications in the optics industry.

(e) The Cu-Fe-Sb-S and Cu-Zn-Sb-S systems which contain the quaternary solid solutions $(CuFe)_{12}Sb_4S_{13}$ and $(CuZn)_{12}Sb_4S_{13}$ respectively. The non-stoichiometry of the solid solutions, which has been noted in the case of zinc, requires investigation.

(f) The factors controlling substitution of Ag for Cu in tetrahedrite (e.g. the presence of other substituting elements)which is important because tetrahedrite is an ore mineral of silver.

(g) Crystal structure studies of:

(1) Cu_3SbS_3 which has a structure similar to wittichenite, Cu_3BiS_3.

(2) $Cu_{12}Sb_4S_{13}$ which has been assumed in the present study to have the crystal structure determined by Wuensch (1964) using a natural specimen. The structure of pure tetrahedrite requires further study in order to explain the high temperature non-stoichiometry and polymorphism of tetrahedrite in the Cu-Sb-S system.

(3) $(CuAg)_3SbS_4$ which differs slightly from stibioluzonite, Cu_3SbS_4.

(h) Spectral reflectivity and colour measurements which may be diagnostic of individual elements in substituted sulphosalts and may contribute to an understanding of bonding in -

(1) Ag-stibioluzonite, $(CuAg)_3SbS_4$,

(2) the $(CuAg)_3SbS_3$ series which transmit long wavelength red light, and

(3) tetrahedrites with Cu substituted by Ag, Fe, Zn and other elements, singly and in combinations.

(i) Unit cell edge and microhardness determination of sulphosalts which contribute to an understanding of bonding.

(j) The feasibility of synthesising substituted tetrahedrites by hydrothermal means which is necessary in

order to investigate, in more detail, factors controlling the crystallisation and composition of natural sulphosalts.

(k) The study of natural sulphosalts in order to define their mineralogical features and guide the experimental work. Theoretical conclusions reached using data obtained by study of synthetic minerals may also be applied to natural sulphosalts and ore deposits containing them.

(N.B.) The Cu-Sb-S and Cu-Sb-As-S systems have been investigated and the tetrahedrite-tennantite series is the subject of an unpublished study by Skinner and Luce (Skinner, personal communication). This work only became known to the author at a late stage in the writing of this thesis.

Conclusions

This project was undertaken in order to investigate the possible contribution to be made by synthetic sulphide mineralogy to the understanding of sulphosalts. Tetrahedrite was selected as a typical sulphosalt and has been the main subject of study.

From the work on synthetic specimens described in Chapter 3, on the phase relations of tetrahedrite in the Cu-Sb-S system, in Chapter 4, on substitution of Sb by As in tetrahedrite (the tetrahedrite-tennantite series), and in Chapter 5, on substitution of Cu by Zn, Fe and Ag in tetrahedrite, it is apparent that the main factor limiting the usefulness of dry sulphide synthesis in this type of study is the high temperature ($>400^{\circ}C$) involved. For example, variations in the composition of tetrahedrite in

the Cu-Sb-S system (this study) and tennantite in the Cu-As-S system (Maske and Skinner 1971) have been shown to be temperature dependant. Metastable high temperature polymorphs of non-stoichiometric tetrahedrite have been obtained in experiments in the Cu-Sb-S system. Lamellae of stibioluzonite in Zn-tetrahedrite indicated the non-stoichiometry of substituted tetrahedrite at high temperature. Silver substitution in tetrahedrite has proved to be temperature dependant.

These complications increase the difficulties of synthesis of sulphosalts and probably have little significance in the study of natural minerals which crystallise in relatively low temperature ($<400^{\circ}C$) environments. Tetrahedrite, for example, is commonly found in hydrothermal-type ore deposits with temperatures of deposition in the order of 200 to $300^{\circ}C$. Guillemin and Picott (1966) report tetrahedrite occurring as an alteration product of bronze Roman coins in hot springs (58 to $68^{\circ}C$) at Bourbonne-les-Bains.

The main contribution to be made by dry sulphide synthesis to the study of natural sulphosalts is indirect. The crystal chemistry of sulphides is little understood and understanding the factors controlling substitution and the effects of different substituting elements on the physical properties of a structure requires the collection of systematic mineralogical data.

It is not always easy to use specimens of natural minerals for the collection of systematic data because of the complexity of compositions and the restricted range in compositions represented in nature.

Systematic information on mineralogical properties can

conveniently be obtained by synthesis of selected compositions. Predictions on the limit of substitution of an element in a structure, or its effect on some physical property, can be tested. In this way a study of synthetic minerals can contribute to theoretical aspects of sulphide crystal chemistry and so contribute to the understanding of mineralogical properties of natural minerals.

REFERENCES

AKINCI, O. T. (1970) The Effect of Iron Substitution on the Cell Size, Reflectivity and Colour of Sphalerite. Unpub. M.Sc.Thesis, University of Durham.

BERNARD, J. H. (1957 & 8) Investigation of Minerals of the Tetrahedrite Group. Min. Abstracts 15, p.23.

BERRY, L. G. (1943) Studies of Mineral Sulpho-Salts: VII - A Systematic Arrangement on the Basis of Cell Dimensions. Univ. of Toronto Studies, Geol. Series, No.48, pp.9-30.

BITHER, T. A. et al. (1968) Transition Metal Pyrite Dichalcogenides. High-Pressure Synthesis and Correlation of Properties. Inorg. Chem. 7, p.2208-2220.

BOHMER, H. (1964) Mineralogy of the Tetrahedrite Series, Econ. Geol., 59, p.1426.

BOYLE, R. W. (1968) The Geochemistry of Silver and its Deposits. Geol. Surv. of Canada, Bull.160.

BROWN, G. I. (1967). A New Guide to Modern Valency Theory. Longmans.

BURNS, R. G. (1970) Mineralogical Applications of Crystal Field Theory. Cambridge University Press.

BURNS, R. G. and Vaughan, D. J. (1970). Interpretation of the Reflectivity Behaviour of Ore Minerals. Amer. Mineral. 55, p.1576-1586.

CAMBI, L. and Elli, M. (1965) Processi idrotermali Sintesi di solfosali da ossidi di metalli e metalloidi. La Chimica e l'Industria, vol.47, No.2.

COMMISION INTERNATIONALE de l'Eclairage (1931). Proceedings of the eighth session. Cambridge.

COMPANION, A. L. (1964) Chemical Bonding. McGraw Hill, Inc., New York.

DANA, J. D. and DANA, E. S. (1944). The System of Mineralogy, edited by Palache, C. Berman, H. and Frondel, C. Vol.I, John Wiley and Sons, Inc., New York.

DAVIES, O. L. (1957) Statistical Methods in Research and Production. Oliver and Boyd.

DUNCUMB, P. and JONES, E. M. Electron Probe Microanalysis. An Easy to Use Computer Program for Correcting Quantitative Data. Report No.260. Tube Investment Research Labs., Hinxton Hall, Saffron Walden, Cambridge, England.

EDWARDS, A. B. (1947) Texture of Ore Minerals. Melbourne.

ELLIOTT, R. P. (1965) Constitution of Binary Alloys. 1st Supplement, McGraw Hill Book Co. Inc., New York.

ENGEL, P. and NOWACKI, W. (1966). Die Verfeinerung der Kristallstruktur von Proustit, (Ag_3AsS_3) und Pyrargyrit, (Ag_3SbS_3). N. Jahrbuch, Miner. Monatsh. p.181-184.

FRUEH, A. J. (1954). The Use of Zone Theory in Problems of Sulphide Mineralogy. Geochim. Cosmochim. Acta 6, p.79-89.

FYFE, W. S. (1964) Geochemistry of Solids: An Introduction. McGraw Hill Inc., New York.

GAINES, R. V. (1957) Luzonite, Famatinite and some Related Minerals. Amer. Mineral., Vol.42.

GAUDIN, A. M. and DICKE, G. (1939). The Pyrosynthesis, Microscope Study and Irridescent Filming of Sulphide Compounds of Copper with Arsenic, Antimony and Bismuth. Econ. Geol. Vol.34, p.49-81 and p.214-232.

GAUDIN, A. M. and McGlashan, D. W. (1938). Sulphide Silver Minerals - A Contribution to their Pyro-synthesis and to their Identification by their Irridescent Filming. Econ. Geol., Vol.33, p.143-193.

G.K.N. (1958) The G.K.N. (Bench Type) Micro-hardness Tester Instruction Booklet. Associated Automation Ltd.

GMELIN (1961) Gmelin's Handbuch der Anorganischen Chemie. 8 Auflage, Kupfer, Teil B - Liefenung 2, p.971-973.

GODOVIKOV, A. A. et al. (1970). New Synthetic Copper and Silver Sulpho-Salts. International Min. Assoc. 7th General Meeting. The Genesis of Ore Deposits. (Collected Abstracts).

GRAESER, S. (1965) Die Mineralfundstellen im Dolomit des Binnatales. Schweiz. Min. Petr. Mitt. Band 45, Heft 2.

GUERTLER, W. and MEISSNER, K. L. (1921). Met.Erz. 18, p.410-415.

GUILLEMIN, C. and Picott, P. (1966). Observations nouvelles sur les sulfures néogènes des sources thermales de Bourbonne-les-Bains. Bull. Soc. Franç. Min. Crist., 89, p.367-371.

HANSEN, M. and Anderko, K. (1958). Constitution of Binary Alloys. 2nd Ed. McGraw Hill Inc., New York.

HARADA, Z. and KITAHAMA, M. (1952). On Some Sulphosalt Minerals (tetrahedrite and tennantite) from Northern Japan. Journ. Fac. Sci., Hokkaido Univ., Ser.4 (Geol. Min.) Vol.8, p.74-81.

HARCOURT, G. A. (1937). The Distinction between Enargite and Famatanite (Luzonite). Amer. Mineral. 22, p.517-535.

HELLNER, E. (1958). A Structural Scheme for Sulfide Minerals. Journ. of Geol. 66, p.503-525.

HOFMANN, W. (1933). Strukturelle und Morphologische Zusammenhänge bei Erzen vom Formeltyp ABC_2 1. Die Struktur von Wolfsbergit $CuSbS_2$ und Emplektit $CuBiS_2$ und deren Beziehungen zu der Struktur von Antimonit Sb_2S_3. Z. Krist., Vol.84, p.177-203.

JELLINEK, F. (1968). Sulphides in Inorganic Sulphur Chemistry. Edited by Nickless, G. p.669-747 (Elsevier)

KEIGHIN, C. W. and HONEA, R. M. (1969). The System Ag-Sb-S from 600°C to 200°C. Mineral Deposita, (Berlin), 4, p.153-171.

KIMBALL, G. E. (1940). Directed Valence. J. Chem. Phys., 8, p.188-198.

KLUG, H. P. and ALEXANDER, L. E. (1962). X-Ray Diffraction Procedure. John Wiley and Sons. Inc., New York.

KOSTOV, I. (1957) On Isomorphism amongst Minerals of the groups of Sulpho-Salts. Trans. All.-Union Min.Soc. 86, No.3, p.336-342 in Aspects of Theoretical Mineralogy in U.S.S.R. by Battey and Tomkeieff, International Series of Monographs on Earth Sciences, Vol.18, p.293-330.

KRETSCHMER, A. (1911). Z. Krist. 48, p.484.

KULLERUD, G. (1958). The Cu-S System. Ann. Rept. of Director of Geophys. Lab., Carnegie Inst., Wash., Year Book 59, p.110-120.

KULLERUD, G. (1960). The Cu-S System. Ann.Rept. of Director of Geophys. Lab., Carnegie Inst., Wash., Year Book 57, p.215-218.

LEVY, C. (1966). Contribution à la Mineralogie des Sulfures de Cuivre du type $Cu_3 \times S_4$. Première thèse, présentée à la Faculté des Sciences de l'Université de Paris, Publié dans les Mémoires du Bureau de Recherches Géologiques et Minières.

LONG, J. V. P. (1967). Electron Probe Microanalysis, in Physical Methods in Determinative Mineralogy. Edit. by J. Zussman, Academic Press.

MacADAM, D. L. (1942). Visual Sensitivities Colour Differences in Daylight. J. Opt. Soc. Am., vol.32, p.247.

MACHATSCHKI, F. (1928)a Formel und Kristallstruktur des Tetraedrites. Norsk. Geol. Tidsskr. 10, 23.

MACHATSCHKI, F. (1928)b Präzisionmessungen der Gitterkonstanten verschiedener Fahlerze. Formel und Struktur derselben. Z.Krist.68, p.204.

MARPLES, J. A. C. and SHAW, J. L. (1966). Two Crystallographic Computor Programs for Lattice Parameter Refinement and for Calculating Expected Line Position. United Kingdom Atomic Energy Authority Research Group Report A.E.R.E. - R.5210.

MARUMO, F. and NOWACKI, W. (1967). A Refinement of the Crystal Structure Luzonite. Z. Krist. Bd. 124. p.1-8.

MASKE, S. and SKINNER, B. J. (1971) Studies of the Sulphosalts of Copper. 1. Phases and Phase Relations in the System Cu-As-S. (In Preparation).

MINGOS, D. M. P. (1971) Geometrics of co-ordinated Ligands. Nature Physical Science, Vol.229.

MINSTER, E. F. (1964). Crystallochemical Factors of Isomorphism in Essentially Covalent Compounds as Illustrated by Sphalerite. Geochem. Intern., p.285-289.

NELSON, J. B. and RILEY, D. P. (1945). An Experimental Investigation of Extrapolation Methods in the Determination of Accurate UnitCell Dimension of Crystals. Phys. Soc., London Proc.

NICKEL, E. H. et al. (1971). Bond Strengths in the Disulphides of Iron Cobalt and Nickel. Canadian Mineralogist.

NOVOTNÝ, J., and NOVAK, F. (1966). The Mineralogical and Geochemical Study of Tetrahedrite from Špani Dolina near Banská Bystrica (central Slovakia). Časopis Min. Geol., Praha, 11, p.239-247.

NOWACKI, W. (1969). Zur Klassification und Kristallchemie der Sulfosalze. Schweiz Min. Petr. Mitt, 49, 109-156.

NUFFIELD, E. W. (1947) Studies of Mineral Sulpho-Salts: XI - Wittichenite (Klaprothite). Econ. Geol., Vol.XIII, No.2.

PARRAVANO, N. and DE CESARIS, P. (1912). Solfoantimoniti Ramosi. Gaz. Chim. Ital., Vol.42, p.189.

PARTHÉ, (1967). In Intermettallic Compounds edited by J. H. Westbrook. John Wiley and Sons Inc.

PAULING, L. (1931) The Nature of the Chemical Bond. Application of results obtained from the quantum mechanics and from a theory of paramagnetic susceptibility to the structure of molecules. J. Amer. Chem. Soc.53, p.1367-1400.

PAULING, L. (1938). The Nature of the Interatomic Forces in Metals. Phys. Rev. 54, p.899-904.

PAULING, L. (1960). The Nature of the Chemical Bond. 3rd Ed. Cornell Univ. Press. Ithaca. New York.

PAULING, L. (1970) Crystallography and Chemical Bonding of Sulfide Minerals. Mineral. Soc. Amer. Spec. Pap.3, p.125-131.

PAULING, L. and NEUMAN, E. W. (1934). The Crystal Structure of Binnite, $(CuFe)_{12}As_4S_{13}$ and the Chemical Composition and Structure of Minerals of the Tetrahedrite Group. Z. Krist. 88, p. 54-62.

PEARSON, W. B. (1964). The Crystal Structures of Semiconductors and a General Valence Rule. Acta Cryst. 17, 1.

PILLER, H. (1966). Colour Measurements in Ore Microscopy. Mineralium Deposita.

PRIOR, G. T. (1916). Analyses of Seligmannite, Zincifferrous Tennantite (binnite) and Fuchsite from the Lengenbach quarry, Binnenthal. Min. Mag. 15, p.385-387.

PRIOR, G. T. and SPENCER, L. J. (1899). The Identity of Binnite with Tennantite and the Chemical Composition of Fahlerz. Min.Mag. 12, p. 184-213.

PROUVOST, J. (1963). Various Aspects of Atomic Displacements in Metallic Sulfides. Min. Soc. Amer. Spec. Pap.I, p.144.

ROSEBOOM, E. H. (1966). An Investigation of the System Cu-S and some Natural Copper Sulfides between 25°C and 700°C. Econ. Geol. 61, p.641-672.

RUCKLIDGE, J. and GASPARRINI, E. L. (1969). EMPADRVII. Dept. of Geol., University of Toronto.

RUNDLE, R. E. (1967). Theories of Bonding in Metals and Alloys - in Intermettallic Compounds edited by J. H. Westbrook.

SAKHAROVA, M. S. (1966). The Basic Problems of Isomorphism and Origin of Tetrahedrite-Tennantite Ores. Academy of Science of the U.S.S.R., Vol.8, No.I.

SCHENCK, R. et al. (1939). Gleichgewichtsstudien über Erzbildende Sulfide. Zeit. für Anorg. und Allgem. Chem., Vol.240, p.173.

SCIENCE OF COLOR (1953) Committee on Colorimetry. Optical Society of America. Cromwell, New York.

SEEL, F. (1965). Atomic Structure and Chemical Bonding. Methuen and Co. Ltd., London.

SKINNER, B. J. (1960). Assemblage Enargite-Famatanite, a possible geologic thermometer. Geol. Soc. Am. Bull., Vol.71, p.1975.

SPRINGER, G. (1969). Electronprobe Analyses of Tetrahedrite. N.Jb. Miner. Mh, p.24-32.

STAPLES, A. B. and WARREN, H. V. (1946). Minerals from the Highland-Bell Silver Mine, Beaverdell, British Columbia, Univ. of Toronto Studies, Geol. Ser. No.50 (for 1945), p.27-33.

TANSEL, T. (1970). On the Mineralogy of Some Base Metal Ores from Ireland. Unpub. M.Sc. Thesis, University of Durham.

TOULMIN, P. III and BARTON, P. B. Jr., (1964). Athermodynamic Study of Pyrite and Pyrrochotite, Geochem. et Cosmochim., Acta, Vol.28, p.641-671.

TRDLIČKA, Z. (1967) Mineralogical Study of the Tetrahedrite from Ore Deposition Fichtenhübel, Slovakia, Časopis. Min. Geol., Praha, 12, p.115-122.

TSCHERMAK (1894) in Pauling and Neuman (1934).

VAUGHAN, D. J., BURNS, R. G. and BURNS, V. M. (1971). Geochemistry and Bonding of Thiospinel Materials. Geochem. et Cosmochim. Acta, Vol.35, p.365-381.

WERNICK, J. H. and BENSON, K. E. (1957). New Semiconducting Ternary Compounds. Jour. Chem. Phys., Solids, vol.3, p.157-159.

WEST, W. A. and MENZIES, A. W. C. (1929). The Vapor pressures of Sulphur between 100°C and 550°C with Related Thermal Data. J. Phys. Chem. 33, p.1880.

WRIGHT, W. D. and PITT, F. H. G. (1934). Hue Discrimination in Normal Colour Vision. Proc. of the Phys. Soc. 46, p.459.

WUENSCH, B. J. (1964). The Crystal Structure of Tetrahedrite $Cu_{12}Sb_4S_{13}$. Z. Krist., Vol.119, p.437-453.

WUENSCH, B. J., TAKÉUCHI, Y. and NOWACKI, W. (1966)a Refinement of the Crystal Structure of Binnite $Cu_{12}As_4S_{13}$. Z. Krist., Vol.23, p.1-20.

WUENSCH, B. J., TAKÉUCHI, Y. and NOWACKI, W. (1966)b Comparison of the Crystal Structures of Binnite $Cu_{12}AsS_{13}$ and Tetrahedrite $Cu_{12}Sb_4S_{13}$. Amer. Min.

YUI, S. (1970) Heterogeneity within a single Grain of Minerals of the Tennantite-Tetrahedrite Series. International Min. Assoc., 7th General Meeting. The Genesis of Ore Deposits. (Collected abstracts).